Summer 2009

New Conceptual Understanding of Lewis Acidity, Coordinate Covalent Bonding, and Catalysis

Joshua A. Plumley

NEW CONCEPTUAL UNDERSTANDING OF LEWIS ACIDITY,

COORDINATE COVALENT BONDING, AND CATALYSIS

A Dissertation

Submitted to the Bayer School

of Natural and Environmental Sciences

Duquesne University

In partial fulfillment of the requirements for

the degree of Doctor of Philosophy

By

Joshua A. Plumley

August 2009

NEW CONCEPTUAL UNDERSTANDING OF LEWIS ACIDITY,

COORDINATE COVALENT BONDING, AND CATALYSIS

By

Joshua A. Plumley

Approved August 2009

_____
Jeffrey D. Evanseck
Professor of Chemistry and Biochemistry
Dissertation Director
Committee Member

_____
Ellen Gawalt
Assistant Professor of Chemistry and
Biochemistry
Committee Member

_____
Douglas J. Fox
Director, Gaussian Inc.
External Reader

_____
Jeffry D. Madura
Chair and Professor of Chemistry and
Biochemistry
Committee Member

_____
David W. Seybert
Dean, Bayer School of Natural &
Environmental Sciences
Professor of Chemistry and Biochemistry

ABSTRACT

NEW CONCEPTUAL UNDERSTANDING OF LEWIS ACIDITY,

COORDINATE COVALENT BONDING, AND CATALYSIS

By

Joshua A. Plumley

August 2009

Dissertation Supervised by Jeffrey D. Evanseck

The focus of this dissertation is to correct misconceptions about Lewis acidity, uncover the physical nature of the coordinate covalent bond, and discusses how Lewis acid catalysts influence the rate enhancement of the Diels-Alder reaction. Large-scale quantum computations have been employed to explore many of Lewis' original ideas concerning valency and acid/base behavior. An efficient and practical level of theory able to model Lewis acid adducts accurately was determined by systematic comparison of computed coordinate covalent bond lengths and binding enthalpies of ammonia borane and methyl substituted ammonia trimethylboranes with high-resolution gas-phase experimental work. Of all the levels of theory explored, M06-2X/6-311++G(3df,2p) provided molecular accuracy consistent with more resource intensive QCISD(T)/6-311++G(3df,2p) computations.

Coordinate covalent bond strength has traditionally been used to judge the strength of Lewis acidity; however, inconsistencies between predictions from theory and computation, and observations from experiment have arisen, which has resulted in consternation within the scientific community. Consequently, the electronic origin of Lewis acidity was investigated. It has been determined that the coordinate covalent bond dissociation energy is an inadequate index of intrinsic Lewis acid strength, because the strength of the bond is governed not only by the strength of the acid, but also by unique orbital interactions dependent upon the substituents of the acid and base. Boron Lewis acidity is found to depend upon both substituent electronegativity and atomic size. Originally deduced from Pauling's electronegativities, boron's substituents determine acidity by influencing the population of its valence by withdrawing electron density. However, size effects manifest differently than previously considered, where greater σ-bond orbital overlap, rather than π-bond orbital overlap, between boron and larger substituents increase the electron density available to boron, thereby decreasing Lewis acidity. The computed electronegativity and size effects of substituents establish unique periodic trends that provide a novel and clearer understanding of boron Lewis acidity, consistent with first principle predictions.

Lastly, it is discovered that the energetics associated with the transition structure converge much slower than what was observed for coordinate covalent bonded ground states. Consequently, it is harder to model activation barriers, as compared to binding energies, to within experimental accuracy, because larger basis sets must be employed. Hyperconjugation within dienophile ground states, initiated by geminal Lewis acid interactions, is found to govern the strength of the coordinate covalent bond between the

Lewis acid and the dienophile. A novel interpretation is presented where the strength of the coordinate covalent bond within the Lewis acid activated dienophile is governed by donor-acceptor orbital interactions between the π-density present on the carbonyl group to the σ^* orbitals on the Lewis acid, rather than the main donor-acceptor motif between the oxygen lone pair and the empty *2p* orbital on the Lewis acid. Moreover, the same hyperconjugation within the dienophile controls the rate enhancement of the Lewis acid catalyzed Diels-Alder reaction, by modulating the energy of the dienophile's lowest unoccupied molecular orbital. A new understanding of Lewis acidity and coordinate covalent bonding has been achieved to better describe and predict the structure and electronic mechanism of organic reactions.

ACKNOWLEDGMENT

have been as successful as I am today. I would like to thank specifically my grandfather, for he is directly responsible for my excellent work ethic. He taught me that nothing is impossible and to never give up. He would have been proud of my accomplishments.

TABLE OF CONTENTS

LIST OF FIGURES

LIST OF TABLES

LIST OF ABBREVIATIONS

A   Helmholtz free energy

AN   Acceptor number

AR   Atomic radii

aug-cc-pVnZ   augmented correlation consistent polarized valence n zeta

B3LYP   Becke's three-parameter exchange functional with the correlation functional provided by Lee, Yang, and Parr

B3P86   Becke's three-parameter exchange functional with Perdew's correlation functional developed in 1986

BLYP   Becke's 1988 exchange functional with the correlation functional provided by Lee, Yang, and Parr

BSSE   Basis set superposition error

BVD   Boron valence deficiency

cc-pVnZ   correlation consistent polarized valence n zeta

CCSD   Coupled cluster with single and double substitutions

CI   Configuration interaction

CID   Configuration interaction with double substitutions

CISD   Configuration interaction with single and double substitutions

CP   Counterpoise method

DFT   Density functional theory

DN   Donor number

E   Energy

EDG   Electron donating group

EN   Electronegativity

EWG	Electron withdrawing group
FMO	Frontier molecular orbital
G	Gibbs free energy
GGA	Generalized gradient approximation
GTO	Gaussian type orbital
H	Enthalpy
HF	Hartree-Fock
H-GGA	Hybrid-generalized gradient approximation
HM-GGA	Hybrid meta-generalized gradient approximation
HOMO	Highest occupied molecular orbital
HSAB	hard soft-acid base
K	Equilibrium constant
k_B	Boltzmann's constant 1.380658×10^{-23} J $\cdot$ K^{-1}
LSDA	Local spin density approximation
LUMO	Lowest unoccupied molecular orbital
LYP	Correlation functional provided by Lee, Yang, and Parr
M05	Minnesota functional developed in 2005
M05-2X	Minnesota functional developed in 2005 with double the Hartree-Fock exchange compared to that of M05
M06	Minnesota functional developed in 2006
M06-2X	Minnesota functional developed in 2006 with double the Hartree-Fock exchange compared to that of M06
M08-HX	Minnesota functional developed in 2008 with 52.23% Hartree-Fock exchange
M08-SO	Minnesota functional developed in 2008 where the gradient expansion is to the second order

MAD	Mean absolute deviation
M-GGA	Meta-generalized gradient approximation
MP2	Møller-Plesset second-order perturbation theory
MPW	The Perdew-Wang 1991 exchange functional as modified by Adamo and Barone
MPW1B95	Modified Perdew-Wang 1-parameter functional with Becke's M-GGA correlation functional developed in 1995/1996 (fit to atomization energies)
MPW1K	Modified Perdew-Wang 1-parameter functional for kinetics
MPWB1K	Modified Perdew-Wang 1-parameter functional with Becke's M-GGA correlation functional developed in 1995/1996 (fit to kinetic data)
NAO	Natural atomic orbital
NBO	Natural bond orbital
NBO 5.G	Natural bond orbital program Version 5 compatible with Gaussian
NBO	Natural bond orbital
NHO	Natural hybrid orbital
NRT	Natural resonance theory
PCM	Polarizable continuum model
PES	Potential energy surface
QCISD	Quadratic configuration interaction with single and double substitutions
QCISD(T)	Quadratic configuration interaction with single and double substitutions incorporating a perturbational treatment of the triples contribution
Q_{CTF}	Charge transfer frustration
QM	Quantum Mechanics
S	Entropy
S43	Secondary orbital [4+3] interaction discovered by Singleton
SAH	Secondary orbital interaction discovered by Salem, Houk, and Alston

SCF	Self consistent field
SOI	Secondary orbital interaction
SP	Single point
STO	Slater-type orbital
STO-nG	Slater-type orbital consisting of n Gaussian type orbitals
VSEPR	Valence shell electron pair repulsion
VSXC	van Voorhis and Scuseria's gradient-corrected correlation functional
VWN3	Vosko, Wilk, and Nusair 1980 correlation functional(III)
WH	Secondary orbital interaction discovered by Woodward and Hoffmann
ZPE	Zero point energy

Chapter 1

Introduction

1.1 The Chemical Bond

The chemical bond is one of the most fundamental assemblies within the framework of chemistry and biochemistry. Most chemical reactions involve the formation or cleavage of bonds; thus, it is of vital importance to understand the physical nature of the chemical bond. The foundation of chemical bonding was laid with the "electronic structure revolution," initiated by Gilbert Lewis.[1-5] Nearly a century later, his concepts pertaining to the "electron pair bond" and the "rule of eight," later coined by Irving Langmuir as the "octet rule",[3, 6] are still discussed and taught in almost all general chemistry text books and courses as an introduction to the marvelous and complex world of the chemical bond.

Of the various types of bonding described by Pauling,[7] Lewis reported that the covalent chemical bond between two atoms is a direct result of sharing pairs of electrons, completing the valence shells of the bonded atoms.[4] However, Lewis was not able to explain the counterintuitive attraction between the electrons, because particles of the same charge should repel each other. However, Lewis was so confident in the formation of the covalent bond through electron-pair sharing that he declared Coulomb's Law invalid for extremely short distances. It was not until Pauli's exclusion principle

was formulated that the electron pair was justified. Regardless of the origin, Lewis

coined the phrase "rule of two" or the "duet rule" to refer to localized electron pairs. As

a manifestation of the "duet rule," Lewis represented the electron pair with an ingenious

double dot symbol, which resembles a colon, to designate a shared bond or nonbonding

pair of electrons. As a result, molecules such as the hydrogen dimer and water can be

easily constructed as "Lewis dot structures" (Figure 1.1).

Figure 1.1. Lewis dot and line structure representations of the hydrogen dimer and water.

Lewis also proposed that atoms following the first period possess electrons in successive

shells containing up to eight electrons. He introduced the cubical atom in which eight

electrons were systematically arranged on the corners of a cube.[4] Consequently, the

"rule of eight" or "octet rule" was born. Lewis was aware of exceptions to the "octet

rule" and thus regarded the "duet rule" to be a more fundamental chemical observation

rather than the "octet rule." For example, BF_3 and PCl_6 violate the "octet rule,"

possessing valencies of six and twelve respectively, as shown by Figure 1.2.

Figure 1.2. Lewis dot structures of BF_3 and PCl_3, clearly illustrating the violation of the octet rule, where boron possesses six valence electrons and phosphorous possesses twelve valence electrons. The three lone pairs on each halogen have been omitted for clarity.

In spite of Lewis' caution regarding the limitations of the octet rule, Langmuir stressed the "octet rule" over the "duet rule". As a consequence of his persuasive lectures and vigorous promotion of the octet rule, it became recognized as a fundamental law rather than a hypothesis based on experimental data.[3, 6, 8] Consequently, when violations of the "octet rule" were discovered, attempts to explain the deviation were reported.[7] However, once the "octet rule" was accepted as merely an empirical observation rather than a law of nature, attempts to retain the validity of the octet rule were no longer needed. The octet rule strictly applies to atoms of the second period (e.g. carbon, nitrogen, oxygen and fluorine). Atoms from other periods may obey the "octet rule," but not all molecules necessarily do so.

BF$_3$ is a common Lewis acid and a known violator of the octet rule; however, in an attempt to adhere to the well promoted "octet rule", justifications were made to show that BF$_3$ does in fact obey the octet rule.[7] For example, Pauling reported that double bonds between boron and fluorine significantly influence the bonding scheme within BF$_3$, as illustrated by three degenerate resonance structures (Figure 1.3). The three

resonance structures illustrate that boron does in fact possess eight electrons in its

valence and thus adheres to the octet rule.
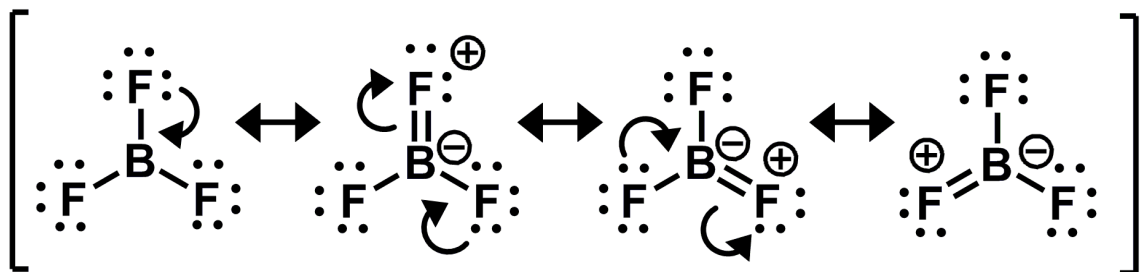
Figure 1.3. Resonance structures of BF_3, justifying that BF_3 does in fact obey the octet rule, since boron possesses eight electrons in its valence shells.

Pauling justified the BF_3 bonding scheme by bringing attention to the fact that

boron has a formally empty $2p$ orbital, which may be filled with fluorine's lone pairs.

Furthermore, the 0.07 Å shorter B–F bond length within BF_3 as compared to within BF_4^-

suggests partial double bond character.[7] However, the shorter B–F bond length within

BF_3 can just as easily be justified by the fact that three atoms can more closely pack

around a central atom as compared to four.[9]

Lewis' theory dictates that electrons exist as localized pairs within a molecule,

fixed between a set of nuclei or as lone pairs. However, this is not true since the

positions of the electrons are not known precisely, according to Heisenberg's uncertainty

principle. A primary example of a molecule that is not accurately represented by one

Lewis dot structure with fixed electrons is that of benzene. Pauling rectified the dilemma

by showing that delocalized structures such as benzene can be represented as a linear combination of resonance structures, yielding a resonance hybrid. However, as the number of delocalized electrons within a structure increases, the resonance hybrid description becomes less accurate, and a molecular orbital description is necessary.[10]

Although pairs of electrons are known to delocalize, Lewis' theory is an excellent first-order approximation for understanding the bonding within a molecule. Furthermore, the approximate localization of electron pairs between atoms also initiated an understanding of molecular geometry. For example, if electrons in an octet are arranged on the corners of a tetrahedron, molecules such as CH_4 were justified to possess a tetrahedral structure. The arrangement of electron pairs also justified the trigonal pyramidal and bent molecular geometries for NH_3 and OH_2 molecules, respectively. Extensions of Lewis' theory by Sidwick and Powell[11] suggested that molecular geometry is a consequence of the total number of electron pairs in the valence shells of the central atom, where electron pairs would arrange themselves around the central atom in order to minimize electron pair repulsions. Lewis, Sidwick, and Powell's pioneering advancements finally led to the construction of Valence Shell Electron Pair Repulsion Theory (VSEPR).[9]

The foundation of the chemical bond, laid by Lewis[1, 2, 4, 5] and other pioneers such as Pauling,[9] Langmuir,[3, 6, 8] J. E. Lennard-Jones,[12] Linnett,[13] Mulliken, Heitler, and London,[14] to mention a few, can hardly be summarized in a single chapter. However, one point remains clear; The nature of the chemical bond is far from lucid, as made evident by the publication of an entire issue of the *Journal of Computational Chemistry* dedicated to chemical bonding, where new and exciting bonding schemes are currently

being explored and reported.[15] For example, Frenking and coworkers reported that nonpolar bonds between main-group elements, which are prototype covalent bonds, have large attractive contributions from electrostatic interactions, which can be stronger than the orbital overlap, which was previously thought to be the primary interaction.[16] Furthermore, unusual bond orders between transition metal structures have been reported, ranging from quadruple to sextuple bonds.[17, 18] Regardless of the new bonding schemes, the "electron pair" remains the primary unit of chemical bonding, introduced nearly a century ago by Lewis.

1.1.1 The Covalent Versus Coordinate Covalent Bond

Pauling classified all chemical bonds as being either covalent, electrostatic, or metallic, indicating that the covalent bond is among the most common and prevalent bonding schemes within the realm of chemical bonding.[7] In addition to the three main bonding motifs, he noted the existence of a subsection within the covalent classification, now recognized as the coordinate covalent bond, also referred to as the dative bond, coordination bond, or coordinate link.[19-22] Pauling was intrigued by the coordinate covalent bond, which he considered to be a type of double bond consisting of one single covalent bond and one ionic bond of unit strength, as demonstrated by trimethylamine oxide within Figure 1.4.[7]
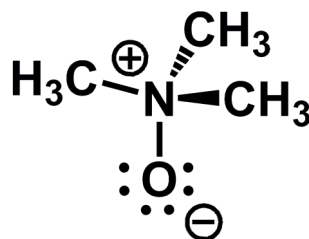
Figure 1.4. The coordinate covalent bond between the donor, oxygen, and the acceptor, nitrogen, within trimethylamine oxide. Illustration of one covalent bond plus one ionic bond to represent the coordinate covalent bond.

Although the coordinate covalent bond is not considered a double bond as Pauling originally proposed, it has been reported to possess both ionic and covalent character.[23-25] The coordinate covalent bond demonstrates an atypical bonding scheme, where covalent and ionic potential energy surfaces become close in energy, where the wavefunction is described by Equation 1.1.

$$\Psi_{\text{coordinate covalent}}(D^+\!-A^-) = a\Psi_{\text{covalent}}(D\!-A) + b\Psi_{\text{ionic}}(D^+,\, A^-) \qquad 1.1$$

The importance of each bonding term depends upon the ability of the atomic partners to share electrons, as well as D to donate electrons and A to accept them.

The archetypical prototypes of the coordinate covalent bond and the covalent bond are ammonia borane (H_3BNH_3) and ethane (H_3CCH_3), respectively, as shown by Figure 1.5. Previously, it was thought that when a coordinate covalent bond forms, the participating electron pair originates solely from one fragment.[19] For example, the electron pair forming the coordinate covalent bond within ammonia borane is donated

from ammonia to the electron-pair acceptor, borane. However, the distinction between the covalent and coordinate covalent bond becomes unclear when ethane is formed by the coordination between a carbanion and a carbocation. Haaland proposed a more lucid distinction between the coordinate covalent and covalent bond by not considering where the electrons originate, as previously done, but by considering the minimum-energy rupture of the bond and then examining the resulting fragments.[19] If the minimum-energy rupture of the bond yields two neutral radicals, then the bond is classified as covalent; however, if the rupture of the bond proceeds by a heterolytic mechanism, then the bond is said to be coordinate covalent (Figure 1.5).

Coordinate Covalent Scheme
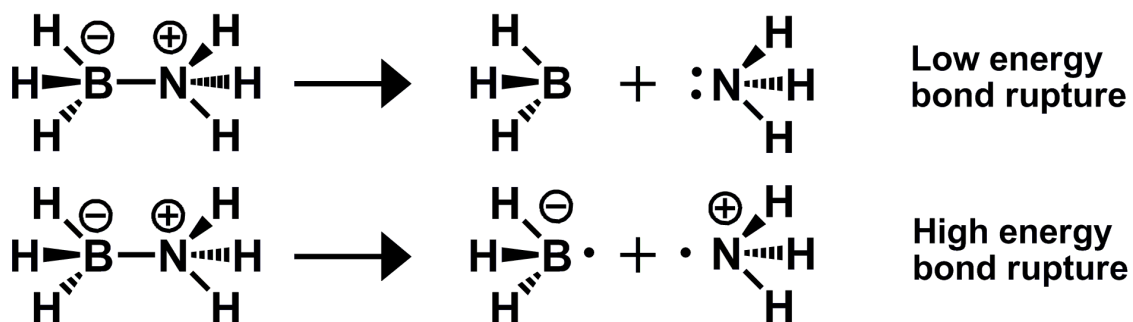
Covalent Scheme
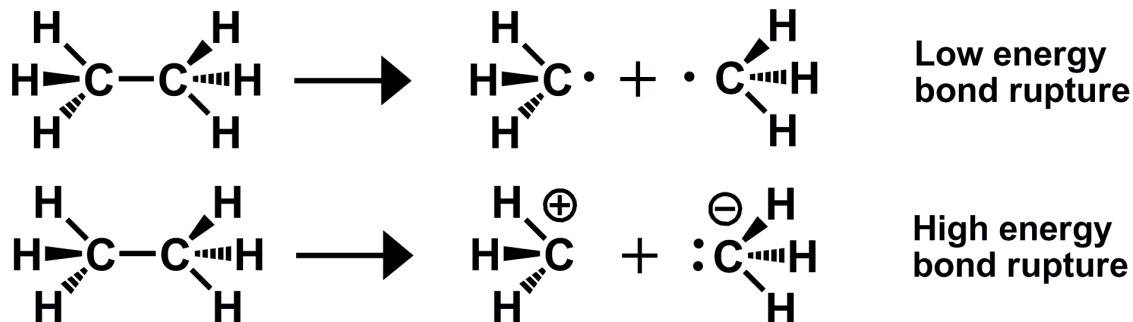
Figure 1.5. Coordinate covalent and covalent bond ruptures within ammonia borane and ethane, respectively. Ethane proceeds via a homolytic minimum energy rupture, yielding two neutral radicals; thus, classified as covalent. Ammonia borane proceeds via a heterolytic minimum energy rupture, yielding two neutral diamagnetic species, and is therefore classified as coordinate covalent.

Ammonia borane and ethane are isoelectronic; however, a comparison between their physical characteristics allows the differences between coordinate covalent and covalent bonds to be recognized. For example, the gas-phase dipole moment of ethane is 0 D, whereas the dipole moment of ammonia borane is 5.13 D, for which the negative pole lies on the acceptor.[26] The difference between the dipole moments demonstrates the donor-acceptor character of the coordinate covalent bond in contrast to that of the

9

covalent bond. However, it is interesting to note that the dipole moment is predicted to be 7.98 D, if the point charge of an electron (1.602×10^{-19} C) and the experimental B–N bond length of 1.658 ± 0.002 Å[26] are used within the formula $\mathbf{d} = Q\mathbf{r}$, where $\mathbf{d}$ is the dipole moment, Q is the equal point charge on each atom, and $\mathbf{r}$ is the distance between the two atoms. The difference between the experimental and predicted dipole moments suggests that the nitrogen does not donate a full pair of electrons as the formal charges on nitrogen and boron within ammonia borane imply. In addition to the dipole moment differences, melting point differences exist as well, where ammonia borane experiences a higher melting point (112 - 114 $^{\circ}$C)[27] as compared to ethane (-182.8°C).[28] The higher melting point observed within ammonia borane arises because the dipole moments allow intermolecular attractions to occur between the adducts, whereas these attractions do not exist within ethane. A difference in bond strength is also observed between the isoelectronic species, where the observed C–C covalent bond dissociation enthalpy for ethane is $\Delta H_{298} = 90.2$ kcal/mol,[29] about three times stronger than the best estimate of $\Delta H_{298} = 27.5$ kcal/mol[24] for the B–N coordinate covalent bond. The difference in bond strengths is reflected by the bond lengths, where the C–C covalent bond is 1.530 ± 0.002 Å[30] and the B–N coordinate covalent bond is 0.125 Å longer. Similar trends are observed when the physical and chemical characteristics of coordinate covalent and covalent bonds are compared within isoelectronic species, such as $(CH_3)_3Si–Si(CH_3)_3$ and $(CH_3)_3Al–P(CH_3)_3$, where the Si–Si covalent bond (2.340 ± 0.009 Å)[31] is shorter than the Al–P coordinate covalent bond (2.53 ± 0.04 Å).[32] In addition, the bond dissociation enthalpy of the Si–Si covalent bond ($\Delta H_{298} = 79.3$ kcal/mol)[33] is stronger than the Al–P coordinate covalent bond ($\Delta H_{298} = 21.0$ kcal/mol)[34] by a factor of four. In

summary, the coordinate covalent bond possesses a longer bond length, a stronger dipole moment, and is about one-third weaker when compared to its isoelectronic covalent counterpart.

Ammonia borane serves as a common prototype of the coordinate covalent bond, which exists within many molecules that have profound consequences in many realms of chemistry and biochemistry, such as the fields of storage and release of hydrogen as a fuel,[35-37] growth of uniform coatings on individual filaments for fiber-reinforced ceramic matrix composites,[38-41] and as new oncological,[42-44] cardiovascular, and anti-inflammatory drugs.[44-48] Consequently, it is of interest to understand the electronics within the coordinate covalent bond and its consequence upon chemical phenomena.

1.2 Acid and Base Theory

In 1887 Svante A. Arrhenius defined acids and bases as chemical species that dissociate in water to yield hydronium and hydroxide ions, respectively.[49] Although the Arrhenius definition was an important contribution to acid-base chemistry, it fails to explain why some molecules such as NH_3 neutralize acids, even though no hydroxide group is present. Arrhenius's definition of the base was modified by Brønsted[50] and Lowry[51, 52] in 1923, where a base was defined as any chemical species that binds with a proton. Brønsted and Lowry's definition consists of an equilibrium reaction, where a proton is exchanged from an acid, HA to a base B, yielding a conjugate base, A^-, and conjugate acid, HB^+, as shown by Equation 1.2.

$$HA + B \rightleftharpoons A^- + HB^+ \qquad\qquad 1.2$$

The strength of a Brønsted-Lowry acid is gauged by the degree of hydrogen dissociation in water. For example, a strong acid, such as H_2SO_4, will dissociate to a greater degree than a weak acid, such as ammonia, favoring the right side of the equilibrium expressed in Equation 1.2. A quantitative measure regarding the strength of acids and bases is defined by determining the concentration of H_3O^+ or ^-OH in an aqueous solution, where a larger amount of H_3O^+ suggests a stronger acid, and thus a weaker base, as the water ion-constant mandates.

$$K_w = [H_3O^+][^-OH] = 1.00 \times 10^{-14} \qquad\qquad 1.3$$

Since the concentration of H_3O^+ may be utilized to gauge the strength of an acid, it is only natural to use the equilibrium constant, specifically the acid-dissociation constant to gauge Brønsted-Lowry acidity (Equation 1.4). Consequently, a larger K_a designates a stronger acid, as shown by Equation 1.4.

$$HA + H_2O \rightleftharpoons H_3O^+ + A^- \qquad K_a = \frac{[H_3O^+][A^-]}{[HA]} \qquad 1.4$$
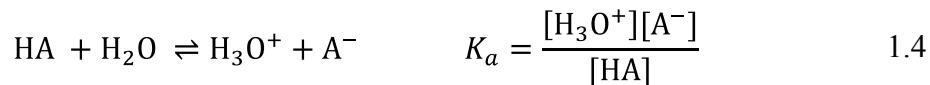
For the sake of convenience, strengths of acids are indicated on a logarithmic scale, in which the $-\log$ of K_a yields the pK_a. Similarly, the strength of a base is related to the concentration of ^-OH and thus the base-dissociation constant, K_b, as shown by Equation 1.5.

$$A^- + H_2O \rightleftharpoons HA + {}^-OH \qquad K_b = \frac{[{}^-OH][HA]}{[A^-]} \qquad 1.5$$
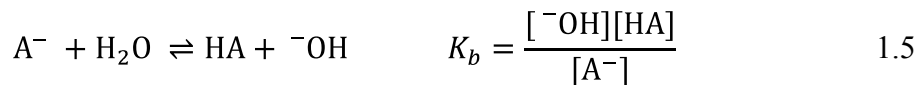
Multiplying K_a and K_b yields Equation 1.3 and thus $pK_a + pK_b = 14$. The relationship

between pK_a and pK_b indicates that a strong acid must possess a weak conjugate base

and a weak acid must possess a strong conjugate base. Consequently, the conjugate base

of a strong acid must be stable in its anionic form; otherwise, the acid would not easily

dissociate.

The stability of a conjugate base may be used as an indicator to gauge the

relative strength of acids. Stable anions tend to be weaker bases and as a result, their

conjugate acids are stronger. Factors that impact the stability of the anion and thus the

strength of an acid are atomic size, electronegativity, and resonance.[53, 54] The negative

charge present on the ion is more stable if it is dispersed over a larger volume, which

means atomic size influences the strength of an acid. For example, F⁻ is smaller than Br⁻,

making F⁻ less stable than Br⁻ and HF a weaker acid than HBr, as reflected by their pK_as

of 3.2 and -9.0 in water, respectively.[54] A more electronegative atom is able to bear a

negative charge more easily than a less electronegative atom, yielding a more stable

anion and thus a stronger acid. For example, nitrogen is less electronegative than

fluorine, thus NH_2^- is less stable than F⁻, and so NH_3 is a weaker acid than HF with pK_as

of 36 and 3.2, respectively.[53] Considering Brønsted-Lowry acids, a binary acid increases

in strength across a period, because the conjugate base is stabilized by increasing

electronegativity without significant size changes. However, within a periodic group,

electronegativity effects become negligible compared to size changes and

Brønsted-Lowry acids strengthen with increasing size. Lastly, resonance can stabilize the negative charge by delocalizing it over two or more atoms. For example, acetic acid ($pK_a = 4.7$) is weaker than methanesulfonic acid ($pK_a = -1.2$) primarily because methanesulfonic acid possesses three important resonance structures that delocalize the negative charge, whereas acetic acid only has two, as shown by Figure 1.6.
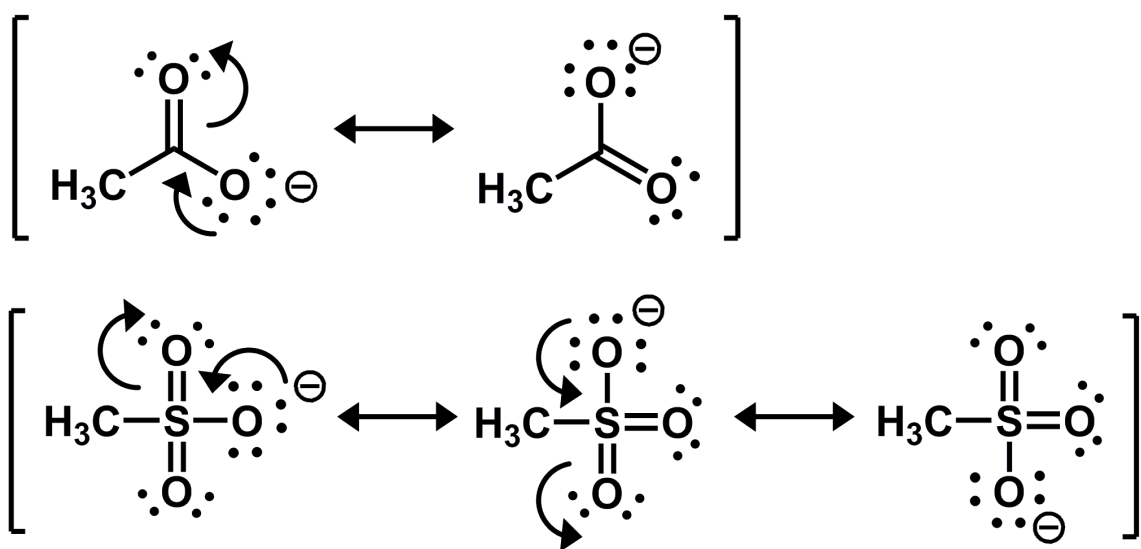
Figure 1.6. Resonance structures corresponding to the acetate ion (top) and methanesulfonate ion (bottom), illustrating the delocalization of the negative charge which ultimately governs the strength of the corresponding conjugate acid. Acetic acid is weaker than methanesulfonic acid, since the negative charge is delocalized across only two structures as compared to three.

Brønsted-Lowry acid-base theory depends on the transfer of a proton from an acid to a base. This is limiting since it is a one element theory, where only species containing hydrogen atoms may be acids. Gilbert Lewis recognized that Brønsted-Lowry bases use a pair of nonbonding electrons to bind to a proton.[2, 55]

Furthermore, he noticed that the transfer of a proton is not necessary to satisfy the nucleophilcity of the base. In fact, Lewis defined an acid as any species that accepts an electron pair, whereas a base is a chemical species that donates an electron pair. As a result, a new bond is formed between the acid and base, specifically, a coordinate covalent bond. Lewis was clear that valence is a crucial element in defining acidity.[55, 56] For example, the Lewis acidity of boronic acids is due to their tendency to complete their octet, or the stable group of four electron-pairs; however, it is a concept that cannot be measured directly. Lewis suggested that the coordinate covalent bond dissociation energy may be used as a preliminary index of acidity; yet, he cautioned that several factors could influence the degree of dissociation.[2] Due to its importance, there have been several indirect methods to gauge relative Lewis acidity.

An overview of different procedures that measure relative Lewis acid and base strengths has been given by Anslyn and Dougherty.[54] Examples include Pearson's hard soft acid base (HSAB) principle,[57-60] Gutmann's donor (DN) and acceptor numbers (AN),[61-63] Drago, Marks, and Wayland's $E\,\&\,C$ and $D\,\&\,O$ equations,[64-66] and Christe and coworker's fluoride affinities.[67] Pearson used acid-base displacement equilibrium constants and aqueous stability constants to deduce that hard (nonpolarizable) acids prefer to bind to hard bases, and that soft (polarizable) acids prefer to bind to soft bases. This classification of hard and soft acids and bases has been exploited to predict the outcome of many acid-base reactions.[57] Gutmann introduced the concept of acceptor numbers (AN) and donor numbers (DN), which scale linearly with the negative heat of reaction of adduct formation. Consequently, AN allows predictions of acidity to be made against measured heats of formation from acid-base reactions. Drago and Wayland

developed a double-scale enthalpy equation, the $E \& C$ equation, to predict acid-base

reaction enthalpies dependent upon terms that represent the electrostatic and covalent

nature of the acid-base interaction. This equation allows for a quantative prediction of

the reaction enthalpy between any acid and base for which the parameters are known.

However, the equation fails when predicting the stability of adducts formed between

highly ionic acids and bases. Subsequently, Drago and Marks derived an improved

equation more suitable for ionic adducts, referred to as the $D \& O$ equations. Christe and

coworkers determined the reaction enthalpy between a variety of Lewis acids and the

fluoride ion, where a larger value indicates a stronger affinity between the Lewis acid

and ion.

Regardless of the scale utilized to predict the relative strengths of Lewis acids, it

is assumed that a stronger coordinate covalent bond is due to the increased Lewis

acidity, when the Lewis base is held constant. However, problems arise from such an

assumption, because the strength of the coordinate covalent bond is influenced by other

forces such as orbital and steric interactions between the substituents present on the

Lewis acid and base.[68-70] Chapter 4 addresses the deficiencies of utilizing the indirect

method of considering the stability of a Lewis acid adduct to gauge the strength of a

Lewis acid, as well as presents a novel approach to gauge the strength of a Lewis acid.

We use the term "intrinsic Lewis acidity" to measure relative Lewis acidity in the

manner originally intended by Lewis, which is by the valence deficiency of the acid of

interest, yielding its desire to accept an electron pair.[55, 56]

1.3 The Diels-Alder Reaction

Otto Diels and Kurt Alder discovered the Diels-Alder reaction in 1928,[71] for which they received the Nobel prize in 1950. The Diels-Alder reaction is among the most common transformations to construct a six member ring in a regio- and stereoselective manner,[72, 73] where a conjugated diene and dienophile react to yield a cycloadduct, as shown by Figure 1.7. However, the Diels-Alder reaction is not limited to carbon-carbon bond formation, where newly formed sigma bonds within the cycloadduct can occur between heteroatoms or between heteroatoms and carbon atoms, as well.[74, 75]
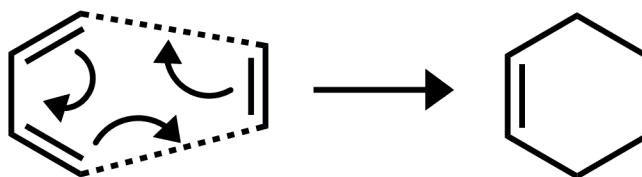
Figure 1.7. Simple Diels-Alder reaction between ethene (dienophile) and 1,3-butadiene (diene) to form the final cycloadduct, cyclohexane. The dashed lines correspond to the new bond formation.

A variety of experimental conditions and factors have been shown to influence the rate enhancement and selectivity of the Diels-Alder reaction, such as pressure,[76-79] aqueous solutions,[76, 80-82] stable cation radicals,[76] ultrasonic radiation,[79] Brønsted-Lowry acids,[76, 83-85] ionic liquids,[78, 86-89] and Lewis acids.[76, 77, 80, 90-92] Although a large amount of data exists, illustrating the practicality and validity of using Lewis acids to catalyze

17

Diels-Alder reactions to enhance rate and synthesize specific asymmetric products, the origin of Lewis acidity and its connection with rate enhancement remains unclear. One primary objective of the research discussed in this dissertation is to understand Lewis acidity and its influence upon the rate of reaction. Specifically, the goal is to acquire a quantitative understanding on the orbital interactions that regulate the frontier molecular orbital (FMO) interactions, as introduced by Fukui's FMO theory.[93-95]

1.3.1 Frontier Molecular Orbitals and Their Influence upon Reactivity and Selectivity.

According to FMO theory the rate and selectivity of a reaction are governed by the in-phase orbital interaction of the highest occupied molecular orbital (HOMO) of one reactant and the lowest unoccupied molecular orbital (LUMO) of the remaining reactant.[95-98] The interaction between the HOMO and the LUMO can occur in two distinct ways. First, the HOMO of the dienophile can interact with the LUMO of the diene to form the cycloadduct, also known as the inverse electron demand Diels-Alder reaction. Second, the HOMO of the diene can interact with the LUMO of the dienophile, also referred to as the normal electron demand Diels-Alder reaction. The normal and inverse electron demand mechanisms are shown by Figure 1.8.
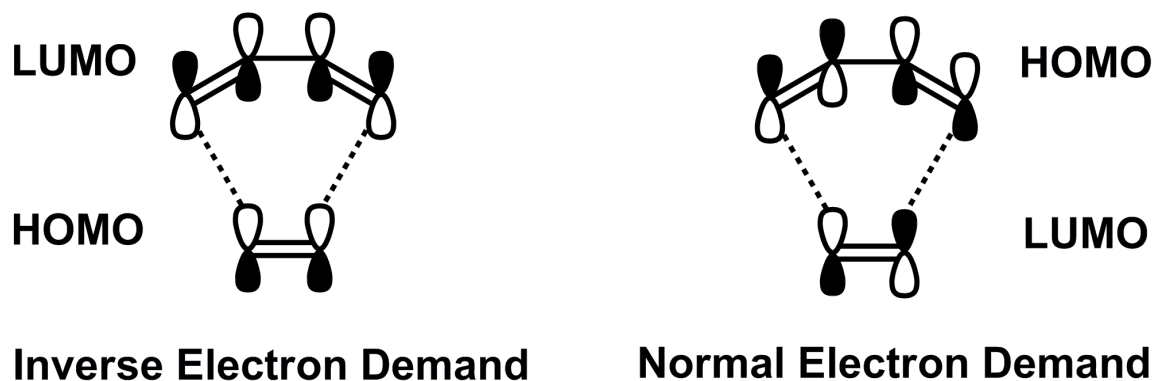
Figure 1.8. In-phase orbital overlap between the HOMO and LUMO of the diene and dienophile for the inverse and normal electron demand. The normal electron demand proceeds via the interaction between the LUMO of the dienophile and the HOMO of the diene, whereas the inverse electron demand proceeds via the interaction between the LUMO of the diene and the HOMO of the dienophile.

       The reactivity of the Diels-Alder reaction depends upon the energy difference between these four orbitals. For example, if the energy difference between the HOMO of the diene and the LUMO of the dienophile is less than the energy difference between of the LUMO of the diene and the HOMO of the dienophile, then the Diels-Alder reaction will proceed via a normal electron demand mechanism. The rate of the reaction is governed by the magnitude of the energy difference between the FMOs, where a smaller energy difference will yield a stabilized transition state (lower energy) and produce an increase in the rate of reaction. An electron donating substituent will increase the energy of a HOMO or LUMO, while an electron withdrawing substituent will decrease their energies. Consequently, if a Lewis acid is coordinated to a dienophile that is participating in a normal electron demand Diels-Alder reaction, the LUMO will decrease in energy, allowing a more favorable orbital interaction with the HOMO of the diene, and ultimately increase the rate of reaction. One of the first reports of a Lewis

acid catalyzed Diels-Alder reaction was by Yates and Eaton, where a rate increase of *ca*.

10^5 was observed for the Diels-Alder reaction between anthracene and maleic anhydride

when the $AlCl_3$ Lewis acid was utilized.[99] Similarly, Inukai and Kojima subsequently

reported the successful rate enhancement of the Diels-Alder reaction between

1,3-butadiene and methyl acrylate in the presence of $AlCl_3$.[100]

In addition to rate enhancement, FMO theory also explains the increased

regioselectivity of Lewis acid catalyzed Diels-Alder reactions.[72, 98] For example, the

para:*meta* ratio of the product for the Diels-Alder reaction between methyl butadiene

and methyl acrylate is 69.5:30.5, whereas the $AlCl_3$ catalysis of the same reaction

increases the *para*:*meta* ratio to 95:5.[101] FMO theory attributes the observed *para*:*meta*

increase to a more favorable orbital overlap during the *para* reaction pathway between

the HOMO and LUMO of the diene and dienophile, respectively, as illustrated by

Figure 1.9. For this example, the *para* cycloadduct is favored, because the corresponding

reaction pathway allows more orbital overlap between the FMOs than the *meta* pathway.

During the *para* reaction pathway, the larger lobes on the LUMO and HOMO of the

dienophile and diene, respectively, overlap, whereas the LUMO-HOMO orbital overlap

is not as great for the *meta* pathway. In general, the reaction pathway that allows the

most orbital overlap will be followed, and thus the corresponding regioisomer will be

formed. Similar accounts of observed increases in the *para:meta* ratio upon Lewis acid

catlaysis of the Diels-Alder reaction have been reported.[101, 102]

More Orbital Overlap: *Para* Pathway
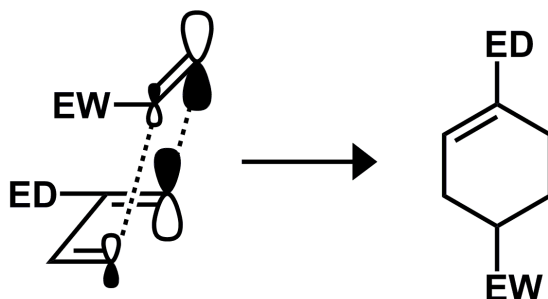
Less Orbital Overlap: *Meta* Pathway
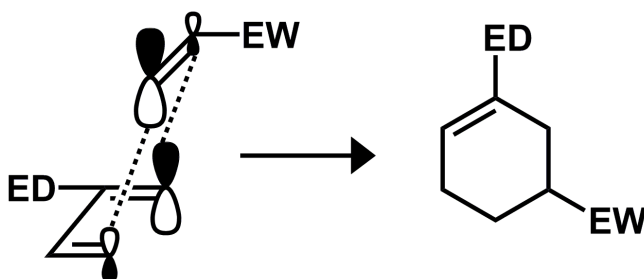
Figure 1.9. Diels-Alder reaction between the LUMO of the dienophile and the HOMO of the diene, illustrating that the *para* cycloadduct is favored over the *meta* cycloadduct because a more favorable orbital overlap is experienced during the *para* reaction pathway.

FMO theory accounts for the observed *endo* stereoselectivity of the Diels-Alder reaction,[73] where the *endo* product is commonly attributed to stabilizing secondary orbital interactions (SOIs) that occur within the transition structure that are unobtainable during the *exo* reaction pathway.[103-108] Three types of SOIs have been reported and are shown by Figure 1.10, specifically, the [4+3] interaction proposed by Singleton (S43),[107] the SAH interaction introduced by Houk, Salem, and Alston,[104-106] and finally, the WH interaction established by Woodward and Hoffmann.[103] The secondary orbital interactions do not initiate any bond formations, but rather the interactions provide a

stability within the *endo* transition structure that cannot be achieved by the *exo* transition

structure, making the *endo* product more preferred. However, the influence of SOIs

upon stereoselectivity remains debated.[109, 110]
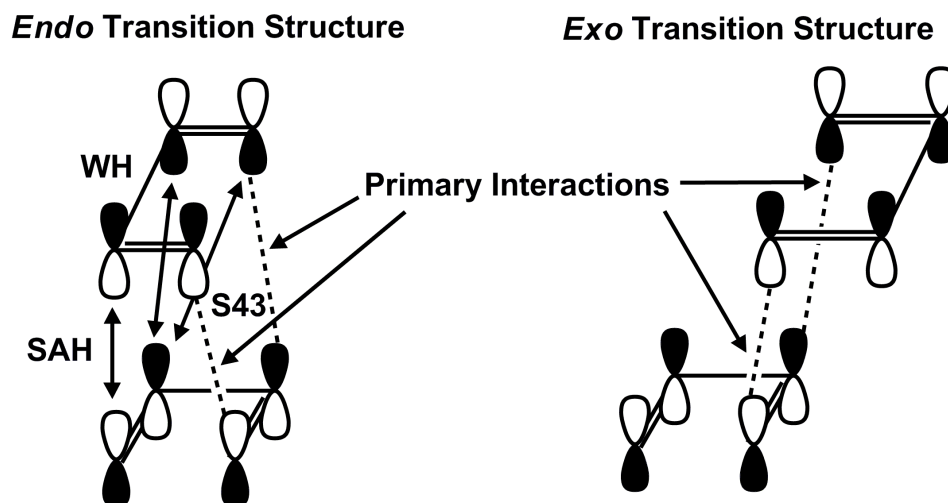
Figure 1.10. Secondary Orbital Interactions (SOIs) introduced by Salem, Houk, and Alston (SAH), Singleton (S43), and Woodward and Hoffman (WH), have been utilized to account for the preference of the *endo* product versus the *exo* product, regarding the Diels-Alder reaction. The stabilizing secondary orbital interactions are shown by the double headed arrow between the corresponding orbitals. *Endo* is favored over *exo* because the latter lacks the stabilizing SOIs.

This dissertation focuses on uncovering the hyperconjugation effects within the

Lewis acid and between the Lewis acid and the dienophile that regulate the rate

enhancement of the Diels-Alder reaction. A novel geminal interaction that is intimately

connected to the rate enhancement of the Diels-Alder reaction has been discovered. The

Lewis acid geminal interaction initiates and governs π-conjugation within the

dienophile, lowers the LUMO energy, and ultimately increases the rate of reaction.

These results provide further quantitative insight into how Lewis acids impact chemical reactivity.

1.4 Objective of Thesis

Due to the fundamental interest and importance of coordinate covalent bonding, Lewis acidity, and their influence upon chemical reactivity, this dissertation presents a critical account of Lewis acidity and differences with Brønsted-Lowry periodic trends, fundamental ideas in coordinate covalent bond strength, and ultimately the Lewis acid rate enhanced Diels-Alder reaction.

First, the goal is to establish an efficient level of theory that is able to model the energetics of the coordinate covalent bond accurately. The binding enthalpy associated with ammonia borane, a well-known prototype of the coordinate covalent bond, has been reported to vary between -14.3 to -37.5 kcal/mol, depending on the level of theory employed. The large discrepancies indicate that the coordinate covalent bond is sensitive to the level of theory utilized. In order to determine an adequate level of theory for modeling the electronics of the coordinate covalent bond, high-level quantum chemical calculations are used to compute energy and bond length convergence as a function of quantum chemical method and basis set. Central to this work is that commonly employed levels of theory are found to be insufficient to characterize the coordinate covalent bond. It is discovered that the charge separation at the equilibrium bond length must be modeled correctly in order for a level of theory to characterize accurately the coordinate covalent bond. The charge separation results from a mismatch in donor and

acceptor strength, which endows the termini with a buildup of electron density. We have coined this mismatch of strength "charge-transfer frustration." This is critical to understanding the electronics within the coordinate covalent bond.

Second, the origin of Lewis acidity has been investigated. Currently, coordinate covalent bond strength is used to assess the strength of Lewis acidity. Inconsistencies between theory, computation, and experiment have arisen, which in turn have spawned a conundrum of interpretations and explanations regarding the origin of Lewis acidity. Currently, it is not possible to predict Lewis acidity accurately, because the chemical and physical origin of acidity is not well understood. A framework that unifies theory, computation, and experiment has been provided which yields periodic trends of substituted Lewis acids based upon first-principles, such as substituent size and electronegativity. Significant differences are observed between the discovered periodic trends of Lewis acidity and those accepted and currently taught for Brønsted-Lowry acidity.

Third, the origin of rate enhancement of the Lewis acid catalyzed Diels-Alder reaction is investigated. Utilizing chiral Lewis acids continues to be an exciting and actively studied area. Lewis acids are known to influence a wide variety of highly enantioselective organic reactions, whereas the Diels-Alder, aldol, ene, hydrocyanation, allylation, ethylation and alkylation reactions have been attributed to stabilized ground state adduct conformations. As an extension, stabilized ground states have been investigated to predict the rate of reaction. Specifically, the binding strength of twelve substituted BF_2X Lewis acids coordinated with 2-propenal have been studied by quantum chemistry and linked back to the rate enhancement of the Diels-Alder reaction.

Although it is known that strength of the Lewis acid influences the strength of the coordinate covalent bond within the ground state and ultimately affects the rate of reaction, a quantitative description is lacking. For the first time, a quantitative description is presented. Specifically, a direct connection between rate enhancement and coordinate covalent bond strength is achieved through a synergistic transfer of electron density initiated by a novel geminal interaction within the Lewis acid. Understanding how substituents influence the rate of organic reactions should give experimentalists the opportunity to utilize boron Lewis acids to control reaction rates, and allow chemical insight into the origin of how Lewis acids regulate reaction rates.

This dissertation lays a foundation for understanding Lewis acidity, chemical bonding, and chemical reactivity, as well as determining the appropriate toolset necessary to model these chemical phenomena. The implementation of these tools have led to a clear and concise explanation of the electronic origins of Lewis acidity and a quantitative rationalization of the rate enhancement of the boron Lewis acid catalyzed Diels-Alder reaction. The data presented should launch unique opportunities in any scientific discipline that exploits coordinate covalent bonds and Lewis acid catalysts, such as the use of ammonia borane as a source of hydrogen fuel, the synthesis of new materials and ceramic matrix composites, the discovery of novel pharmaceutical drugs that treat oncological, cardiovascular, and anti-inflammatory disorders, and the dual Lewis acid/base catalysis of reactions.

Chapter 2

Electronic Structure Modeling

2.1 Quantum Mechanical Calculations

Quantum mechanics (QM) is the mathematical description of a set of principles that explain the electronic behavior of atoms and molecules. Of the vast electronic structure programs available, the chemical phenomena described within this Ph.D. dissertation have been investigated with Gaussian 03,[111] NWChem 5.1,[112] and NBO.[113] The theoretical underpinnings of QM have the ability to predict all observables associated with molecular systems. However, in practice, only hydrogenic systems or systems that possess one electron can be solved exactly.[114, 115] Although exact analytical solutions do not exist for two-electron systems, the Schrödinger equation has been solved numerically for the helium atom and isoelectronic ions with forty digits of accuracy.[116, 117] For those systems containing more than one electron, approximations must be utilized. The problem resides in the electron-electron repulsion term within the Hamiltonian. Consequently, many approximations have been developed to treat the electron-electron repulsion. It is at the discretion of the computational chemist to decide which approximation to employ, understanding that a balance of accuracy and efficiency is usually the goal. Since the birth of QM, the number of approximations has increased dramatically. Consequently, computational chemistry has become an art as much as a

science. The remainder of this chapter discusses the methodology and foundation of computational chemistry, starting with the non-relativistic time-independent Schrödinger equation.

2.2 Schrödinger's equation

It is natural to begin a discussion of QM by beginning with Schrödinger's time-independent equation (Equation 2.1).[115]

$$\hat{H}(\mathbf{r}, \mathbf{R})\psi(\mathbf{r}, \mathbf{R}) = E(\mathbf{r}, \mathbf{R})\psi(\mathbf{r}, \mathbf{R}) \qquad 2.1$$

The $\hat{H}(\mathbf{r}, \mathbf{R})$, $\psi(\mathbf{r}, \mathbf{R})$, and $E(\mathbf{r}, \mathbf{R})$, refer to the Hamiltonian, wavefunction, and total energy of the molecular system, respectively, where nuclear coordinates are denoted by $\mathbf{R}$ and electronic coordinates are denoted by $\mathbf{r}$. Psi, $\psi(\mathbf{r}, \mathbf{R})$ refers to the wavefunction and characterizes the behavior of the molecular system, while the Hamiltonian operates on $\psi(\mathbf{r}, \mathbf{R})$ yielding the total energy, $E(\mathbf{r}, \mathbf{R})$.

In general, the Hamiltonian for N electrons and M nuclei in atomic units is represented by Equation 2.2.

$$\hat{H}(\mathbf{r}, \mathbf{R}) = -\sum_{i}^{N} \frac{1}{2}\nabla_i^2 - \sum_{A}^{M} \frac{1}{2M_A}\nabla_A^2 - \sum_{i}^{N}\sum_{A}^{M} \frac{Z_A}{|\mathbf{r}_i - \mathbf{R}_A|} + \qquad 2.2$$

$$\sum_{i}^{N}\sum_{j>i}^{N}\frac{1}{|\mathbf{r}_i - \mathbf{r}_j|} + \sum_{A}^{M}\sum_{B>A}^{M}\frac{Z_A Z_B}{|\mathbf{R}_A - \mathbf{R}_B|}$$

$$\nabla^2 = \frac{\partial^2}{\partial x^2} + \frac{\partial^2}{\partial y^2} + \frac{\partial^2}{\partial z^2} \qquad\qquad 2.3$$

The first and second term in Equation 2.2 represents the kinetic energy of the electrons and nuclei of the system, respectively. The third term is the columbic attraction between electrons and nuclei. The fourth and fifth terms represent the electron-electron and nuclei-nuclei repulsions, respectively.

It is possible to simplify Schrödinger's time-independent equation by employing the Born-Oppenheimer approximation.[118] The Born-Oppenheiner approximation takes advantage of the fact that the proton is about 1836 times heavier than an electron. The large difference in mass between the proton and electron suggests that the nuclear velocities are much smaller than the electron velocities and thus the electrons adjust instantaneously to changes in nuclear geometry. Consequently, it is assumed that the coupling between the motion of the electrons and the motion of the nuclei is zero and the nuclei are stationary from the electronic perspective.

As a result of employing the Born-Oppenheiner approximation, the total wavefunction, $\psi_{\text{total}}(\mathbf{r}, \mathbf{R})$, becomes a product of two wavefunctions, one of which corresponds to the nuclei, $\psi_{\text{nuclear}}(\mathbf{R})$, while the other corresponds to the electrons, $\psi_{\text{electronic}}(\mathbf{r}, \mathbf{R})$ (Equation 2.4). In addition, the second term of the Hamiltonian (Equation 2.2) is eliminated, yielding $\hat{H}_{\text{electronic}}(\mathbf{r}, \mathbf{R})$. Consequently, the Schrödinger

time-independent equation is simplified and is represented by Equation 2.5. The electronic wavefunction is independent of nuclei momenta and depends only upon their position. The total energy of the system is simply the sum of the electronic and nuclear energies.

$$\psi_{\text{total}}(\mathbf{r}, \mathbf{R}) = \psi_{\text{nuclear}}(\mathbf{R})\psi_{\text{electronic}}(\mathbf{r}, \mathbf{R}), \qquad 2.4$$

$$\widehat{H}_{\text{electronic}}(\mathbf{r}, \mathbf{R})\psi_{\text{electronic}}(\mathbf{r}, \mathbf{R}) = E_{\text{electronic}}(\mathbf{r}, \mathbf{R})\psi_{\text{electronic}}(\mathbf{r}, \mathbf{R}) \qquad 2.5$$

Considering the hydrogen atom, where only a single electron and proton exists, the Hamiltonian takes the form of Equation 2.6, since the second, fourth, and fifth terms in the Hamiltonian are eliminated. Consequently, Schrödinger's time-independent equation can be solved exactly for those systems similar to the hydrogen atom, where only one electron is present.

$$\widehat{H}(\mathbf{r}) = -\frac{1}{2}\nabla^2 - \frac{Z}{\mathbf{r}} \qquad 2.6$$

However, considering systems with two or more interacting electrons, Schrödinger's time-independent equation cannot be solved exactly. This is because the electron-electron repulsions couple the electrons. In order to solve Schrödinger's equation, further approximations must be considered, as explained throughout this chapter. However, appropriate approximations coupled with high performance computers provide high accuracy results in excellent agreement with experiment. For example, as of March 3, 2009, Kraken, the fastest academic supercomputer, features

66,048 computational cores and more than 100 terabytes of memory, pushing the limits of computational science by computing 607 teraflops. Kraken is a Cray XT5 system, located at the National Institute for Computational Sciences, managed by the University of Tennessee, and funded by the National Science Foundation.

It may seem disconcerting to continue with QM, since Schrödinger's equation cannot be solved exactly for polyatomic systems with more than one electron. However, powerful tools are available to computational chemists in order to investigate chemical phenomena. The remainder of this chapter explains the tools available.

2.3 The Variational Theorem

Ab initio indicates that the computation considers first principles and utilizes no empirical or experimental data. The *ab initio* chemical methods employ mathematical approximations to simplify the quantum mechanical calculation, such as simpler functional forms or approximate solutions to complicated differential equations. Before the relevant *ab initio* chemical methods are explained, the variational theorem is discussed, which provides a foundation for assessing the accuracy of a trial wavefunction.

The variational theorem[119] is a useful tool that allows the quality of the wavefunction to be assessed. The theorem states that the eigenvalue or energy ($\langle E \rangle$) yielded from solving Schrödinger's time-independent equation, employing a trial

wavefunction, is always greater than that yielded (E_0) from the true wavefunction (Equation 2.7).

$$\langle E \rangle = \frac{\int \psi^* \widehat{H} \psi d\tau}{\int \psi^* \psi \, d\tau} \geq E_0 \qquad\qquad 2.7$$

Equation 2.7 states that the expectation value or average energy, $\langle E \rangle$, of the system is achieved by performing the integral over all space, $d\tau$, and will always be greater than the true energy of the ground state wavefunction, E_0. For most polyatomic systems, the true wavefunction is not known. Consequently, a trial wavefunction is assumed. Since the energy calculated from the trial wavefunction is always greater than that yielded from the true wavefunction, the lowest energy corresponds to the more accurate wavefunction and is therefore a better representation of the true wavefunction. Thus, the variational theorem allows the accuracy of the trial wavefunction to be assessed.

2.4 Hartree-Fock

The Hartree-Fock approximation is an important contribution to quantum mechanics, because it allows Schrödinger's time-independent equation to be solved for a many-electron system. The Hartree-Fock (HF) equations have been derived and explained in detail elsewhere.[115, 120, 121] Briefly, The HF scheme partitions the many-electron wavefunction in terms of one electron wavefunctions (or orbitals) in the form of a Slater determinant. Expressing the wavefunction in terms of a Slater

31

determinant satisfies the criteria that the electronic wavefunction must be antisymmetric, where the sign of the wavefunction must invert upon exchange of any two electrons. Equation 2.8 displays the wavefunction for a *N*-electron wavefunction as a Slater determinant of orbitals, where $\phi_2(1)$ refers to electron number "1" in the second spin orbital, which is the product of the spatial function and spin function, and $\frac{1}{\sqrt{N!}}$ ensures the wavefunction is normalized. Another important property of the Slater determinant is that when any row or column is equal to zero, then the determinant is equal to zero.

$$\psi = \frac{1}{\sqrt{N!}} \begin{vmatrix} \phi_1(1) & \phi_2(1) & \cdots & \phi_N(1) \\ \phi_1(2) & \phi_2(2) & \ddots & \phi_N(2) \\ & \vdots & \ddots & \vdots \\ \phi_1(N) & \phi_2(N) & \cdots & \phi_N(N) \end{vmatrix} \qquad 2.8$$

A severe consequence of expressing the wavefunction as a Slater determinant is that the movement of electrons is considered uncorrelated. Consequently, each electron does not experience repulsion with each individual electron within the system, but rather experiences repulsion with an average field generated by the remaining electrons. Thus, the HF approximation neglects electron correlation, and is the major source of error within the HF scheme. Regardless of the neglect of electron correlation, one advantage of the HF approximation is that it simplifies the many-electron Schrödinger equation into multiple simpler one-electron equations, such as Equation 2.9, each yielding a single-electron wavefunction, referred to as an orbital, ϕ_i, and an orbital energy, ε_i. The orbital describes the behavior of an electron in the net field generated by all the other electrons.

$$\hat{f}_i \phi_i = \varepsilon_i \phi_i \qquad\qquad 2.9$$

The effective one-electron Hamiltonian, $\hat{f}_i$, (Equation 2.10) otherwise known as the Fock operator, accounts for three contributions to the total energy of the electron. Specifically, the core (H^{Core}), Coulomb (J_i), and exchange (K_i) energies are determined by performing their corresponding operators, as shown by Equations 2.11 through 2.13.

$$\hat{f}_i = H^{Core} + \sum_{i}^{N} [J_i - K_i] \qquad\qquad 2.10$$

$$H^{\text{Core}} = -\frac{1}{2} \nabla_i^2 - \sum_{A}^{M} \frac{Z_A}{|\mathbf{r}_i - \mathbf{R}_A|} \qquad\qquad 2.11$$

$$J_i \phi_i = \phi_i \int \phi_j^* \frac{1}{|\mathbf{r}_i - \mathbf{r}_j|} \phi_j d\tau_2 \qquad\qquad 2.12$$

$$K_i \phi_i = \phi_j \int \phi_j^* \frac{1}{|\mathbf{r}_i - \mathbf{r}_j|} \phi_i d\tau_2 \qquad\qquad 2.13$$

The core energy represents the kinetic energy of the electron i and the coulomb attraction between electron i and nucleus A, which make favorable contributions to the electronic energy, as reflected by the negative signs within Equation 2.11. The coulomb interaction refers to the unfavorable repulsions between electron i and the average field generated by the remaining electrons. The exchange energy has no classical counterpart

and arises because of the antisymmetric nature of the wavefunction. This is a manifestation of the Pauli Exclusion Principle, which states that no two electrons can possess the same quantum numbers. Therefore, electrons with the same spin cannot possess the same spatial coordinates and tend to be farther apart.

To solve the Hartree-Fock equations, it is important to remember that each electron is assumed to move in an average field comprised of the nuclei and electrons. This is a consequence of expressing the multi-electron wavefunction in terms of one electron wavefunctions. Consequently, the solution of the one electron eigenvalue equation (Equation 2.9) will affect the solutions to the remaining one electron eigenvalue equations. The method of solving such a set of equations is called the self-consistent field method. First, a trial set of solutions, ϕ_i, to the HF equations are obtained and are then used to calculate the Coulomb and exchange operators. The one electron eigenvalue equations are then solved, giving a new set of orbitals and corresponding energies, which are subsequently used in the second iteration of the HF equations. In other words, a new set of Coulomb and exchange operators are determined and a new set of orbitals and orbital energies are determined. The process continues until differences between subsequent solutions are below a certain threshold. The convergence of such a solution means self-consistency is achieved.

Although the HF method was a major breakthrough in solving quantum mechanical calculations, it does have several major drawbacks. The most significatnt drawback is that HF neglects the effects of electron correlation. In other words, the electron-electron repulsions are not considered explicitly, but rather, each electron is merely moving in an average potential generated by the remaining electrons.

Consequently, the position of an electron is completely independent of the positions of the remaining electrons and the tendency of electrons to avoid each other is less than HF suggests. The lack of electron correlation is primarily responsible for the poor performance of HF. However, HF is useful for first-level predictions of chemical systems, such as geometric parameters.[122] Furthermore, it serves as the theoretical foundation for most other chemical methods, such as Møller-Plesset and Configuration Interaction. The next few subsections describe chemical methods that are based on the HF scheme but are improved upon by correcting the neglect of electron correlation.

2.5 Møller-Plesset Perturbation Theory

Møller-Plesset (MP) perturbation theory[123, 124] starts with the HF result and adds a small perturbation that accounts for electron correlation. Consequently, MP is commonly referred to as a post-self consistent field method (post-SCF). MP perturbation theory has been explained in detail elsewhere.[115, 120] Briefly, Møller and Plesset account for the electron correlation by expressing the true Hamiltonian, $\widehat{H}$, as a sum of a zeroth order Hamiltonian, $\widehat{H}_0$, and a small perturbation, commonly denoted V, which is not to be confused with the potential.

$$\widehat{H} = \widehat{H}_0 + \lambda V \qquad\qquad 2.14$$

The λ is a parameter that can vary from 0 to 1. When $\lambda = 0$ the Hamiltonian is equal to the zeroth-order Hamiltonian, but when $\lambda = 1$, the Hamiltonian is equal to its exact form.

As a result of implementing λ, the corresponding wavefunction, ψ, and energy, E, is expressed as a power series of λ.

$$\psi = \sum_{n=0}^{N} \lambda^n \psi^{(n)} \qquad\qquad 2.15$$

$$E = \sum_{n=0}^{N} \lambda^n E^{(n)} \qquad\qquad 2.16$$

The number n, within the superscripted parentheses, refers to the order of correction. For example, $E^{(1)}$ refers to the first order correction to the energy. The perturbed wavefunction and energy are then substituted into Schrödinger's equation and solved. To solve such an equation, the MP formalism defines the unperturbed Hamiltonian, $\widehat{H}_0$, as the sum of the one-electron Fock operators, which yields the zeroth-order energy, $E^{(0)}$, a value that is simply the sum of the orbital energies, ε_i. In order to achieve higher order corrections to the energy, the perturbation must be considered. As Equation 2.14 states, the perturbation is the difference between the true and zeroth-order Hamiltonians. Solving the Schrödinger equation to determine the contribution of each ordered energy term reveals that the sum of the zeroth and first-order energies is simply the HF result for the closed shell system. Therefore, in order to obtain any corrections to the HF energy, second-order perturbations (MP2) must be considered. Higher order perturbations of the form MPN (N = 3, 4, 5 … etc.) exist as well, where the summations expressed by Equations 2.15 and 2.16 are truncated at some order N; however,

employing higher order perturbations increases the time of the computation on the order of $O_{,}^{N+3}$ where O is the number of basis functions and N is the order of truncation.[121, 125]

The advantage of MP2 is that it typically accounts for about 80 to 90% of the electron correlation neglected by HF.[121] However, a disadvantage is that MP perturbation theory is not variational. This means that the energies computed with MP theory may be lower or higher than the exact energy. Although MP2 does have its deficiencies, it is a vast improvement upon HF theory, as it is able to predict structures and energetics more accurately.[122] For example, HF/6-311++G(3df,3pd) predicts hydrogen fluoride binding energy to be 97.9 kcal/mol, which differs from the experimental value of 141.2 kcal/mol by 43.3 kcal/mol.[122] In contrast, MP2 predicts the binding energy to be 144.9 kcal/mol, in much better agreement with the experimental observation.[122] Furthermore, MP2 is size consistent, which is not the case for some other post-SCF methods, such as Configuration Interaction. The concept of size consistency is expanded upon in Chapter 2.6.

2.6 Configuration Interaction

Another post-SCF method that accounts for electron correlation is the Configuration Interaction (CI) method.[126-129] The theoretical foundation of CI assumes that the true wavefunction is a linear combination of excited Slater determinants. In fact, the CI wavefunction starts with a single Slater determinant, as used in HF theory, and subsequently adds singly, doubly, triply, etc., excited determinants relative to the HF configuration. The CI wavefunction, ψ_{CI}, can therefore be written as,

$$\psi_{CI} = a_0\Phi_{HF} + \sum_{S}^{\infty} a_S\Phi_S + \sum_{D}^{\infty} a_D\Phi_D + \sum_{T}^{\infty} a_T\Phi_T + \cdots = \sum_{i=0}^{\infty} a_i\Phi_i \qquad 2.17$$

Subscripts S, D, T, etc., indicate determinants that are singly, doubly, triply, etc. For example, singly substituted determinants replace a single occupied orbital with a virtual spin orbital, whereas doubly substituted determinants replace two occupied orbitals with two virtual spin orbitals. This is equivalent to exciting an electron from a filled to a vacant orbital. The energy of the system is minimized by determining the coefficients, a_i, utilizing the variational theorem. As one can guess, the CI approach becomes quite complex and resource intensive as more excited determinants are considered. Depending on the basis set (Chapter 2.8), the number of Slater determinants can increase rapidly (Equation 2.18). The number of ways to permute N electrons and K orbitals is reflected by the binomial coefficient,

$$\frac{K!}{N!\,(K-N)!} \qquad 2.18$$

It is not difficult to conceive that the implementation of CI is generally limited to molecular systems containing a small number of atoms. Nevertheless, CI is a powerful breakthrough in quantum mechanics, because if all possible permutations (full CI) are considered in the presence of a complete basis set, then the exact quantum mechanical result is achieved, at least when relativistic effects are not considered. If full CI is employed in the presence of a complete basis set, it is referred to as complete CI.

It is impractical to consider all possible permutations for anything but the smallest of systems, such as H_2O^{121} and the proton transfer process $He + H_2^+ \rightarrow$ $HeH^+ + H.^{130}$ Consequently, limitations are imposed on the number of excited state configurations allowed, truncating Equation 2.17 to consider specific excited determinants. For example, a CI calculation that considers only single substitutions is termed CIS. However, truncating the expansion to maintain only singly substituted determinants does not improve the HF energy, as CIS is equal to HF for the ground state energy. This is a manifestation of Brillouin's theorem.[121] Further excitations beyond singly substituted determinants are necessary to improve upon the HF result. For example, CID considers only double substitutions and CISD considers both single and double substitutions. Triple and quadruple excitations exist as well. Even with the number of excite determinants limited, the number of permutations can be too large for practical computations.

An advantage of CI is that it is variational in nature, which means that the energy obtained from employing CI is always greater than the true energy of the system. However, it is not size consistent. The only version of CI that is size consistent is complete CI. Size consistency guarantees that the energy of N noninteracting molecules is equal to N times the energy of the isolated molecule. Size consistency becomes important when computing dissociation energies. A quadratic correction, introduced by Pople, allows CI to account for size consistency. [131, 132] The quadratic correction to the configuration interaction (QCI) ensures size consistency by accounting for excited state configurations that are quadratic in nature.[131, 132] In addition, Pople elaborated upon QCISD by evaluating the triples contribution by perturbation theory.[132] Note that the

letter in parentheses refers to the perturbational treatment. Inclusion of the triples correction at the QCISD(T) level yields substantial improvements to the calculated total energies over QCISD when compared to the complete CI energies.[132] QCISD has been shown to be very similar to coupled cluster singles and doubles (CCSD), where some of the terms from the CCSD formalism are omitted.[132, 133] The omitted terms are computationally inexpensive and it is normally considered unnecessary to utilize the QCISD formalism over the CCSD implementation.[121] Furthermore, CCSD is size consistent without any corrections, in contrast to CI, where the quadratic correction is necessary. However, in practice QCISD and CCSD along with QCISD(T) and CCSD(T) yield similar results,[134] but severe exceptions do exist such as that reported for the Cu–C dissociation energy within $CuCH_3$, where a 42 kcal/mol difference was observed.[135]

CI and QCI are chemical methods that account for electron correlation and provide substantial improvements over MP2 and HF, but not without a drastic increase in computational resources. For example, QCISD(T) and QCISD scale O^7 and O^6, respectively, where O indicated the number of basis functions (Chapter 2.8).[121, 125] Consequently, CI and QCI are limited by the number of atoms they can model within the electronic structure calculation, depending on the completeness of the basis set, and are thus impractical for larger systems. At this point, it seems that accounting for electron correlation may only be viable for small molecules. However, density functional theory, discussed in Chapter 2.7, allows computational chemists to account for electron correlation with little increase in computational resources (O^3),[125] as compared to post-SCF methods.

2.7 Density Functional Theory

Density functional theory (DFT)[121, 125, 136, 137] is a popular choice for modeling medium to larger sized systems due to its efficiency and accuracy, in contrast to more resource intensive post-SCF methods, such as QCISD(T). DFT accounts for electron correlation; however, it lacks the description of dispersive forces, which are important for binding affinities dominated by van der Waals interactions.[138-140] Dispersion interactions originate from instantaneous dipoles that arise from fluctuations in electron density. Instantaneous dipoles can induce a dipole in a neighboring atom, which gives an attractive inductive effect. DFT methods that account for dispersion and van der Waals interactions are currently being developed.[136, 141-146]

The previous chemical methods discussed, such as HF, MP2, and QCISD(T) utilize a wavefunction to determine observables. DFT provides an alternative by assuming that the energy of a system can be determined from the electron density rather than the wavefunction. The direct mathematical relationship between electron density and the ground state energy of the system was proposed by Hohenberg and Kohn;[147] however, the initial proposal only provided a mathematical link. No method of describing how to achieve the energy was explained until Kohn and Sham provided a simple solution.[148] The theorems proposed by Hohenberg, Kohn, and Sham are discussed in Chapter 2.7.1.

2.7.1 Hohenberg-Kohn and Kohn-Sham

A rigorous mathematical framework relating electron density to ground state energy was proposed by Hohenberg and Kohn.[147] Hohenberg and Kohn's theorem has been discussed in detail elsewhere.[115, 120] Briefly, assume the electrons within a given system are moving within a field potential, V, of positively charged nuclei. If the potential is unique, then the Hamiltonian and corresponding energy of the system is unique as well. Assume that two separate potentials, V_A and V_B, with corresponding Hamiltonians, H_A and H_B, exact energies, E_A^{True} and E_B^{True}, and wavefunctions, ψ_A and ψ_B, yield the same electron density, $\rho(\boldsymbol{r})$. According to the variational theorem:

$$E_A^{\text{True}} < \langle \psi_A | H_A | \psi_B \rangle = \langle \psi_A | H_A - H_B + H_B | \psi_B \rangle$$

$$E_A^{\text{True}} < E_B^{\text{True}} + \langle \psi_A | H_A - H_B + H_B | \psi_B \rangle$$

$$E_A^{\text{True}} < E_B^{\text{True}} + \int (V_A - V_B)\rho d\tau \qquad\qquad 2.19$$

Interchanging A with B yields:

$$E_B^{True} < E_A^{True} + \int (V_B - V_A)\rho d\tau \qquad\qquad 2.20$$

Finally, adding Equations 2.19 and 2.20 yields Equation 2.21, which is obviously false.

$$E_A^{True} + E_B^{True} < E_A^{True} + E_B^{True} \qquad\qquad 2.21$$

This proof concludes that two different potentials cannot result in one distinct electron density. Consequently, a unique electron density supports the existence of a unique wavefunction and thus a unique energy as well as other observables. It must be remembered that the proof only shows a relationship between the electron density and the energy of the system. A methodology to compute the energy of a system utilizing its electron density was not introduced until the Kohn-Sham formalism was developed in 1965.[149]

Kohn and Sham proposed a method for determining the density and thus the energy of a system.[149] Employing ideas from HF theory, they proposed that the true density of a system containing interacting electrons is identical to the density of a system consisting of noninteracting electrons. Consequently, Schrödinger's equation may be separated and the self consistent manipulations employed throughout HF theory may be applied within DFT as well. Similar equations to 2.9 are constructed and solved (Equation 2.22 and 2.23); however, electron correlation is introduced in the exchange-correlation term, $V_{XC}[\rho]$.

$$\hat{f}_i^{KS}\phi_i = \varepsilon_i\phi_i \qquad\qquad 2.22$$

$$\hat{f}_i^{KS} = -\frac{1}{2}\nabla_i^2 - \sum_i^M \frac{Z_A}{r_{iA}} + \int \frac{\rho(r')}{r_{ii'}}dr' + V_{XC}[\rho] \qquad\qquad 2.23$$

The first term in Equation 2.23 represents the kinetic energy of the noninteracting electrons, the second term represents the attraction between electrons and nuclei, the

third term corresponds to the Coulombic repulsions between the charge distribution at r_i and $r_{i'}$. The last term, the exchange-correlation term, corrects the kinetic energy for the interacting nature of electrons, and all non-classical interactions that arise due to the electron-electron exchange energy. If the exact exchange-correlation functional was known, the exact energy could be computed. Consequently, within the realm of one electron Kohn-Sham equations, DFT approximates $V_{XC}[\rho]$ to determine the exchange-correlation energy, $E_{XC}[\rho]$. $V_{XC}[\rho]$ may be further dissected into $V_X[\rho]$ and $V_C[\rho]$, with corresponding exchange, $E_X[\rho]$ and correlation energies, $E_C[\rho]$, respectively. There is no systematic way of improving the approximation of $V_{XC}[\rho]$ as done for wavefunction-based methods, such as considering higher order perturbations (MPn) or excited state configurations (CI). However, a variety of approximations to $V_{XC}[\rho]$ exists as discussed in Chapters 2.7.2 through 2.7.6 .

2.7.2 Exchange-Correlation Functional

Kohn-Sham density functional theory (DFT)[149] has become a well-established tool in the computational chemistry community. It is known that DFT accuracy is dependent upon the approximation of $V_{XC}[\rho]$ within the Kohn-Sham formalism.[125, 149] Current DFT implementations, such as the local spin density approximation (LSDA),[149-151] generalized gradient approximation (GGA),[152-157] meta-GGA (M-GGA),[158, 159] hybrid-GGA (H-GGA),[152, 156, 158, 160, 161] and hybrid meta-GGA (HM-GGA),[141, 162, 163] treat $V_{XC}[\rho]$ differently. LSDA assumes that the $E_{XC}[\rho]$ at any point in space depends only on the spin density at that specific spatial region. GGA

improves upon LSDA by considering the gradient of the density along with the spin density. Further improvements of GGA include the spin-dependent electronic kinetic energy density (M-GGA) and a certain percentage of Hartree-Fock exchange (H-GGA). Finally, the HM-GGA incorporates both approximations from M-GGA and H-GGA.

All DFT calculations performed throughout this dissertation employ either B3LYP,[156, 164] MPW1K,[161] MPW1B95,[162] MPWB1K,[162] M05-2X,[141] M05,[141, 165] M06-2X[163] or M06.[163] Consequently, each is discussed in the following subsections.

2.7.3 B3LYP

B3LYP employs the H-GGA, where the exchange-correlation energy is defined as

$$E_{B3LYP}^{XC} = (1-a)E_{LSDA}^{X} + aE_{HF}^{X} + b\Delta E_{B88}^{X} + cE_{LYP}^{C} + (1-c)E_{VWN3}^{C} \qquad 2.24$$

The coefficients a, b, and c are empirically derived[164] from a least squares fit to 56 atomization energies, 42 ionization potentials, 8 proton affinities, and 10 first row total atomic energies determined by experiment.[166] The values of the optimized coefficients are $a = 0.20$, $b = 0.72$, and $c = 0.81$.[164] The first term of Equation 2.24 is the exchange energy determined by the local spin density approximation proposed by Slater.[149-151] The second term represents the exact Hartree-Fock exchange energy. The third term is the gradient corrected exchange energy proposed by Becke.[164] The fourth term corresponds to the correlation energy (which includes the gradient term) determined by

Lee, Yang, and Parr.[156] Finally, the last term represents the standard correlation energy predicted by the VWN3 functional developed by Vosko, Wilk and Nusair.[167]

B3LYP is one of the most popular density functionals available today, where, as of March 2009, a SciFinder Scholar 2009 "Research Topic" search for B3LYP yields 32,880 references, whereas searches for other functionals such as MPW1K, B3P86, and BLYP yield 240, 558, and 1697 references, respectively. B3LYP's popularity originates from its ability to correct the inherent deficiencies within previous functionals. Consequently, B3LYP predicts chemical phenomena in better agreement with experiment such as molecular structure, atomization energies, ionization potentials, proton affinities, and total energies.[115, 125, 164] However, B3LYP does suffer from its own deficiencies. For example, B3LYP underestimates barrier heights,[168] noncovalent interactions,[169, 170] and bond energies and lengths involving transition metals.[171, 172] Furthermore, one of the principal ideas of this dissertation is that the commonly employed B3LYP method is unable to model accurately the electronic nature of coordinate covalent B–N bonds.[24, 173]

2.7.4 MPW1K

Truhlar and coworkers developed the modified Perdew-Wang 1 parameter functional for kinetics (MPW1K)[161] with the goal of devising a method that would yield increased accuracy for transition state energies. MPW1K employs the H-GGA, similar to B3LYP; however, MPW1K is a one parameter functional and B3LYP is a three parameter functional. Truhlar's MPW1K functional starts with a version of the

Perdew-Wang exchange functional,[174, 175] modified by Adamo and Barone[176] and the Perdew-Wang correlation functional.[177] The amount of HF exchange energy (the single parameter) was then optimized to fit the experimental data of 20 forward barrier heights, 20 reverse barrier heights, and 20 energies of reaction,[161] otherwise referred to as a training data set. The exchange-correlation energy determined by MPW1K is displayed in Equation 2.25, where the amount of HF exchange, X, was optimized to be $X = 42.8$.

$$E_{MPW1K}^{XC} = (1 - \frac{X}{100})(E_{LSDA}^{X} + \Delta E_{MPW}^{X}) + \frac{X}{100}E_{HF}^{X} + E_{LSDA}^{C} + \Delta E_{PW}^{C} \qquad 2.25$$

The first and second terms within the parentheses of Equation 2.25 represent the exchange energy, as determined by the local spin density approximation and the modified version of the Perdew-Wang gradient corrected exchange energy developed by Adamo and Barone. The third term is the exact Hartree-Fock exchange energy. Finally, the fourth and last term account for the correlation energy represented by the local spin density approximation and the Perdew-Wang gradient corrected correlation energy, respectively.

MPW1K reproduces experimental activation barriers accurately;[161, 178] however, one of the conclusions drawn from this dissertation is that MPW1K is unable to model the electronic nature of coordinate covalent B–N bonds accurately.[24, 173]

2.7.5 MPW1B95 and MPWB1K

MPW1B95[162] and MPWB1K[162] are based on a version of the Perdew-Wang exchange functional,[174, 175] modified by Adamo and Barone[176] with Becke's meta correlation functional.[158] As discussed previously, meta implies that the exchange-correlation energy depends on the kinetic energy density as well as the density and gradient of the density. MPW1B95 and MPWB1K are similar to the MPW1K functional, except that the ΔE_{PW}^{C} term within Equation 2.25 is replaced by Becke's meta correlation functional. Furthermore, X was optimized to fit an atomization energy database,[179] yielding $X = 31$ for the MPW1B95 functional, whereas the MPWB1K functional possesses $X = 44$, optimized to fit a database consisting of kinetic data.[160]

MPWB1K was constructed for general applications in thermochemistry and thus was suggested by Truhlar for thermochemical kinetics and noncovalent interactions but not for activation barriers.[162, 180] Similarly, MPW1B95 was constructed for kinetics and was recommended by Truhlar for covalent and noncovalent chemistry, performing well for hydrogen bonding and weak interactions.[162, 180] However, a principal conclusion from this dissertation is that neither MPW1B95 nor MPWB1K are able to model the short- and medium-range noncovalent interactions accurately within sterically congested coordinate covalent B–N bonded systems.[173]

2.7.6 M05-2X, M05, M06-2X and M06

Truhlar's new generation of density functional methods, primarily M05-2X,[141] M05,[141, 165] M06-2X[163] and M06.[163] (M-functionals) employ a HM-GGA. The M-functionals incorporate a balance of kinetic energy density within the exchange and correlation functionals, differing from MPWB1K and MPW1B95, where kinetic energy density is incorporated within the correlation functional only. The training data sets used to parameterize M05 and M05-2X include the training data sets utilized for MPWB1K and MPW1B95, and have been expanded to include several other training data sets possessing binding energies, total atomic energies, ionization potentials, electron affinities, and bond dissociation energies. M05 and M05-2X differ in that M05-2X excludes metals from the training data set. In addition, the parameterization of M05-2X ($X = 56$) yields two times (2X) the amount of Hartree–Fock exchange, compared to M05 ($X = 28$). The M06 and M06-2X functionals are a linear combination of the M05 and VSXC functionals developed by Van Voohris and Scuseria.[159, 181, 182] Training data sets were expanded upon compared to the M05 suite as well as the data sets used for accuracy assessment. M06-2X ($X = 54$) and M06 ($X = 27$) are similar to M05-2X and M05, respectively since those with the "-2X" extension possess double the exchange than their respective "non-2X" functional. Furthermore, methods with the "-2X" extension omit training data sets consisting of transition metals.

Before the existence of the M-functionals, MPWB1K and MPW1B95 were among the best for analyzing noncovalent interactions dominated by medium-range exchange-correlation energy.[162, 180] Before the existence of the M06 suite of functionals, M05-2X and M05 were initially recommended when a combination of non-metallic

thermochemistry, kinetics, and noncovalent interactions were investigated,[141, 165] while

M05 was suggested for exploring organometallic and inorganometallic

thermochemistry.[141, 165] Subsequently, M06-2X and M06 have been recommended for a

wide range of chemical phenomena.[163] A recent review by Truhlar assessed the accuracy

of many functionals against 496 data values within 32 databases including

thermochemistry, barrier heights, noncovalent interactions, electronic spectroscopy, and

structural data.[136] It was suggested that, M06-2X, M05-2X, and M06 be employed for

systems where main-group thermochemistry, kinetics, and noncovalent interactions are

important.[136] M06 was recommended specifically for transition metal thermochemistry

involving both reactive organic and transition metal bonds.[136] The claim that M06-2X,

M05-2X, and M06 are able to model noncovalent interactions is in agreement with this

dissertation. Specifically, M06-2X, M06 and M05-2X are able to reproduce the

experimental trend associated with the binding enthalpies of four methylated ammonia

trimethylboranes, $(CH_3)_3B-N(CH_3)_n H_{3-n}$ (n = 0 to 3), where noncovalent interactions

exist between the sterically congested methyl groups.[173] This is expanded upon in

Chapter 3.

Recently Truhlar and coworkers have developed two new density functional

methods, M08-HX and M08-SO, providing slightly better results than that achieved by

employing M06-2X, but significantly better than M05-2X and B3LYP.[183] Briefly, the

M08-HX functional form has been improved, compared to that for M06-2X, where the

uniform electron gas limit is enforced. The M08-SO functional enforces a different

constraint, where the gradient expansion is correct to the second order within the

exchange and correlation functionals. M08-HX and M08-SO have been recommended for investigating main-group thermochemistry, kinetics, and noncovalent interactions.[183]

2.8 Basis Sets

A variety of chemical methods have been discussed in terms of approximating Schrödinger's equation. However, solutions cannot be obtained without a description of how the wavefunction is constructed. This leads to a discussion on basis sets. Basis sets have been reviewed in the past.[120-122, 184, 185] Briefly, a basis set is a set of functions or basis functions that mathematically describe the atomic orbitals, the molecular orbitals, and finally the entire wavefunction. Initially, it may seem appropriate to construct a basis set from Slater type orbitals (STOs), since such functions behave correctly.[120, 186] For example, STOs possess the appropriate functional form regarding the radial wavefunction, where the wavefunction is non-zero at the nucleus and exponentially decays upon moving further away from the nucleus. However, the necessary two-electron integrals are cumbersome, to evaluate when the atomic orbitals are present on different atomic centers.[120]

Boys proposed an alternative to using STOs by approximating the STO as a linear combination of simpler Gaussian type orbital functions (GTOs).[128, 129] This is accomplished by using a least squares fitting approach by optimizing the coefficients and exponents to maximize the integral overlap between the STO and corresponding linear combination of GTOs. A general GTO takes the form

$$\phi_{GTO} = \left(\frac{2\alpha}{\pi}\right)^{3/4} \left[\frac{(8\alpha)^{i+j+k} i! \, j! \, k!}{(2i)! \, (2j)! \, (2k)!}\right]^{1/2} x^i y^j z^k e^{-\alpha(x^2+y^2+z^2)} \qquad 2.26$$

where α is the exponent that controls the radial spread of the Gaussian function and $i, j,$ and k are integers that reflect the angular momentum quantum numbers. For example, when the sum of the indices are zero, an s-type GTO is yielded. Similarly, when the sum of the indices is one, a p-type GTO is yielded. There exist three possible combinations of $i+j+k$ to equal a sum of one. As a result, the p_x, p_y, and p_z orbitals are formed. In the same manner, higher angular momentum orbitals are constructed. Although the term GTO is commonly used, it is probably incorrect to refer to GTOs as "orbitals," since they are not orbitals *per se*; they are merely simpler functions, more correctly referred to as Gaussian primitives. In other words, each atomic orbital is expressed as a linear combination of Gaussian primitives.

The primary difference between STOs and GTOs is the radial decay, where an STO decays as e^{-r}, and a GTO decays as e^{-r^2}. Although employing a linear combination of Gaussian functions to represent an STO allows efficient computation of integrals, deficiencies are present. Figure 2.1 illustrates the deficiencies by comparing a $1s$ STO to several GTO linear truncated to one, two, three, four and five GTOs, referred to as STO-1G, STO-2G, STO-3G, STO-4G, and STO-5G, respectively.[187] No matter how many GTOs are used to approximate the STO, the linear combination never accurately models the cusp at the origin. Furthermore, GTOs decay more rapidly than STOs. Consequently, Gaussian functions underestimate the long-range overlap between atoms and the electron density present near the nucleus.
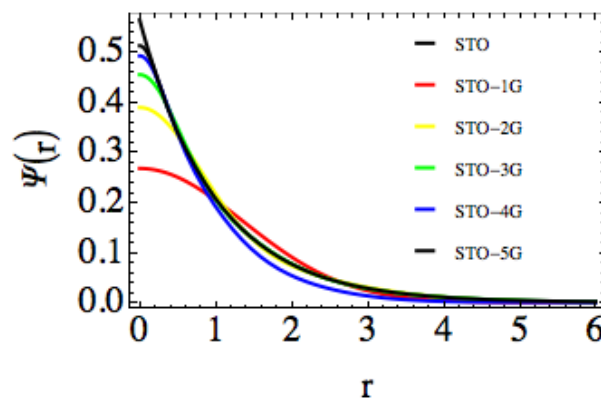
Figure 2.1. A comparison between a 1s Slater type orbital (STO) and five linear combinations of Gaussian primitives truncated at specific orders (STO-1G, STO-2G, STO-3G, STO-4G, STO-5G) that approximate the STO by a least square fitting approach.[187]

The STO-nG series (n = 1, 2, 3, 4 and 5 etc.) are known as minimal basis sets, where each basis function is represented by n Gaussian primitives. This is referred to as a single-zeta basis set, because each atomic orbital (core and valence) are represented by one basis function. However, this imposes severe limitations to the movement of electrons in response to a molecular environment. Increasing the number of basis functions per atom increases the size of the basis set, imposing fewer constraints on the electrons and more accurately describes molecular orbitals.[122, 185] A double-zeta basis set imposes fewer constraints compared to a single-zeta basis set by representing each atomic orbital with two basis functions. Similarly, a triple-zeta basis set extends the atomic orbital representation to three basis functions.

53

One can imagine increasing the basis set size by systematically increasing the number of basis functions per atomic orbital. As a result, the calculation demands more computational resources. However, from a chemical standpoint, chemical bonding is primarily a consequence of interacting valence orbitals. Therefore, there is more to be gained by increasing the flexibility of the valence orbitals compared to the core orbitals. This introduced the idea of split-valence basis sets, where each core orbital is represented by a single basis function, and each valence orbital is represented by multiple basis functions. Common split-valence basis sets developed by Pople are denoted 6-31G or 6-311G.[187-193] The number before the hyphen refers to the number of Gaussian primitives used to represent each core atomic orbital. The number of digits after the hyphen refers to the number of basis functions utilized to represent each valence atomic orbital, while the number itself represents how many primitives are used to describe each basis function. For example, the 6-31G basis set utilizes two basis functions for each valence atomic orbital, and is therefore a double-zeta basis set. Similarly, the 6-311G basis set is of triple-zeta character. The "3" implies that three primitives are used to describe the first basis function of the valence atomic orbitals, while the first "1" implies one primitive is used for the description of the second basis function, and the last "1" indicates one primitive is used for the description of the third basis function.

Basis set size can be increased by introducing polarization functions beyond what is required for the ground state description of each atom. For example, 6-31G(d,p) is a double-zeta basis set with additional d polarization functions on non-hydrogen or heavy atoms, and p functions on hydrogen atoms. Note that angular momenta preceding

the comma within the parentheses refer to additional polarization functions on heavy atoms, while angular momenta after the comma refer to increasing polarization on hydrogen atoms. Yet another way to increase basis set size is to add diffuse functions, which are larger orbitals that are added to the atomic orbital description. Diffuse functions are necessary to model negatively charge anions accurately, because electron density is farther away from the nucleus.[184] Diffuseness is denoted by a "++" or "+" within the basis set. For example, the 6-31++G(d) basis set includes diffuse *s* and *p* functions on both heavy atoms and hydrogen atoms, whereas the 6-31+G(d) basis set includes diffuse *s* and *p* functions on only the heavy atoms. A common basis set referred to within dissertation is the 6-311++G(3df,2p) basis set. This is a Pople-style triple-zeta basis set that includes three sets of *d* polarization functions (not *3d* orbitals) and one set of *f* functions on the heavy atoms. In addition, two sets of *p* functions are present on the hydrogen atoms, and both heavy and hydrogen atoms include diffuse functions. Functions of the same angular momentum vary in their coefficients and exponents.[187-193]

Independent of Pople, Dunning and coworkers developed the correlation consistent basis sets, which include polarization and diffuse functions by employing a more systematic approach.[194-196] The benefit of Dunning's strategy is that the correlation consistent basis sets are designed to converge to the complete basis set limit utilizing extrapolation methods.[197-200] The complete basis set imposes no restriction to the number of functions, thus an infinite set of functions are utilized. Examples of correlation consistent basis sets include cc-pVnZ and aug-cc-pVnZ, where n = D, T, Q and 5 and "aug" signifies the addition of diffuse functions. Higher orders of n do exist but are extremely resource intensive for large chemical systems and therefore have not been

considered here. The value of n designates how many polarization functions are included. For example, the cc-pVDZ includes a set of s and p polarization functions to the existing s function of a hydrogen atom, totaling two sets of s and one set of p. Increasing D to T adds another set of s, p, and d to the functions included when $n = D$, totaling three sets of s, two sets of p, and one set of d. As a final illustration, increasing T to Q adds an additional set of s, p, d, and f functions, totaling four sets of s, three sets of p, two sets of d, and one set of f.

Regarding the implementation of basis sets, it is important to note that electronic structure programs may utilize different coordinate systems to cover the same spatial volume. For example, the indices i, j, and k within Equation 2.26 yield six d functions when Cartesian coordinates are utilized. However, they may be transformed to five spherical d-functions and one s-function. Similarly, the ten Cartesian f-functions may be transformed into seven spherical f-functions and three p functions. The resource savings from employing spherical rather than Cartesian coordinates can be quite substantial if many d, f, and higher angular momentum functions are considered within a calculation. Consequently, many programs take advantage of the resource savings by using spherical functions. It is known that the default for Gaussian03 and NWChem 5.1 is to utilize spherical and Cartesian angular momentum basis functions for triple-zeta basis sets, respectively. In order to make a direct comparison between different programs while using the same triple-zeta basis set, the SPHERICAL keyword has been implemented within NWChem to utilize five d- and seven f-functions, consistent with Gaussian03.

As a final note, the level of theory used to approximate Schrödinger's equation is always comprised of a chemical method and a basis set, which is usually denoted as

"chemical method/basis set". For example, a common level of theory employed throughout this dissertation is M06-2X/6-311++G(3df,2p). M06-2X/6-311++G(3df,2p) indicates that the M06-2X method was utilized in conjunction with the 6-311++G(3df,2p) basis set. Another common notation is "method/basis set//method//basis set". The "//" indicates that two computations are involved. First, a geometry optimization is performed using the level of theory following "//", then a single point energy evaluation is employed using the level of theory preceding "//". The single point energy evaluation yields the energy of the system without varying the coordinates of the atoms, as is done for a geometry optimization. The geometry optimization is often performed at a lower level of theory, while the single point energy evaluation is conducted at a higher level of theory. This approach is more efficient and practical when compared to employing a full geometry optimization at a higher level of theory.[115]

2.9 Basis Set Superposition Error

A basis set is a mathematical approximation of the wavefunction. A complete basis set is rarely used, since the resources necessary are demanding. Consequently, a linear combination of Gaussian functions is utilized, truncated at a specific order, as discussed previously. The truncated basis set inevitably introduces error into the computation, since it restricts electron movement. However, another error introduced by incomplete basis sets is basis set superposition error (BSSE).[201] Consider computing the binding energy, ΔE, between two molecules, A and B. The simplest strategy is to

compute the energy of the complex, $E(A-B)$, monomer A, $E(A)$, and monomer B,

$E(B)$, and take the difference, as shown by Equation 2.27.

$$\Delta E = E(A-B) - E(A) - E(B) \qquad\qquad 2.27$$

However, basis functions from A can compensate for the basis set incompleteness on

monomer B, and vice versa. The swapping of orbital space is the origin of the name

"superposition" error. BSSE results in an artificial lowering of the energy of $E(A-B)$.

Consequently, the predicted binding energy will invariably be an overestimate of the

true value. As the complete basis set limit is approached, the deficiencies in the basis set

are reduced, and the BSSE is eliminated. However, larger basis sets become

cumbersome for systems containing many atoms. Thus, approximations of assessing

BSSE have been considered.

A common approach is the counterpoise method (CP) developed by Boys and

Bernardi.[202, 203] It is helpful to remember that the inaccuracy only lies within the energy

of the complex. The calculated energies of the monomers are correct, at least within the

accuracy of the method and basis set. To correct the energy of the complex, four

additional computations are necessary, according to the CP method. First, the energy of

A, $E(A)_{ab}$, is computed in the presence of the basis functions that represent A and B, but

without the nuclei of B present. Second, the energy of B, $E(B)_{ab}$, is computed in the

presence of the basis functions that represent A and B, but without the nuclei of A

present. Basis functions consisting of fixed coordinates in space with no corresponding

nuclei are often referred to as ghost orbitals. Third, the energy of A, $E(A)_a$, is computed

in the presence of the basis functions that represent A only. Lastly, the energy of B,

$E(B)_b$, is computed in the presence of the basis functions that represent B only. It must

be remembered that since the error lies within the complex, the energies of the

fragments are determined with respect to their geometries within the complex, not the

isolated monomers. The amount of BSSE, ΔE_{BSSE}, is then computed according to

Equation 2.28

$$\Delta E_{BSSE} = [E(A)_{ab} - E(A)_a] + [E(B)_{ab} - E(B)_b] \qquad 2.28$$

In essence, the first quantity refers to the BSSE introduced by A "stealing" basis

functions from B, and the second quantity refers to the BSSE introduced by B "stealing"

basis functions from A. The BSSE corrected binding energy, determined by the CP

method, is represented by Equation 2.29.

$$\Delta E_{CP\ corrected} = \Delta E - \Delta E_{BSSE} \qquad 2.29$$

When computing accurate binding energetics, it has been reported that BSSE should be

corrected by utilizing the counterpoise method.[184, 201, 204-208] A review of BSSE and a

variety of methods that attempt to eliminate BSSE is given by Kestner and

Combariza.[201]

2.10 Natural Bond Orbital Analysis

The Hamiltonian operator is associated with the total energy of a quantum mechanical system. However, other chemical properties are of interest, such as atomic charge and bond order. Population analysis is a method of partitioning the wavefunction or electron density into charges on each atomic nuclei. It must be noted that atomic charges cannot be observed experimentally, since charge does not correspond to a unique physical property.[121, 209] Thus, there is no quantum mechanical operator that is associated with atomic charge. Each partitioning scheme is completely arbitrary. Consequently, many methods have been devised, such as Mulliken's[210] and Löwdin's[211] population analysis, atoms in molecules,[212] and natural population analysis, NPA.[213] In general, the electron density and nuclear charges are condensed to a partial charge and assigned to each corresponding nucleus. This is an effective approach for predicting sites susceptible to nucleophilic or electrophilic attack, and the prediction of other molecular properties dependent upon charge. Since each approach is arbitrary, the choice to select an analysis must be based on chemical intuition. Suggestions on which algorithm to use have been made.[214] Atomic charges derived from NPA have been successful as effective measures of substituent induced pKa shifts within a variety of anilines and phenols, able to model the pKa shifts better than other charge partitioning schemes.[215] Similarly, predicted NPA atomic charges were able to replicate electron density donating and withdrawing trends within substituted actinide complexes better than other methods of analysis.[216] Lastly, it was reported that the electronegativity equalization method should be based on atomic charges derived from the NPA scheme, rather than those derived from other methods.[209] Consequently, NPA has been used for

the derivation of atomic charges in this dissertation work, as implemented through the natural bond orbital (NBO) program.[113]

NBO analysis of Weinhold and coworkers is an electron population analysis algorithm that provides an intuitive framework for investigating chemical phenomena in terms of familiar concepts such as Gilbert Lewis' dot structures. The transformation from basis set to NBOs has been discussed in detail elsewhere.[217-221] However a brief description outlining the process is warranted. NBO transforms the non-orthogonal atomic orbitals from the HF wavefunction into orthonormal natural atomic orbitals (NAO),[213] natural hybrid orbitals (NHO),[222] and natural bond orbitals (NBO).[220] This allows electron density to be treated in a more intuitive manner, *i.e.* localized onto bonds, atoms, and lone pairs, leading to the best possible description of the molecule as a localized Lewis structure. Figure 2.3 illustrates the transformation performed on the basis set for methane.
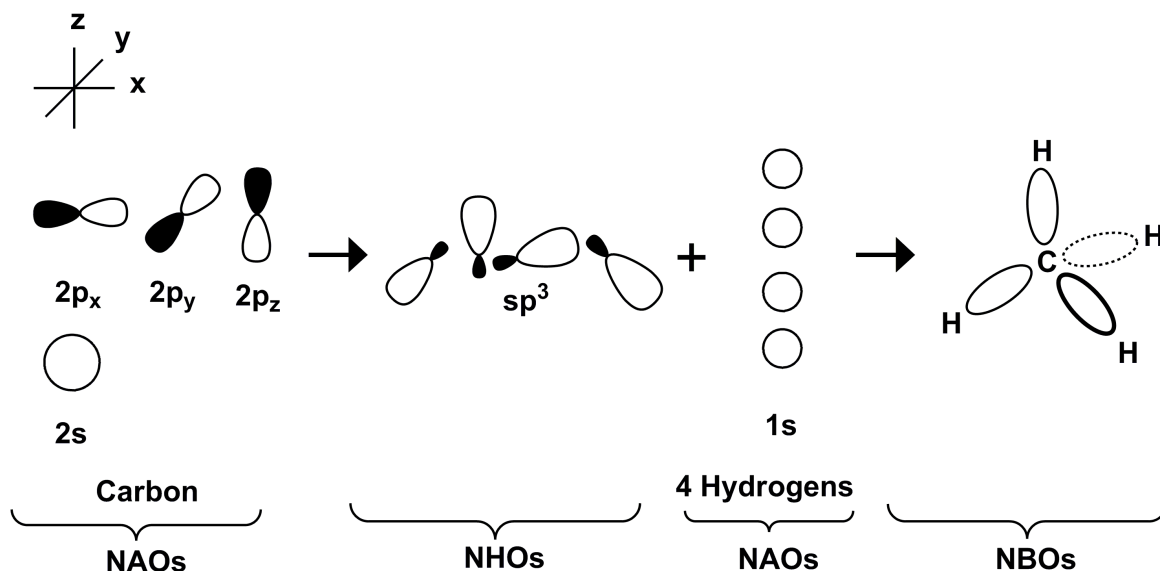
Figure 2.2. Transformation from natural atomic orbitals (NAOs) to natural hybrid orbitals (NHOs) to natural bond orbitals (NBOs) for methane

The NBO transformation provides filled orbitals that are more concentrated or localized in terms of occupancies. Subsequently, hyperconjugation between filled and empty orbitals may be determined. An interesting example of hyperconjugation involves an explanation of the internal rotation barrier of ethane. It has been reported that a vicinal stereoelectronic effect between a filled C–H sigma bond and an unfilled C–H sigma antibond, denoted $\sigma(\text{C–H}) \rightarrow \sigma^*(\text{C–H})$, is responsible for the staggered ethane conformer possessing a lower energy than that of the eclipsed form;[223, 224] however, this is still highly debated.[225-229]

NBO computes bond descriptors such as bond order, percent bond covalency and iconicity by employing natural resonance theory (NRT).[217-219, 221] NRT determines localized resonance structures and their corresponding weighting factors, which express
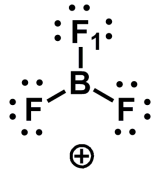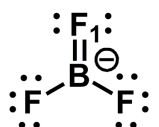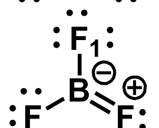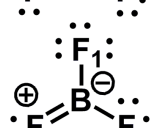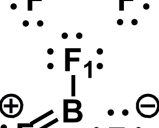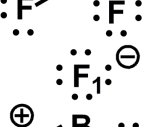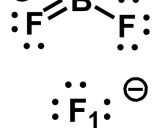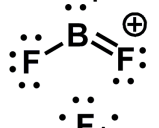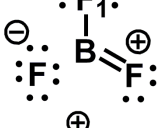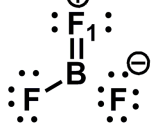
the contribution of each structure to the resonance hybrid. Subsequently, properties of a

given delocalized system may be attained in resonance-averaged form. For example,

consider the ten BF_3 resonance structures found by a default NBO analysis,

corresponding $B–F_1$ bond orders, and percent contribution of each resonance structure to

the overall resonance hybrid, shown in Table 2.1. The bond order for the $B–F_1$ bond may

be determined by Equation 2.30, where γ represents the quantity of interest (in this case

the bond order) corresponding to each individual resonance structure, θ, and its percent

contribution, ξ, to the averaged resonance form, Θ.

$$\Theta^{\text{Bond Order}} = \sum_i \xi_i \theta_i \gamma_i \qquad 2.30$$

Consequently, Equation 2.30 becomes Equation 2.31, and the bond order of $B–F_1$ equals

1.0, as expected.

$$
\begin{aligned}
\Theta^{\text{Bond Order}} = {} & (I)1.0(.811) + (II)2.0(0.043) + (III)1.0(0.043) \\
& + (IV)1.0(0.043) + (V)1.0(0.01) + (VI)0.0(0.01) \\
& + (VII)0.0(0.01) + (VIII)1.0(0.01) + (IX)2.0(0.01) \\
& + (X)2.0(0.01) = 1.0
\end{aligned}
\qquad 2.31
$$

Table 2.1. Resonance Structures, B–F$_1$ Bond Orders, and Percent Contribution of Each Resonance Structure to the Averaged-Resonance Form.

	Resonance Structure	Bond Order	Percent Contribution
I		1.0	81.1
II		2.0	4.3
III		1.0	4.3
IV		1.0	4.3
V		1.0	1.0
VI		0.0	1.0
VII		0.0	1.0
VIII		1.0	1.0
IX		2.0	1.0
X		2.0	1.0

2.11 Potential Energy Surfaces

As expected, the energy of a molecular system changes as the coordinates of the nuclei are modified. The way in which the energy varies as a function of nuclear coordinates is reflected by a potential energy surface (PES). A common goal among chemists is to locate different points along the PES to investigate reaction pathways. Specifically, energy minima connected by maxima on the PES are of interest because relative energy differences between the appropriate points, otherwise known as saddle points, allow the prediction of activation barriers and heats of reaction.

In order to locate saddle points along the PES, it is common to employ geometry optimizations where derivatives of the energy with respect to the atomic coordinates are used to determine critical information about the PES. It is helpful to consider a Taylor series expansion of the energy function, $V(x)$, about the point x_0, shown in Equation 2.32. [120-122]

$$V(x) = V(x_0) + (x - x_0)\frac{\partial V(x)}{\partial x}\bigg|_{x=x_0} + \frac{(x - x_0)^2}{2}\frac{\partial V^2(x)}{\partial x^2}\bigg|_{x=x_0} + \cdots \qquad 2.32$$

In order to locate stationary points, geometry optimizations proceed by first computing the energy of an initial structure, the first derivative of the energy (gradient), and then making a decision as to how far and in what direction the atoms should move in order to reduce the forces between all the atoms. The gradient is defined as the negative forces between each atom as well as the magnitude of the slope. Consequently, the gradient indicates the direction along the PES in which the energy decreases most rapidly from

the current point or increases if a transition structure is of interest. When the gradient is zero or extremely close to zero, the forces demonstrated between each atom are also close to zero. When the forces and the calculated displacements between all atoms are below a certain threshold, the structure is considered optimized.

If the gradient is zero and the potential is assumed to be zero at x_0, truncation of the Taylor series expansion, retaining the second order term, yields the form of the harmonic oscillator, which in turn results in an expression consisting of the force constant (Equation 2.33).

$$V(x) \cong \frac{(x - x_0)^2}{2} \frac{\partial V^2(x)}{\partial x^2}\bigg|_{x=x_0} = \frac{\Delta x^2}{2} k \qquad 2.33$$

For a system containing multiple atoms, k is replaced by a matrix containing all the second derivatives of the energy with respect to the coordinates and is referred to as a Hessian. Some optimization algorithms utilize second derivatives to assess the curvature of the function, providing additional information as to how the next step is taken along the PES in search for the stationary point.

As mentioned previously, certain points along the PES are of interest to chemists, specifically transition structures, groundstates, and stable intermediates. Up till now, there has been no discussion as to how to distinguish between the varieties of structures. Ultimately, the question becomes, "Does does the structure correspond to an energy minima or maxima?" To determine the answer to this question, the eigenvalues of the Hessian are analyzed. If zero negative eigenvalues are present, the corresponding

structure is an energy minima. If one negative eigenvalue is present, the corresponding

structure is a first order saddle point, otherwise known as a transition structure. As found

within the literature, it is common to find negative force constants referred to as

imaginary frequencies. This is easy to understand after referring to the mathematical

relationship between force constants, k, and frequencies of vibration, v, (Equation

2.34), as the square root of a negative force constant divided by the reduced mass, μ,

yields an imaginary result.

$$v = \frac{1}{2\pi} \sqrt{\frac{k}{\mu}} \qquad\qquad 2.34$$

It is critical to always confirm the identity of a saddle point as either an energy minima

or maxima.[230]

2.12 Thermodynamics

Thermodynamic quantities are derived from basic statistical mechanics.[121, 231, 232]

Although electronic structure calculations are usually performed on one molecule, it is

important to make direct comparisons with thermodynamic and kinetic data determined

by experiment. The question arises of how quantities computed for microscopic systems

can be extended and compared to experimental data determined for macroscopic

systems. The answer is statistical mechanics, specifically, the application of the partition

function and the Boltzmann distribution. The partition function is analogous with the

wavefunction from quantum mechanics. As properties can be determined by applying the correct operator on the wavefunction for microscopic systems, the partition function allows the calculation of macroscopic functions. The Boltzmann distribution recognizes that although all molecules exist in their energetic ground state at 0 K, there is a distribution of molecules at finite temperatures that occupy higher energy states with a certain probability. The probability is proportional to the exponential of the negative ratio between the energy state, ϵ, and the Boltzmann factor, k, multiplied by the temperature, T (Equation 2.35). Thus, the probability of finding a molecule with a certain energy, ϵ_i, is expressed by Equation 2.36.

$$P \propto e^{-\frac{\epsilon}{k_B T}} \qquad\qquad 2.35$$

$$P(\epsilon_i) = \frac{e^{-\frac{\epsilon_i}{k_B T}}}{\sum_i^\infty e^{-\frac{\epsilon_i}{k_B T}}} \qquad\qquad 2.36$$

Experimental thermodynamic and kinetic data acquired at a finite temperature include contributions from molecules with higher energy states (electronic, translational, rotational, and vibrational). However, the computational result will include only the lowest energy quantum state. In order for proper comparison with experiment, the contributions from higher energy quantum states must be accounted for.

The higher energy quantum states are considered by employing two important approximations. First, it is assumed that the system of interest contains non-interacting particles (i.e. the ideal gas approximation). Second, it is assumed that the electronic,

translational, rotational, and vibrational contributions to the total energy are not coupled. Therefore, the total energy may be expressed as a sum of the individual components (Equation 2.37), and the total partition function may be expressed as a product of the electronic, translational, rotational, and vibrational partition functions (Equation 2.38).

$$\epsilon = \epsilon_{\text{trans}} + \epsilon_{\text{rot}} + \epsilon_{\text{vib}} + \epsilon_{\text{elec}} \qquad 2.37$$

$$Q = q_{\text{trans}} q_{\text{rot}} q_{\text{vib}} q_{\text{elec}} \qquad 2.38$$

The derivation and application of each partition function has been reported.[121, 231, 232] In short, each individual partition function is solved by considering a generic equation (Equation 2.39), where ϵ_r is the energy corresponding to each quantum degree of freedom, as determined by the Schrödinger equation, and r is the quantum number of interest. Each partition function includes the summation of all possible energy levels corresponding to each quantum degree of freedom. Thus, higher energy states are accounted for in the total partition function.

$$q = \sum_{r}^{\infty} e^{\frac{-\epsilon_r}{k_B T}} \qquad 2.39$$

Once each partition function has been solved, the total partition function can be found, and common thermodynamic functions can be determined according to Equations 2.40 to 2.44.

The thermodynamic functions investigated throughout this dissertation are internal energy (E), enthalpy (H), Helmholtz free energy (A), entropy (S), and Gibbs free energy (G), which are represented by Equations 2.40, 2.41, 2.42, 2.43, and 2.44, respectively.[114, 121, 232, 233]

$$E = k_B T^2 \left(\frac{\partial \ln Q}{\partial T}\right)_V \tag{2.40}$$

$$H = E + PV = k_B T^2 \left(\frac{\partial \ln Q}{\partial T}\right)_V + k_B TV \left(\frac{\partial \ln Q}{\partial V}\right)_T \tag{2.41}$$

$$A = -k_B T \ln Q \tag{2.42}$$

$$S = \frac{E + A}{T} = k_B T \left(\frac{\partial \ln Q}{\partial T}\right)_V + k_B \ln Q \tag{2.43}$$

$$G = H - TS = k_B TV \left(\frac{\partial \ln Q}{\partial V}\right)_T - k_B T \ln Q \tag{2.44}$$

Electronic structure programs employ frequency analyses to provide the absolute thermodynamic property, which is merely the sum of the electronic energy and the thermal correction of interest. For example, the enthalpy of a system is expressed as

$$H_{298} = E_{\text{elec}} + H_{298}^{\text{thermal}} \tag{2.45}$$

However, the absolute thermodynamic quantity is rarely of interest. The change or difference in the thermochemical property is of importance. Consequently, a difference in the same thermodynamic quantity is taken to yield values associated with chemical phenomena, such as bond dissociation enthalpies at finite temperatures, ΔH_{298}, or Gibbs free activation energies, $\Delta^{\ddagger}G_{298}$. These two quantities will be referred to often throughout this dissertation.

In practice, computed thermal corrections often possess a known amount of systematic error due to the approximation employed by the chemical method and/or basis set.[234-236] Consequently, scaling factors have been developed to realign thermodynamic quantities with corresponding experimental phenomena. If high level computed thermodynamic quantities are desired, it is often advantageous to optimize the structure at a high level of theory to acquire the electronic energy, and subsequently perform a frequency analysis with a low level of theory on an optimized structure determined with the same low level of theory. The absolute thermodynamic quantity can then be scaled and added to the electronic energy determined with the high level of theory. Equation 2.46 illustrates the absolute enthalpy predicted by a scaling approach.

$$H_{298} = E_{\text{elec}}^{\text{QCISD(T)}/6-311+G(3df,2p)} + 0.9989 H_{298}^{\text{B3LYP}/6-31G(d)} \qquad 2.46$$

Equation 2.46 is the same as 2.45 except for the fact that the thermal correction is scaled. The electronic energy is computed by a high level of theory, QCISD(T)/6-311++G(3df,2p), where the enthalpy correction is computed with a low level of theory, B3LYP/6-31G(d). It is important to note that the scaling factor is

dependent on the level of theory. Radom and coworkers recommended a scaling factor of 0.9989 with the use with B3LYP/6-31G(d).[235] It is also important to note that scaling factors for thermodynamic quantities are temperature dependent. Consequently, Radom and coworkers derived scaling factors for enthalpy corrections at temperatures of 298.15, 450 and 600 K, so that scaling factors may be interpolated within the 298.15 to 600 K range.[235] For example, an appropriate scaling factor for a B3LYP/6-31G(d) thermal correction at T = 373 K is 0.9941, as determined by the interpolation performed in Figure 2.3.
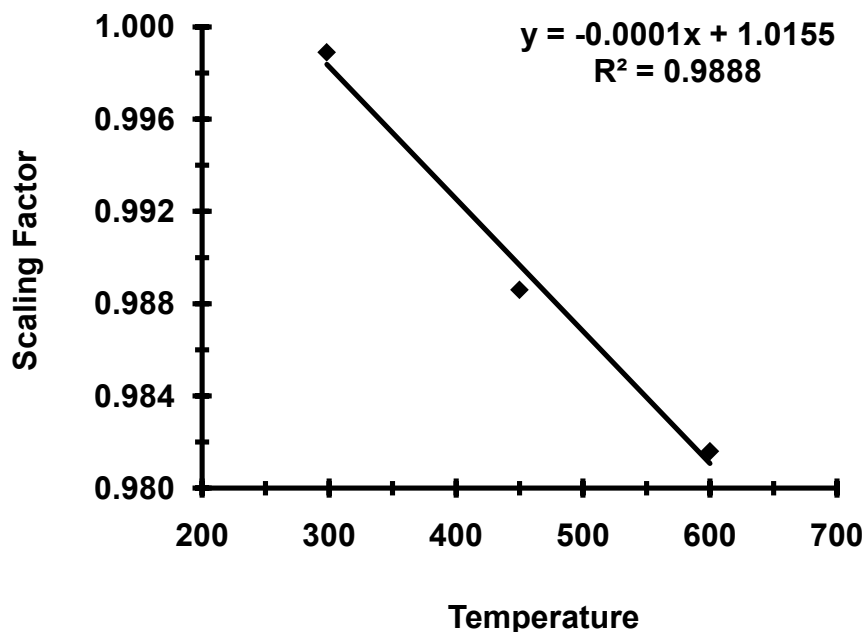
Figure 2.3. Line of best fit regarding the enthalpy scaling factors derived by Radom and coworkers.[235] Scaling factors are 0.9989, 0.9886, and 0.9816 for T = 298.15, 450, and 600 K, respectively. Using the equation that describes the line of best fit, a scaling factor of 0.9941 is calculated for T = 373 K.

Chapter 3

Covalent and Ionic Nature of the Coordinate Covalent Bond and Account of Accurate Binding Enthalpies

The inherent difficulty in modeling the energetic character of the B–N coordinate covalent bond has been investigated utilizing density functional theory (DFT) and *ab initio* methods. The underlying influence of basis set size and functions, thermal corrections, and basis set superposition error (BSSE) on the predicted binding enthalpy of ammonia borane ($H_3B–NH_3$) and four methyl substituted ammonia trimethylboranes [$(CH_3)_3B–N(CH_3)_nH_{3-n}$; n = 0-3] has been evaluated and compared with experiment. HF, B3LYP, MPW1K, MPW1B95, MPWB1K, M05, M05-2X, M06, M06-2X, MP2, QCISD, and QCISD(T) have been utilized with a wide range of Pople-style and correlation consistent basis sets. Overall, DFT and HF result in less BSSE and converge to binding enthalpies with fewer basis functions than post-SCF techniques. However, of the DFT methods explored, only M06, M05-2X, and M06-2X model experimental binding enthalpies and trends accurately, producing MADs of 3.9, 1.6, and 0.3 kcal/mol, respectively. Despite slow basis set convergence, MP2, QCISD, and QCISD(T)

employed with the 6-311++G(3df,2p) basis set reproduce the experimental binding

enthalpy trend and result in lower MADs of 1.9, 2.3, and 0.4 kcal/mol, respectively,

when corrected for BSSE and a residual convergence error of *ca*. 1.3-1.6 kcal/mol.

Accuracy of the predicted binding enthalpy is linked to correct determination of the

bond's coordinate covalent character given by charge-transfer frustration, $Q_{CTF} \cong$

$-\left(\Delta Q_B + \Delta Q_N\right)$. Frustration gauges the incompleteness of charge-transfer between the

donor and acceptor. The binding enthalpy across ammonia borane and methylated

complexes is correlated to its coordinate covalent character ($R^2 = 0.91$), where more

coordinate covalent bond character (less charge-transfer frustration) results in a weaker

binding enthalpy. However, a balance of electronic and steric factors must be considered

to explain trends in experimentally reported binding enthalpies. Coordinate covalent

bond descriptors, such as bond ionicity and covalency are important in the accurate

determination of the coordinate covalent bond. The B–N coordinate covalent bond in

ammonia borane is characterized as being 65% ionic, moderately strong (-27.5 ± 0.5

kcal/mol), and structurally flexible on the donor side to relieve steric congestion.

3.1 Introduction

The coordinate covalent bond, also known as the semipolar double bond,[19-21] or

coordinate link,[22] has been less defined and studied as compared to either covalent or

ionic bonds.[7, 10, 237] Depending upon the field of study, molecular systems with

coordinate covalent bonds are typically referred to as coordination compounds,[238] Lewis

acid-base adducts,[69] or electron donor-acceptor complexes.[57, 239, 240] Despite the

nomenclature, these molecular systems employ an atypical bonding scheme, where covalent and ionic potential energy surfaces become close in energy.[25] The wavefunction for coordinate covalent bonding is described as

$$\Psi_{\text{coordinate covalent}}(D^+\!-\!A^-) = a\Psi_{\text{covalent}}(D\!-\!A) + b\Psi_{\text{ionic}}(D^+,\,A^-) \qquad 3.1$$

The importance of each bonding term depends upon the ability of the atomic partners to share electrons, as well as D to donate electrons and A to accept them. It has been reported previously that the B–N bond strength includes contributions from both covalent and ionic terms, making trends in bond energies difficult to predict *a priori*.[241] Thus, a difficult situation results for the computational treatment of the structure, energetics, and dynamics of the coordinate covalent bond, since the employed chemical theory must simultaneously treat the partial covalent and ionic contributions accurately without compensation of errors.

To date, the binding energetics for ammonia borane, $H_3B\text{–}NH_3$, a well-known prototype of the coordinate covalent bond,[19] have not been directly measured by experiment. As a result of the computational challenge in modeling both the covalent and ionic character of the coordinate covalent bond, the predicted binding energetics vary widely.[19, 204, 242-248] Table 3.1 is a noncomprehensive summary of the predicted binding energetics reported using different levels of theory with and without basis set superposition error (BSSE) and thermal corrections.

Table 3.1. H_3B–NH_3 Binding Enthalpies, ΔH, Electronic Binding Energies, ΔE_{elec}, and Zero-Point Corrected Binding Energies, ΔE_0, Determined by Different Approaches.

Method	BE[a]	BSSE[c]
Gurvich's estimation[249]	ΔH_{298} = -37.5 ± 4.3	-
B3LYP/6-31G(d)[246]	ΔE_{elec} = -32.8	no
BAC-MP4[250]	ΔH_{298} = -31.3	no
Haaland's estimation[19]	ΔH_{298} = -31.1 ± 1.0	-
CCSD(T)/aug-cc-pVTZ[246]	ΔE_{elec} = -31.1	no
MP2/TZ2P[241]	ΔH_{298} = -30.7	no
MP2/6-31G(d,p)[243]	ΔH_{298} = -30.0	no
MP2/aug-cc-pVDZ[204]	ΔE_{elec} = -29.3[b]	yes
CCSD(T)/aug-cc-pVDZ[204]	ΔE_{elec} = -28.5[b]	yes
BLYP/6-31G(d)[247]	ΔE_0 = -28.5	no
MP2/TZ2P[247]	ΔE_0 = -28.3	no
MPW1K/6-311++G(d,p)[245]	ΔE_0 = -28.1	no
MP2/6-311++G(d,p)[245]	ΔE_0 = -26.5	no
CCSD(T)/cc-pVTZ[247]	ΔE_0 = -26.5	no
B3LYP/6-31G(d)[246]	ΔE_0 = -26.3	no
G2(MP2)[251]	ΔE_0 = -26.0	no
Piela's estimation[204]	ΔH_{298} = -25.7 ± 2.0[b]	yes
CCSD(T)/6-311++G(d,p)[244]	ΔE_0 = -25.5	no
CCSD(T)/aug-cc-pVTZ[246]	ΔE_0 = -24.6	no
CCSD(T)/aug-cc-pVDZ[204]	ΔH_{298} = -24.5[b]	yes
MP2/6-31G(d,p)[243]	ΔH_{298} = -24.1	yes
B3LYP/6-311++G(d,p)[245]	ΔE_0 = -23.5	no
MP2/aug-cc-pVDZ[204]	ΔE_0 = -23.5[a]	yes
CCSD(T)/aug-cc-pVDZ[204]	ΔE_0 = -22.7[b]	yes
HF/aug-cc-pVDZ[204]	ΔE_{elec} = -20.1[b]	yes
HF/aug-cc-pVDZ[204]	ΔE_0 = -14.3[b]	yes

[a] All values are in kcal/mol.
[b] The aug-cc-pVDZ basis set has been supplemented with diffuse *f* functions on the boron and nitrogen atoms, and one diffuse *d* function on each hydrogen atom.
[c] Designates whether basis set superposition error was corrected.

To the best of our knowledge, there exist two estimates of the H_3B–NH_3 binding enthalpy derived indirectly from experimental data. The earliest H_3B–NH_3 binding

enthalpy was provided by Haaland, extrapolated from the experimental binding enthalpies of seven methylated boranes.[19] The estimation was reproduced (Figure 3.1) by using a quadratic fit of the plotted binding enthalpies for $(CH_3)_3B–N(CH_3)_nH_{3-n}$, $n = 0$-3, versus the number of methyl substituents on nitrogen, n, as done by Brown and co-workers.[252] Subsequently, a second quadratic equation was fitted to the binding enthalpies for $H_3B-N(CH_3)_nH_{3-n}$ versus the same x-axis. The binding enthalpy of H_3B-NH_3 was taken as the value that allowed the coefficient of the quadratic term within the two equations to be equivalent. Haaland's resulting binding enthalpy of ammonia borane is ΔH_{298} -31.1 ± 1.0 kcal/mol.[19] Haaland's estimation is expected to incorporate some error because the binding enthalpies for the $H_3B-N(CH_3)_nH_{3-n}$ (omitting $n = 0$) series were derived from standard enthalpies of reactions.[19] However, subsequent refinement of the $H_3B-N(CH_3)_3$ binding enthalpy by experiment revealed that the derived value was underestimated by 3.5 kcal/mol.[29] Thus, binding enthalpies for the $H_3B-N(CH_3)_nH_{3-n}$ series (omitting $n = 0$) yield a linear relationship with increasing n rather than a quadratic relationship, as assumed by Haaland to estimate the binding enthalpy of ammonia borane.

$y = -1.38x^2 + 5.38x + 31.07$
$R^2 = 1.00$

$y = -1.38x^2 + 5.44x + 13.74$
$R^2 = 0.99$

Binding Energy

Number of Methyls on Nitrogen
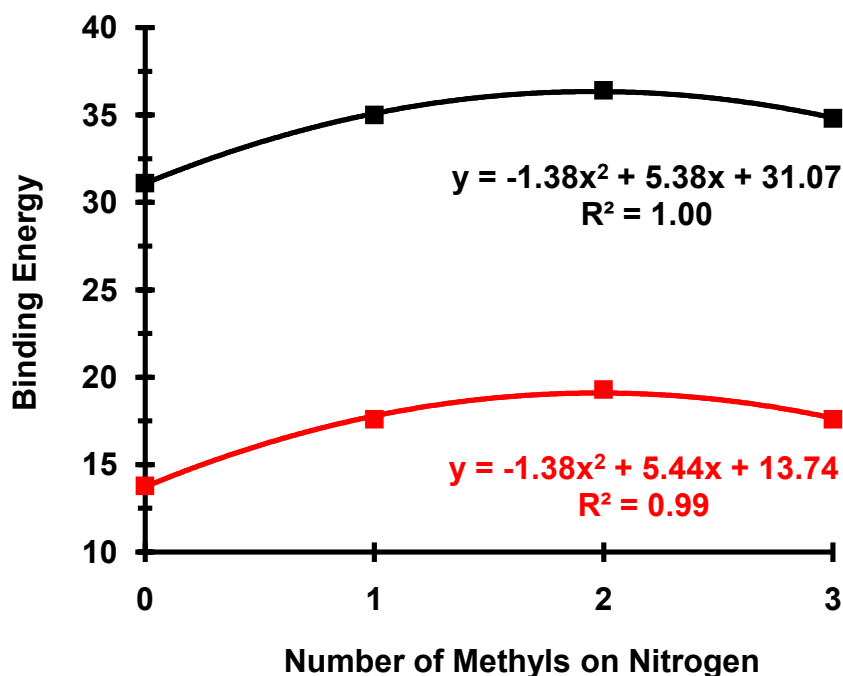
Figure 3.1. Haaland's estimation. The estimation was reproduced by using a quadratic fit of the plotted binding enthalpies for $(CH_3)_3B–N(CH_3)_nH_{3-n}$, n = 0-3 (red line), versus the number of methyl substituents on nitrogen. Subsequently, a second quadratic equation was fit to the plotted binding enthalpies for $H_3B–N(CH_3)_nH_{3-n}$ (black line) versus the same x-axis. The binding enthalpy of H_3B-NH_3 was then taken as the value that allowed the coefficient of the quadratic term within the two equations to be equivalent. Haaland's resulting binding enthalpy value is ΔH_{298} = -31.1 ± 1.0 kcal/mol.

Second, Gurvich et al. used four experimental studies to estimate the heat of formation (ΔH_f^o = -27.5 ± 3.6 kcal/mol) for $H_3B–NH_3$,[249] which yields a B–N binding energy of -37.5 ± 4.3 kcal/mol when the ΔH_f^o for borane (ΔH_f^o = 21.0 ± 2.4 kcal/mol),[249] and ammonia (ΔH_f^o = -11.0 ± 0.1 kcal/mol)[253] are considered. It has been noted that Gurvich's estimated heats of formation were based upon experimental data not firmly established, and that the large uncertainty could yield an inaccurate B–N binding enthalpy.[250]

Computational predictions of the $H_3B–NH_3$ binding enthalpy are significantly weaker than the Haaland and Gurvich estimations. Predicted binding energies (ΔE_0, corrected for ZPE at 0 K) are -24.6 kcal/mol from CCSD(T)/aug-cc-pVTZ,[246] -26.5 kcal/mol from MP2/6-311++G(d,p),[245] and -22.7 from CCSD(T)/aug-cc-pVDZ.[204] Piela and coworker's enthalpic estimation was determined by computing the binding enthalpy using MP2/aug-cc-pVDZ supplemented with a $3s3p2d1f$ set of functions centered in the middle of the B–N dative bond. The resulting binding enthalpy at 298 K was -26.5 kcal/mol. The MP2 binding enthalpy was corrected by adding the correlation contribution of 0.8 kcal/mol, which is the difference between CCSD(T) and MP2 binding energies with the aug-cc-pVDZ basis set. The final estimated binding enthalpy reported at 298 K was -25.7 ± 2.0 kcal/mol.[204]

The B–N coordinate covalent bond has been investigated computationally in substituted systems as well.[36, 242-248, 251, 254] In particular, an investigation critiquing the ability of density functional theory (DFT) to model B–N coordinate covalent bonds accurately has been reported.[245] Systematic addition of methyl groups to the donor and acceptor atoms of ammonia borane revealed increasing error in B3LYP predicted binding energetics, whereas MP2 provided energetic trends consistent with experiment.[245] Other borate systems containing B–N coordinate covalent bonds also have been analyzed in which B3LYP was unable to model the coordinate covalent bond accurately.[244] Further analysis showed that CCSD(T) predicted and ZPE corrected binding energies[244] compare well with MP2 predicted binding energies.[245]

The wide range of predicted binding energetics for $H_3B–NH_3$ from -14.3 to -37.5 kcal/mol (Table 3.1) and the divergence of predicted binding energetics of substituted

ammonia borane systems are symptomatic of the inherent difficulty in modeling the coordinate covalent bond. The obvious variables contributing to the reported variability include the chemical method and basis set employed, whether BSSE corrections were implemented, and if the appropriate thermal corrections were applied to the electronic energy. Many of the reported studies recognize the need for one computational factor over another; however, in many of the reports, the energies were not corrected for BSSE, even though it is generally recognized that it ranges between 1 to 3 kcal/mol for DFT methods[245] and 3 to 10 kcal/mol for post-SCF methods when small basis set are utilized.[204, 243, 244, 255] BSSE corrections are important, since smaller basis sets are commonly used to predict the binding energetics of B–N coordinate covalent bonds.

Due to the need for accurate computational modeling and characterization of the coordinate covalent bond, a systematic computational approach has been implemented to investigate ammonia borane and methyl substituted ammonia trimethylboranes [$(CH_3)_3B-N(CH_3)_nH_{3-n}$; $n = 0-3$]. The $(CH_3)_3B-N(CH_3)_nH_{3-n}$ complexes have been chosen for analysis rather than $H_3B-N(CH_3)_nH_{3-n}$ systems, since more prominent effects on binding enthalpies have been observed.[19] Furthermore, the binding enthalpies of the $H_3B-N(CH_3)_nH_{3-n}$ adducts have not been directly determined by experiment, but rather derived from standard heats of reaction,[19] with the exception of $H_3B-N(CH_3)_3$.[29] The influence of electron correlation, basis set size, and BSSE has been explored by performing electronic structure calculations with a variety of basis sets, quantum chemical methods, and corrections in order to identify appropriate levels of theory that model the coordinate covalent bond accurately. The relationship between the accurate prediction of charge-transfer frustration, ionicity and covalency, and the structural and

energetic characterization of the coordinate covalent bond has been evaluated to provide a more comprehensive understanding of the coordinate covalent bond. Besides interest in the fundamental chemical physics of coordinate covalent bonds,[19, 240] this approach may be used as a predictive strategy for the structural and energetic properties of coordinate covalent bonds that have important consequences in the fields of storage and release of hydrogen as a fuel,[35-37] growth of uniform coatings on individual filaments for fiber-reinforced ceramic matrix composites,[38-41] and as new oncological,[42-44] cardiovascular, and anti-inflammatory drugs.[44-48]

3.2 Computational Approach

All electronic structure calculations have been explained in Chapter 2 and were carried out with Gaussian03[111] and NWChem 5.1[112] using the computational resources at the Center for Computational Sciences at Duquesne University.[256] Specifically, NWChem 5.1 was utilized for all M06-2X and M06 calculations while Gaussian03 was utilized for all HF, B3LYP, MPW1K, MPW1B95, MPWB1K, M05-2X, M05, MP2, QCISD, and QCISD(T) computations. It is important to note that due to computer resource limitations, full QCISD(T) optimizations were not possible, unless otherwise noted. However, single point (SP) energy calculations have been employed utilizing QCISD(T)//QCISD, where the basis set is the same for both the SP and geometry optimization.

Basis set superposition error corrected and uncorrected binding energetics for $H_3B–NH_3$ were predicted by HF, B3LYP, MPW1K, MP2, QCISD, and QCISD(T) in

combination with 48 Pople basis sets, ranging from 6-31G(d) to 6-311++G(3d2f,3p2d) and from Dunning's cc-pVDZ to aug-cc-pV5Z correlation consistent basis sets. Due to resource limitations, FOPTs could not be performed with QCISD or QCISD(T) with the aug-cc-pV5Z basis set. Consequently, single point energy calculations were performed with QCISD(T)/aug-cc-pV5Z and QCISD/aug-cc-pV5Z on MP2/6-311++G(3df,2p) optimized H_3B-NH_3 geometries. The basis sets employed are shown in Table 3.2.

Table 3.2. The Number of Basis Functions for Each Basis Set Pertaining to H_3B-NH_3.

Pople Basis Sets						
(X,Y)	6-31G (X,Y)	6-31+G (X,Y)	6-31++G (X,Y)	6-311G (X,Y)	6-311+G (X,Y)	6-311++G (X,Y)
(d)	42	50	56	54	62	68
(d,p)	60	68	74	72	80	86
(2d,p)	72	80	86	82	90	96
(2d,2p)	90	98	104	100	108	114
(3df,2p)	116	124	130	124	132	138
(3df,pd)	134	142	148	136	144	150
(3df,3pd)	170	178	184	172	180	186
(3d2f,3p2d)	220	228	234	216	224	230

Correlation Consistent Basis Sets		
X	cc-pVXZ	aug-cc-pVXZ
D	58	100
T	144	230
Q	290	436
5	512	734

At the time of this investigation, the MPW1B95, MPWB1K, M05-2X, M05, M06-2X, and M06 density functionals were unavailable. Consequently, the systematic analysis of basis set size and BSSE was not performed with MPW1B95, MPWB1K,

M05-2X, M05, M06-2X, or M06. However, as will be discussed, binding energies converge at the 6-311++G(3df,2p) basis set when employed with HF and the B3LYP and MPW1K density functionals. Thus, MPW1B95, MPWB1K, M05-2X, M05, M06-2X, and M06 BSSE corrected binding energies are predicted with the 6-311++G(3df,2p) basis set.

All energy minima have been confirmed by the absence of imaginary frequencies by vibrational frequency calculations utilizing B3LYP/6-31G(d). Enthalpy corrections were predicted utilizing B3LYP/6-31G(d) and scaled by 0.9989 in order to compute binding enthalpies at 298 K for the H_3B–NH_3 adduct. Enthalpy corrections have been scaled by 0.9941 to compute binding enthalpies for the remaining four adducts, for which the experimental binding enthalpies have been determined at 373 K. Scaling factors are known to be temperature dependent and are discussed in Chapter 2.12.

All NBO computations have been performed with HF, B3LYP, MPW1K, MPW1B95, MPWB1K, M05, M05-2X, and MP2 utilizing the 6-311++G(3df,2p) basis set on the corresponding optimized H_3B–NH_3 and methyl substituted ammonia trimethylborane structures to determine bond orders, bond covalencies, and bond ionicities corresponding to the B–N coordinate covalent bond. All NBO computations have been performed utilizing the NBO 5.G[220,113] program embedded within Gaussian03.

3.3 Convergence Rate and Value of the H_3B–NH_3 Coordinate Covalent Bond Length

A systematic evaluation of H_3B–NH_3 bond length across different chemical methods and basis sets has been carried out. The rate of bond length convergence as a function of the number of basis functions and the converged value have been compared to the reported experimental B–N bond length of 1.658 ± 0.002 Å, determined by microwave spectra of nine isotopic species of ammonia borane between 308 and 318 K.[26] A prior microwave spectra analysis of two isotopic species determined that the B–N bond length was 1.66 ± 0.03 Å,[257] where assumptions made resulted in a larger standard deviation than the more recent analysis. The latest account performed a full isotopic substitution of ammonia borane, allowing the assumed parameters in the first account to be determined directly; therefore, a more accurate B–N bond length was able to be determined. All computations in this study have been compared to the more recent account, where the B–N bond length was reported as 1.658 ± 0.002 Å.

The correlation consistent basis sets, ranging from cc-pVDZ to aug-cc-pV5Z, have been used for the geometry optimization of H_3B–NH_3, due to the systematic inclusion of electron correlation and possible extrapolation to the complete basis set limit. Convergence was estimated when the change in bond length between consecutive basis sets was less than 1×10^{-3} Å and for all subsequent pair-wise comparisons. For each chemical method utilized, smooth convergence is observed with and without augmentation, as shown by Figure 3.2.
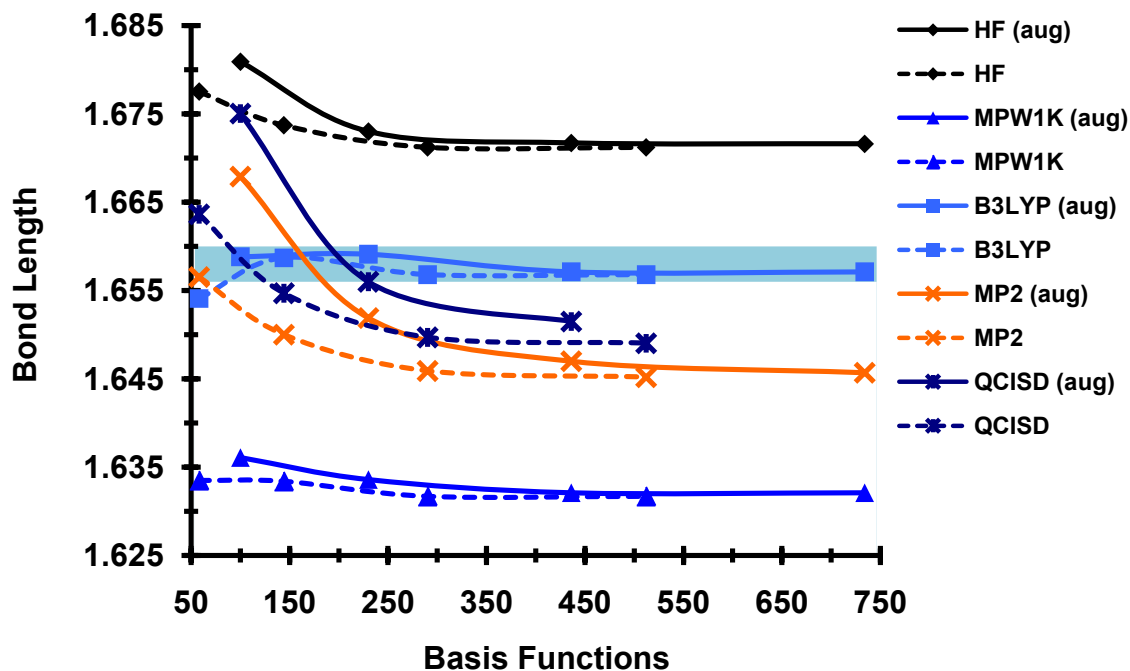
Figure 3.2. Convergence behavior of the $H_3B–NH_3$ coordinate covalent bond length (Å) vs. the number of basis functions employed with aug-cc-pVXZ (solid line) and cc-pVXZ (dashed line), where X is D, T, Q, or 5. The correspondence between the number of basis functions and the basis set is given in Table 3.2. The light blue area represents the range of uncertainty for the experimental gas phase result of 1.658 ± 0.002 Å.[26]

A number of important issues arise when considering how the bond length depends upon the number and type of basis functions utilized by a basis set. First, the inclusion of diffuse functions lengthens post-SCF bond lengths for smaller basis sets. Second, bond lengths modeled from correlation consistent basis sets with augmentation converge between aug-cc-pVQZ (436 basis functions) and aug-cc-pV5Z (734 basis functions) for each post-SCF method, where the bond lengths modeled with the cc-pVXZ basis sets (no augmentation) converge by 290 basis functions. Third, DFT and HF need less than half the basis functions to achieve convergence as compared to post-SCF methods. Fourth, considering converged values, HF overestimates the

experimental bond length by 0.014 Å, whereas B3LYP, QCISD, MP2 and MPW1K underestimate experiment by 0.001, 0.009, 0.012, and 0.026 Å, respectively. Thus, all methods using correlation consistent basis sets converge within 1% of the reported experimental value, except MPW1K. The B–N bond length predicted by B3LYP is the only method that converges within the uncertainty of 0.002 Å using the correlation consistent basis sets. Converged bond lengths predicted by HF, QCISD, MP2, and MPW1K differ from the experimental bond length by 0.013, 0.006, 0.011 and 0.026 Å, respectively. Importantly, post-SCF methods converge to shorter B–N bond lengths than predicted by experiment. This behavior is anticipated since the predicted geometries are computed at 0 K, whereas the experimental values were determined between 308 and 318 K. Figure 3.3 displays the convergence behavior of the B–N coordinate covalent bond lengths as a function of basis functions implemented by the Pople style 6-311++G(X,Y) basis sets for each chemical method. Predicted lengths by post-SCF methods converge to a B–N bond length near 150 basis functions [6-311++G(3df,pd)], whereas bond lengths predicted by DFT and HF converge earlier at 96 basis functions [6-311++G(2d,p)]. All converged bond lengths range between 1.632 and 1.672 Å, which is in moderate agreement with experiment.[26] The same order in increasing bond length with Pople basis sets is observed as with the correlation consistent basis sets (HF > B3LYP > QCISD > MP2 > MPW1K). Only bond lengths predicted by B3LYP converge within the accuracy of 0.002 Å, similarly to that observed with the correlation consistent basis sets. HF, MP2, and QCISD converge within 0.011 Å of the upper bound error (1.658 + 0.002 Å), 0.009 Å of the lower bound error (1.658 - 0.002 Å), and 0.004 Å of the lower bound, respectively. All B–N bond lengths predicted by the 6-311++G(X,Y)

basis sets converged to the bond lengths predicted by the correlation consistent basis sets within 0.2%.
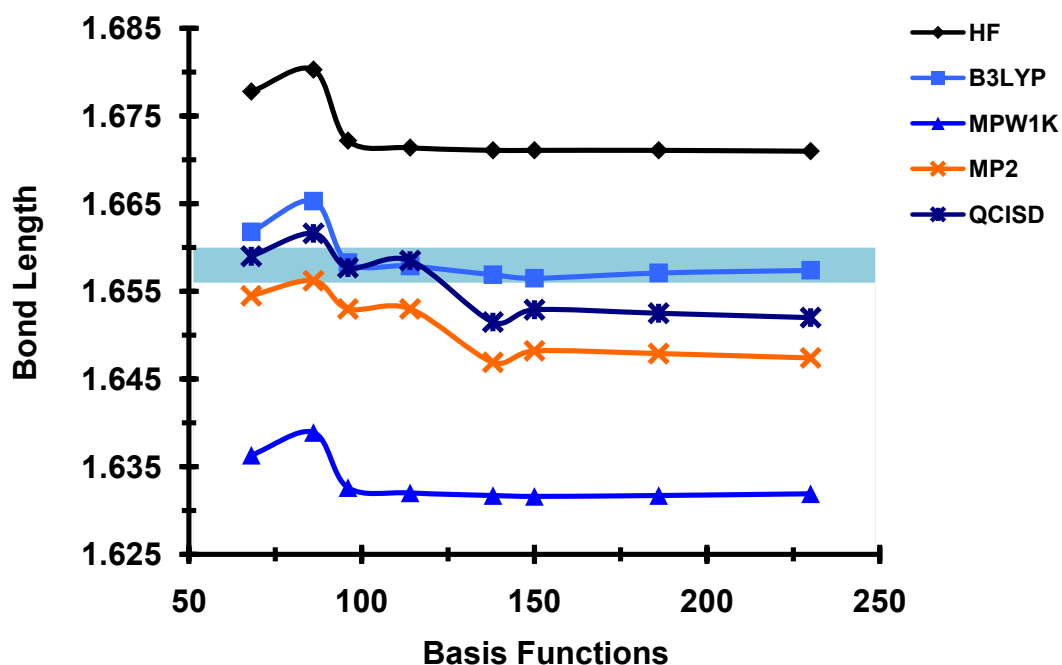
Figure 3.3. Convergence behavior of the $H_3B–NH_3$ coordinate covalent bond length (Å) vs. the number of basis functions employed with 6-311++G(X,Y). The correspondence between the number of basis functions and the basis set is given in Table 3.2. The light blue area represents the range of uncertainty for the experimental gas phase result of 1.658 ± 0.002 Å.[26]

The rate of convergence for the 6-31G(X,Y), 6-31+(X,Y), 6-31++(X,Y), 6-311G(X,Y), and 6-311++(X,Y) basis sets is shown by Figure 3.4 and was analyzed in the same manner as the 6-311++G(X,Y), cc-pVXZ, and aug-cc-pVXZ basis sets. The predicted bond lengths (converged and not converged) by all chemical methods and basis sets utilized in this study range between 1.631 and 1.689 Å, (Table 3.3) again in moderate agreement with experiment.[26] There are a few notable points. For example,

double-zeta split-valence quality basis sets [i.e., 6-31G(X,Y), 6-31+G(X,Y), and 6-31++G(X,Y)] do not necessarily produce a converged B–N bond length. In fact, the predicted change in bond length by DFT methods and HF never converged. Post-SCF methods also had trouble yielding a converged B–N bond length for the double-zeta basis sets, but converged when employing $3df$ and $3dp$ polarization functions on the heavy and hydrogen atoms, respectively.
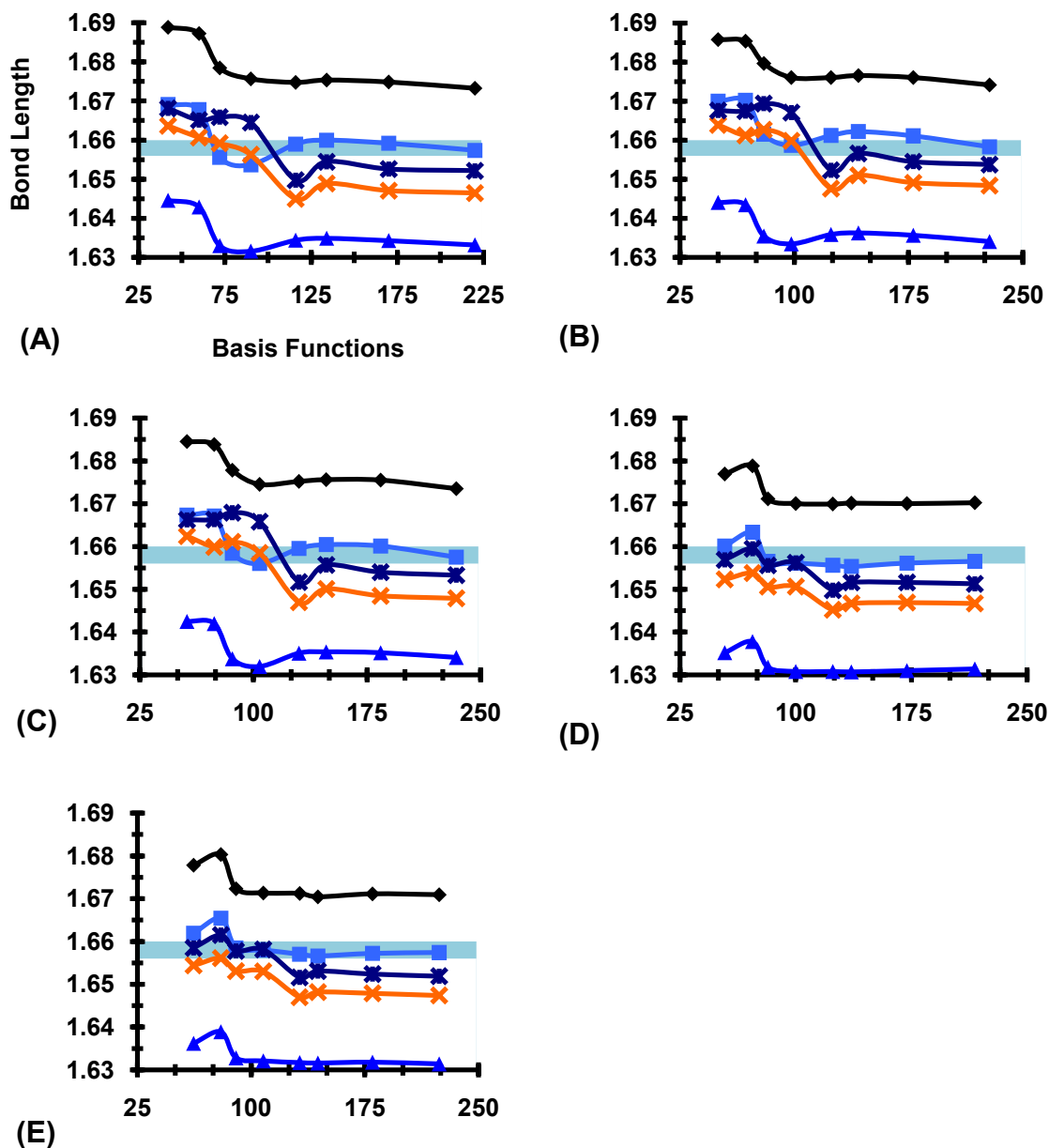
Figure 3.4. Convergence behavior of the $H_3B–NH_3$ coordinate covalent bond length (Å) vs. the number of basis functions employed with 6-31G(X,Y) (A), 6-31+G(X,Y) (B), 6-31++G(X,Y) (C), 6-311G(X,Y) (D), and 6-311+G(X,Y) (E). The correspondence between the number of basis functions and the basis set is given in Table 3.2. The light blue area represents the range of uncertainty for the experimental gas phase result of 1.658 ± 0.002 Å.[26]

89

Table 3.3. Predicted $H_3B–NH_3$ Coordinate Covalent Bond Lengths (Å). Experimental B–N Bond Length is 1.658 ± 0.002 Å.

	Basis Functions	MPW1K	B3LYP	MP2	HF	QCISD
6-31G(d)	42	1.6446	1.6691	1.6637	1.6889	1.6681
6-31G(d,p)	60	1.6429	1.6678	1.6607	1.6873	1.6651
6-31G(2d,p)	72	1.6330	1.6556	1.6592	1.6785	1.6659
6-31G(2d,2p)	90	1.6316	1.6537	1.6563	1.6757	1.6645
6-31G(3df,2p)	116	1.6344	1.6590	1.6450	1.6748	1.6498
6-31G(3df,pd)	134	1.6349	1.6600	1.6489	1.6754	1.6545
6-31G(3df,3pd)	170	1.6343	1.6592	1.6471	1.6749	1.6526
6-31G(3d2f,3p2d)	220	1.6332	1.6574	1.6465	1.6733	1.6522
6-31+G(d)	50	1.6441	1.6700	1.6639	1.6857	1.6676
6-31+G(d,p)	68	1.6435	1.6702	1.6612	1.6853	1.6675
6-31+G(2d,p)	80	1.6355	1.6615	1.6627	1.6796	1.6694
6-31+G(2d,2p)	98	1.6335	1.6587	1.6598	1.6760	1.6671
6-31+G(3df,2p)	124	1.6359	1.6612	1.6476	1.6760	1.6523
6-31+G(3df.pd)	142	1.6363	1.6622	1.6510	1.6765	1.6566
6-31+G(3df,3pd)	178	1.6357	1.6611	1.6491	1.6760	1.6545
6-31+G(3d2f,3p2d)	228	1.6341	1.6583	1.6484	1.6741	1.6538
6-31++G(d)	56	1.6425	1.6673	1.6624	1.6845	1.6662
6-31++G(d,p)	74	1.6420	1.6671	1.6599	1.6838	1.6663
6-31++G(2d,p)	86	1.6338	1.6584	1.6611	1.6778	1.6679
6-31++G(2d,2p)	104	1.6320	1.6560	1.6585	1.6745	1.6658
6-31++G(3df,2p)	130	1.6351	1.6595	1.6470	1.6752	1.6517
6-31++G(3df,pd)	148	1.6354	1.6604	1.6501	1.6756	1.6557
6-31++G(3df,3pd)	184	1.6352	1.6601	1.6485	1.6755	1.6540
6-31++G(3d2f,3p2d)	234	1.6341	1.6575	1.6479	1.6735	1.6533
6-311G(d)	54	1.6352	1.6601	1.6523	1.6769	1.6569
6-311G(d,p)	72	1.6378	1.6633	1.6538	1.6788	1.6595
6-311G(2d,p)	82	1.6318	1.6565	1.6506	1.6711	1.6556
6-311G(2d,2p)	100	1.6308	1.6561	1.6506	1.6700	1.6562
6-311G(3df,2p)	124	1.6308	1.6556	1.6452	1.6699	1.6498
6-311G(3df,pd)	136	1.6307	1.6553	1.6467	1.6701	1.6516
6-311G(3df,3pd)	172	1.6310	1.6561	1.6469	1.6700	1.6516
6-311G(3d2f,3p2d)	216	1.6314	1.6565	1.6467	1.6702	1.6513
6-311+G(d)	62	1.6362	1.6619	1.6544	1.6778	1.6585
6-311+G(d,p)	80	1.6389	1.6654	1.6561	1.6803	1.6615
6-311+G(2d,p)	90	1.6328	1.6585	1.6531	1.6723	1.6578
6-311+G(2d,2p)	108	1.6321	1.6580	1.6530	1.6713	1.6581
6-311+G(3df,2p)	132	1.6317	1.6570	1.6470	1.6712	1.6516
6-311+G(3df,pd)	144	1.6316	1.6566	1.6482	1.6704	1.6531
6-311+G(3df,3pd)	180	1.6318	1.6572	1.6479	1.6711	1.6524
6-311+G(3d2f,3p2d)	224	1.6314	1.6574	1.6474	1.6709	1.6519

Table 3.3. (continued).

6-311++G(d)	68	1.6363	1.6618	1.6545	1.6778	1.6590
6-311++G(d,p)	86	1.6389	1.6653	1.6562	1.6803	1.6616
6-311++G(2d,p)	96	1.6326	1.6583	1.6530	1.6722	1.6577
6-311++G(2d,2p)	114	1.6320	1.6579	1.6530	1.6714	1.6585
6-311++G(3df,2p)	138	1.6317	1.6569	1.6469	1.6711	1.6515
6-311++G(3df,pd)	150	1.6316	1.6565	1.6482	1.6711	1.6529
6-311++G(3df,3pd)	186	1.6317	1.6571	1.6479	1.6711	1.6525
6-311++G(3d2f,3p2d)	230	1.6319	1.6574	1.6474	1.6710	1.6520
cc-pVDZ	58	1.6335	1.6541	1.6565	1.6775	1.6636
cc-pVTZ	144	1.6334	1.6587	1.6500	1.6737	1.6547
cc-pVQZ	290	1.6317	1.6568	1.6459	1.6712	1.6497
cc-pV5Z	512	1.6317	1.6568	1.6452	1.6712	1.6490
aug-cc-pVDZ	100	1.6361	1.6588	1.6679	1.6809	1.6750
aug-cc-pVTZ	230	1.6336	1.6591	1.6519	1.6730	1.6560
aug-cc-pVQZ	436	1.6321	1.6571	1.6470	1.6717	1.6515
aug-cc-pV5Z	734	1.6321	1.6571	1.6457	1.6716	na

In general, quality of the basis set is important to predicting the B–N bond length. The triple-zeta split-valence quality basis sets [e.g. 6-311G(X,Y), 6-311+G(X,Y), and 6-311++G(X,Y)] yielded converged B–N bond lengths. In particular, the bond length predicted with the 6-311++G(X,Y) basis sets converged smoothly to the bond length yielded by the correlation consistent basis sets, and was found to be within 1% of the experimental accuracy of ± 0.002 Å for most methods employed. In the final assessment, the 6-311++G(3df,pd) and 6-311++G(2d,p) basis sets (150 and 96 basis functions, respectively) or greater are necessary to ensure a converged B–N coordinate covalent bond length for post-SCF methods and DFT or HF methods, respectively.

3.4 Sensitivity of Binding Enthalpy upon Variations in the H_3B–NH_3 Coordinate Covalent Bond Length

In order to investigate the energetic sensitivity upon bond length variation, binding enthalpies determined by MP2/aug-cc-pVXZ (X = D, T and Q) single point energy calculations on ammonia borane structures that possess the shortest and longest B–N bond lengths across all levels of theory considered were compared to binding enthalpies determined from full geometry optimizations at the MP2/aug-cc-pVXZ level of theory. MP2 has been chosen due to its accuracy and efficiency, as discussed in Chapter 3.7. The longest B–N bond length of 1.689 Å resulted from HF/6-31G(d) and the shortest of 1.632 Å was located using MPW1K/6-31G(2d,2p). Table 3.4 displays the predicted binding enthalpies, B–N coordinate covalent bond lengths, and corresponding differences between the higher and lower levels of theory. The largest binding enthalpy difference predicted was 0.2 kcal/mol. Thus, the data indicate that the predicted B–N bond length variation using different levels of theory (Table 3.1) does not account for the wide discrepancy of 23.2 kcal/mol in binding energies.

Table 3.4. Predicted $H_3B–NH_3$ Binding Enthalpies, ΔH_{298}, from Single Point (SP) Energy Evaluations and Full Geometry Optimizations (FOPT).[a,b]

	ΔH_{298} SP	ΔH_{298} FOPT Higher level	B–N FOPT Higher Level	B–N FOPT Lower Level	ΔB–N	$\Delta\Delta H_{298}$
MP2/aug-cc-pVDZ// HF/6-31G(d)	-26.7	-26.6	1.668	1.689	0.021	0.1
MP2/aug-cc-pVTZ// HF/6-31G(d)	-27.6	-27.8	1.652	1.689	0.037	0.2
MP2/aug-cc-pVQZ// HF/6-31G(d)	-27.9	-28.1	1.647	1.689	0.042	0.2
MP2/aug-cc-pVDZ// MPW1K/6-31G(2d,2p)	-26.5	-26.6	1.668	1.632	0.036	0.1
MP2/aug-cc-pVTZ// MPW1K /6-31G(2d,2p)	-27.8	-27.8	1.652	1.632	0.020	0.0
MP2/aug-cc-pVQZ// MPW1K /6-31G(2d,2p)	-28.1	-28.1	1.647	1.632	0.015	0.0
QCISD/aug-cc-pVDZ// MP2/6-311++G(3df,2p)	-24.7	-24.6	1.675	1.647	0.028	0.1
QCISD/6-311++G(d,p)// MP2/6-311++G(3df,2p)	-26.1	-26.1	1.662	1.647	0.015	0.0
QCISD/6-311++G(3df,2p)// MP2/6-311++G(3df,2p)	-26.2	-26.2	1.652	1.647	0.005	0.0
QCISD(T)/aug-cc-pVDZ// MP2/6-311++G(3df,2p)	-25.7	-25.7	1.677	1.647	0.030	0.0
QCISD(T)/6-311++G(d,p)// MP2/6-311++G(3df,2p)	-27.4	-27.4	1.662	1.647	0.015	0.0
QCISD(T)/6-311++G(3df,2p)// MP2/6-311++G(3df,2p)	-27.5	-27.5	1.653	1.647	0.006	0.0

[a] All energies are in kcal/mol.
[b] All bond lengths are in Å

Considering post-SCF methods, the B–N bond length converges at the

6-311++G(3df,pd) basis set. However, binding enthalpies converge earlier at the similar

6-311++G(3df,2p) basis set as discussed in Chapter 3.6. The use of 6-311++G(3df,2p)

instead 6-311++G(3df,dp) saves 12 basis functions for $H_3B–NH_3$ and 36 for the largest methyl substituted ammonia trimethylborane considered. Despite the resource savings, FOPTs remain impractical on the larger methyl substituted ammonia trimethylborane structures with available resources utilizing QCISD and QCISD(T) with either basis set. However, SP energy evaluations and BSSE corrections were possible with QCISD and QCISD(T) using the 6-311++G(3df,2p) basis set. To justify this approach, QCISD SP energy evaluations using small (aug-cc-pVDZ) to large (6-311++G(3df,2p)) basis sets on MP2/6-311++G(3df,2p) optimized $H_3B–NH_3$ structures were compared to QCISD/6-311++G(3df,2p) FOPT energies. As shown in Table 3.4, there is a negligible (< 0.1 kcal/mol) difference between binding enthalpies determined by the QCISD FOPTs and SPs. Finally, QCISD(T) SP energies on MP2 optimized structures were compared to QCISD(T) FOPT energies. As seen in Table 3.4, QCISD(T) FOPT binding enthalpies differ from QCISD(T)//MP2 values by an insignificant amount (< 0.0 kcal/mol). The data suggest that performing QCISD and QCISD(T) SP energy evaluations on MP2 optimized structures is a valid approximation to analyze the larger trimethylboranes. Consequently, energy evaluations were conducted using the 6-311++G(3df,2p) basis set rather than the unbalanced 6-311++G(3df,pd) basis set.

3.5 Impact of Basis Set Superposition Error upon Binding Enthalpies between BH_3 and NH_3

The influence of BSSE has been well-documented,[184, 201, 204, 206-208, 243, 244] but has been inconsistently applied to the energetics concerning the coordinate covalent bond, as

summarized by Table 3.1. To investigate the impact of this factor on coordinate covalent bonding systematically, the amount BSSE has been determined for each method utilizing the correlation consistent basis sets, as shown by Figure 3.5. In general, the BSSE corrected binding enthalpies are weaker than those not corrected for BSSE.
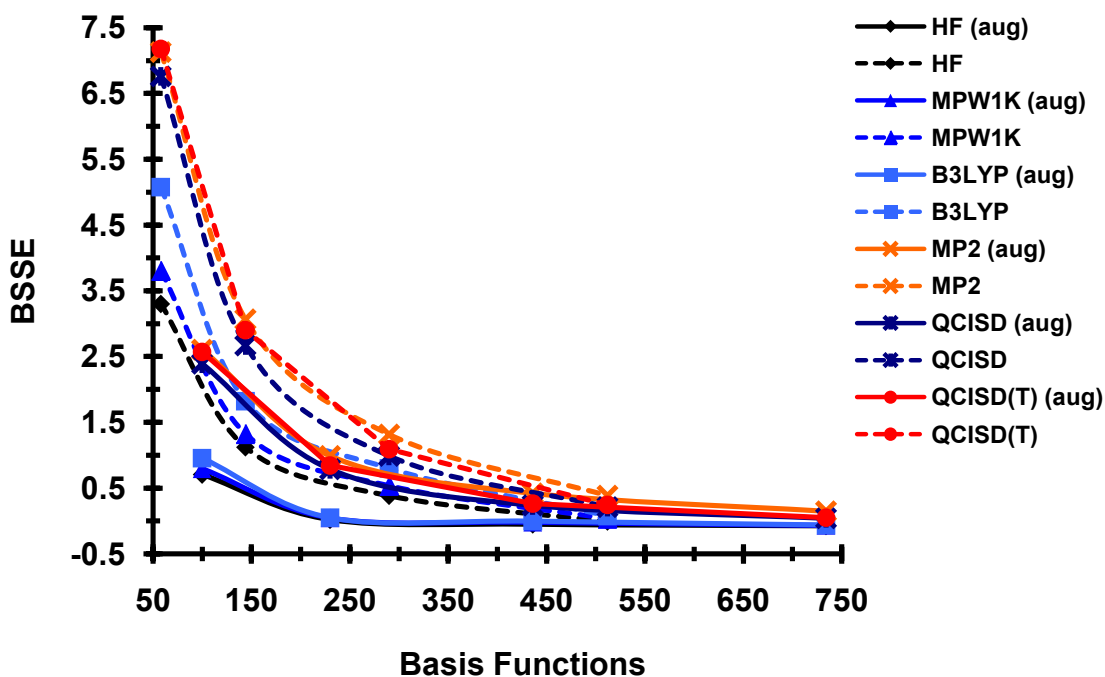
Figure 3.5. Basis set superposition error (BSSE) (kcal/mol) for HF, B3LYP, MPW1K, MP2, QCISD, and QCISD(T) utilizing the cc-pVXZ (dashed lines) and aug-cc-pVXZ (solid lines) basis sets. The BSSE is determined by subtracting the uncorrected ΔH_{298} from the BSSE corrected ΔH_{298}. QCISD and QCISD(T) BSSE corrections employed with the aug-cc-pv5z basis set are performed on the MP2/6-311++G(3df,2p) optimized structure.

Two interesting trends are observed for the BSSE corrected binding enthalpies. First, cc-pVXZ basis sets result in more BSSE than the augmented basis sets, especially with smaller basis sets. Second, post-SCF computations result with increased BSSE, as

compared to DFT and HF. It has been previously noted that methods incorporating

electron correlation result in more BSSE as compared to HF and DFT methods with

smaller basis sets.[201, 243, 244, 255] For example, the cc-pVDZ basis set (58 basis functions)

with post-SCF, DFT, and HF methods incorporates BSSE on the order of *ca*. 7.0, 4.5,

and 3.5 kcal/mol, respectively. BSSE is practically eliminated (0.0 to 0.4 kcal/mol) with

the use of the cc-pV5Z basis set (512 basis functions). More specifically, BSSE is

completely removed for DFT and HF with the use of the aug-cc-pVTZ basis set (230

basis functions), whereas aug-cc-pVQZ (436 basis functions) is needed to eliminate

BSSE (0.2 to 0.4 kcal/mol) for post-SCF methods. The same trend is seen for the Pople

basis sets, where basis sets lacking diffuse functions incorporate more BSSE than those

that include diffuseness. The amount of BSSE yielded for all basis sets and HF, B3LYP,

MPW1K, MP2, QCISD, and QCISD(T) are reported in Table 3.5. In general, the basis

sets typically employed (Table 3.1) in the evaluation of the coordinate covalent bond are

too small and require the adjustment for BSSE.

Table 3.5. Amount of BSSE in Predicted Binding Enthalpies for H_3B–NH_3 at 298 K.[a]

	Basis Functions	MPW1K	B3LYP	MP2	HF	QCISD	QCISD(T)
6-31G(d)	42	2.6	3.0	6.2	2.4	6.2	6.6
6-31G(d,p)	60	2.5	3.1	5.8	2.2	5.8	6.2
6-31G(2d,p)	72	2.2	3.1	4.7	1.9	4.5	4.8
6-31G(2d,2p)	90	2.4	3.4	4.7	2.1	4.4	4.7
6-31G(3df,2p)	116	2.5	3.5	5.0	2.1	4.5	4.8
6-31G(3df,pd)	134	2.4	3.2	4.7	2.0	4.3	4.6
6-31G(3df,3pd)	170	2.3	2.9	4.0	2.0	3.5	3.8
6-31G(3d2f,3p2d)	220	2.3	2.9	3.8	2.0	3.4	3.6
6-31+G(d)	50	1.9	1.7	5.2	1.8	5.3	5.7
6-31+G(d,p)	68	1.4	1.3	4.5	1.2	4.6	4.9
6-31+G(2d,p)	80	0.6	0.7	2.7	0.5	2.6	2.9
6-31+G(2d,2p)	98	0.5	0.6	2.3	0.4	2.1	2.4
6-31+G(3df,2p)	124	0.2	0.2	2.2	0.2	1.9	2.2
6-31+G(3df.pd)	142	0.3	0.2	2.1	0.3	2.0	2.2
6-31+G(3df,3pd)	178	0.3	0.2	1.6	0.3	1.4	1.5
6-31+G(3d2f,3p2d)	228	0.3	0.4	1.5	0.3	1.2	1.3
6-31++G(d)	56	1.8	1.7	5.2	1.6	5.3	5.6
6-31++G(d,p)	74	1.4	1.4	4.5	1.2	4.6	5.0
6-31++G(2d,p)	86	0.6	0.7	2.7	0.5	2.7	2.9
6-31++G(2d,2p)	104	0.5	0.6	2.3	0.4	2.2	2.4
6-31++G(3df,2p)	130	0.2	0.3	2.2	0.2	1.9	2.2
6-31++G(3df,pd)	148	0.2	0.3	2.2	0.3	2.1	2.3
6-31++G(3df,3pd)	184	0.3	0.2	1.6	0.3	1.4	1.5
6-31++G(3d2f,3p2d)	234	0.3	0.4	1.4	0.3	1.2	1.3
6-311G(d)	54	4.2	4.9	8.7	3.6	8.4	8.9
6-311G(d,p)	72	3.1	3.9	6.9	2.8	6.5	7.0
6-311G(2d,p)	82	2.6	3.4	5.4	2.3	5.1	5.4
6-311G(2d,2p)	100	2.5	3.2	4.9	2.2	4.5	4.8
6-311G(3df,2p)	124	2.5	3.3	4.8	2.2	4.2	4.5
6-311G(3df,pd)	136	2.6	3.4	4.8	2.3	4.3	4.5
6-311G(3df,3pd)	172	1.7	2.1	3.3	1.5	2.9	3.1
6-311G(3d2f,3p2d)	216	1.6	1.9	3.0	1.4	2.6	2.7
6-311+G(d)	62	2.7	2.6	6.7	2.3	6.6	7.0
6-311+G(d,p)	80	1.1	1.1	4.3	1.0	4.2	4.6
6-311+G(2d,p)	90	0.6	0.6	2.8	0.5	2.8	3.0
6-311+G(2d,2p)	108	0.3	0.3	2.1	0.2	1.9	2.1
6-311+G(3df,2p)	132	0.2	0.2	1.7	0.2	1.5	1.6
6-311+G(3df,pd)	144	0.3	0.2	1.7	0.2	1.5	1.7
6-311+G(3df,3pd)	180	0.2	0.2	1.4	0.2	1.2	1.3
6-311+G(3d2f,3p2d)	224	0.2	0.2	1.3	0.2	1.1	1.2

Table 3.5. (continued)

6-311++G(d)	68	2.6	2.5	6.5	2.2	6.5	6.8
6-311++G(d,p)	86	1.1	1.1	4.3	0.9	4.2	4.6
6-311++G(2d,p)	96	0.6	0.6	2.8	0.4	2.7	3.0
6-311++G(2d,2p)	114	0.3	0.3	2.1	0.2	1.9	2.1
6-311++G(3df,2p)	138	0.2	0.2	1.7	0.2	1.5	1.6
6-311++G(3df,pd)	150	0.3	0.2	1.7	0.2	1.5	1.7
6-311++G(3df,3pd)	186	0.2	0.2	1.4	0.2	1.2	1.3
6-311++G(3d2f,3p2d)	230	0.2	-0.1	1.3	0.2	1.1	1.2
cc-pVDZ	58	3.8	5.1	7.1	3.3	6.8	7.2
cc-pVTZ	144	1.3	1.8	3.1	1.1	2.7	2.9
cc-pVQZ	290	0.5	0.8	1.3	0.4	1.0	1.1
cc-pV5Z	512	0.0	0.1	0.4	0.0	0.2	0.2
aug-cc-pVDZ	100	0.8	1.0	2.6	0.7	2.4	2.6
aug-cc-pVTZ	230	0.0	0.0	1.0	0.0	0.8	0.8
aug-cc-pVQZ	436	0.0	0.0	0.4	0.0	0.2	0.3
aug-cc-pV5Z	734	-0.1	-0.1	0.1	-0.1	0.0[b]	0.0[b]

[a] All energies are in kcal/mol. The difference between BSSE corrected and uncorrected ΔH_{298} is the amount of BSSE each basis set incorporates.
[b] SP energy evaluations have been performed on MP2/6-311++G(3df,2p) optimized structures.

BSSE was not systematically investigated for the M06-2X, M06, M05-2X, M05, MPW1B95, and MPWB1K functionals due to their unavailability at the time of this analysis. However, a brief account of BSSE regarding the untested functionals is warranted and thus presented. As will be discussed in Chapter 3.6, binding enthalpies converge at the 6-311++G(3df,2p) basis set as a function of the number of basis functions. Consequently, the impact of BSSE on binding enthalpies predicted by M06-2X, M06, M05-2X, M05, MPW1B95, and MPWB1K in conjunction with the 6-311++G(3df,2p) basis set has been explored and compared to the BSSE yielded with HF, B3LYP, and MPW1K and the same basis set. The amount of BSSE for all DFT methods and HF utilizing the 6-311++G(3df,2p) basis set is summarized in Table 3.6. M06, M06-2X, M05, M05-2X, MPWB1K, and MPW1B95 yield BSSEs comparable to

that found for HF, B3LYP, and MPW1K. Since HF, B3LYP and MPW1K yield a

converged binding enthalpy at this basis set, it is reasonable to assume that the

remaining functionals behave similarly. A M06-2X/aug-cc-pVQZ optimization of

ammonia borane supports this assumption; where the B–N coordinate covalent bond

length and BSSE corrected binding enthalpy differ from that predicted by

M06-2X/6-311++G(3df,2p) by 0.0008 Å and 0.2 kcal/mol, respectively. Consequently,

M06-2X is used with the 6-311++G(3df,2p) basis set to deliver a value near

convergence with a minimum amount of BSSE without jeopardizing efficiency and

practicality.

Table 3.6. Amount of BSSE in Predicted Binding Enthalpies for $H_3B–NH_3$ and $(CH_3)_3B−N(CH_3)_nH_{3-n}$ (n = 0 to 3).[a]

	BH_3-NH_3	n=0	n=1	n=2	n=3	Average
HF[24]	0.2	0.3	0.3	0.3	0.4	0.3
M05[173]	0.2	0.4	0.3	0.4	0.4	0.4
B3LYP[24]	0.2	0.3	0.3	0.4	0.4	0.3
MPW1K[24]	0.2	0.3	0.4	0.4	0.5	0.4
M06[173]	0.3	0.4	0.5	0.6	0.7	0.5
MPW1B95[173]	0.2	0.3	0.3	0.4	0.5	0.3
MPWB1K[173]	0.2	0.3	0.3	0.3	0.4	0.3
M05-2X[173]	0.2	0.3	0.4	0.5	0.6	0.4
M06-2X[173]	0.2	0.3	0.5	0.5	0.7	0.4

[a] BSSE computed by subtracting the ΔH BSSE corrected value from the ΔH uncorrected value. The 6-311++G(3df,2p) basis set has been utilized. All values in kcal/mol.

3.6 Convergence Rate of $H_3B–NH_3$ Binding Enthalpy

The binding enthalpy convergence for $H_3B–NH_3$ was analyzed in the same

manner as for the bond length. The rate of binding enthalpy convergence with BSSE

corrections as a function of the number of basis functions has been determined, and the

converged value has been compared to estimations provided by Haaland (-31.1 ± 1.0

kcal/mol),[19] Gurvich (-37.5 ± 4.3 kcal/mol),[249] and Piela (-25.7 ± 2.0 kcal/mol).[204] The

experimental binding enthalpy has not been reported. Convergence was identified when

the change in binding enthalpy between consecutive basis sets, and for all subsequent

pair-wise comparisons, was less than 0.3 kcal/mol. For each chemical method utilized,

smooth convergence is observed for the correlation consistent basis sets with and

without augmentation, as shown by Figure 3.6.
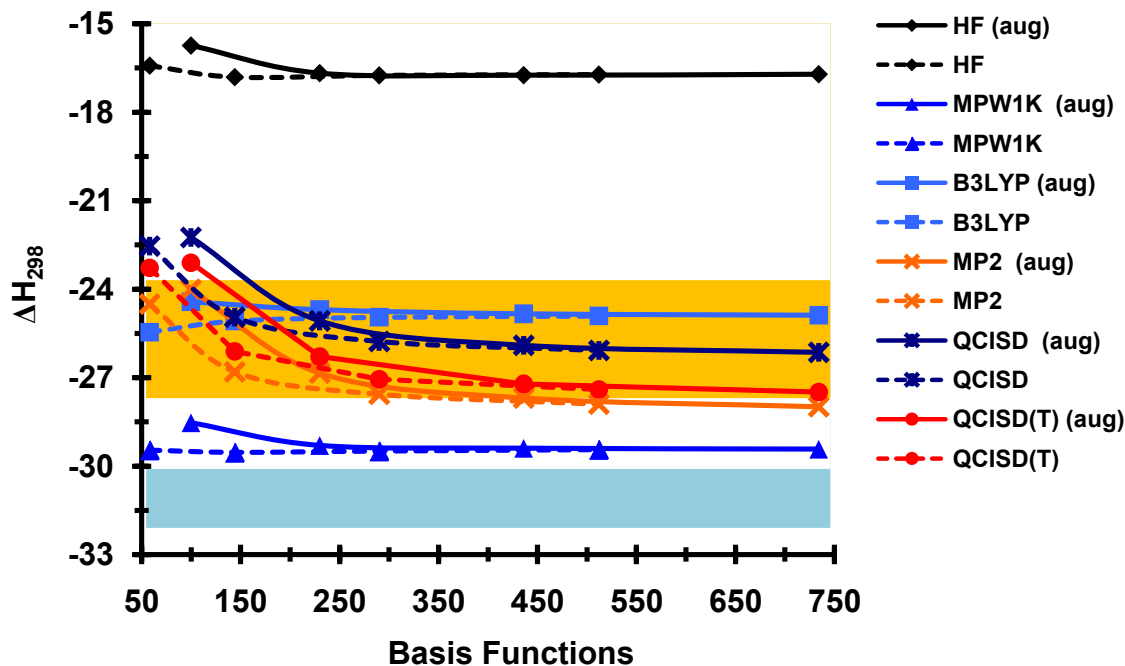
Figure 3.6. BSSE corrected H_3B–NH_3 binding enthalpies, ΔH_{298} (kcal/mol), vs. basis functions for aug-cc-pVXZ (solid line) and cc-pVXZ (dashed line) (X = D, T, Q, and 5). The blue and orange areas represent Haaland's estimation (-31.1 ± 1.0 kcal/mol) and Piela's estimation (-25.7 ± 2.0 kcal/mol), respectively. Gurvich's estimation (-37.5 ± 4.3 kcal/mol) is not shown on the figure. The QCISD(T)/aug-cc-pV5Z data point is a SP energy evaluation on the MP2/6-311++G(3df,2p) optimized structure.

Three important conclusions can be drawn concerning the predicted BSSE corrected ΔH_{298}, utilizing the correlation consistent basis sets. First, the inclusion of diffuse functions is significant for smaller basis set computations, such as those reported in Table 3.1. Each method with augmentation underestimates the converged binding enthalpy by several kcal/mol up until about 225 basis functions. Second, the binding enthalpy convergence is slower using post-SCF methods, as compared to DFT and HF. For example, MP2, QCISD, and QCISD(T) binding enthalpies continue to change by 0.2

to 0.3 kcal/mol between cc-pVQZ and cc-pV5Z with and without augmentation. Further

evaluation using cc-pV6Z is currently not possible due to resource limitations. In

contrast, binding enthalpies predicted by DFT and HF converge earlier between

cc-pVTZ (144 basis functions) and aug-cc-pVTZ (230 basis functions). Third, DFT and

post-SCF binding enthalpy predictions fall between the Piela and Haaland estimates. As

expected, the order of converged binding enthalpies supports the order of B–N bond

lengths. The weakest to strongest binding enthalpies are HF < B3LYP < QCISD <

QCISD(T) < MP2 < MPW1K. Both HF and MPW1K are in poor energetic agreement

with the previous estimates. Lastly, BSSE corrected ΔH_{298} converge to the same BSSE

uncorrected ΔH_{298} for each method. Consequently, the BSSE approaches zero in the

limit of the complete basis set, as discussed in Chapter 2.9.

For Pople basis sets, the convergence of the BSSE corrected ΔH_{298} has been

analyzed using the 6-311++G(X,Y) basis sets, which is shown by Figure 3.7. All

methods yield converged binding enthalpies at the 6-311++G(3df,2p) basis set, the same

converged value as predicted by the correlation consistent basis sets, except post-SCF

methods. MP2, QCISD, and QCISD(T) in conjunction with the 6-311++G(3df,2p) basis

set predict weaker binding enthalpies than with the aug-cc-pV5Z basis set by 1.5, 1.3

and 1.6 kcal/mol, respectively. It is found that the post-SCF predicted and BSSE

corrected binding enthalpies converge slowly and do not converge even when the largest

Pople basis set is employed. It is assumed that post-SCF predicted and BSSE corrected

binding enthalpies will converge eventually to that predicted by the aug-cc-pV5Z basis

set when polarization functions are added to the 6-311++G(X,Y) basis sets, as found for

the B–N bond lengths. As a consequence, the residual error of 1.5, 1.3 and 1.6 kcal/mol

for MP2, QCISD, and QCISD(T), respectively, called the "convergence correction," will

be subtracted (increase the magnitude) from the predicted ΔH_{373} for methyl substituted

ammonia trimethylboranes discussed in the Chapter 3.7. All BSSE corrected binding

enthalpies predicted by all levels of theory are reported in Table 3.7. It must be

remembered that although all binding enthalpies have been corrected for BSSE, the

larger basis sets incorporate a negligible amount of BSSE; therefore, in practice, BSSE

does not need to be corrected when larger basis sets are utilized.
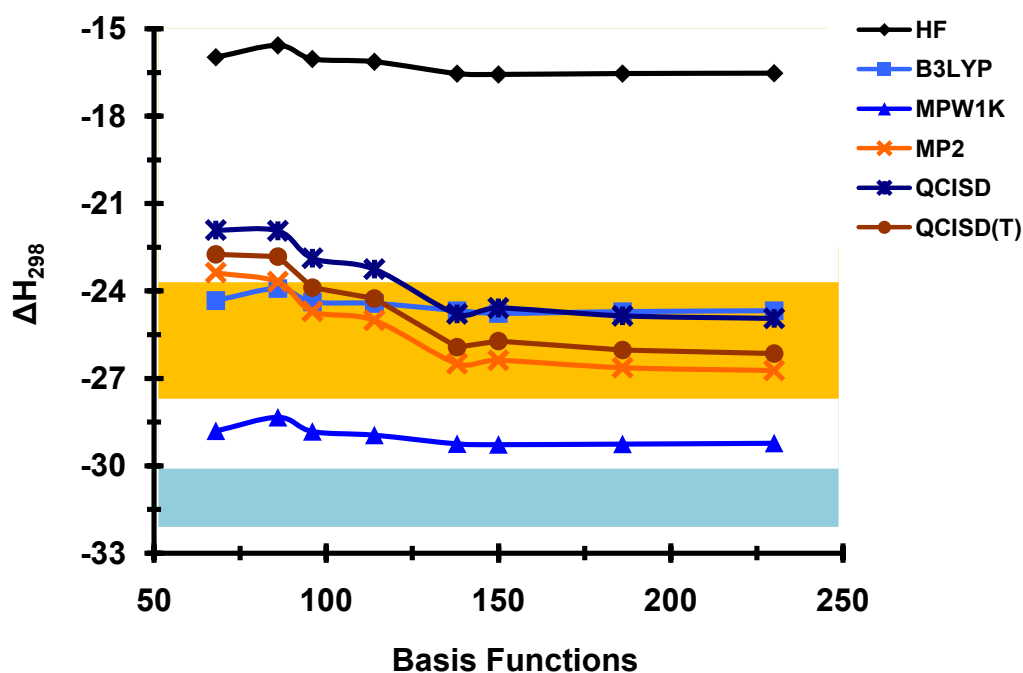
Figure 3.7. BSSE corrected $H_3B–NH_3$ binding enthalpies, ΔH_{298} (kcal/mol), vs. basis functions for 6-311++G(X,Y). The light blue and light orange areas represent Haaland's estimation (-31.1 ± 2.0 kcal/mol) and Piela's estimation (-25.7 ± 1.0 kcal/mol), respectively. Gurvich's estimation (-37.5 ± 4.3 kcal/mol) is not shown on the figure.

Table 3.7. BSSE Corrected Binding Enthalpies for $H_3B–NH_3$ at 298 K.[a]

	Basis Functions	MPW1K	B3LYP	MP2	HF	QCISD	QCISD(T)
6-31G(d)	42	-30.2	-25.7	-24.2	-17.1	-22.6	-23.3
6-31G(d,p)	60	-29.8	-25.3	-23.9	-16.7	-22.1	-22.8
6-31G(2d,p)	72	-29.2	-24.7	-24.0	-16.0	-21.9	-22.7
6-31G(2d,2p)	90	-29.1	-24.6	-24.4	-15.9	-22.4	-23.2
6-31G(3df,2p)	116	-28.6	-23.7	-25.3	-16.0	-23.6	-24.6
6-31G(3df,pd)	134	-28.7	-23.8	-25.3	-16.1	-23.5	-24.5
6-31G(3df,3pd)	170	-28.7	-23.8	-25.7	-16.0	-24.0	-25.0
6-31G(3d2f,3p2d)	220	-28.9	-24.3	-26.2	-16.2	-24.5	-25.6
6-31+G(d)	50	-29.0	-24.3	-22.7	-16.0	-21.3	-22.0
6-31+G(d,p)	68	-28.5	-23.9	-22.4	-15.7	-20.8	-21.6
6-31+G(2d,p)	80	-28.4	-23.8	-23.0	-15.4	-21.1	-21.9
6-31+G(2d,2p)	98	-28.4	-23.8	-23.5	-15.4	-21.7	-22.6
6-31+G(3df,2p)	124	-28.8	-24.1	-25.6	-16.1	-23.9	-24.9
6-31+G(3df.pd)	142	-28.8	-24.1	-25.5	-16.2	-23.7	-24.7
6-31+G(3df,3pd)	178	-28.9	-24.2	-26.0	-16.2	-24.3	-25.4
6-31+G(3d2f,3p2d)	228	-29.0	-24.5	-26.4	-16.3	-24.7	-25.8
6-31++G(d)	56	-29.2	-24.6	-22.9	-16.2	-21.6	-22.3
6-31++G(d,p)	74	-28.7	-24.2	-22.6	-15.8	-21.0	-21.8
6-31++G(2d,p)	86	-28.6	-24.1	-23.2	-15.6	-21.3	-22.2
6-31++G(2d,2p)	104	-28.7	-24.1	-23.7	-15.6	-21.9	-22.8
6-31++G(3df,2p)	130	-28.9	-24.3	-25.8	-16.3	-24.1	-25.1
6-31++G(3df,pd)	148	-28.9	-24.3	-25.6	-16.3	-23.9	-24.9
6-31++G(3df,3pd)	184	-29.0	-24.3	-26.2	-16.3	-24.4	-25.5
6-31++G(3d2f,3p2d)	234	-29.1	-24.6	-26.6	-16.4	-24.8	-26.0
6-311G(d)	54	-29.4	-25.2	-24.2	-16.5	-22.6	-23.4
6-311G(d,p)	72	-29.0	-24.8	-24.5	-16.1	-22.6	-23.5
6-311G(2d,p)	82	-29.4	-25.1	-25.3	-16.5	-23.4	-24.4
6-311G(2d,2p)	100	-29.4	-25.0	-25.6	-16.6	-23.8	-24.8
6-311G(3df,2p)	124	-29.5	-25.0	-26.8	-16.8	-25.0	-26.2
6-311G(3df,pd)	136	-29.6	-25.1	-26.7	-16.8	-24.8	-25.9
6-311G(3df,3pd)	172	-29.5	-24.9	-26.8	-16.7	-25.0	-26.2
6-311G(3d2f,3p2d)	216	-29.4	-24.8	-26.8	-16.6	-25.0	-26.2
6-311+G(d)	62	-28.8	-24.3	-23.3	-15.9	-21.9	-22.7
6-311+G(d,p)	80	-28.3	-23.9	-23.7	-15.6	-21.9	-22.8
6-311+G(2d,p)	90	-28.8	-24.4	-24.7	-16.0	-22.9	-23.9
6-311+G(2d,2p)	108	-28.9	-24.4	-25.0	-16.1	-23.2	-24.2
6-311+G(3df,2p)	132	-29.2	-24.7	-26.5	-16.5	-24.8	-25.9
6-311+G(3df,pd)	144	-29.3	-24.8	-26.4	-16.6	-24.6	-25.7
6-311+G(3df,3pd)	180	-29.3	-24.7	-26.6	-16.5	-24.9	-26.0
6-311+G(3d2f,3p2d)	224	-29.2	-24.7	-26.7	-16.5	-24.9	-26.1
6-311++G(d)	68	-28.8	-24.3	-23.4	-16.0	-21.9	-22.7
6-311++G(d,p)	86	-28.3	-23.9	-23.7	-15.6	-21.9	-22.8

Table 3.7. (continued)

6-311++G(2d,p)	96	-28.8	-24.4	-24.7	-16.0	-22.9	-23.9
6-311++G(2d,2p)	114	-28.9	-24.4	-25.0	-16.1	-23.3	-24.3
6-311++G(3df,2p)	138	-29.2	-24.7	-26.5	-16.5	-24.8	-25.9
6-311++G(3df,pd)	150	-29.3	-24.8	-26.4	-16.6	-24.6	-25.7
6-311++G(3df,3pd)	186	-29.3	-24.7	-26.6	-16.5	-24.9	-26.0
6-311++G(3d2f,3p2d)	230	-29.2	-24.7	-26.7	-16.5	-24.9	-26.1
cc-pVDZ	58	-29.5	-25.5	-24.5	-16.4	-22.5	-23.3
cc-pVTZ	144	-29.5	-25.1	-26.8	-16.8	-25.0	-26.1
cc-pVQZ	290	-29.5	-25.0	-27.6	-16.8	-25.8	-27.1
cc-pV5Z	512	-29.4	-24.9	-27.9	-16.7	-26.1	-27.4
aug-cc-pVDZ	100	-28.5	-24.4	-24.0	-15.7	-22.3	-23.1
aug-cc-pVTZ	230	-29.3	-24.7	-26.9	-16.7	-25.1	-26.3
aug-cc-pVQZ	436	-29.4	-24.8	-27.7	-16.7	-25.9	-27.2
aug-cc-pV5Z	734	-29.4	-24.9	-28.0	-16.7	-26.1[b]	-27.5[b]

[a] All energies are in kcal/mol.
[b] SP energy evaluation on MP2/6-311++G(3df,2p) optimized structures.

Our final prediction for the binding enthalpy at 298 K for ammonia borane is

-27.5 ± 0.5 kcal/mol, using QCISD(T)/aug-cc-pV5Z with BSSE corrections on the

MP2/6-311++G(3df,2p) optimized geomertry. However, BSSE is insignificant at such a

large basis set (Table 3.5) and can be ignored. The error of 0.5 kcal/mol is estimated

from the QCISD(T) mean absolute deviation (MAD) of four methyl substituted

ammonia trimethylboranes analyzed and discussed in Chapter 3.7. The error of 0.5

kcal/mol is not unreasonable, because high accuracy compound methods, such as

Gaussian-4, report energetics with an average absolute deviation of 0.80 kcal/mol.[258]

Our prediction is within the uncertainty of Piela's -25.7 ± 2.0 kcal/mol,[204] yet

significantly weaker than Haaland's estimate of -31.1 ± 1.0 kcal/mol,[19] and Gurvich's

recommendation of -37.5 ± 4.3 kcal/mol.[249]

3.7 Accuracy Assessment of Binding Enthalpies for Methyl Substituted Ammonia Trimethylboranes

The binding enthalpies of four methyl substituted ammonia trimethylboranes, $(CH_3)_3B–NH_3$, $(CH)_3B–NH_2CH_3$, $(CH)_3B–NH(CH_3)_2$, and $(CH)_3B–N(CH_3)_3$ have been predicted with HF, B3LYP, MPW1K, MPW1B95, MPWB1K, M05-2X, M05, M06-2X, M06, MP2, QCISD, and QCISD(T) using the 6-311++G(3df,2p) basis set and compared with experiment.[252] Although the MPW1B95, MPWB1K, M05-2X, M05, M06-2X, and M06 density functionals were not systematically analyzed with regard to basis set size and BSSE, as completed for HF, B3LYP, MPW1K, MP2, QCISD, and QCISD(T), the convergence rate observed with other DFT methods, such as MPW1K and B3LYP, allow us to assume that the untested DFT methods will converge similarly at the 6-311++G(3df,2p) basis set. Support for this assumption is discussed in Chapter 3.5. Consequently, all methods employ the 6-311++G(3df,2p) basis set to achieve a converged binding enthalpy. BSSE corrections as well as the appropriate convergence corrections for MP2 (1.5 kcal/mol), QCISD (1.3 kcal/mol), and QCISD(T) (1.6 kcal/mol) have been applied. Table 3.8 displays the BSSE corrected binding enthalpies at the appropriate temperature.

Table 3.8. Predicted and Experimental Binding Enthalpies for Ammonia Borane and $(CH_3)_3B-N(CH_3)_nH_{3-n}$ (n = 0 to 3), ΔH_T.[a]

	BH_3-NH_3	n = 0	n = 1	n = 2	n = 3	MAD
HF[24]	-16.5	-2.0	-3.5	-1.2	3.6	15.2
M05[173]	-23.2	-6.8	-9.0	-7.3	-2.4	9.4
B3LYP[24]	-24.7	-6.8	-8.8	-7.0	-2.4	9.2
MPW1K[24]	-29.2	-11.9	-14.2	-12.9	-9.1	4.4
M06[173]	**-25.3**	**-10.3**	**-14.0**	**-14.5**	**-12.5**	**3.9**
MPW1B95[173]	-30.0	-12.5	-15.4	-14.9	-12.5	3.1
QCISD//MP2[24,a]	**-26.1**	**-12.6**	**-13.8**	**-16.8**	**-14.7**	**2.3**
MPWB1K[173]	-30.3	-13.4	-16.4	-16.1	-13.9	2.3
MP2[24,a]	**-28.0**	**-15.6**	**-20.1**	**-21.4**	**-20.2**	**1.9**
M05-2X[173]	**-25.9**	**-12.2**	**-16.3**	**-17.3**	**-16.1**	**1.6**
QCISD(T)//MP2[24,a]	**-27.5**	**-14.4**	**-18.6**	**-19.5**	**-17.8**	**0.4**
M06-2X[173]	**-27.8**	**-14.2**	**-18.4**	**-19.2**	**-17.8**	**0.3**
Experiment[252]	-27.5 ± 0.5[b]	-13.8 ± 0.3	-17.6 ± 0.2	-19.3 ± 0.3	-17.6 ± 0.2	

[a] BSSE corrections and convergence corrections of 1.5, 1.3 and 1.6 kcal/mol for MP2, QCISD, and QCISD(T), respectively, have been applied. The temperatures are 298 K for BH_3-NH_3, and 373 K for $(CH_3)_3B-N(CH_3)_nH_{3-n}$; n = 0 to 3. The 6-311++G(3df,2p) basis set has been employed with all chemical methods. Chemical methods in boldface indicate that the experimental trend was reproduced.
[b] Best estimate predicted by QCISD(T)/aug-cc-pV5Z//MP2/6-311++G(3df,2p).

All methods predict a stronger ammonia borane B–N coordinate covalent bond as compared to the trimethylboranes. However, beyond $(CH)_3B-NH_3$, experiment yields an increase in B–N coordinate covalent bond strength for each methyl group added to the nitrogen atom, until the third methyl group, in which the B–N coordinate covalent bond strength decreases to that of the one methyl case. Although DFT and HF are less affected by BSSE, only M06-2X, M06, and M05-2X are found to replicate the B–N coordinate covalent bond strengthening upon methyl substitution on the donor side (n = 0 to 2) with subsequent weakening as the last methyl group is added (n = 3). The HF, M05, B3LYP, MPW1K, MPW1B95, and MPW1BK methods predict that the addition of the second methyl group will decrease the B–N coordinate covalent bond strength,

which contradicts the experimental trend. Furthermore, HF, M05, B3LYP, MPW1K, MPW1B95, and MPW1BK are also unable to model the B–N binding enthalpies on a quantitative level as well, evident by MADs of 15.2, 9.4, 9.2, 4.4, 3.1, and 2.3 kcal/mol (Table 3.8), respectively.

All post-SCF methods with the 6-311++G(3df,2p) basis set incorporating BSSE and convergence corrections reproduced the experimental trend of B–N coordinate covalent bond strength with MADs of 2.3, 1.9, and 0.4 kcal/mol for MP2, QCISD, and QCISD(T), respectively. The BSSE and convergence corrected QCISD(T) binding enthalpies are within the experimental uncertainty for trimethylboranes ($n = 2$ and 3), and slightly outside the experimental accuracy by 0.3 and 0.8 kcal/mol for $n = 0$ and 1, respectively. The data suggest that the triples correction to the wavefunction is critical, accounting for *ca*. 10 to 25% of the ΔH_{373} in order to align QCISD computations with experiment. Similar results regarding the importance of the triples contribution were reported by Pople and Head-Gordon, where electronic energies predicted by QCISD(T) and QCISD differed from FCI results by 4.3 and 1.3 kcal/mol respectively.[132]

M06 yields the highest MAD (3.9 kcal/mol) out of the functionals able to reproduce the experimental trend, and consistently underestimates the strength of the B−N coordinate covalent bond. M05-2X yields a comparable MAD to MP2 at a much lower computational cost. Formally, MP2 scales as N^5, while DFT scales as N^3 (N = number of basis functions).[125] M05-2X and MP2 MADs are 1.6 and 1.9 kcal/mol, respectively; however, MP2 tends to overestimate the strength of the coordinate covalent bond, while M05-2X underestimates it. M06-2X is comparable to QCISD(T), yielding a MAD of 0.3 kcal/mol, 0.1 kcal/mol lower than that of QCISD(T)'s MAD. Consequently,

M06-2X is a practical and efficient functional suitable for modeling the energetic character of the B–N coordinate covalent bond. Comparing resources, QCISD(T) scales as N^7 compared to DFT methods which grow as N^3.[125] Furthermore, M06-2X does not require a convergence correction for the basis set limit, a requirement for QCISD(T) to realign predicted results with experiment, due to the slow convergence of predicted post SCF results.

3.7.1 Possible Origins of M06-2X's Success

M06-2X, M06, and M05-2X are the only DFT methods found in this study that reproduce the experimental trend in binding enthalpies. Furthermore, only M06-2X and M05-2X yield comparable MADs to QCISD(T) and MP2, respectively. The Minnesota functionals were designed with a balance of kinetic energy density between the exchange and correlation functionals. In contrast, MPWB1K and MPW1B95 incorporate kinetic energy density within the correlation functional only, while B3LYP and MPW1K consider it in neither the exchange nor the correlation functionals. However, this cannot be the only reason for the relative quantitative success of M06-2X and M05-2X, since M05 also incorporates kinetic energy density in both the exchange and correlation functionals and is unable to model the experimental trend. The two main differences between the successful functionals (M06-2X and M05-2X) and M05 involves nearly double the amount of Hartree–Fock exchange (M06-2X and M05-2X) and a different formulation of the functional form (M06-2X). The linear combination of the M05 class functional and VSXC[159, 182] (yielding the M06 style) allows both M06 and M06-2X to

model the experimental binding enthalpy *trend* accurately; however, doubling the

Hartree–Fock exchange allows a more *quantitative* assessment of the B–N coordinate

covalent bond by M06-2X compared to M06. The empirical nature of the functional

forms associated with M06-2X, M06, M05-2X, and M05, possessing 33, 36, 23, and 23

optimized parameters, respectively, may contribute to the high accuracy as well.

However, M05 possesses the same number of optimized parameters as M05-2X and is

unable to account for the experimental trend. In contrast, M05-2X is able to reproduce

the experimental trend by just doubling the amount of Hartree-Fock exchange, but with

a higher MAD compared to M06-2X. Consequently, the balance of kinetic energy

density in both the exchange and correlation functionals, the higher amount of

Hartree-Fock exchange, and the functional forms of the exchange and correlation

functionals within the M06 class of functionals are critical in order to model a balance of

short and medium range exchange-correlation interactions that exist within the sterically

hindered B–N coordinate covalent bonded adducts.

3.8 Significance of Thermal Corrections

The ability of theory to predict accurate B–N coordinate covalent binding

enthalpies has been shown to depend upon the method, basis set size, and BSSE.

However, thermal corrections can also make important contributions to the predicted

binding energetics. For example, the thermal adjustments with BSSE corrections

associated with the highest level of theory employed,

QCISD(T)/6-311++G(3df,2p)//MP2/6-311++G(3df,2p), are listed in Table 3.9.

As expected, thermal factors are found to influence the predicted binding energetics significantly, yet are not always applied for comparison with experiment (Table 3.1). BSSE alone can account for an absolute difference from the binding electronic energy by up to 3.6 kcal/mol, BSSE and zero-point energy corrections up to 7.9 kcal/mol, and BSSE and enthalpic (thermal) corrections up to 6.9 kcal/mol. This does not mean that the predicted binding energetics are necessarily incorrect; however, care must be taken for valid comparison with experiment. For example, the predicted ΔE_{elec} for $H_3B–NH_3$ is -31.5 kcal/mol using QCISD(T)/6-311++G(3df,2p)//MP2/6-311++G(3df,2p), which is in fortuitous agreement with Haaland's estimation of -31.1 ± 1.0 kcal/mol. Haaland's estimation is not a ΔE_{elec} value, rather an extrapolation from ΔH_{298} values. When the appropriate thermal corrections are applied to the QCISD(T) prediction, ΔH_{298} is predicted to be -25.9 kcal/mol, which is 5.2 kcal/mol different from Haaland's estimation. Thus, without a systematic study, it is possible for theory and experimental values to match accidentally; however, this could be avoided when proper corrections are applied and comparisons are made. Consequently, the methyl substituted ammonia trimethylboranes require enthalpic adjustments at T = 373 for accurate experimental comparison, as performed in Chapter 3.7.

Table 3.9. Factors Influencing QCISD(T) Predicted Binding Energetics for H_3B-NH_3 and $(CH_3)_3B-N(CH_3)_nH_{3-n}$; n = 0-3.[a]

	Average Difference	H_3B-NH_3[b]	$n = 0$[b]	$n = 1$[b]	$n = 2$[b]	$n = 3$[b]
ΔE_{elec}	0.0	-31.5	-18.1	-22.6	-24.1	-23.1
ΔE_{elec}[c]	2.7	-29.9 (1.7)	-15.7 (2.4)	-19.9 (2.7)	-21.0 (3.1)	-19.5 (3.6)
ΔE_0[c]	7.2	-24.3 (7.3)	-11.2 (6.9)	-15.9 (6.7)	-17.0 (7.1)	-15.2 (7.9)
ΔH_T[c]	5.9	-25.9 (5.6)	-12.8 (5.3)	-17.0 (5.6)	-17.9 (6.2)	-16.2 (6.9)

[a] Relative values to the predicted binding electronic energy, ΔE_{elec}, are given in parentheses. The convergence correction of 1.6 kcal/mol for QCISD(T) is not applied. The 6-311++G(3df,2p) basis set has been employed. All energies are in kcal/mol.
[b] T = 298 K for BH_3-NH_3 and T = 373 K for $(CH_3)_3B-N(CH_3)_nH_{3-n}$; n = 0 to 3. Geometries optimized with MP2/6-311++G(3df,2p)
[c] BSSE corrected.

When a lower level of theory is utilized, such as with MP2/6-311++G(d,p), the corrections are larger (Table 3.10) due to BSSE. Since each level of theory is corrected by the same scaled frequencies (refer to Chapter 2.12 and 3.2), BSSE is the only variable in this study. However, the binding electronic energy can change up to 8.2 kcal/mol, BSSE and ZPE corrections up to 12.4 kcal/mol, and BSSE and enthalpic (thermal) corrections up to 11.4 kcal/mol. The results demonstrate the importance of thermal corrections and BSSE.

Table 3.10. Factors Influencing MP2 Predicted Binding Energetics for H_3B–NH_3 and $(CH_3)_3B$-$N(CH_3)_nH_{3-n}$; n = 0-3.[a]

	Average Difference	H_3B–NH_3[b]	n = 0[b]	n = 1[b]	n = 2[b]	n = 3[b]
ΔE_{elec}	0.0	-32.0	-19.9	-24.4	-26.1	-25.7
ΔE_{elec}[c]	6.4	-27.6 (4.3)	-13.9 (6.0)	-18.0 (6.4)	-19.0 (7.1)	-17.5 (8.2)
ΔE_0[c]	11.0	-21.1 (10.8)	-9.4 (10.5)	-14.0 (10.4)	-14.9 (11.1)	-13.3 (12.4)
ΔH_T[c]	9.6	-23.7 (8.3)	-11.0 (8.9)	-15.1 (9.3)	-15.9 (10.2)	-14.3 (11.4)

[a] Relative values to the predicted binding electronic energy, ΔE_{elec}, are given in parentheses. The 6-311++G(d,p) basis set has been employed. All energies are in kcal/mol.
[b] T = 298 K for BH_3-NH_3 and T = 373 K for $(CH_3)_3B$–$N(CH_3)_nH_{3-n}$; n = 0 to 3.
[c] BSSE corrected.

It has been previously recommended that the MP2 method be employed with at least a triple-zeta split-valence basis set to model the B–N coordinate covalent bond accurately.[244, 245] Evaluation of the methyl substituted ammonia trimethylboranes utilizing MP2/6-311++G(d,p) reveals that BSSE ranges between 4.3 to 8.2 kcal/mol, as shown in Table 3.10. The comparison with experiment should include thermal and BSSE corrections. For example, the MP2/6-311++G(d,p) BSSE uncorrected binding energies employing only ZPE corrections for $(CH_3)_3B$–$N(CH_3)_nH_{3-n}$, where n is 0, 1, 2 and 3, are -15.4, -20.4, -22.1, -21.4 kcal/mol (MAD of 2.8 kcal/mol),[245] respectively. The reported values are significantly different than the MP2/6-311++G(d,p) predicted binding enthalpies of -11.0, -15.1, -15.9, -14.3 kcal/mol (MAD of 3.0 kcal/mol), respectively, which are adjusted for thermal factors (373 K) and BSSE.

When a DFT method, such as M06-2X, is utilized in conjunction with 6-311++G(3df,2p) the corrections are smaller (Table 3.11), since there is less BSSE. However, the binding electronic energy can change up to 0.6 kcal/mol, BSSE and ZPE

corrections up to 4.8 kcal/mol, and BSSE and enthalpic (thermal) corrections up to 3.9

kcal/mol. The results demonstrate the importance of thermal corrections and BSSE.

Table 3.11. Factors Influencing M06-2X Predicted Binding Energetics for for H_3B–NH_3 and $(CH_3)_3B$–$N(CH_3)_nH_{3-n}$; n = 0-3.[a]

	Average Difference	H_3B–NH_3[b]	$n = 0$[b]	$n = 1$[b]	$n = 2$[b]	$n = 3$[b]
ΔE_{elec}	0.0	-32.0	-17.4	-21.7	-22.8	-21.7
ΔE_{elec}[c]	0.4	-31.7 (0.3)	-17.1 (0.3)	-21.3 (0.4)	-22.3 (0.5)	-21.1 (0.6)
ΔE_0[c]	4.9	-26.1 (5.9)	-12.6 (4.8)	-17.3 (4.4)	-18.3 (4.5)	-16.9 (4.8)
ΔH_T[c]	3.6	-27.8 (4.2)	-14.2 (3.2)	-18.4 (3.3)	-19.2 (3.6)	-17.8 (3.9)

[a] Relative values to the predicted binding electronic energy, ΔE_{elec}, are given in parentheses. The 6-311++G(3df.2p) basis set has been employed. All energies are in kcal/mol.
[b] T = 298 K for BH_3-NH_3 and T = 373 K for $(CH_3)_3B$–$N(CH_3)_nH_{3-n}$; n = 0 to 3.
[c] BSSE corrected.

There are three key conclusions. First, the electronic energy should be adjusted

with the necessary thermodynamic corrections at the appropriate temperature in order to

make proper comparisons with experiment. Second, the 6-311++G(3df,2p) basis set

should be utilized to ensure a negligible amount of BSSE and a converged binding

enthalpy. Lastly, BSSE must be corrected when small basis sets are utilized. It is

recommended that if accurate binding enthalpies are desired on a quantitative level

(MAD of 0.3 kcal/mol) then M06-2X/6-311++G(3df,2p) should be utilized,

incorporating BSSE corrections. This level of theory may be utilized in order to model

the structural and energetic properties of B–N coordinate covalent bonds.

3.9 Chemical Descriptors of the B–N Coordinate Covalent Bond

In order to probe the electronic nature of the coordinate covalent bond, NBO and NRT analysis has been employed to provide the chemical descriptors (atomic charges, bond orders, bond covalency, bond ionicity, and charge-transfer frustration) of H_3B-NH_3 and the four methyl substituted ammonia trimethylboranes. QCISD(T)/6-311++G(3df,2p) with BSSE and convergence corrections has been shown to predict accurate binding enthalpies for substituted trimethyl boranes. However, the electronic wavefunction predicted by QCISD(T) cannot be analyzed by NBO, since the requisite density matrix is not available. M06-2X provides accuracies comparable to QCISD(T); however, the NBO analysis was not available within NWChem 5.1 at the time of this investigation. Consequently, QCISD(T), M06-2X, and M06 are omitted from the NBO and NRT discussion.

To uncover the "physical" reasons for the wide variability in predicted binding enthalpies by different levels of theory, NBO and NRT analysis has been performed with HF, B3LYP, MPW1K, MPWB1K, MPW1B95, M05, M05-2X and MP2 utilizing the 6-311++G(3df,2p) basis set on the corresponding optimized structures to explore the relationship between the variation in binding enthalpies and the error in predicted charges, bond orders, covalencies, and ionicities. Due to its proven semi-quantitative results, MP2/6-311++G(3df,2p) predicted charges, bond orders, covalencies, ionicities, and binding enthalpies with BSSE and convergence corrections are taken as the reference or "exact" value for percent error calculations. M05-2X provides comparable accuracies to that of MP2 (Table 3.8); however, due to the high empirical nature of the

M05-2X exchange-correlation functional, MP2 data is considered to be the reference rather than M05-2X.

3.9.1 Charge Transfer Frustration

From the Lewis perspective, the formation of a coordinate covalent bond within $H_3B–NH_3$ occurs when two electrons are donated by the nitrogen atom and accepted by boron.[221] This is an oversimplification of the coordinate covalent bond concept, where the strength of the donor does not necessarily match that of the acceptor. A mismatch in donor and acceptor strength endows the termini with a reduction or build-up of electron density, which we refer to as "frustration." The frustrated termini utilize their immediate substituents to satisfy further electronic needs and provide a unique character of chemical bonding.

Frustration is quantified by examining the differences in charges between the bonded and separated states. The atomic termini of the coordinate covalent bond experience a change in atomic charge [Q_N^{coord} and Q_B^{coord}] compared to their separated states [Q_N^{sep} and Q_B^{sep}] by approximately equal but opposite amounts, as shown by Equation 3.2.[221]

$$Q_N^{coord} - Q_N^{sep} \cong -\left[Q_B^{coord} - Q_B^{sep}\right]$$

3.2

$$\Delta Q_N \cong -\Delta Q_B$$

In other words, the donation (loss) of electron density from the donor (ΔQ_N) will be approximately equal in magnitude to the electron density accepted (gained) by the acceptor (ΔQ_B). Consequently, the extent in which ΔQ_N equals $-\Delta Q_B$ is used to gauge the coordinate covalent character of a chemical bond. If ΔQ_N equals $-\Delta Q_B$, then the B–N bond is considered fully coordinate covalent, indicating no offset from equality, where a perfect match between donating and accepting electron density is achieved. If ΔQ_N does not equal $-\Delta Q_B$, then the difference represents the charge-transfer frustration, Q_{CTF}, or mismatch of donor and acceptor strength, between the two atoms (Equation 3.3).

$$Q_{CTF} = -\left(\Delta Q_B + \Delta Q_N\right) \qquad 3.3$$

For example, considering H_3B–NH_3 and isolated species, MP2/6-311++G(3df,2p) predicts ΔQ_N and $-\Delta Q_B$ to be 0.230 and 0.503 e, respectively, resulting in a Q_{CTF} of 0.273 e, which is considered to have relatively weak coordinate covalent character in comparison to F_3B–NH_3, where a Q_{CTF} of 0.000 e is computed at the same level of theory. This is in good agreement with the B3LYP/6-311++G(d,p) predicted value of -0.013 e by Weinhold.[221] This suggests that BF_3 is more compatible with NH_3 than BH_3, which agrees with Pearson's Hard Soft Acid Base (HSAB) principles, because BF_3 and NH_3 are both hard and BH_3 is soft.[57-59]

In addition, the B–N bond strength is stronger in H_3B–NH_3 as compared to F_3B-NH_3.[241, 246] Therefore, the relationship between the trend of binding enthalpies from methyl substituted ammonia boranes and the extent of predicted charge-transfer

frustration is of interest in characterizing the coordinate covalent bond. Figure 3.8

displays the BSSE and convergence corrected MP2/6-311++G(3df,2p) predicted binding

enthalpies vs. Q_{CTF} A strong linear correlation ($R^2 = 0.91$) is found suggesting that as

the coordinate covalent character of the B–N bond increases, its corresponding strength

decreases.
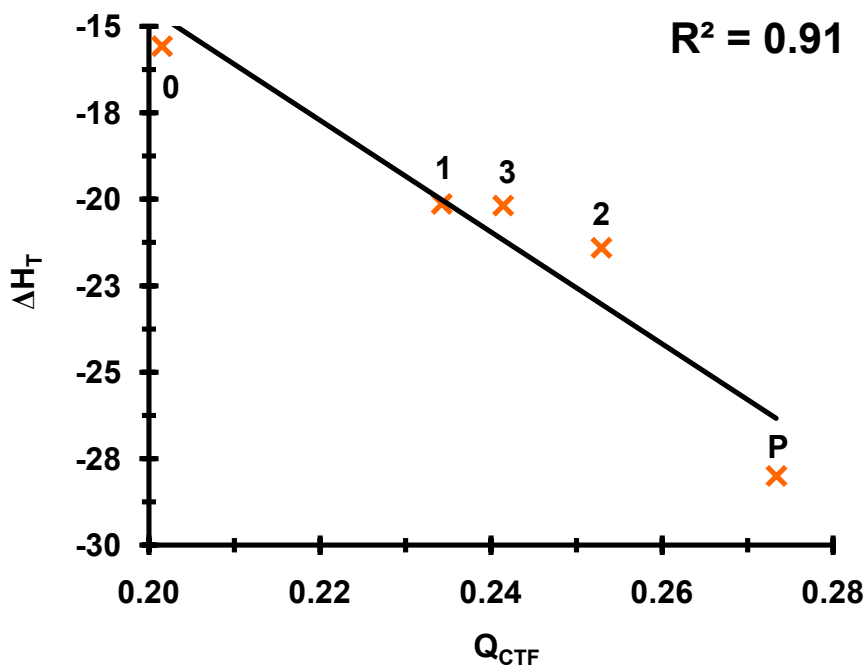
Figure 3.8. MP2/6-311++G(3df,2p) predicted binding enthalpies (BSSE and convergence corrections included) for $(CH_3)_3B–N(CH_3)_nH_{3-n}$ (n = 0-3) and ammonia borane vs. the charge-transfer frustration, $Q_{CTF} = -(\Delta Q_B + \Delta Q_N)$. Labels near each data point refer to n, or number of methyl substitutions. P refers to the prototype coordinate covalent, $H_3B–NH_3$. T = 298 K for P and T = 373 when n = 0-3.

Figure 3.9 shows the percent error in the corrected predicted binding enthalpies

for $H_3B–NH_3$ and four trimethylboranes utilizing HF, B3LYP, MPW1K, MPWB1K,

MPW1B95, M05, M05-2X and MP2 employing the 6-311++G(3df,2p) basis set versus

the percent error in charge-transfer frustration between boron and nitrogen for each

corresponding method. A linear correlation ($R^2 = 0.79$) exists, which suggests that

modeling the B–N coordinate covalent bond character accurately is critical to achieving

accurate binding enthalpies. Errors as large as 118% occur in the predicted binding

enthalpy, if Q_{CTF} is underestimated by 28%, as predicted for $(CH)_3B–N(CH_3)_3$ by HF.

All Q_{CTF}, percent error in Q_{CTF}, and percent error in binding enthalpies are reported in

Table 3.12, 3.13, and 3.14 respectively.
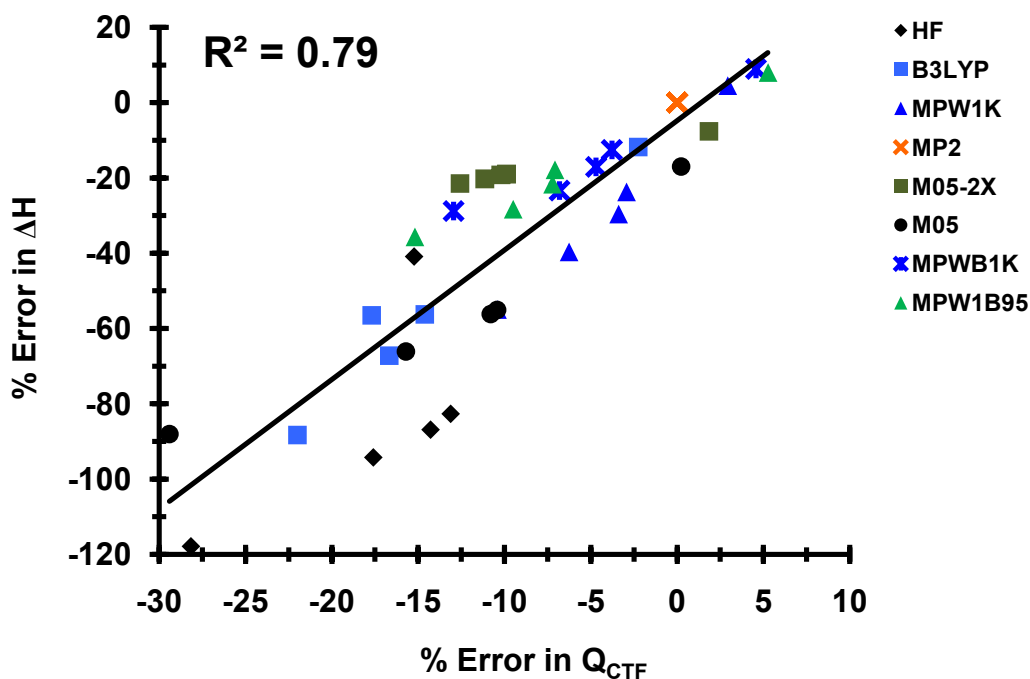
Figure 3.9. Percent error in the predicted binding enthalpy versus the percent error in the predicted charge-transfer frustration, $Q_{CTF} = -(\Delta Q_B + \Delta Q_N)$ for HF, B3LYP, MPW1K, MPWB1K, MPW1B95, M05, and M05-2X utilizing the 6-311++G(3df,2p) basis set on the corresponding optimized $H_3B–NH_3$ and $(CH_3)_3B–N(CH_3)_nH_{3-n}$ (n = 0-3) structures.

Table 3.12. Charge Transfer Frustration for $H_3B–NH_3$ and $(CH_3)_3B–N(CH_3)_nH_{3-n}$; n = 0-3.[a, b]

	$H_3B–NH_3$	$n = 0$	$n = 1$	$n = 2$	$n = 3$
HF	0.232	0.173	0.204	0.208	0.173
B3LYP	0.267	0.166	0.200	0.211	0.188
M05	0.274	0.180	0.210	0.213	0.170
MPW1K	0.281	0.196	0.226	0.237	0.216
MPW1B95	0.288	0.187	0.217	0.229	0.205
MPWB1K	0.286	0.194	0.223	0.236	0.210
M05-2X	0.278	0.176	0.211	0.227	0.215
MP2	0.273	0.202	0.234	0.253	0.241

[a] Q_{CTF} = -(ΔQ_B + ΔQ_N) in electrons.
[b] All methods utilize the 6-311++G(3df,2p) basis set.

Table 3.13. Percent Error in Charge Transfer Frustration for $H_3B–NH_3$ and $(CH_3)_3B–N(CH_3)_nH_{3-n}$; n = 0-3.[a, b]

	$H_3B–NH_3$	n = 0	$n = 1$	$n = 2$	$n = 3$
HF	-15.2	-14.3	-13.1	-17.6	-28.2
B3LYP	-2.3	-17.7	-14.6	-16.7	-22.0
M05	0.2	-10.8	-10.4	-15.7	-29.4
MPW1K	2.9	-2.9	-3.4	-6.3	-10.4
MPW1B95	5.3	-7.1	-7.2	-9.5	-15.2
MPWB1K	4.6	-3.8	-4.7	-6.8	-12.9
M05-2X	1.8	-12.6	-9.9	-10.2	-11.1
MP2	0.0	0.0	0.0	0.0	0.0

[a] MP2/6-311++G(3df,2p) data is taken as the exact data for percent error calculations.
[b] The sign is maintained to determine if the error corresponds to an over or underestimation.

Table 3.14. Percent Error in Binding Enthalpy for $H_3B–NH_3$ and $(CH_3)_3B–N(CH_3)_nH_{3-n}$; n = 0-3.[a, b]

	$H_3B–NH_3$	$n = 0$	$n = 1$	$n = 2$	$n = 3$
HF	-40.9	-86.9	-82.7	-94.3	-117.9
B3LYP	-11.9	-56.5	-56.3	-67.2	-88.3
M05	-17.0	-56.1	-55.1	-66.1	-88.0
MPW1K	4.5	-23.7	-29.6	-39.7	-55.0
MPW1B95	7.9	-17.9	-21.7	-28.4	-35.7
MPWB1K	8.9	-12.6	-17.1	-23.4	-28.8
M05-2X	-7.6	-21.5	-19.0	-19.2	-20.3
MP2	0.0	0.0	0.0	0.0	0.0

[a] MP2/6-311++G(3df,2p) data is taken as the exact data for percent error calculations.
[b] The sign is maintained to determine if the error corresponds to an over or underestimation.

The charge-transfer frustration predicted by MP2/6-311++G(3df,2p) for

BH_3-NH_3, $(CH_3)_3B–NH_3$, $(CH)_3B–NH_2CH_3$, $(CH)_3B–NH(CH_3)_2$, and $(CH)_3B–N(CH_3)_3$

is 0.273, 0.202, 0.234, 0.253, and 0.241 e, respectively. The Q_{CTF} trend across the

coordinate covalent bond with methyl substitution at either the donor or acceptor is

rationalized by the electronegativities for nitrogen, carbon, hydrogen and boron, which

are 3.0, 2.5, 2.1, and 2.0, respectively.[7] Methyl substitution of boron(comparing

H_3B-NH_3 and $(CH_3)_3B–NH_3$)) withdraws electron density from boron, due to the

difference in electronegativities, resulting in a decrease of charge-transfer frustration and

weakening of the B–N bond, as observed by experiment.[252] For the donor, increasing n

within $(CH_3)_3B–N(CH_3)_nH_{3-n}$ results in more donation of electron density to nitrogen,

allowing nitrogen to become a stronger Lewis base. Thus, the charge-transfer frustration

across the B–N bond increases from $n = 0$ to $n = 2$ yielding a stronger B–N bond, except

for when $n = 3$. Steric congestion cannot be ignored in the methyl substituted adduct

when $n = 3$; therefore, a balance of sterics and electronics must be considered, as

discussed in Chapter 3.10.

3.9.2 Bond Covalency and Ionicity

Although no strong correlation exists between bond order and binding enthalpy

($R^2 = 0.30$, Figure 3.10) moderate correlations were found between the errors in binding

enthalpy and both the errors in percent bond ionicity and percent bond covalency. Table

3.15 through Table 3.20 report the B–N bond order, percent bond covalency, percent

bond ionicity, and percent error of each descriptor with MP2 data taken as the reference.

Figure 3.11 displays a liner correlation ($R^2 = 0.70$) between the percent error in binding enthalpy versus percent error in percent bond covalency. Large errors in the predicted binding enthalpy result from moderate errors in the percent bond covalency. For example, HF underestimates the percent bond covalency of the B–N coordinate covalent bond within $(CH_3)_3B–N(CH_3)_3$ by 16.3%, resulting in a predicted binding enthalpy of $\Delta H_{373} = 3.6$ kcal/mol, a 118% underestimation of the BSSE and convergence corrected MP2 predicted value of -20.2 kcal/mol. DFT and HF underestimate the binding enthalpy of the B–N bond for all systems, except for $H_3B–NH_3$, as predicted with MPW1K, MPWB1K and MPW1B95. The data support that the bond covalency must be predicted correctly in order to model an accurate binding enthalpy.

Figure 3.10. Percent error in the predicted binding enthalpy vs. the percent error in the B–N bond order for HF, B3LYP, MPW1K, MPWB1K, MPW1B95, M05, M05-2X and MP2 utilizing the 6-311++G(3df,2p) basis set on the corresponding optimized $H_3B–NH_3$ and $(CH_3)_3B–N(CH_3)_nH_{3-n}$ (n = 0-3) structures.

Table 3.15. B–N Bond Order for $H_3B–NH_3$ and $(CH_3)_3B–N(CH_3)_nH_{3-n}$; n = 0-3

	$H_3B–NH_3$	n = 0	n = 1	n = 2	n = 3
HF	1.003	0.973	0.967	0.955	0.940
B3LYP	1.012	0.972	0.965	0.951	0.932
M05	1.011	0.967	0.961	0.944	0.925
MPW1K	1.012	0.974	0.966	0.954	0.934
MPW1B95	1.013	0.974	0.965	0.952	0.932
MPWB1K	1.012	0.974	0.962	0.953	0.934
M05-2X	1.007	0.971	0.965	0.952	0.934
MP2	1.026	0.964	0.930	0.911	0.897

Table 3.16. Percent Error in B–N Bond Order for $H_3B–NH_3$ and $(CH_3)_3B–N(CH_3)_nH_{3-n}$; n = 0-3.[a, b]

	$H_3B–NH_3$	$n = 0$	$n = 1$	$n = 2$	$n = 3$
HF	-2.2	0.9	3.9	4.8	4.7
B3LYP	-1.3	0.8	3.8	4.4	3.9
M05	-1.4	0.3	3.3	3.6	3.1
MPW1K	-1.4	1.0	3.9	4.7	4.2
MPW1B95	-1.3	1.1	3.8	4.5	3.9
MPWB1K	-1.4	1.0	3.4	4.6	4.2
M05-2X	-1.9	0.7	3.7	4.4	4.1
MP2	0.0	0.0	0.0	0.0	0.0

[a] MP2/6-311++G(3df,2p) data is taken as the exact data for percent error calculations.
[b] The sign is maintained to determine if the error corresponds to an over or underestimation.

Table 3.17. Percent B–N Bond Covalency for $H_3B–NH_3$ and $(CH_3)_3B–N(CH_3)_nH_{3-n}$; n = 0-3

	$H_3B–NH_3$	$n = 0$	$n = 1$	$n = 2$	$n = 3$
HF	33.8	30.3	29.5	27.4	24.2
B3LYP	36.8	34.3	33.2	30.8	28.0
M05	35.4	32.9	31.5	28.8	24.7
MPW1K	37.6	35.2	33.8	31.5	28.8
MPW1B95	37.5	35.4	33.9	31.6	28.8
MPWB1K	37.3	35.1	33.8	31.5	28.6
M05-2X	36.6	34.2	33.2	31.3	28.7
MP2	35.4	33.5	33.4	31.7	28.9

Table 3.18. Percent Error in Percent B–N Bond Covalency for $H_3B–NH_3$ and $(CH_3)_3B-N(CH_3)_nH_{3-n}$; n = 0-3.[a, b]

	$H_3B–NH_3$	$n = 0$	$n = 1$	$n = 2$	$n = 3$
HF	-4.5	-9.6	-11.7	-13.5	-16.3
B3LYP	4.2	2.3	-0.8	-2.7	-3.2
M05	0.0	-1.8	-5.8	-9.2	-14.4
MPW1K	6.2	4.9	1.2	-0.5	-0.3
MPW1B95	6.1	5.6	1.6	-0.1	-0.4
MPWB1K	5.6	4.7	1.2	-0.6	-1.1
M05-2X	3.6	1.9	-0.6	-1.4	-0.6
MP2	0.0	0.0	0.0	0.0	0.0

[a] MP2/6-311++G(3df,2p) data is taken as the exact data for percent error calculations.
[b] The sign is maintained to determine if the error corresponds to an over or underestimation.

Table 3.19. Percent B–N Bond Ionicity for $H_3B–NH_3$ and $(CH_3)_3B–N(CH_3)_nH_{3-n}$; n = 0-3.

	$H_3B–NH_3$	$n = 0$	$n = 1$	$n = 2$	$n = 3$
HF	66.2	69.7	70.5	72.6	75.8
B3LYP	63.2	65.7	66.8	69.1	72.0
M05	64.6	67.1	68.5	71.2	75.3
MPW1K	62.4	64.8	66.2	68.5	71.2
MPW1B95	62.5	64.6	66.1	68.3	71.2
MPWB1K	62.7	64.9	66.2	68.5	71.4
M05-2X	63.4	65.8	66.8	68.7	71.3
MP2	64.6	66.5	66.6	68.3	71.1

Table 3.20. Percent Error in Percent B–N Bond Ionicity for $H_3B–NH_3$ and $(CH_3)_3B–N(CH_3)_nH_{3-n}$; n = 0-3.[a, b]

	$H_3B–NH_3$	$n = 0$	$n = 1$	$n = 2$	$n = 3$
HF	2.5	4.8	5.8	6.3	6.6
B3LYP	-2.3	-1.1	0.4	1.2	1.3
M05	0.0	0.9	2.9	4.3	5.9
MPW1K	-3.4	-2.5	-0.6	0.2	0.1
MPW1B95	-3.3	-2.8	-0.8	0.1	0.2
MPWB1K	-3.0	-2.4	-0.6	0.3	0.5
M05-2X	-2.0	-0.9	0.3	0.7	0.3
MP2	0.0	0.0	0.0	0.0	0.0

[a] MP2/6-311++G(3df,2p) data is taken as the exact data for percent error calculations.
[b] The sign is maintained to determine if the error corresponds to an over or underestimation.
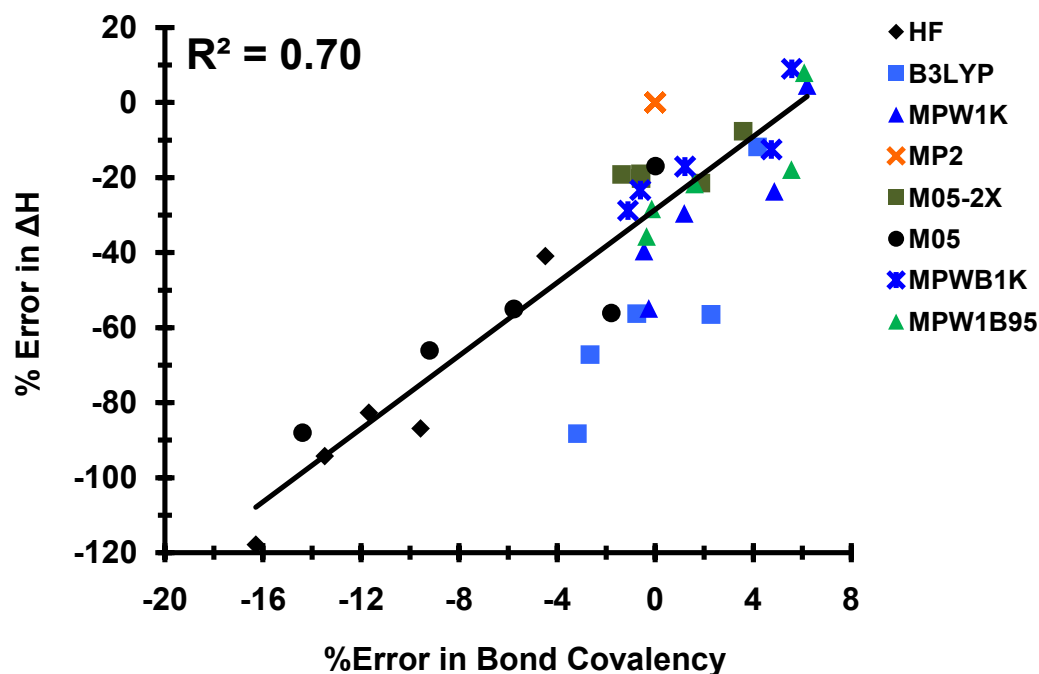
Figure 3.11. Percent error in the predicted binding enthalpy vs. the percent error in the percent B-N bond covalency for HF, B3LYP, MPW1K, MPWB1K, MPW1B95, M05, M05-2X and MP2 utilizing the 6-311++G(3df,2p) basis set on the corresponding optimized $H_3B–NH_3$ and $(CH_3)_3B-N(CH_3)_nH_{3-n}$ (n = 0-3) structures. The equation of the line that fits the data is y = 4.87x – 28.6.

MP2/6-311++G(3df,2p) predicts the percent bond covalency for the coordinate covalent bond between boron and nitrogen to decrease with increasing methyl substitutions within $H_3B–NH_3$, $(CH_3)_3B–NH_3$, $(CH)_3B–NH_2CH_3$, $(CH)_3B–NH(CH_3)_2$, and $(CH)_3B–N(CH_3)_3$ with values of 35.4, 33.5, 33.4, 31.7, 28.9%, respectively. The data suggest that the covalency must be modeled correctly in order to predict an accurate binding enthalpy; however, it does not explain the trend in predicted or observed binding enthalpies, which is in agreement with Jonas and coworkers.[241] Jonas and coworkers found that strong coordinate covalent bonds may be primarily bound by either covalent or ionic interactions, and that no correlation exists between the strength of the bond and

the degree of covalency or ionicity.[241] A balance of electronics and steric factors must be considered in such crowded systems, as discussed in Chapter 3.10.

A correlation ($R^2 = 0.69$) exists between errors in percent bond ionicity and binding enthalpy, as shown in Figure 3.12. HF overestimates the percent bond ionicity, which results in weaker predicted binding enthalpies compared to MP2. In addition, HF and DFT result in weaker binding enthalpies, except for H_3B-NH_3, as predicted by MPW1K, MPWB1K, and MPW1B95. As with the error in covalency, moderate errors in ionicity yield large errors in the binding enthalpy. For example, an error of 6.7% in percent ionicity results in a 118% error in binding enthalpy. The data support that the percent bond ionicity must be predicted correctly in order to predict an accurate binding enthalpy. MP2/6-311++G(3df,2p) predicts the percent bond ionicity for the coordinate covalent bond between boron and nitrogen to increase with increasing methyl substitutions within H_3B-NH_3, $(CH_3)_3B-NH_3$, $(CH)_3B-NH_2CH_3$, $(CH)_3B-NH(CH_3)_2$, and $(CH)_3B-N(CH_3)_3$, with percentages of 64.6, 66.5, 66.6, 68.3, 71.1%, respectively. The ionicity increases by approximately the same amount as the decrease in covalency with methyl substitution. As discussed with the covalency, the extent to which the bond is ionic does not explain the binding enthalpy trend. The percent error in binding enthalpy is more sensitive to the percent error in ionic character over covalent character as indicated by the magnitude of the slope of the fitted line displayed in Figure 3.11 and Figure 3.12 (10.3 vs. 4.9). The data suggest that the ionic nature of the wavefunction is more difficult to model than the covalent character.
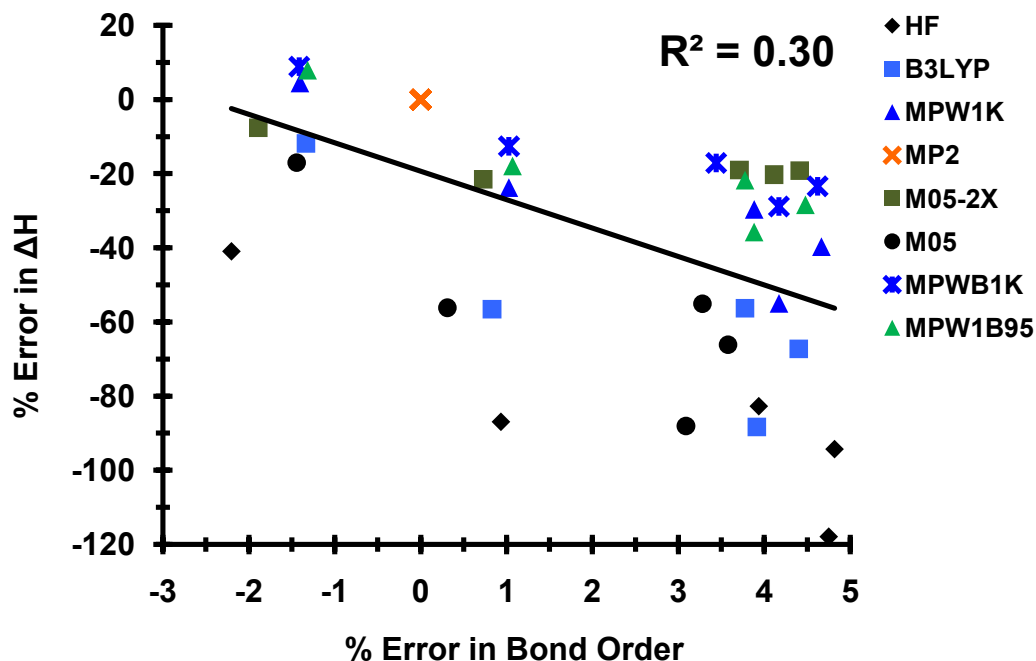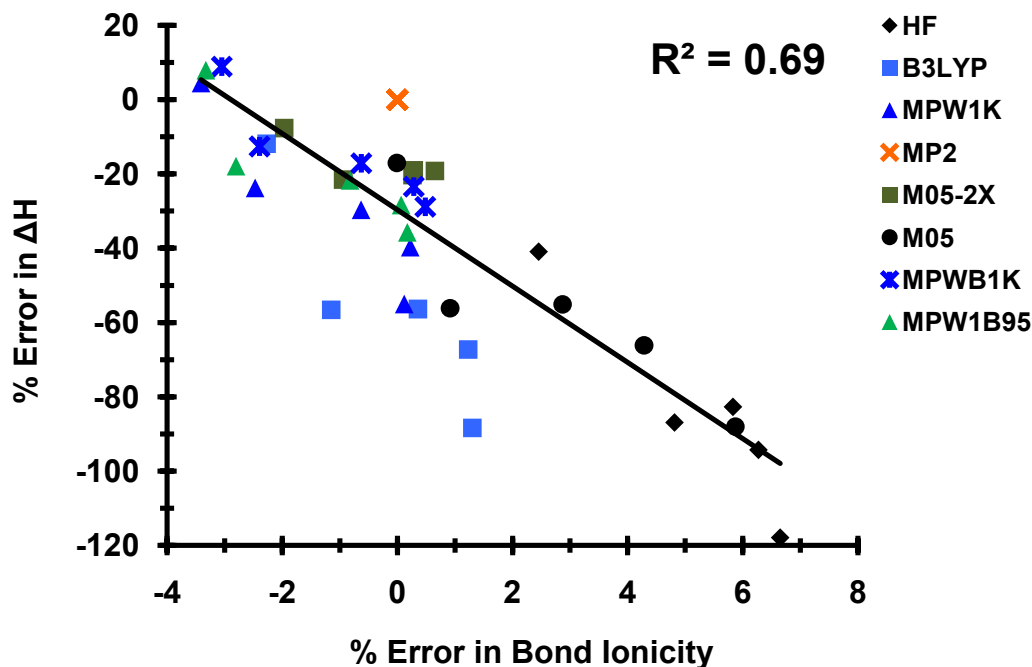
Figure 3.12. Percent error in the predicted binding enthalpy vs. the percent error in the percent bond ionicity for HF, B3LYP, MPW1K, MPWB1K, MPW1B95, M05, and M05-2X utilizing the 6-311++G(3df,2p) basis set on the corresponding optimized $H_3B–NH_3$ and $(CH_3)_3B–N(CH_3)_nH_{3-n}$ (n = 0-3) structures. The equation of the line that fits the data is y = -10.3x – 29.6.

A few points may be summarized. First, as the charge-transfer frustration approaches zero, the donor and acceptor are perfect matches and thus the bond becomes purely coordinate covalent. Second, the ammonia borane coordinate covalent bond is 64.6 % ionic and 35.4% covalent. Finally, coordinate covalent bond descriptors such as the charge-transfer frustration, bond covalency and ionicity are important factors that must be modeled accurately in order to achieve results comparable with experiment. Consequently, the correct modeling of the coordinate covalent bond descriptors allows MP2/6-311++G(3df,2p) to predict accurately the binding enthalpy trend of the

$(CH_3)_3B\text{-}N(CH_3)_nH_{3-n}$ (n = 0-3) adducts. If the coordinate covalent bond descriptors are not modeled accurately, errors in predicted binding energetics can be as large as 118%.

3.10   A Balance of Steric and Electronic Effects Accounts for the Binding Enthalpy Trend within $(CH_3)_3B−N(CH_3)_nH_{3-n}$

The charge-transfer frustration at equilibrium is crucial to characterizing the nature of the coordinate covalent bond, and subsequently predicting accurate binding enthalpies. However, from the previous discussion, the predicted coordinate covalent bond descriptors do not fully explain the reported experimental trend for $n = 2$ to $n = 3$. The MP2/6-311++G(3df,2p) predicted binding enthalpies (with BSSE and convergence corrections) vs. Q_{CTF} displays a strong linear correlation ($R^2 = 0.91$), implying the nature of the coordinate covalent bond has consequences on the binding enthalpy. However, the reason for *why* the binding enthalpy decreases and the coordinate covalent character has increased upon methyl substitution ($n = 2$ to $n = 3$) is not revealed by analyzing the coordinate covalent bond descriptors. A balance of sterics and electronics must be considered.

In an analysis of the predicted geometries, it is found that the atomic termini of the coordinate covalent bond allow for the substituted groups to relieve steric strain by the bending of angles (Figure 3.13). The acceptor's tetrahedral geometry is rigid compared to the donor's. The predicted acceptor XBN angles (X = H or C) vary only by 3.1°, whereas the donor XNB angles vary by 14.2° depending upon the number of

methyl substitutions. As methyl groups are added to the donor, steric congestion is relieved by expanding the CNB angles with a corresponding angle compression of $\angle$HNB for $n = 1$ and $n = 2$. The donor group appears to "rotate" to relieve the steric congestion away from the three methyl groups on the acceptor. For example, when one methyl is added ($n = 1$), the CNB angle becomes 117.2° (6.4° greater than $\angle$HNB when $n = 0$), while the HNB angles compress to 106.7° (4.1° less than $\angle$HNB when $n = 0$). With the combined relief of steric strain and the donation of electron density by the methyl group, the computed B–N bond is strengthened and shortens by 0.005 Å. The result is an experimentally observed energy lowering of 3.8 kcal/mol, compared to when $n = 0$. When two methyl groups are added, the CNB angles become 114.0° (3.2° greater than $\angle$HNB when $n = 0$) with a corresponding HNB angle of 103.0° (7.8° less than $\angle$HNB when $n = 0$). There is less rotation of the methyl groups for steric relief; however, the two methyl groups donate electron density to nitrogen, decreasing the coordinate covalent character of the B–N bond. Consequently, the combined effect is a 1.7 kcal/mol stabilization observed experimentally. Finally, addition of the last methyl group cannot utilize the rotation mechanism for stabilization due to the symmetric nature of the substitution. When $n = 3$ the CNB angle is found to be nearly tetrahedral at 110.9°, contracting by only 0.1° when $n = 0$. Despite the electron donation by three methyl groups, the lack of steric relief by rotation prevents potential stabilization. Consequently, a destabilization of 3.4 kcal/mol occurs with a B–N bond elongation of 0.027 Å, as compared to when $n = 0$, decreasing the charge-transfer frustration and subsequently increasing the coordinate covalent character. The B–N destabilization and corresponding Q_{CTF} decrease is observed within Figure 3.8, correlating well with the

remaining ammonia borane data. In summary, the data suggest that methyl substitution stabilizes the B–N bond by decreasing the coordinate covalent (and thus covalent) nature. The bond is further stabilized as a result of relieving steric congestion by geometric distortion. Subsequent methyl substitutions become increasingly crowded and difficult to accommodate despite the stabilization offered by reducing the coordinate covalent nature of the bond. In addition, N–C and B–C elongations participate very little in the relief of steric congestion, if at all, since only a 0.003 and 0.007 Å variation is predicted across the methylated ammonia boranes, respectively.
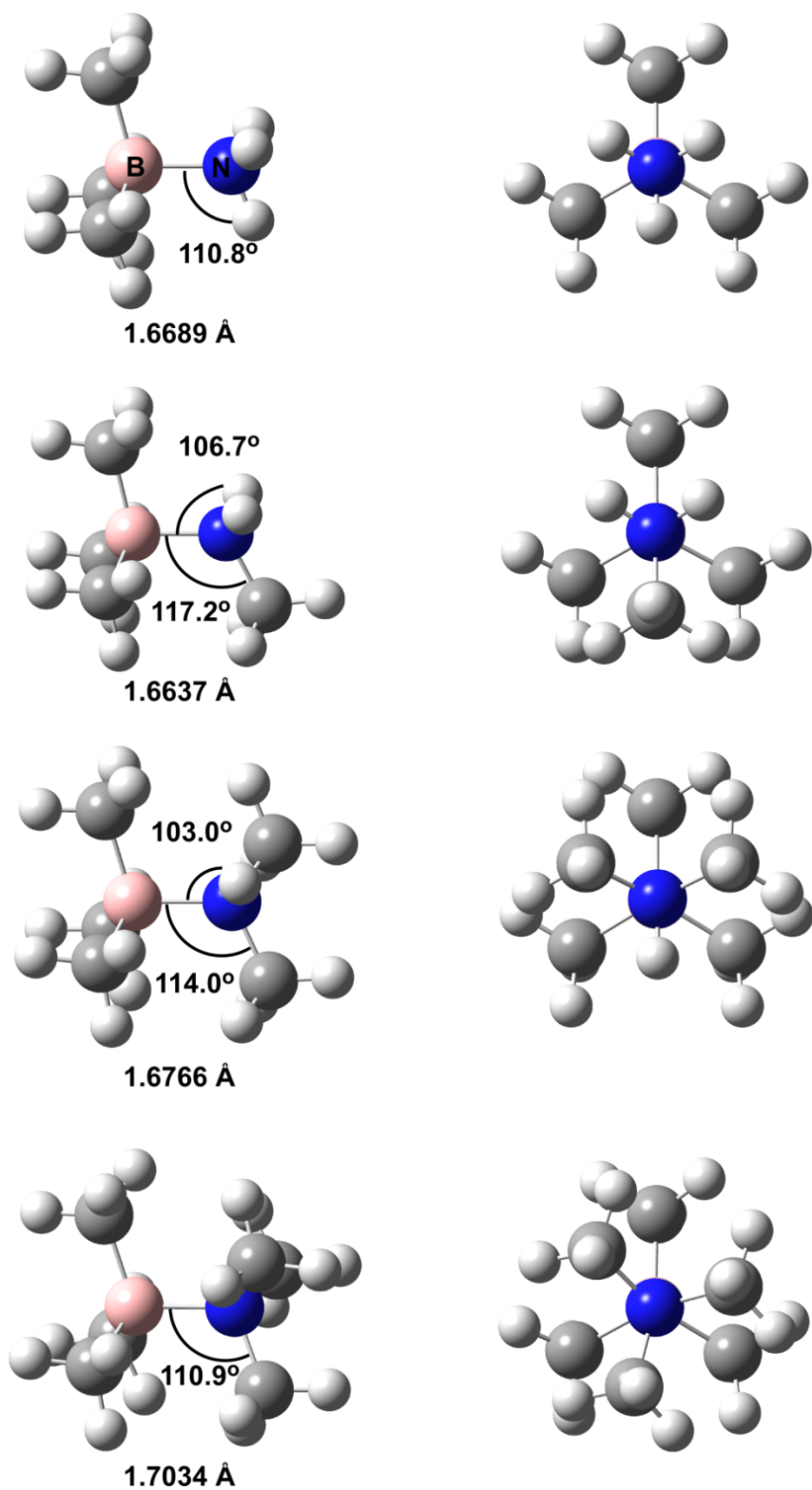
Figure 3.13. $(CH_3)_3B–N(CH_3)_nH_{3-n}$ (n = 0-3) MP2/6-311++G(3df,2p) optimized geometries. B-N bond lengths are reported under each structure. BNC and BNH angles are reported as well.

3.11 Conclusion

The coordinate covalent bond of ammonia borane is 64.6 % ionic and 35.4% covalent, where the charge-transfer frustration between boron and nitrogen is 0.273. It is discovered that a balance of coordinate covalent bond descriptors and steric factors at the equilibrium distance are necessary to model and characterize the coordinate covalent bond. Discrepancies in the binding energetics reported within the literature are not a consequence of varying coordinate covalent bond length, but rather of how the specific method and basis set models the electronics within the system. More specifically, the charge-transfer frustration between boron and nitrogen must be predicted correctly, in order to model the B–N coordinate covalent bond accurately. The binding enthalpy trend is a consequence of the coordinate covalent character of the bond, which is measured by the completeness of charge-transfer. In these particular methyl substituted systems, steric forces cannot be ignored. The Lewis donor has been found to be more flexible than the acceptor, allowing steric congestion to be relieved for the addition of two methyl groups. However, addition of the final methyl group results in severe steric congestion (n = 3), and the binding enthalpy weakens, since the molecule can no longer distort to lower its energy.

M06-2X, M06 and M05-2X in conjunction with the 6-311++G(3df,2p) basis set are able to reproduce the experimental trend with MADs of 0.3, 3.9 and 1.6 kcal/mol, respectively. M05-2X (MAD = 1.6 kcal/mol) and M06-2X (MAD = 0.3 kcal/mol) yield comparable MADs to that of MP2 (MAD = 1.9 kcal/mol) and QCISD(T) (MAD = 0.4 kcal/mol), respectively. M06-2X is able to model the B–N coordinate covalent bond efficiently and accurately without the residual convergence correction and intense

computational resources necessary for post-SCF methods. M06-2X incorporates the proper balance of short-range exchange-correlation energy necessary to model the electronics within the B–N coordinate covalent chemical bond, as well as the medium-range exchange-correlation energy demonstrated by sterically congested environments near the coordinate covalent bond. M06-2X/6-311++G(3df,2p) is a practical and efficient choice for investigating chemical systems possessing B–N coordinate covalent bonds, where quantitative trends in energetics are necessary. In summary, this study provides a comprehensive evaluation of computational protocols used in the study of coordinate covalent bonds. However, it is suspected that weaker Lewis acid-base adducts or stronger organometallic compounds may have different sensitivity and response to the computational factors studied here.

Chapter 4

Periodic Trends and Index of Boron Lewis Acidity

Lewis acidity is customarily gauged by comparing the relative magnitude of coordinate covalent bonding energies, where the Lewis acid moiety is varied and the Lewis base is kept constant. However, the prediction of Lewis acidity from first principles is sometimes contrary to that suggested by experimental bond energies. Specifically, the order of boron trihalide Lewis acidities predicted from substituent electronegativity arguments is opposite to that inferred by experiment. Contemporary explanations for the divergence between theory, computation, and experiment have led to further consternation. Due to the fundamental importance of understanding the origin of Lewis acidity, we report periodic trends for twenty-one boron Lewis acids, as well as their coordinate covalent bond strengths with NH_3, utilizing ab initio, density functional theory and natural bond orbital analysis. Coordinate covalent bond dissociation energy has been determined to be an inadequate index of Lewis acid strength. Instead, acidity is measured in the manner originally intended by Lewis, which is defined by the valence of the acid of interest. Boron Lewis acidity is found to depend upon substituent

electronegativity and atomic size, differently than for known Brønsted-Lowry periodic

trends. Across the second period, stronger substituent electronegativity correlates ($R^2 =$

0.94) with increased Lewis acidity. However, across the third period, an equal

contribution from substituent electronegativity and atomic radii is correlated ($R^2 = 0.98$)

with Lewis acidity. The data suggest that Lewis acidity depends upon electronegativity

solely down Group 14, while equal contribution from both substituent electronegativity

and atomic size are significant down Groups 16 and 17. Originally deduced from

Pauling's electronegativities, boron's substituents determine acidity by influencing the

population of its valence by withdrawing electron density. However, size effects

manifest differently than previously considered, where greater sigma bond (not pi bond)

orbital overlap between boron and larger substituents increase the electron density

available to boron's valence thereby decreasing Lewis acidity. The computed

electronegativity and size effects of substituents establish unique periodic trends that

provide a novel explanation of boron Lewis acidity, consistent with first principle

predictions. The findings resolve ambiguities between theory, computation, and

experiment, and provide a clearer understanding of Lewis acidity.

4.1 Introduction

In 1923, Gilbert N. Lewis published landmark ideas on acid-base theory, where a

base and acid donate and accept a pair of electrons, respectively.[55, 56] Lewis originally

defined acids and bases merely from chemical behavior in reactions without the need for

any theory of molecular structure.[55] Despite the fact that Lewis' revered concept of

valency made it easier to understand the essential characteristics of acids and bases, he

was hesitant in its use in the definition, because valency could not be measured directly.

Without other recourse, indirect measurements of acidity have ensued, principally based

upon the assumption that a stronger acid is more willing to accept an electron pair to

complete its valence, thus resulting in a stronger coordinate covalent bond. An overview

of different procedures that measure relative Lewis acid and base strengths has been

given by Anslyn and Dougherty.[54] Examples include Pearson's hard soft acid base

(HSAB) principle,[57-60] Gutmann's donor (DN) and acceptor numbers (AN),[61-63] Drago,

Marks, and Wayland's *E & C* and *D & O* equations,[64-66] and Christe and coworker's

fluoride affinities.[67] Regardless of the scale utilized to predict the relative strengths of

Lewis acids, it is assumed that a stronger coordinate covalent bond is due to the

increased Lewis acidity when the Lewis base is held constant.

From the beginning, Lewis cautioned that other factors could be important in

determining the adduct's bond strength, other than its tendency to accept an electron

pair.[55] Subsequently, it has been reported that the coordinate covalent bond is influenced

by other forces between the Lewis acid and base, such as orbital and steric

interactions.[68-70] Lewis observed that relative Lewis acidity depends on the choice of

Lewis base. For example, BH_3 forms a more stable adduct with thioethers as compared

to BF_3; however, the reverse is true when the Lewis acids are bound to ethers.[259] A

similar exchange is observed when BF_3 and BH_3 are bound to pyridine N-oxide and p-

methyl pyridine oxide, where BF_3 forms a more stable adduct with pyridine N-oxide as

compared to BH_3; however, BH_3 forms a more stable adduct with p-methyl pyridine

oxide.[260] Lewis summarized "that the relative strength depends not only upon the chosen

solvent but also upon the particular base or acid used for reference."[55] Nevertheless, the indirect gauge of Lewis acidity based upon bond strengths remains.

Even today, valency cannot be directly measured by experimental means, but computational methods and resources have now evolved such that valency and perturbations can be evaluated. As a result, a quantitative value indicating the degree of Lewis acidity is possible from the computed valency of boron. Thus, we use the term "intrinsic Lewis acidity" to measure relative Lewis acidity in the manner originally intended by Lewis,[55] which we define as the valence deficiency of the acid of interest.

Among the Lewis acids available, boron halides are commonly and widely utilized, due to their simplicity and strong influence over many diverse organic reactions.[74, 261-273] The problem of assessing Lewis acidities based upon coordinate covalent bond strength is illustrated by a long-standing problem in organic chemistry, where opposite to that expected, the Lewis acidity of boron trihalides has been reported to increase as $BF_3 < BCl_3 < BBr_3$.[260, 274-282] The observed trend eludes explanations based upon Pauling's electronegativity indices,[7] Bent's Rule of hybridization,[283] steric hinderance,[284] and HSAB.[285] Despite extensive theoretical[286-294] and experimental investigations,[260, 274-282, 290, 295-298] the origin of Lewis acidity differences between boron halides remains controversial, primarily due to the assessment of Lewis acidity as referenced against coordinate covalent bond dissociation energies.

Other ideas have been explored to account for Lewis acidities determined by coordinate covalent bond strengths. Specifically, the importance of halogen lone pairs in Lewis acids has been considered in terms of resonance,[277, 295] $p(\pi) \to p(\pi)$

hyperconjugation,[290, 291, 297] π-bonding,[296] and energy necessary to reorganize planar Lewis acids during adduct formation.[70, 286, 287, 290-292, 298] Despite the terms used, the underlying mechanism involved is the same, where halogen lone pairs interact with boron's formally empty $2p$ orbital, yielding coordinate covalent π-bonds. The question of which halogen demonstrates a larger resonance or $p(\pi) \rightarrow p(\pi)$ hyperconjugation within boron halides continues to be debated.[7, 299-302] Furthermore, the $p(\pi) \rightarrow p(\pi)$ hyperconjugation cannot account for the observed differences in Lewis acidity regarding BH_3 when compared to BF_3[259, 260, 275, 282] or BCl_3.[275, 281, 282] Thus, the impact of halogen lone pairs upon understanding Lewis acidity is dubious.

Computational studies of boron halides coordinated to nitrogen centered Lewis bases and ammonia borane have been reported.[241, 245, 247, 250, 286-289, 292-294, 299, 300, 303-307] However, it has been shown that the electronic description of coordinate covalent bonding is highly sensitive to the level of theory applied, and that post-SCF methods or M06-2X coupled with large basis sets are necessary to predict the binding energies of coordinate covalent systems accurately.[24, 173] Commonly employed computational methods can result in binding enthalpy errors as great as 87% (15.2 kcal/mol), as found for methyl substituted ammonia boranes.[24, 173, 245] Consequently, lower levels of theory have resulted in conflicting ideas on coordinate covalent bonding and gauging Lewis acidity.[24, 173, 241, 245, 247, 250, 286-289, 292, 293, 299, 300, 303-307]

Due to the importance of understanding Lewis acidity, twenty-one isolated boron Lewis acids ($BH_{(3-n)}F_n$, $BH_{(3-n)}Cl_n$, $BCl_{(3-n)}F_n$, $BH_{(3-n)}(OH)_n$, $BH_{(3-n)}(SH)_n$, $BH_{(3-n)}(CH_3)_n$, and $BH_{(3-n)}(SiH_3)_n$; $n = 0$ to 3) as well as their corresponding adducts with NH_3 have been analyzed. Unique to this study is that second and third period substituents are

assessed in a systematic evaluation of boron Lewis acidity to capture periodic trends. Lewis acidity trends down Groups 14, 16, and 17 are also reported. The intrinsic ability of a Lewis acid to accept electron density is investigated in terms of boron's valence, and its stereoelectronic dependence upon substituents. Our observations are rationalized in terms of first principle concepts including the Pauling electronegativity[7, 308] and atomic radii[309] of the atom from the substituent that is directly coordinated to boron. The periodic trends are contrasted against well-known Brønsted-Lowry acid-base behavior and extended to explain aluminum halide Lewis acidity.

4.2 Computational Approach

All electronic structure calculations have been explained in Chapter 2 and were carried out with Gaussian03[111] and NWChem 5.1,[112] using the computational resources at the Center for Computational Science at Duquesne University.[256] Specifically, NWChem 5.1 was utilized for all M06-2X computations while Gaussian03 was utilized for all QCISD(T) and MP2 computations. Ab initio, density functional theory, and natural bond orbital (NBO) analysis have been utilized to analyze stereoelectronic effects of substituted boron Lewis acids. A systematic computational investigation is employed utilizing a level of theory suitable for coordinate covalent bonds within Lewis acid adducts, as discussed in Chapter 3.[24, 173] All adducts with NH_3 and isolated Lewis acids have been fully optimized with M06-2X and the 6-311++G(3df,2p) Pople style basis set. In addition, all isolated boron halide Lewis acids and corresponding adducts with NH_3 have been optimized with MP2/6-311++G(3df,2p). Subsequently, single point

energy calculations have been employed on MP2 optimized structures utilizing QCISD(T)/aug-cc-pVQZ correlation consistent basis set. As discussed in Chapter 3 the QCISD(T)/6-311++G(3df,2p) was found to deliver a low MAD of 0.4 kcal/mol; however, the 6-311++G(3df,2p) basis set has been exchanged with aug-cc-pVQZ to avoid the convergence correction factor necessary for QCISD(T).

Basis set superposition error (BSSE) has been corrected with the counterpoise method developed by Boys and Bernardi. All minima have been confirmed by the absence of imaginary frequencies utilizing B3LYP/6-31G(d). Enthalpy corrections were predicted utilizing B3LYP/6-31G(d) and scaled by 0.9989 in order to predict binding enthalpies at 298 K for all Lewis acids adducts.

All NBO computations have been performed with HF/cc-pVQZ on the M06-2X/6-311++G(3df,2p) optimized structures utilizing the NBO 5.G[113, 220] program embedded within Gaussian03. Goodman reported inadequacies in the triple-split 6-311++G Pople basis set, where diffuse function augmentation lead to misleading conclusions drawn from NBO analysis regarding the stability of common four heavy atom molecules.[310] However, double-split 6-31G Pople-style and correlation consistent basis set are less sensitive to diffuse augmentation, and allow for accurate assessments. Consequently, specific stereoelectronic effects have been investigated utilizing HF/cc-pVQZ//M06-2X/6-311++G(3df,2p) since the requisite density matrix necessary for these types of analyses are not available for MP2 or QCISD(T) computations. The NBO analysis has been employed to determine the natural hybrid overlap (NHO) integral, S, as well as the atomic charge and boron valence deficiency. Briefly, atomic charge is defined as the nuclear charge minus the sum of electron populations from each

natural atomic orbital on the corresponding atom, including core and valence orbitals.[213] In contrast, valence deficiency is the formal valence minus the sum of electron populations from each valence natural atomic orbital.

4.3 Intrinsic Lewis Acidity

Boron's electrophilicity within the isolated Lewis acid is considered in terms of boron's atomic charge and its valence deficiency, calculated by subtracting the NBO predicted valence (HF/cc-pVQZ//M06-2X//6-311++G(3df,2p))[310] from the formal valence of three (Table 4.1). As expected, boron's valence deficiency and atomic charge are highly correlated ($R^2 = 0.999$; Figure 4.1), indicating that both similarly reflect the degree of boron's electrophilicity and thus Lewis acidity. However, boron's valence deficiency and binding enthalpy are not correlated (Figure 4.2; $R^2 = 0.28$), which underscores the need for a new paradigm regarding the prediction of Lewis acidity. Confidence in the data is engendered, since the same trend in binding enthalpy is predicted by using both QCISD(T)//MP2 and the M06-2X functional. Furthermore, the M06-2X predicted binding enthalpy for $(CH_3)B–NH_3$ lies within the uncertainty of the experimental value, $\Delta H_{298} = -13.8 \pm 0.3$ kcal/mol.[19] In addition, the M06-2X and QCISD(T)//MP2 predicted binding enthalpies of -25.1 and -23.8 kcal/mol, respectively, are in excellent agreement with the experimental value of -24.0 kcal/mol regarding the $Cl_3B–NH_3$ adduct.[311] As far as we are aware, there are no other experimental binding enthalpies regarding the NH_3 adducts of interest for further comparison.

Table 4.1. Binding enthalpies with NH_3,[a] Boron's valence deficiency (BVD),[b] and atomic charge (q_B).[b]

	BVD	q_B	QCISD(T)[c] ΔH_{298}	M06-2X[d] ΔH_{298}
BF_3	1.64	1.60	-19.6	-20.2
$B(OH)_3$	1.42	1.38	-	1.1
$BClF_2$	1.35	1.30	-20.8	-21.9
BHF_2	1.30	1.27	-15.2	-16.1
$BH(OH)_2$	1.11	1.08	-	-1.3
$B(CH_3)_3$	1.00	0.98	-	-14.1
BCl_2F	0.97	0.91	-22.2	-23.5
BH_2F	0.92	0.90	-18.8	-19.6
$BH(CH_3)_2$	0.79	0.77	-	-17.5
BH_2OH	0.77	0.76	-	-10.1
BH_2CH_3	0.61	0.60	-	-22.0
BCl_3	0.50	0.44	-23.8	-25.1
$BHCl_2$	0.50	0.46	-24.0	-25.4
BH_2Cl	0.47	0.45	-25.2	-26.2
BH_3	0.43	0.43	-27.1	-27.7
BH_2SH	0.26	0.24	-	-18.1
BH_2SiH_3	0.17	0.16	-	-30.9
$BH(SH)_2$	0.17	0.14	-	-12.6
$B(SH)_3$	0.11	0.07	-	-9.3
$BH(SiH_3)_2$	-0.11	-0.14	-	-33.1
$B(SiH_3)_3$	-0.41	-0.44	-	-35.1

[a] Energies are in kcal/mol.
[b] Charges are in electrons.
[c] QCISD(T)/aug-cc-pVQZ//MP2/6-311++G(3df,2p).
[d] M06-2X/6-311++G(3df,2p).
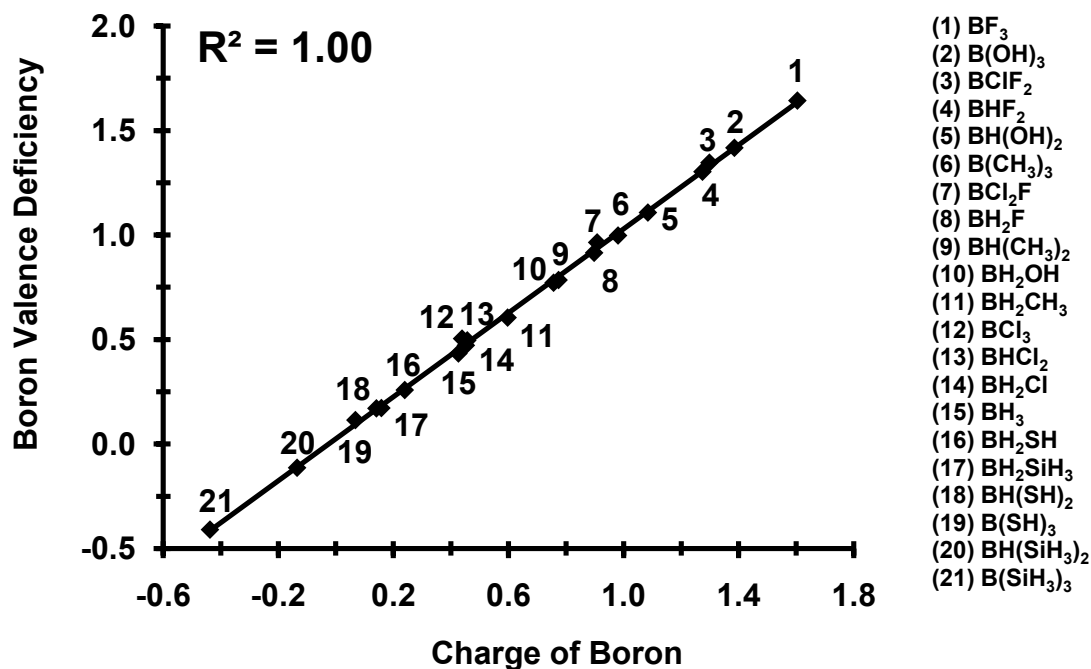
Figure 4.1. Boron valence deficiency vs. boron's charge within the isolated Lewis acid.
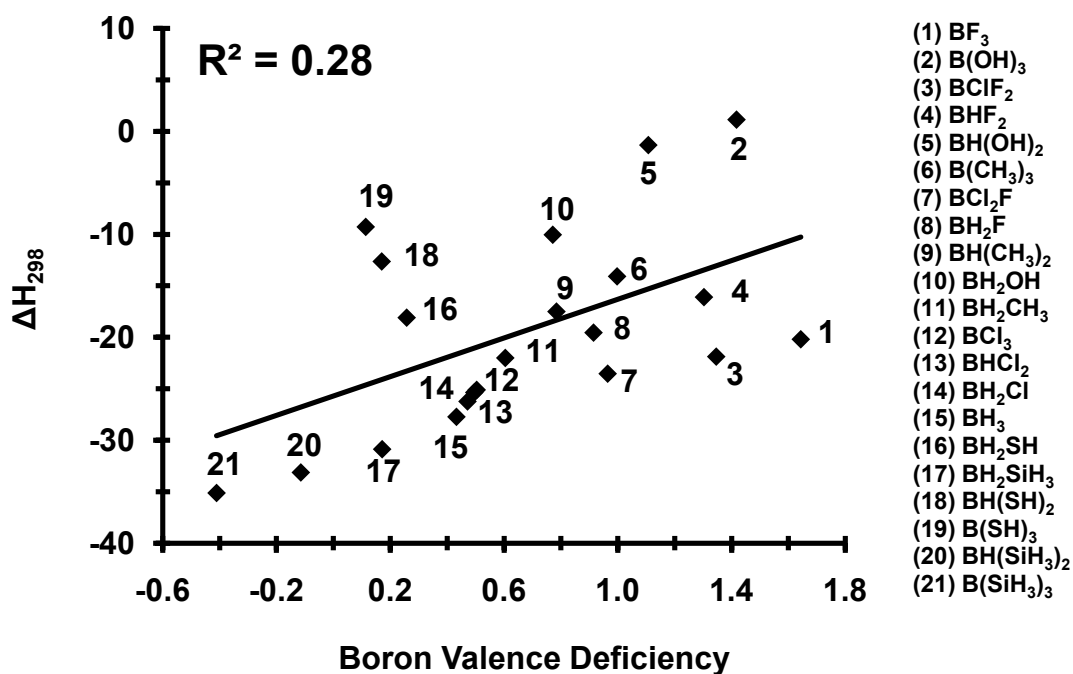
Figure 4.2. M06-2X/6-311++G(3df,2p) predicted BSSE corrected binding enthalpies with NH_3, ΔH_{298} (kcal/mol) vs. boron's valence deficiency (electrons).

The average substituent electronegativity is estimated as one-third the sum of all atomic electronegativities coordinated to boron. Considering all twenty-one Lewis acids, a moderate linear correlation is observed ($R^2 = 0.74$; Figure 4.3A), indicating that as substituents coordinated to boron become more electronegative, boron's valence becomes more deficient, yielding a stronger Lewis acid. The Allen,[312] Sanderson, [313] Allred-Rochow,[314] and Mulliken-Jaffe[315-317] electronegativity scales have been considered, yielding comparable results as shown by Figure 4.3B to Figure 4.3E. Considering Brønsted-Lowry acids,[68] a binary acid increases in strength across a period, because the conjugate base is stabilized with increasing electronegativity without significant atomic size changes. However, within a periodic group, electronegativity effects become negligible compared to atomic size changes and Brønsted-Lowry acids strengthen with increasing size. In contrast to Brønsted-Lowry acid behavior, increasing substituent atomic radii results in weaker Lewis acids for all systems considered ($R^2 = 0.72$, Figure 4.4).
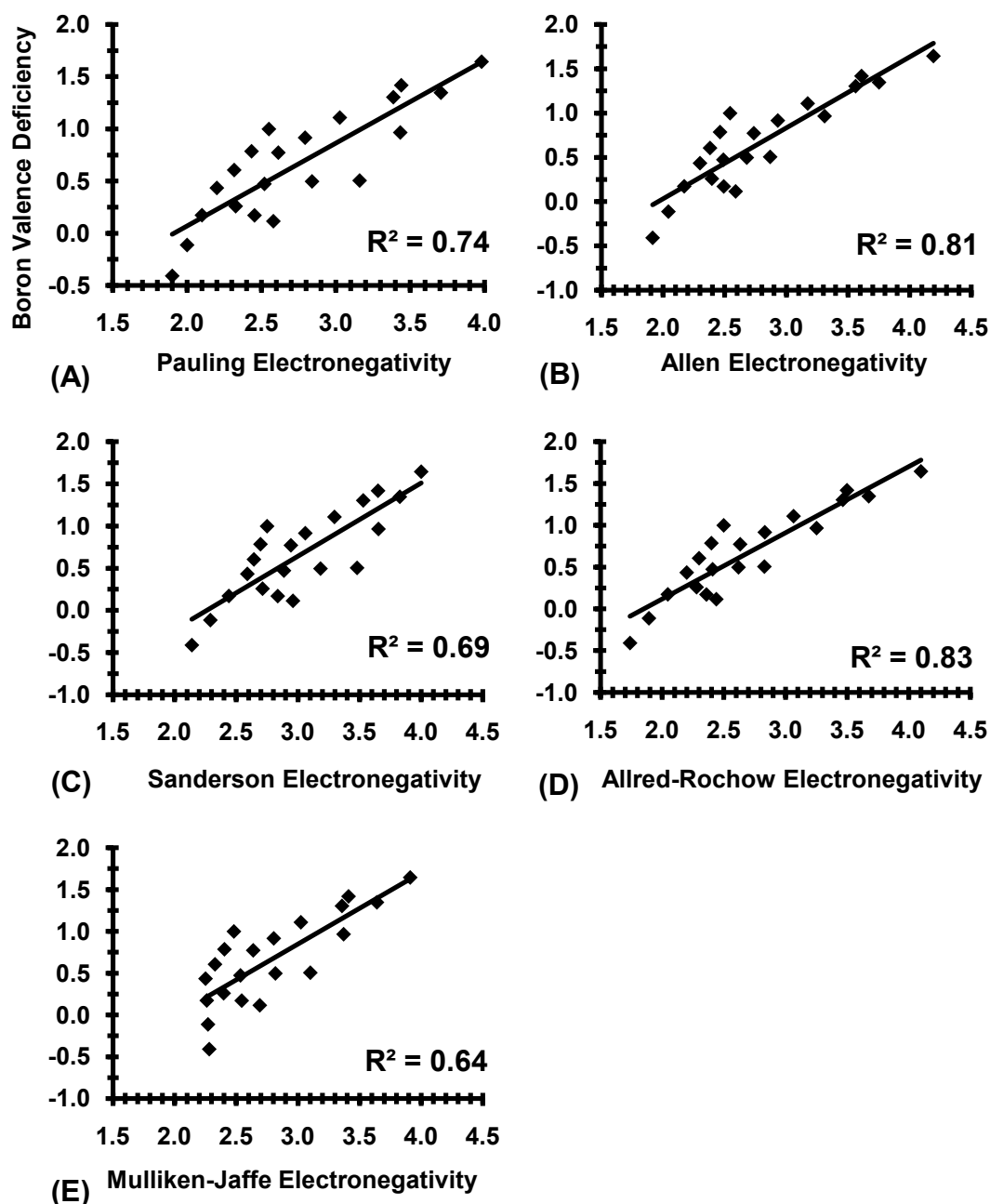
Figure 4.3. (A) Boron's valence deficiency (electrons) vs. the average Pauling electronegativity of the atoms coordinated to boron. (B) vs. Allen electronegativitity[312] (C) vs. Sanderson electronegativitiy[313] (D) Allred-Rochow electronegativity[314] (E) vs. Mulliken-Jaffe electronegativity.[315-317] Second and third period atoms as well as hydrogen are considered. Boron's valence deficiency is the formal valence of three minus the valence electrons predicted by NBO employing HF/cc-pVQZ//M06-2X//6-311++G(3df,2p).
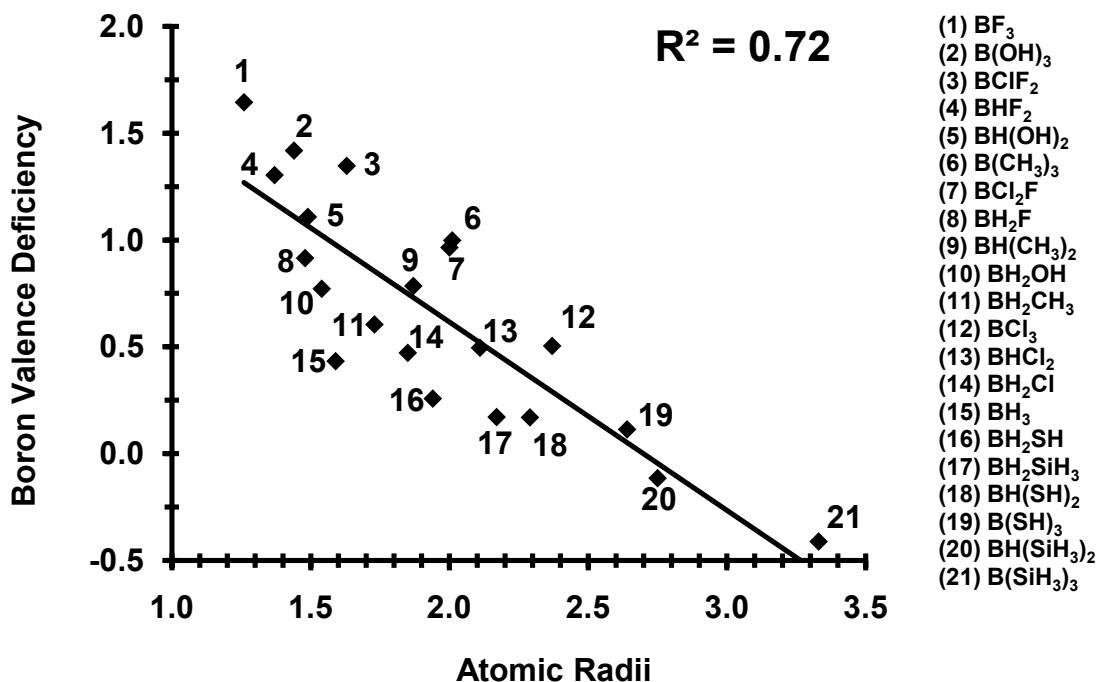
Figure 4.4. Boron's valence deficiency vs. the sum of atomic radii (Å) coordinated to boron. Second and third period atoms as well as hydrogen are considered.

4.3.1 Trends Across Periods

When second period substituted boron Lewis acids ($BH_{(3-n)}(CH_3)_n$, $BH_{(3-n)}(OH)_n$ and $BH_{(3-n)}F_n$; $n = 0$ to 3) are considered, boron's valence deficiency is highly correlated with substituent electronegativity ($R^2 = 0.94$; Figure 4.5A), but not with atomic radii ($R^2 = 0.33$, ; Figure 4.5B). This suggests that substituent electronegativity accounts for 61% more of the observed differences in Lewis acidity for second period substituted boron Lewis acids than does substituent atomic radii. This is in accordance with Brønsted-Lowry theory, where substituent electronegativity differences explain the differences in strength of acids within the same period. In contrast, when third period substituted boron Lewis acids ($BH_{(3-n)}Cl_n–NH_3$, $BH_{(3-n)}(SH)_n$, and $BH_{(3-n)}(SiH_3)_n$; $n = 0$ to 3) are

considered, little correlation is observed with electronegativity ($R^2 = 0.54$; Figure 4.6A) and only a moderate correlation is observed with atomic radii ($R^2 = 0.72$; Figure 4.6B). In order to achieve 94% of the variance in third period substituted boron Lewis acidity, an equal balance of electronegativity and atomic radii is necessary ($R^2 = 0.98$; Figure 4.6C). The coefficients of partial determination (r^2)[318] have been determined to gauge which independent variable is more prominent in explaining the variance in boron's valence deficiency. The coefficients of partial determination are discussed in Chapter 4.3.3.

A linear combination of substituent electronegativities and atomic radii explains the observed variance in boron's valence deficiency when considering second period substituents, similarly to that discovered for third period substituents. As Figure 4.5C displays, a 0.05 increase in the R^2 value is observed. Although the R^2 value is increased by considering the atomic radii in addition to the substituent electronegativity, only 5% more of the variance in boron's valence deficiency is ascribed. When second period substituents are coordinated to boron, a simpler and more concise explanation of differences in valence deficiency is achieved by considering only the substituent electronegativity.

Figure 4.5. (A) Boron's valence deficiency (electrons) vs. the average substituent Pauling electronegativity. (B) vs. the sum of atomic radii (Å) coordinated to boron. (C) vs. a linear combination of average substituent electronegativities (E.N.) and atomic radii sums (A.R.) of atoms coordinated to boron. The line of best fit for the linear combination is y = -2.2 + 0.82×E.N. + 0.56×A.R. Only second period atoms and hydrogen are considered.

Figure 4.6. (A) Boron's valence deficiency (electrons) vs. the average substituent Pauling electronegativity. (B) vs. the sum of atomic radii (Å) coordinated to boron. (C) vs. a linear combination of average substituent electronegativities (E.N.) and atomic radii sums (A.R.) of atoms coordinated to boron. The line of best fit for the linear combination is y = 0.17 + 0.41×E.N.- 0.41×A.R. Only third period atoms and hydrogen are considered.

Coordinate covalent π-bonds between halogen lone pairs and boron's formally empty $2p$ orbital were previously thought to regulate boron halide Lewis acidity and explain periodic trends. It was reported that fluorine lone pairs yield stronger coordinate covalent π-bonds, thus occupying more of boron's $2p$ orbital and accounting for the weaker acidity of BF_3 compared to BCl_3.[7, 287, 295] However, heavier halogens with more

diffuse polarizable lone pairs were predicted to form stronger coordinate covalent π-bonds.[299-301] Thus, a weaker interaction between fluorine's lone pair and boron's formally empty $2p$ orbital is expected when compared to chlorine.[299-301] However, the overlap integral, S_π, representing the magnitude of π-overlap between p_B and p_F, is marginally greater than that between p_B and p_{Cl} (Figure 4.7), in accord with previous reports.[7, 287, 295] Thus, the importance of substituent effects on Lewis acidity solely through coordinate covalent π-bond interactions is questionable.[70, 277, 286, 287, 290-292, 295-298]
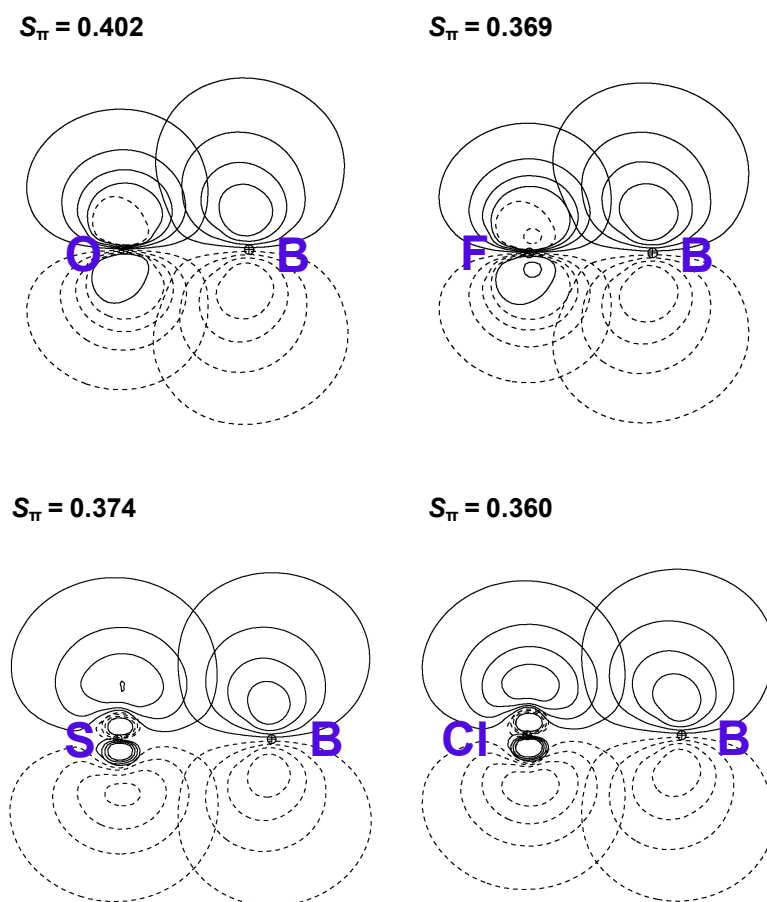
Figure 4.7. Natural hybrid orbital overlap yielding coordinate covalent π bonds between boron and X (X = OH, F, SH, and Cl) within BH_2X. S_π is the overlap integral corresponding to the natural hybrid orbitals involved.

Sigma bond orbital overlap, S_σ, reported in this work represents a novel approach to understanding the correlation between atomic size and Lewis acidity. S_σ between sp^n hybrid orbitals on boron and substituents is correlated with atomic radii (Figure 4.8), where both decrease upon moving across the second and third period from carbon to fluorine ($S_\sigma = 0.82 > 0.78 > 0.72$) and from silicon to chlorine ($S_\sigma = 0.83 > 0.79 > 0.76$), respectively. Differences in S_σ are also correlated with atomic sizes, where both increase upon moving down a periodic group. Larger atoms possess larger sp^n orbitals and thus result in a greater S_σ with boron's hybrid sp^n orbital. Increased S_σ provides additional electron density for electron deficient boron, decreasing its valence deficiency, and ultimately decreasing its acidity. The increase in S_σ between the second and third period within the same group underscores the need to consider a balance of both electronegativity and size effects for a complete description of third period substituted boron Lewis acid strength.

$S_\sigma = 0.824$ $S_\sigma = 0.779$ $S_\sigma = 0.720$

$S_\sigma = 0.827$ $S_\sigma = 0.789$ $S_\sigma = 0.761$
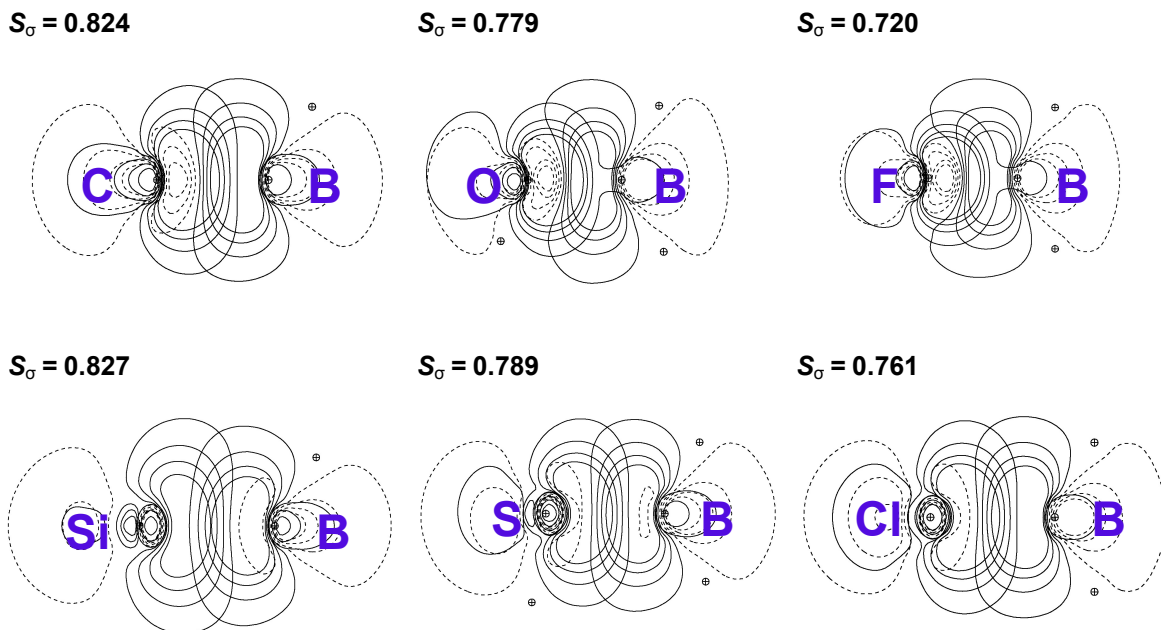
Figure 4.8. Natural hybrid orbital overlap yielding the σ between boron and X (X = CH_3, OH, F, SiH_3, SH, and Cl) within BH_2X. S_σ is the overlap integral corresponding to the natural hybrid orbitals involved.

4.3.2 Trends Down Groups

Only two elements in Groups 14 (carbon and silicon), 16 (oxygen and sulfur), and 17 (fluorine and chlorine) have been considered due to basis set limitations. Interesting differences with Brønsted-Lowry trends are apparent. Group 14 substituent electronegativity is highly correlated with boron's electron deficiency ($R^2 = 0.98$; Figure 4.9A) and atomic radii is only moderately correlated ($R^2 = 0.68$, Figure 4.9B). For example, the difference in S_σ of 0.003, concerning BH_2SiH_3 and BH_2CH_3 can hardly explain the variance in boron's valence deficiency of 0.44 e (Figure 4.8). Consequently, the large differences in electronegativity between carbon and silicon are necessary to

account for the differences in boron's valence deficiency. Electronegativity best explains the variance in boron's valence deficiency as compared to substituent size regarding Group 14 substituents. An equal balance of electronegativity and atomic size is required when considering Groups 16 and 17, as shown by Figure 4.10C and Figure 4.11C, respectively. Again, S_σ influences boron's valence in the same manner as described in Chapter 4.3.1. It is suspected that considering atoms further down Groups 16 and 17 will reveal that boron's valence deficiency exhibits an even greater dependence on size effects through sigma bond orbital overlap.

(1) $B(CH_3)_3$
(2) $BH(CH_3)_2$
(3) BH_2CH_3
(4) BH_3
(5) BH_2SiH_3
(6) $BH(SiH_3)_2$
(7) $B(SiH_3)_3$
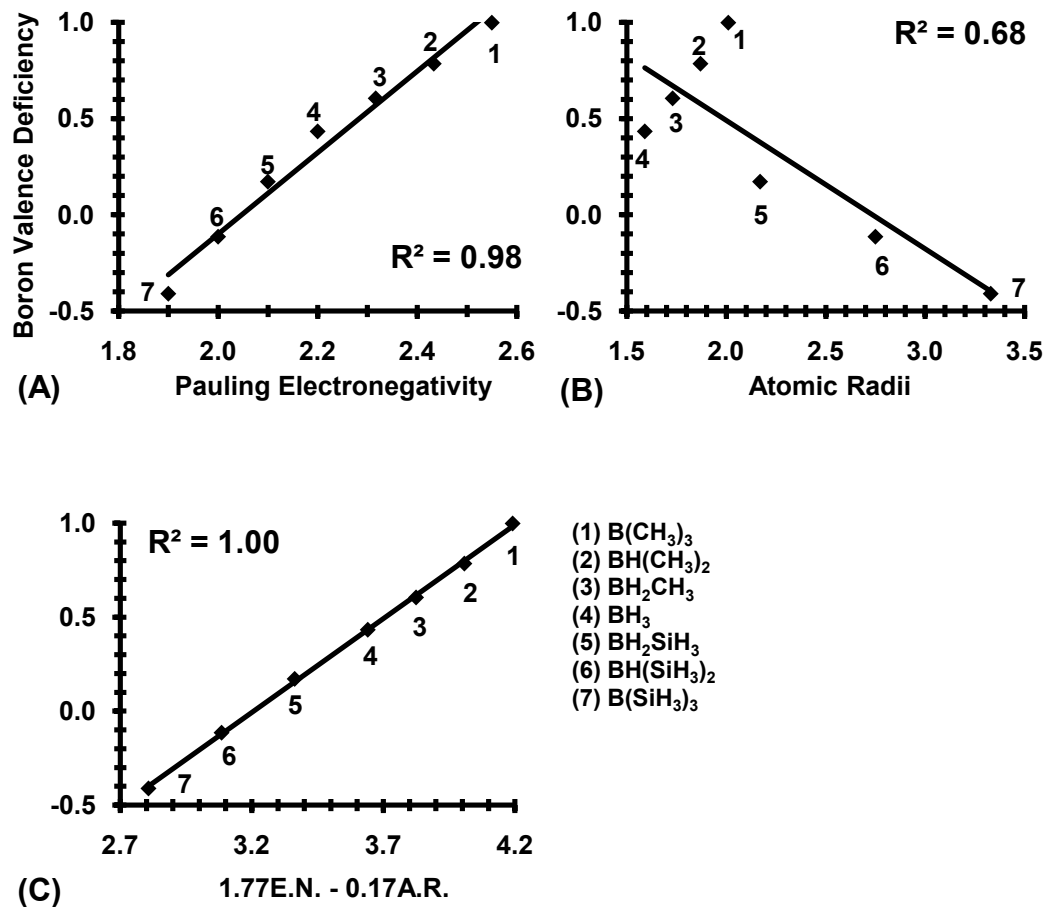
Figure 4.9. (A) Boron's valence deficiency (electrons) vs. the average substituent Pauling electronegativity. (B) vs. the sum of atomic radii (Å) coordinated to boron. (C) vs. a linear combination of average substituent electronegativities (E.N.) and atomic radii sums (A.R.) of atoms coordinated to boron. The line of best fit for the linear combination is y = -3.02 + 1.77×E.N.- 0.17×A.R. Only Group 14 atoms and hydrogen are considered.
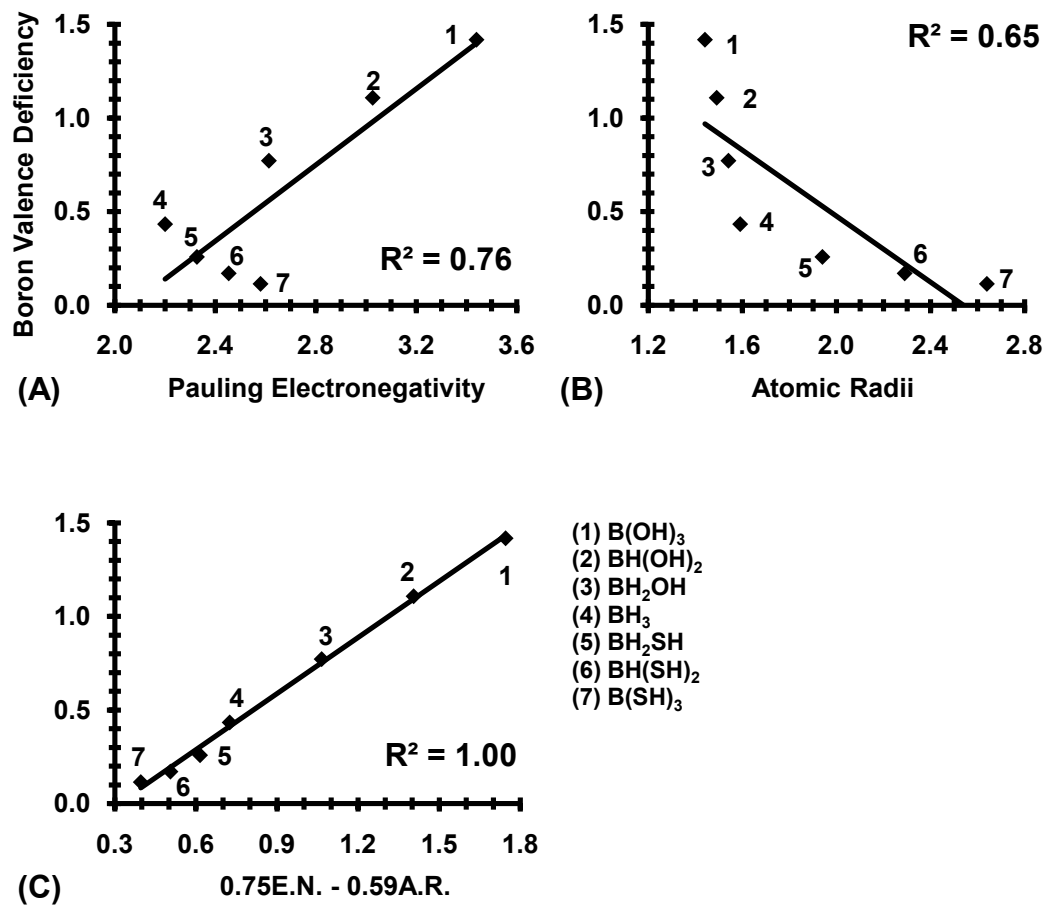
Figure 4.10. (A) Boron's valence deficiency (electrons) vs. the average substituent Pauling electronegativity. (B) vs. the sum of atomic radii (Å) coordinated to boron. (C) vs. a linear combination of average substituent electronegativities (E.N.) and atomic radii sums (A.R.) of atoms coordinated to boron. The line of best fit for the linear combination is y = -0.31 + 0.75×E.N.- 0.59×A.R. Only Group 16 atoms and hydrogen are considered.
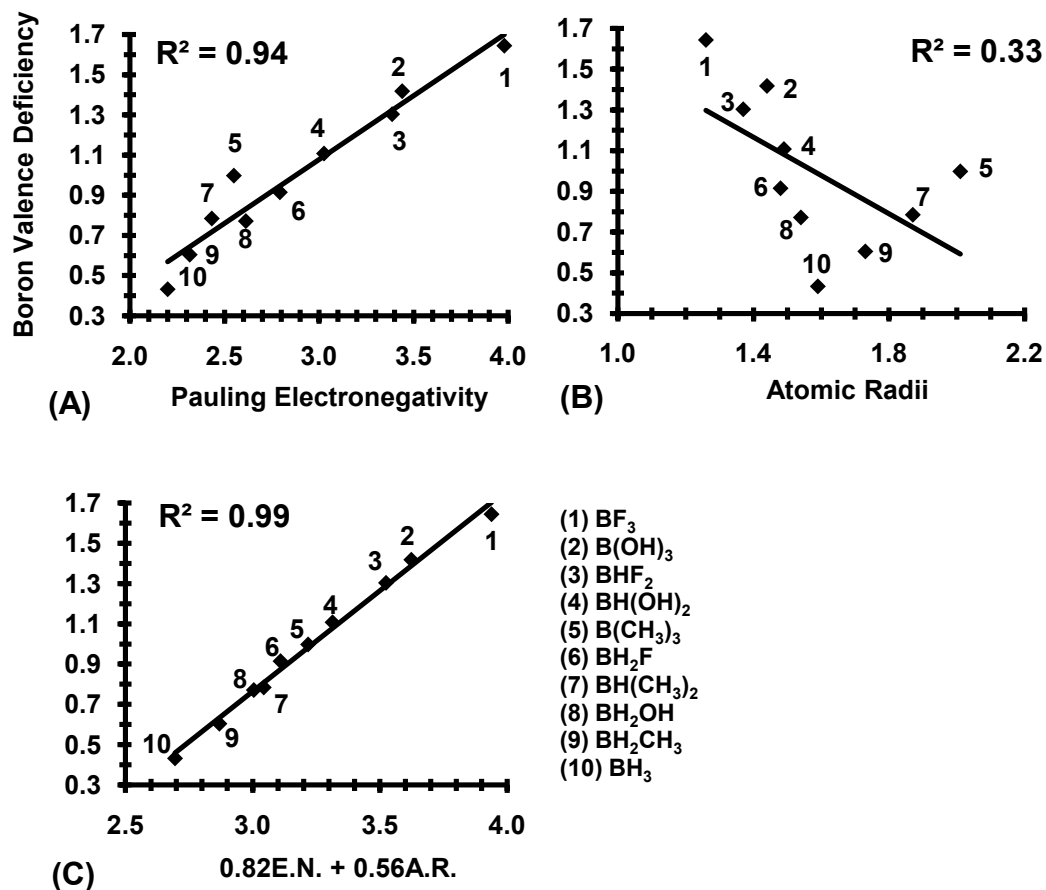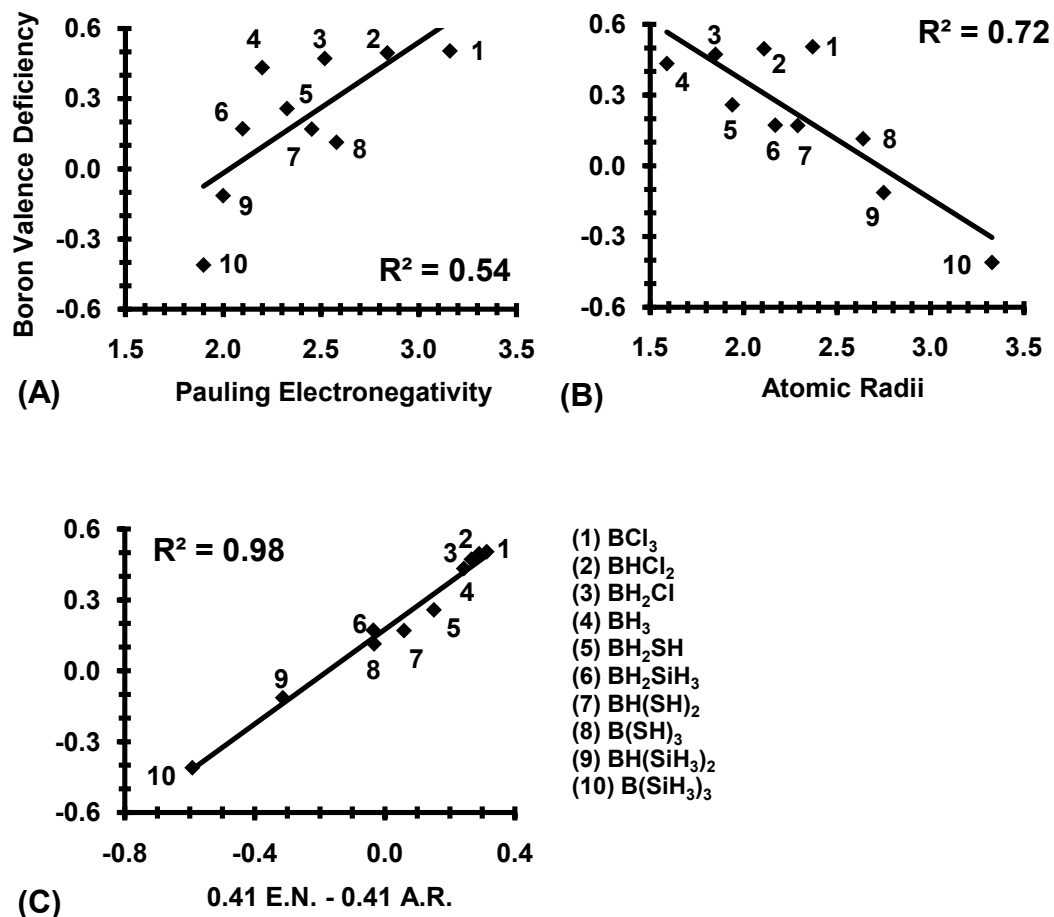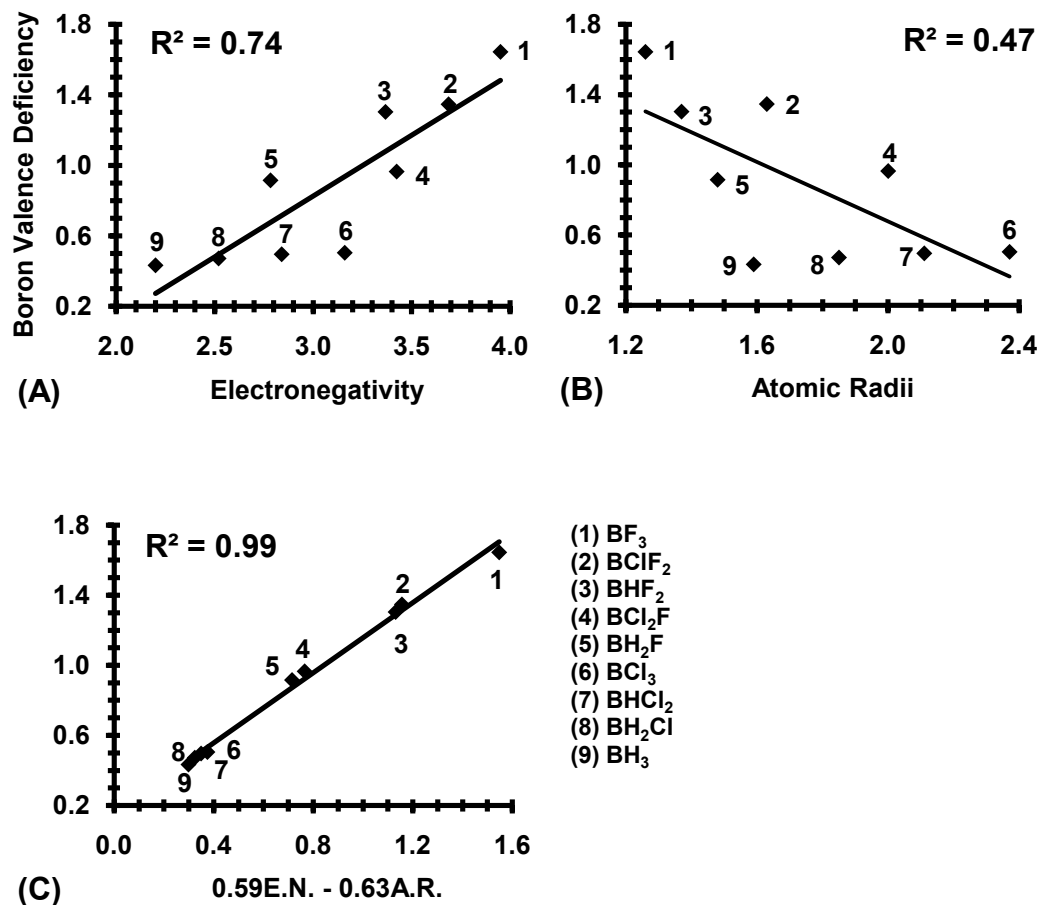
Figure 4.11. (A) Boron's valence deficiency (electrons) vs. the average substituent Pauling electronegativity. (B) vs. the sum of atomic radii (Å) coordinated to boron. (C) vs. a linear combination of average substituent electronegativities (E.N.) and atomic radii sums (A.R.) of atoms coordinated to boron. The line of best fit for the linear combination is y = -0.16 + 0.59×E.N.- 0.63×A.R. Only Group 17 atoms and hydrogen are considered.

4.3.3 Coefficients of Partial Determination

The coefficient of partial determination (r^2)[318] has been analyzed in order to determine the importance of each independent variable (substituent electronegativity and atomic radii) in explaining the dependent variable's variance (boron's valence deficiency). The coefficient of partial determination measures the contribution of one

independent variable when added to a model containing other independent variables. For example, the r^2 regarding a multiple linear regression containing a dependent variable (Y) and two independent variables (X_1 and X_2) would take the following form:

$$r^2_{Y2.1} = \frac{SSE(X_1) - SSE(X_1, X_2)}{SSE(X_1)} \qquad 4.1$$

Where *SSE* is defined as the error sum of squares of the regression incorporating the independent variables within the parentheses. The entries to the right of the dot within the subscript of $r^2_{Y2.1}$ indicate the variable that is already within the model where the entries to the left indicate the dependent variable as well as the independent variable being introduced to the model. Multiplying the result by 100 yields a percent decrease in the error sum of squares when X_2 is added to the model that already contains X_1. Comparing coefficients of partial determination allows the importance of each variable to be assessed. For example, if X_2 is added to a model that contains only X_1, and the error sum of squares is decreased to a greater extent than when X_1 is added to the model that contains only X_2, than X_2 is more important than X_1 when modeling the variance of Y. Table 4.2 summarizes the coefficients of partial determination for each multiple linear regression discussed throughout Chapter 4.

Table 4.2. Partial Coefficients of Determination Regarding Boron's Valence Deficiency (Y) vs. a Linear Combination of Substituent Electronegativity (EN) and Atomic Radii (AR).

Plot	$r^2_{YEN.AR}$	$r^2_{YAR.EN}$
Figure 4.6C[a]	0.94	0.96
Figure 4.10C[b]	0.99	0.99
Figure 4.11C[c]	0.99	0.98

[a] Only third period atoms and hydrogen are considered.
[b] Only Group sixteen atoms (oxygen periodic group) and hydrogen are considered.
[c] Only Group seventeen atoms (fluorine periodic group) and hydrogen are considered.

Regarding, third period, Group 16, and Group 17 trends, the data indicates that when substituent electronegativity or atomic radii are added to a model that contains the remaining independent variable, the error sum of squares decreases by about the same extent. This indicates that each is equally important when modeling the boron valence deficiency.

4.4 Comparison to Previous Models

The present work demonstrates that boron's valence deficiency is an innate chemical property that accounts for the electrophilicity of boron and ultimately determines its Lewis acidity. The influence of $p(\pi) \rightarrow p(\pi)$ hyperconjugation on Lewis acid reorganization energy[70, 286, 287, 290, 291, 298] was previously assumed to be an intrinsic property of the acid, independent from external Lewis bases. However, Drago and coworkers have shown a weakness with this assumption and that reorganization energies are a function of the coordinate covalent bond strength.[290] Furthermore, our results suggest that the $p(\pi) \rightarrow p(\pi)$ hyperconjugation strength is not consistent with boron's valence deficiency. Consequently, our comparison to other models is limited to that described by the lowest unoccupied molecular orbital (LUMO).[287, 288, 293, 303, 305]

It has been reported, utilizing ab initio electronic structure theory, that BCl_3 is a stronger Lewis acid than BF_3 when coordinated to NH_3 due to BCl_3's lower energy LUMO.[287, 288, 293, 303, 305] Thus, the relationship between boron halide LUMOs and its acidity in terms of valence deficiency were re-investigated in this study. First, only BX_3 (X = H, F, Cl) Lewis acids are considered to establish a direct comparison with previous theoretical investigations, where only homogenous Lewis acids such as BF_3 and BCl_3 were analyzed.[287, 288, 293, 303, 305] Indeed, a moderately strong correlation (Figure 4.12; R^2 = 0.82) is found between increasing boron valence deficiency (stronger Lewis acidity) and higher energy LUMOs. The relative LUMOs regarding BF_3 and BCl_3 are in accord with previous studies.[287, 288, 293, 303, 305] To further probe the boron Lewis acid LUMO and its consequence upon Lewis acidity, the systematic halogen substituted Lewis acids, $BH_{(3-n)}F_n–NH_3$, $BH_{(3-n)}Cl_n–NH_3$, and $BCl_{(3-n)}F_n–NH_3$ (n = 0 to 3) were analyzed. Upon analyzing all nine boron halide Lewis acids, the correlation decreases from R^2 = 0.82 to 0.42 (Figure 4.12) essentially eliminating the correlation that was demonstrated when only BX_3 Lewis acids were considered. When the mixed halogen substituted Lewis acids are considered, more subtle differences are revealed indicating that Lewis acidity is not a strict consequence of the LUMO energy level.
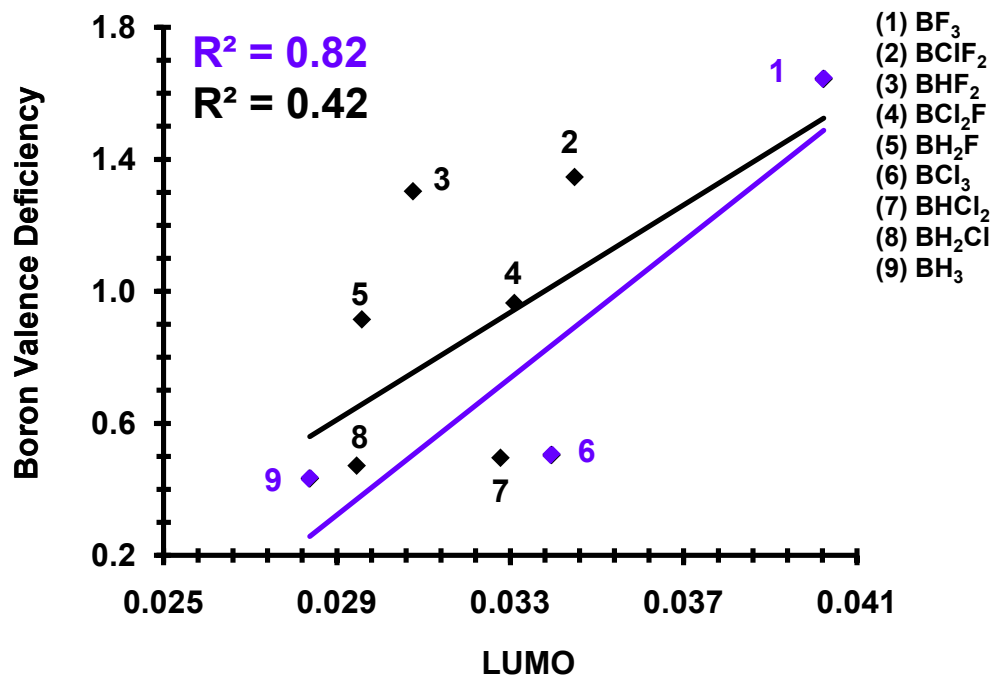
Figure 4.12. Boron's valence deficiency (electrons) vs. the LUMO energy level (hartrees). Energy levels refer to Hartree Fock-orbitals. The black trend line indicates that all boron halide Lewis acids are considered. The blue trend line considers only BX_3 homogenous Lewis acids (X = H, F, Cl).

It is common to gauge the strength of a Lewis acid from the strength of the coordinate covalent bond formed with a common base, as discussed in the Introduction. The binding enthalpies of $X_3B–NH_3$ adducts (X = H, F, Cl) vs. the corresponding boron valence deficiency supports previous results, where Lewis acidity increases as $BF_3 <$ $BCl_3 < BH_3$ (Figure 4.13; $R^2 = 0.91$) with $(CH_3)_3P$ and $(CH_3)_3As$ as Lewis bases;[281] however, when the systematic halogen substituted Lewis acids were analyzed the correlation decreases from $R^2 = 0.91$ to 0.63 (Figure 4.13) More subtle differences are revealed, similarly to that observed for boron's valence deficiency vs. LUMO,

supporting that adduct stability is not a useful indicator of Lewis acidity, as discussed previously and shown by Figure 4.2.
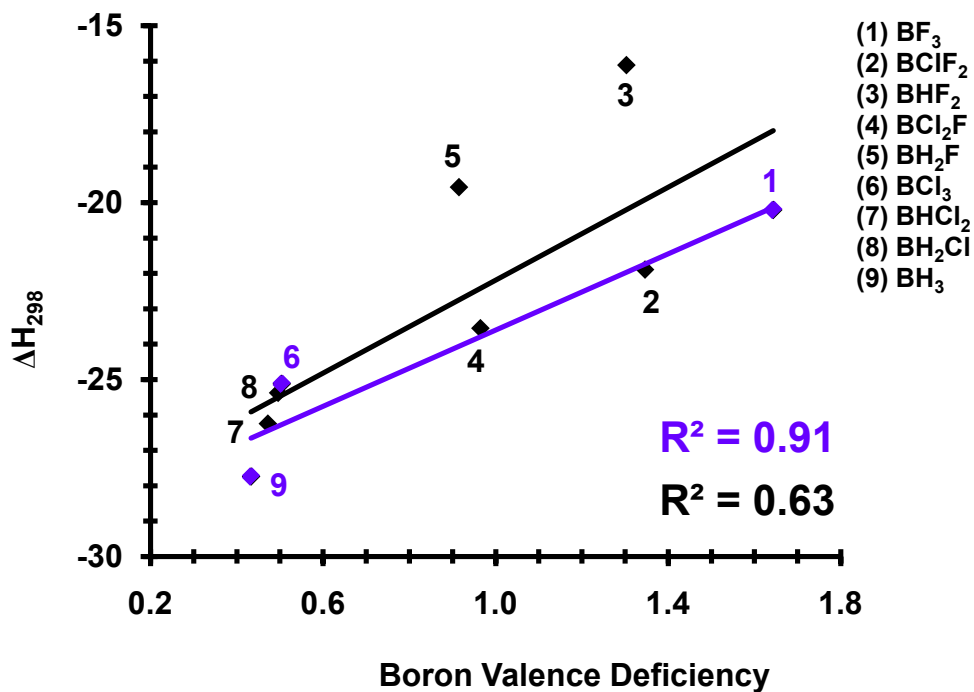
Figure 4.13. Binding enthalpy with NH_3 vs. the boron valence defciency (electrons). The black trend line indicates that all boron halide Lewis acids are considered. The blue trend line considers only BX_3 homogenous Lewis acids (X = H, F, Cl).

4.5 Extension to Aluminum Halides

A similar conundrum between predicted and observed Lewis acidities is found for the aluminum halide series, where complications arise from using coordinate covalent bond strengths as an acidity index, insufficient levels of theory, and different Lewis bases.[67, 299, 319-326] It was initially predicted, utilizing MP2/PDZ, that AlF_3 had a stronger fluoride affinity than $AlCl_3$.[67] However, experimental evaluation in conjunction

162

with additional theoretical work revealed that $AlCl_3$ had a larger affinity for fluoride than AlF_3.[320, 323] Furthermore, MP2/II+//MP2/II predicts that $AlCl_3$ forms a stronger coordinate covalent bond with NH_3 than with AlF_3.[319] However, when NH_3 is exchanged with CO or H_2O, reverse trends are predicted by MP2/II+//MP2/II,[319] MP2/VTZ+D+P,[299] and MP2/6-31G(d,p)[324] calculations. Furthermore, inappropriate levels of theory obscure clear conclusions. For example, coordinate covalent bond strengths between AlX_3 (X = F, Cl, Br, and I) and NH_3 predicted by B3LYP in conjunction with effective core potentials were reported to decrease as the halogen size increased.[322] In contrast, $AlBr_3$[325] forms a stronger bond with NH_3 than with $AlCl_3$[326] according to experimental bond dissociation energies, and $AlCl_3$ forms a stronger bond than found for AlF_3, according to MP2/II+//MP2/II predicted results.[319] Interestingly, a quantitative Lewis acid scale regarding AlX_3 (X = F, Cl, Br, and I) was attempted by comparing electron pair affinities.[327] It was reported that AlX_3 Lewis acidities increase as the halogen size increases. Although the external effects of the Lewis base were eliminated, the reorganization energy demonstrated by the Lewis acid remains as a contaminant in describing the innate ability of a Lewis acid to capture electron density.

Extension of our ideas on boron Lewis acidity indicates that both atomic size and electronegativity regulate aluminum halide Lewis acidity. For example, fluorine possesses a larger electronegativity compared to other halides, thus creating a more electrophilic aluminum center and a stronger Lewis acid. In addition, fluorine possesses a smaller atomic radius, yielding a smaller S_σ by 0.02, decreasing the electron population available to boron's valence, increasing its deficiency and thus its Lewis acidity. NBO results support this prediction, where the aluminum valence deficiency for AlF_3 is

greater than that predicted for $AlCl_3$ by 0.77 electrons. It is also of interest to predict

Lewis acidities by exchanging the Group 13 atom rather than the substituent. The

intrinsic Lewis acidity of YX_3 (Y = Group 13 atom) should increase upon moving down

Group 13 due to electronegativity differences between the Group 13 atom and the

halide. For example, the electronegativity difference between aluminum and fluorine (Δ

= 2.37) is greater than that between boron and fluorine (Δ = 1.94). Therefore, the

valence deficiency and ultimately the Lewis acidity of aluminum halides should be

greater than that exhibited by boron halides. A NBO analysis of AlF_3 and BF_3 supports

this prediction, where the valence deficiency on aluminum and boron is 2.43 and 1.64

electrons, respectively. Preliminary data suggest that size is not important when

comparing the acidity of Group 13 substituted Lewis acids. For example, S_σ is greater

between boron and fluorine than predicted for aluminum and fluorine by only 0.06. This

may be an indication that the large electronegativity difference found between aluminum

and fluorine dominates over size differences. Electron density is more localized on

fluorine when coordinated to aluminum than when coordinated to boron and therefore

overlap with aluminum is decreased. Aluminum halide Lewis acids follow the same

periodic trends as boron halides, further illustrating that valence deficiency is an

apparent index of Lewis acidity that may be rationalized utilizing first principle ideas

such as substituent atomic radii and electronegativity.

4.6 Conclusion

Two main points are realized in describing Lewis acidity from a systematic analysis of twenty-one isolated boron Lewis acids. First, coordinate covalent bond strengths are not an adequate measure of Lewis acidity. Rather, Lewis acidity should be gauged by determining boron's valence deficiency, or its ability to accept an electron-pair. Second, Lewis acidity may be rationalized by the same principles that regulate Brønsted-Lowry acidity, but by different contributions. Specifically, substituent electronegativity explains boron Lewis acidity when second period atoms are coordinated to boron, while an equal balance of substituent electronegativity and atomic size are necessary when third period atoms are considered. Furthermore, substituent electronegativity explains Group 14 substituted boron Lewis acidity, while an equal balance of substituent electronegativity and atomic size are necessary when Group 16 and 17 substituents are considered. Atomic size is found to influence intrinsic boron Lewis acidity, through σ-bond overlap, independent of π-overlap. Specifically, the overlap between the hybrid orbitals present on boron and the substituents that form the σ bond are found to regulate Lewis acidity. A larger overlap increases the electron population available to boron's valence, decreasing its deficiency and thus its Lewis acidity. The present analysis delivers a fundamental report on Lewis acidity, consistent with first principle periodic trends, such as substituent electronegativity and atomic size, which has the potential to realign our understanding and prediction of Lewis acidities.

Chapter 5

Geminal Interactions Key to Lewis Acid Activation of Diels-Alder Reactions

Geminal interactions are fundamental to the binding strength of Lewis acid adducts, and ultimately the rate enhancement of eleven BF_2X catalyzed Diels-Alder reactions between 2-propenal and 1,3-butadiene. Geminal interactions lower sigma anti-bonding energy levels between boron and substituents to facilitate π-conjugation and decrease the energy of the dienophile's lowest unoccupied molecular orbital. The results are consistent with FMO theory, yet provide a novel and quantitative explanation on the activation of organic reactions by Lewis acids.

5.1 Introduction

It is well known that Lewis acids enhance the rate of organic reactions, especially those involving α,β enals.[263, 328-333] Lewis acid catalysis is traditionally explained using Fukui's FMO theory for Diels-Alder and other pericyclic reactions,[72, 95] as recently reviewed by Houk and coworkers.[334] The main idea is that electron density withdrawal from the dienophile provides a better energetic match between the dienophile LUMO and diene HOMO, allowing a more favorable interaction and activation energy lowering in normal electron demand Diels-Alder processes.[93]

A key assumption regarding Lewis acid catalysis is that the acid withdraws electron density from the dienophile. However as originally proposed by Lewis,[4, 55, 56] the acid accepts an electron pair to complete its valence in coordinate covalent bond formation (Figure 5.1). Once the adduct forms and the valency of boron is essentially satisfied, the mechanism of electron density withdrawal from the dienophile becomes much less obvious. Consequently, the purpose of this study is to bring clarity to Lewis acid activation of organic reactions, and report our findings involving stereoelectronic features of Lewis acid activation that correlate with the catalysis of the Diels-Alder reaction.
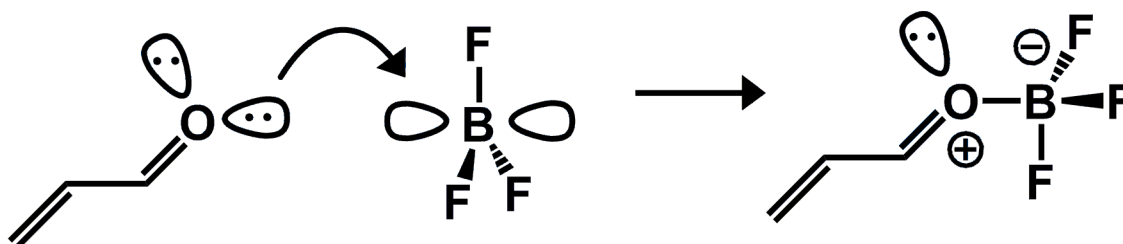
Figure 5.1. Main donor-acceptor interaction of the coordinate covalent bond in Lewis adduct formation.

The present analysis utilizes density functional theory and natural bond orbital (NBO) analysis to determine the stereoelectronic features[335] within Lewis acid adducts that govern the decrease in Gibbs free activation energy, $\Delta^{\ddagger}G_{298}$, of eleven $BF_2\mathbf{X}$ catalyzed Diels-Alder reactions between 1,3-butadiene and 2-propenal. Lewis acid substituents, $\mathbf{X}$ (Table 5.1), have been chosen to cover a full range of strong electron

donor groups (EDG) and acceptor groups (EWG), as given by Hammett's substituent constants,[336, 337] to investigate the impact of such variance upon rate enhancement.

Table 5.1. Hammett Constants Pertaining to the Substituents Investigated.

X	σ_p[336, 337]
$-N_2^+$	1.910
$-NO_2$	0.778
$-CN$	0.660
$-CF_3$	0.540
$-CO_2H$	0.450
$-F$	0.062
$-H$	0.000
$-CH_2CH_3$	-0.151
$-CH_3$	-0.170
$-OCH_3$	-0.268
$-OH$	-0.370
$-NH_2$	-0.660

5.2 Computational Approach

Electronic structure calculations have been explained in detail within Chapter 2, and were carried out with NWChem 5.1[112] and Gaussian09,[338] using the computational resources at the Center for Computational Science at Duquesne University.[256] All gas phase results are acquired by using NWChem 5.1, while solvent effects are included by utilizing the polarizable continuum model, as implemented by Gaussian09 and discussed below. All geometry optimizations and frequency analyses pertaining to Lewis acid catalyzed Diels-Alder reactions between 2-propenal and 1,3-butadiene were performed in the gas phase with the M06-2X[163] density functional method in conjunction with the 6-311++G(3df,2p) basis set.[187-193] The M06-2X/6-311++G(3df,2p) level of theory has

been found to be accurate within experimental accuracy when predicting the binding

energies of coordinate covalent bonded complexes.[24, 173] The performance of

M06-2X/6-311++G(3df,2p) is critical to this study, because Lewis acid adducts involve

the coordinate covalent bond. The performance of M06-2X and M05-2X[141] in

conjunction with the correlation consistent basis sets[194-196] (cc-pVXZ; X = D, T, Q, 5)

was also evaluated and compared to the experimental activation energy of the

uncatalyzed Diels-Alder reaction between 2-propenal and 1,3-butadiene. In addition, the

performance of the B3LYP density functional method was also assessed, due to its

popularity and wide-spread use. M06-2X/6-311++G(3df,2p) has been used to determine

the activation energy of the AlCl$_3$ catalyzed and uncatalyzed Diels-Alder reaction

between methyl acrylate and 1,3-butadiene to determine if M06-2X/6-311++G(3df,2p)

is capable of reproducing the experimental difference in activation energies between

catalyzed and uncatalyzed reactions.

Binding enthalpies predicted by M06-2X/6-311++G(3df,2p) have been corrected

for basis set superposition error (BSSE) by using the counterpoise method developed by

Boys and Bernardi.[201-203] As expected with such a basis set, the amount of BSSE is

found to be about 1 kcal/mol or less for these specific adducts. All minima and first

order saddle points have been confirmed by the absence of imaginary frequencies and

the presence of one imaginary frequency, respectively. Regarding Lewis acid catalyzed

reactions, enthalpy and entropy corrections were predicted utilizing

M06-2X/6-311++G(3df,2p) in order to compute binding enthalpies, ΔH_{298}, and Gibbs

free activation barriers, $\Delta^{\ddagger}G_{298}$. Activation energies, $\Delta^{\ddagger}E_{298}$, determined with the

cc-pVXZ (X = D, T, Q, 5) basis sets become resource intensive as X increases.

Consequently, employing frequency calculations to compute the appropriate thermal corrections, using the cc-pVQZ and cc-pV5Z basis sets, are not possible at this time. For the sake of maintaining consistency across the four different correlation consistent basis sets, the appropriate thermal corrections were determined by M05-2X, M06-2X, and B3LYP in conjunction with the 6-311++G(3df,2p) basis set and were subsequently added to the corresponding electronic energy predicted by each method and correlation consistent basis set.

Natural bond orbital (NBO) analysis[221] was performed using the NBO 5.G program,[113] embedded within NWChem 5.1. NBO is discussed in detail elsewhere.[213, 220-222, 339] Goodman reported inadequacies in the triple-split 6-311++G Pople basis set, where diffuse function augmentation lead to misleading conclusions drawn from NBO analysis regarding the stability of common four heavy atom molecules.[310] However, double-split 6-31G Pople and correlation consistent basis sets are less sensitive to diffuse augmentation, and allow for accurate assessments. Consequently, specific stereoelectronic effects have been investigated utilizing HF/cc-pVQZ on the M06-2X/6-311++G(3df,2p) computed minima.

The activation energies corresponding to the $AlCl_3$ catalyzed and uncatalyzed Diels-Alder reaction between methyl acrylate and 1,3 butadiene have been experimentally determined in benzene.[100] In order for a direct comparison between theory and experiment, solvent effects must be included. Consequently, the polarizable continuum model (PCM) developed by Tomasi and coworkers[340-342] has been employed, as implemented by Gaussian09.[338] The implicit model involves effective Hamiltonian methods that use continuum distributions to describe the solvent.[343] The advantage of

such a scheme is that bulk solvent effects calibrated against macroscopic properties can be efficiently included within the quantum mechanical framework.[344] The PCM model has been used to investigate successfully the effect of solvent upon the energetics and equilibria of other small molecular systems, such as the similar Diels-Alder reaction between 2-propenal and 1,3-butadiene.[345] The PCM method has been described in detail.[343] Briefly, the solute is represented by a charge distribution in a cavity embedded in an infinite polarizable dielectric medium. The cavity shape is obtained from the van der Waals radii of the atoms of the solute. The solvent used in this study is benzene, which possesses a dielectric constant of $\varepsilon = 2.27$. Full geometry optimizations and frequency analyses were performed on the appropriate ground states and transition structures to determine the activation energies, $\Delta^{\ddagger}E_{298}$.

5.3 Geometries of BF_2X Ground State Adducts

Four dienophile adducts are possible by the coordination between boron and the carbonyl oxygen lone pair *syn* to the formyl proton, with B–**X** *synclinal*, *antiperiplanar*, *synperiplanar*, or *anticlinal* to the uncomplexed oxygen lone pair, as illustrated by Figure 5.2.
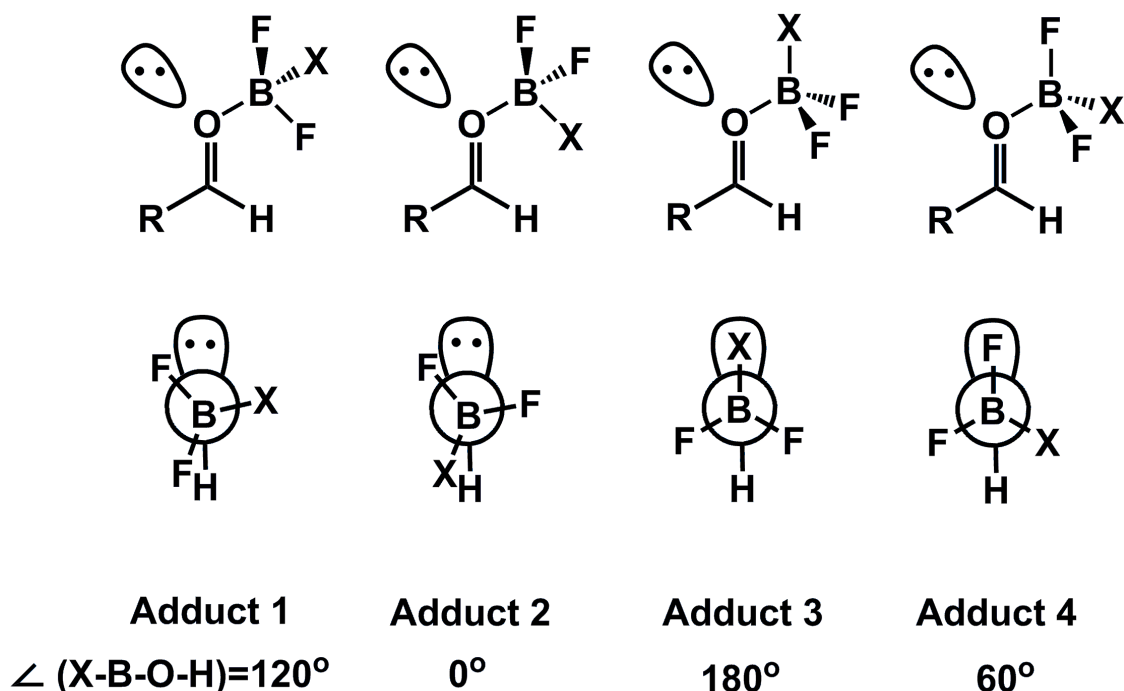
Figure 5.2. Newman projections that illustrate the four possible adduct conformations between BF_2X and 2-propenal. Adduct 1 possesses the substituent, **X**, *synclinal* ($\angle($ **X**–B–O–H) = 120.0°) to the uncomplexed oxygen lone pair. Adduct 2, Adduct 3, and Adduct 4 represent the *antiperiplanar* ($\angle($ **X**–B–O–H) = 0.0°), *synperiplanar* ($\angle($ **X**–B–O–H) = 180.0°), and *anticlinal* ($\angle($**X**–B–O–H) = 60.0°) conformations, respectively.

All four possible conformations are investigated for each substituted BF_2X adduct. Thus, the relative energies between all four adducts regarding each BF_2X substitution are revealed by Table 5.2. Only the lowest energy adducts are discussed and considered for further computations regarding activation barriers and stereoelectronic effects. Previous reports attribute conformational preferences to an electrostatic interaction, known as *nontraditional hydrogen bonding* (O=C–H$\cdots$X, X=F or O).[346-348] In contrast, theoretical analyses suggest that a generalized anomeric effect between the uncomplexed oxygen lone pair on the carbonyl group and the *antiperiplanar* antibonding sigma orbital between boron and the heteroatom (n(O) → σ*(B–X) (X=H,

O, F, or Cl)) is responsible for the conformational preference.[349-352] Other

stereoelectronic effects have been reported to govern the conformational preference as

well, including $\pi(C=O) \rightarrow \sigma^*(B–X)$, $n(X) \rightarrow \pi^*(C=O)$, and $\sigma(B–X) \rightarrow \pi^*(C=O)$.[352] It is

not within the scope of this dissertation to address the factors that govern the

conformational preferences between the various adducts. Only the lowest energy

adducts are of interest and are shown by Figure 5.3.

Table 5.2. Relative Energies between Each Adduct for All Substituted BF_2**X** Lewis Acids Coordinated to 2-propenal.[a]

X	Adduct 1	Adduct 2	Adduct 3	Adduct 4
$-N_2^{+}$ [b]	0.0	3.5	3.7	0.0
$-NO_2$	NA[c]	0.0	2.1	NA[c]
-CN	0.6	0.0	1.8	0.5
$-CF_3$	NA[c]	2.3	2.3	0.0
$-CO_2H$	NA[c]	3.3	4.5	0.0
-F [d]	0.0	-	0.4	-
-H	0.0	1.4	0.4	NA[c]
$-CH_2CH_3$	0.0	2.7	0.3	NA[c]
$-CH_3$	0.0	2.4	0.1	NA[c]
$-OCH_3$	0.0	3.0	4.3	0.1
-OH	0.0	NA[c]	NA[c]	0.2
$-NH_2$	NA[c]	NA[c]	0.0	NA[c]

[a] All values are in kcal/mol.
[b] The lowest energy adduct forms a planar sp^2 boron center with each fluorine *synperiplanar* and *antiperiplanar* to the uncomplexed oxygen lone pair, as shown by Figure 5.3, possessing characteristics of Adduct 1 and Adduct 4, and thus is considered in both columns.
[c] After exhaustive searches, a local minimum could not be found or the saddle point corresponds to a first order transition state.
[d] Adduct 1 and Adduct 2 are equivalent. Adduct 3 and Adduct 4 are equivalent.

X = N$_2^+$ r(O–B) = 1.43 Å   ∠(X–B–O–H) = 88.1°

X = NO$_2$ r(O–B) = 1.61Å   ∠(X–B–O–H) = 0.0° (Adduct 2)

X = CN   r(O–B) = 1.65Å   ∠(X–B–O–H) = 0.0°(Adduct 2)
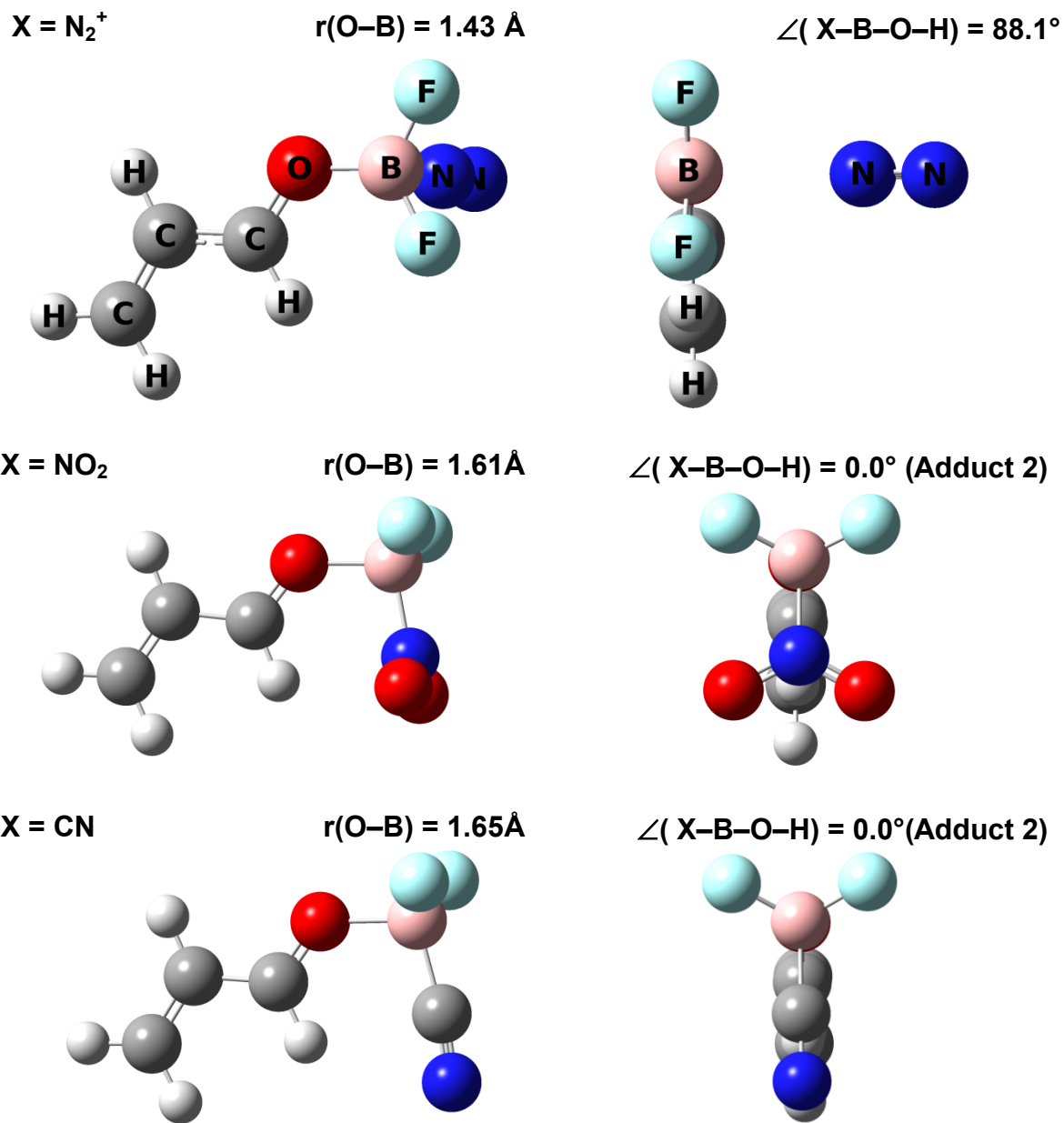
Figure 5.3. BF$_2$**X** Lewis acids coordinated to 2-propenal, forming a coordinate covalent bond between oxygen and boron.   B–O bond lengths are reported above each structure to the left and the **X**–B–O–H dihedral angle is reported above each structure to the right. Small white balls are hydrogen atoms, large white balls are fluorine atoms, grey atoms are carbon atoms, red balls are oxygen atoms, and blue balls are nitrogen atoms.

174

X = CF₃　　　　**r(O–B) = 1.63Å**　　　∠(X–B–O–H) = 86.9° (Adduct 4)

X = CO₂H　　　**r(O–B) = 1.60Å**　　　∠(X–B–O–H) = 70.7°(Adduct 4)

X = F　　　　　**r(O–B) = 1.69Å**　　　∠(X–B–O–H) = 0.0°(Adduct 2 = 1)

X = H　　　　　**r(O–B) = 1.71 Å**　　　∠(X–B–O–H) = 116.5° (Adduct 1)

Figure 5.3. (continued).

175
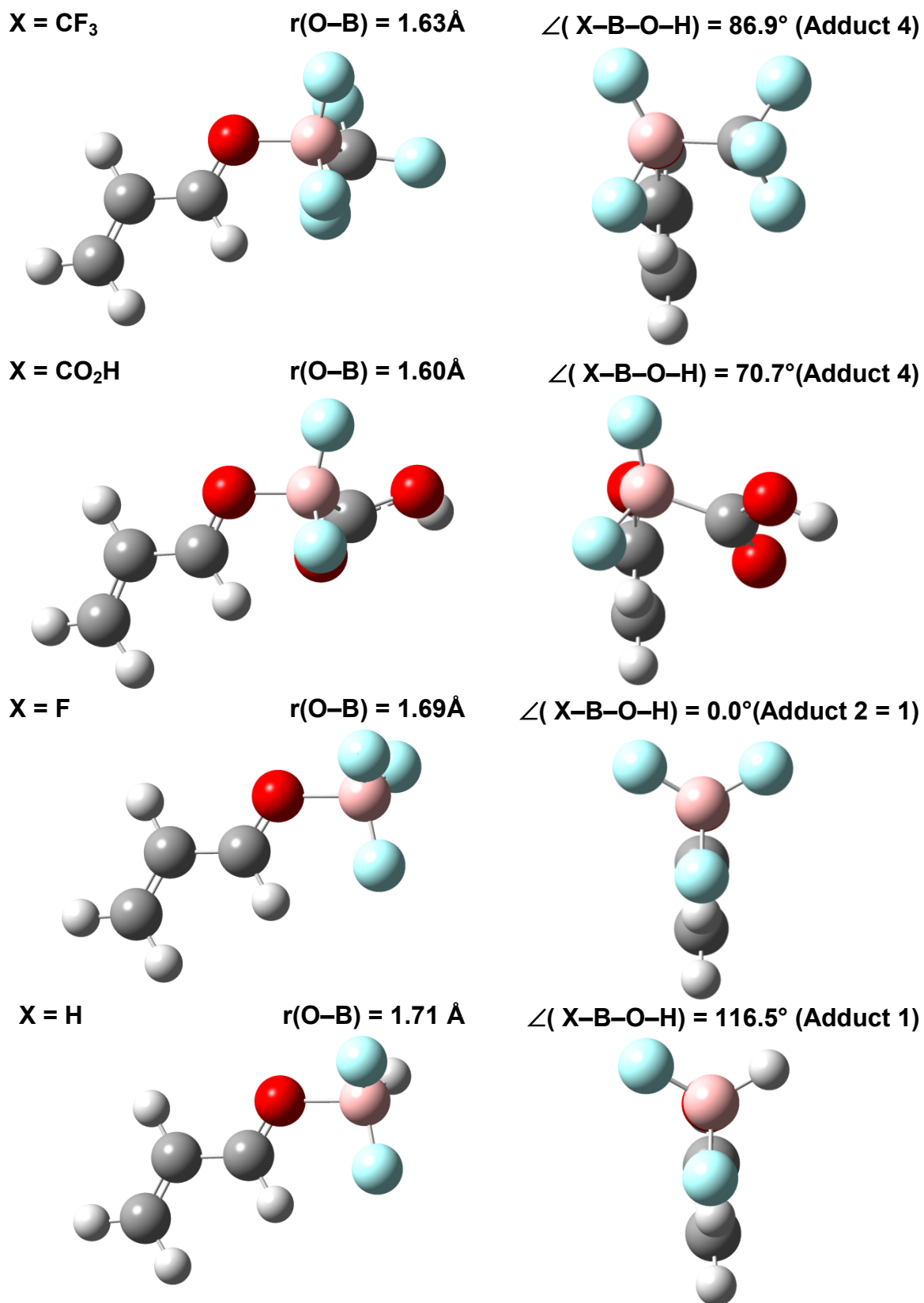
X = CH₂CH₃   **r(O–B) = 1.81 Å**   ∠(X–B–O–H) = 177.0° (Adduct 3)
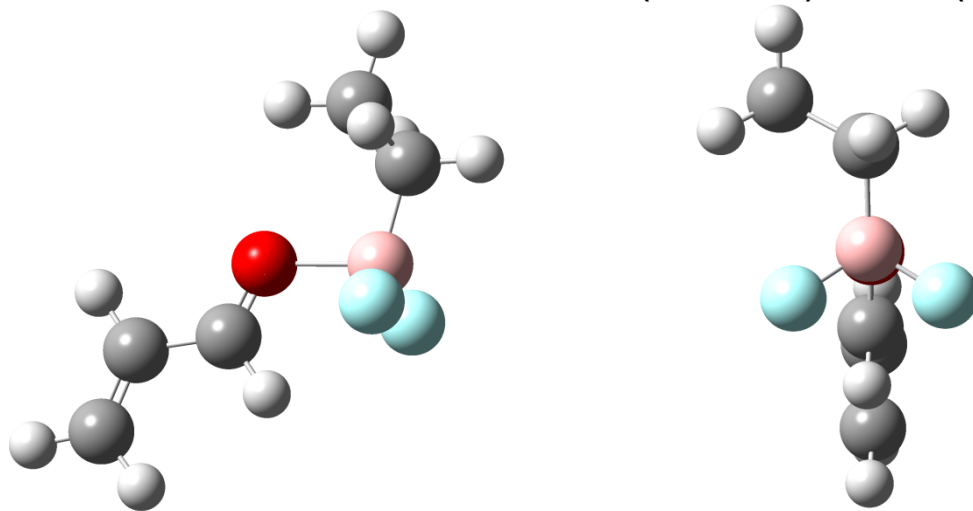
X = CH₃   **r(O–B) = 1.78 Å**   ∠(X–B–O–H) = 126.3° (Adduct 1)
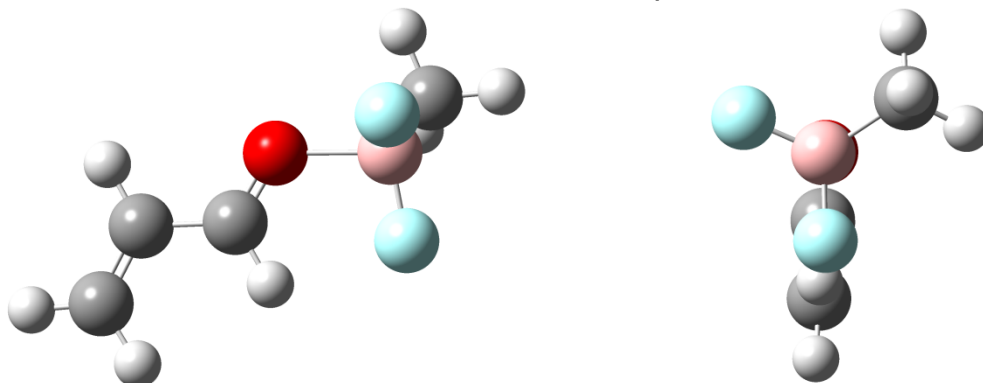
X = OCH₃   **r(O–B) = 2.32 Å**   ∠(X–B–O–H) = 121.1° (Adduct 1)

Figure 5.3. (continued).

176

X = OH　　　　r(O–B) = 1.89 Å　　∠(X–B–O–H) = 113.6° (Adduct 1)

X = NH$_2$　　　　r(O–B) = 2.58 Å　　∠(X–B–O–H) = 180.0° (Adduct 3)
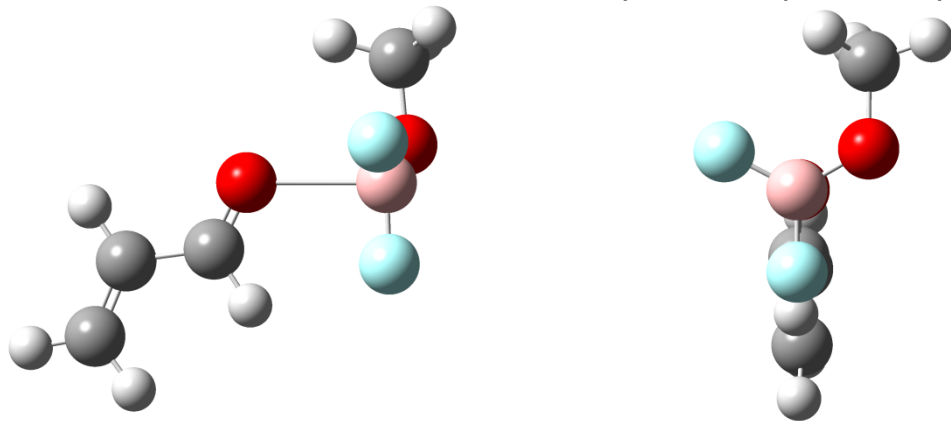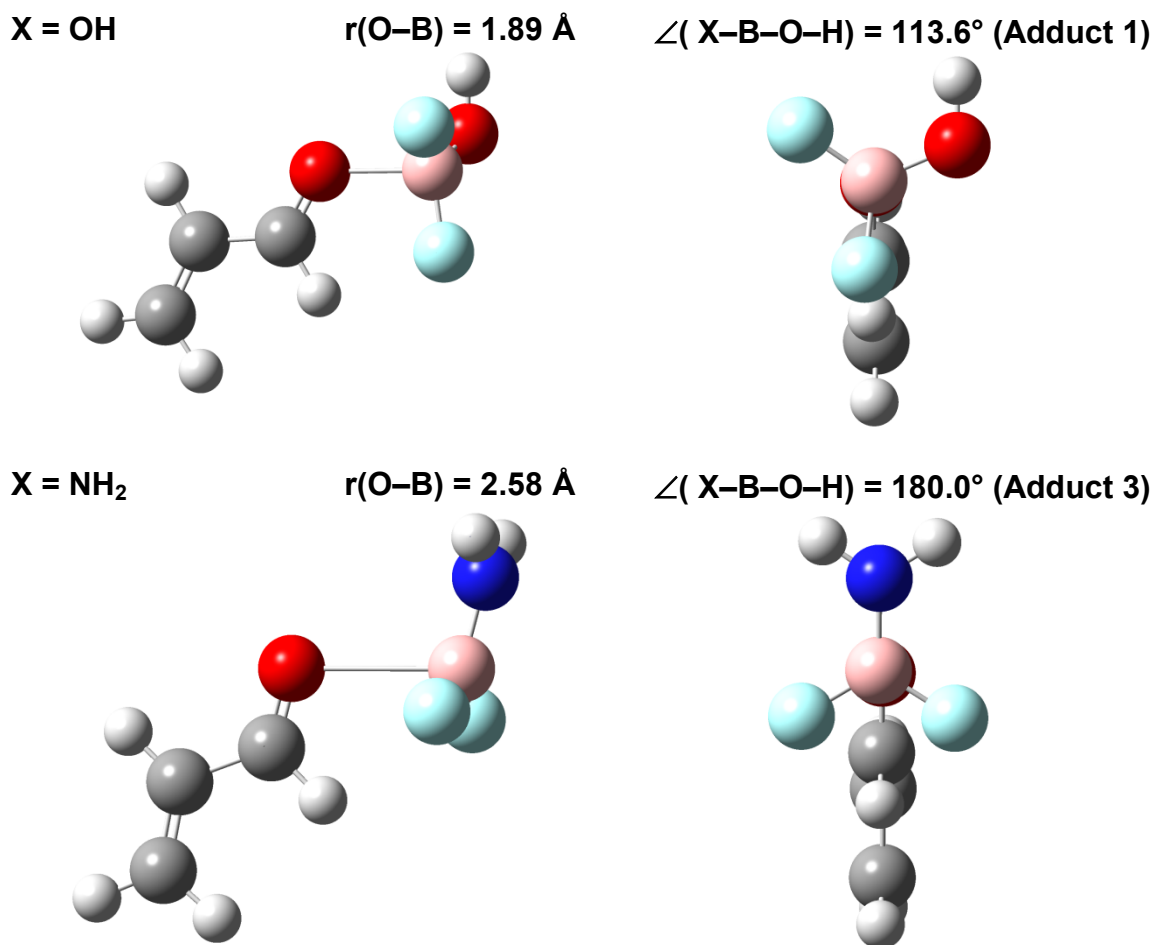
Figure 5.3. (continued).

5.4 Binding Enthalpies between BF$_2$X and 2-Propenal

Binding enthalpies, ΔH_{298}, between the BF$_2$**X** Lewis acids and 2-propenal are reported in Table 5.3. A strong linear correlation (Figure 5.4; $R^2 = 0.87$) is found between σ_p and ΔH_{298}, where stronger EWGs coordinated to BF$_2$**X** yield an increase in affinity. Thus, as expected in coordinate covalent bond formation, the stronger the electron withdrawing substituent on the Lewis acid, the stronger the binding affinity of the adduct. Hammett's constants were originally derived to understand reaction

mechanisms by taking advantage of linear free energy relationships.[336, 353] Consequently,

the strong linear correlation found between the binding enthalpy and Hammett's

constants should not be overinterpreted, since free energy is not considered. Hammett's

constants are merely being used as a tool to gauge the electron donating and

withdrawing tendency of the substituent.

Table 5.3. Substituents, Hammett Constants, and Binding Enthalpies between BF_2**X** and 2-propenal.

X	σ_p [336, 337]	ΔH_{298}
$-N_2^+$	1.910	-76.1
$-NO_2$	0.778	-24.2
$-CN$	0.660	-16.6
$-CF_3$	0.540	-19.7
$-CO_2H$	0.450	-18.1
$-F$	0.062	-11.7
$-H$	0.000	-8.3
$-CH_2CH_3$	-0.151	-6.7
$-CH_3$	-0.170	-6.0
$-OCH_3$	-0.268	-5.5
$-OH$	-0.370	-5.1
$-NH_2$	-0.660	-3.2

[a] All energies are in kcal/mol.
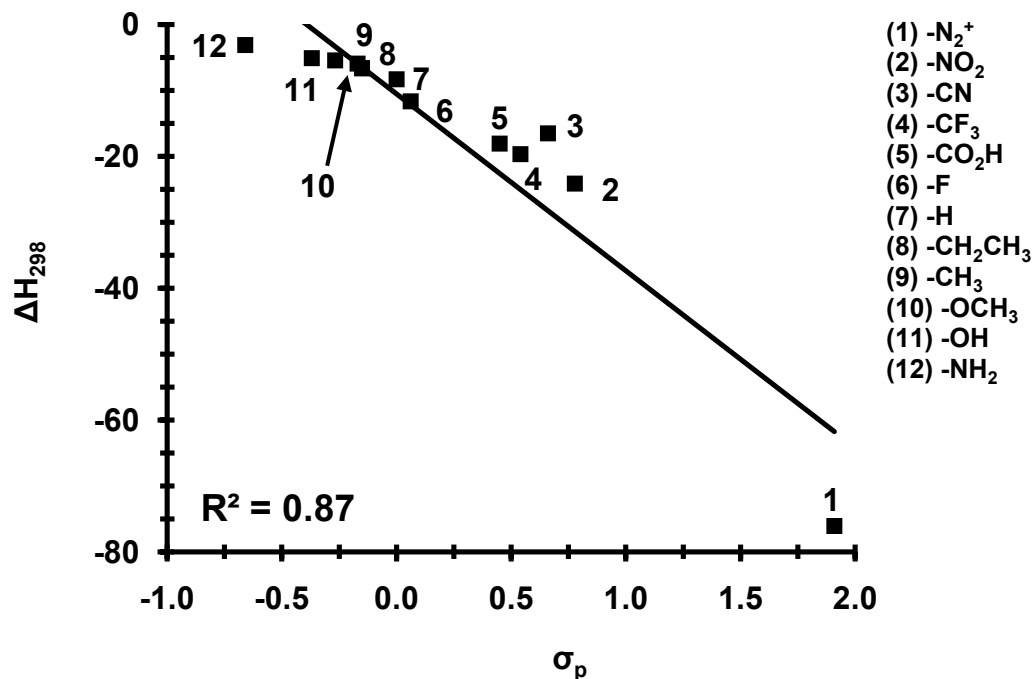
Figure 5.4. Binding enthalpy between BF_2X and 2-propenal vs. the Hammett substituent constant, σ_p. All energies are in kcal/mol.

Eighteen stereoelectronic effects presumed to influence ΔH_{298} between the dienophile and BF_2X have been investigated and reported in Table 5.4. Unsurprisingly, the principal FMO interaction responsible for the formation of the coordinate covalent bond through donation from the carbonyl oxygen lone pair to the empty $2p$ orbital on boron $(n(O) \rightarrow n^*(B))$ is orders of magnitude stronger than all other interactions (Table 5.4). However, $n(O) \rightarrow n^*(B)$ does not explain ΔH_{298} variation satisfactorily (Figure 5.5D; $R^2 = 0.59$). Thus, despite its strength, the traditional donor-acceptor interaction does not correlate with the binding affinity of adduct formation.

Table 5.4. Total Strength of Each Stereoelectronic Effect within Each Substituted Lewis Acid Adduct.[a]

	$\pi(C=O) \rightarrow \sigma^*(B–X)$	$\pi(C=O) \rightarrow \sigma^*(B–F)$
$-N_2^+$	NA[c]	20.28
$-NO_2$	0.00	6.34
$-CN$	0.00	5.26
$-CF_3$	2.63	2.25
$-CO_2H$	2.75	2.66
$-F$	0.00	3.94
$-H$	0.98	2.04
$-CH_2CH_3$	0.00	2.75
$-CH_3$	0.61	1.93
$-OCH_3$	0.08	0.12
$-OH$	0.79	0.76
$-NH_2$	0.00	0.00
	$\sigma(B–X) \rightarrow \sigma^*(B–O)$	$\sigma(B–F) \rightarrow \sigma^*(B–O)$
$-N_2^+$	NA[c]	0.45
$-NO_2$	3.44	1.40
$-CN$	3.12	2.44
$-CF_3$	3.23	3.17
$-CO_2H$	3.04	3.01
$-F$	2.75	5.51
$-H$	3.14	5.80
$-CH_2CH_3$	1.68	7.47
$-CH_3$	1.63	6.69
$-OCH_3$	2.04	10.15
$-OH$	1.39	7.16
$-NH_2$	0.38	0.45
	$n(O) \rightarrow \sigma^*(B–X)$	$n(O) \rightarrow \sigma^*(B–F)$
$-N_2^+$	NA[c]	7.67
$-NO_2$	2.95	2.06
$-CN$	1.80	2.70
$-CF_3$	0.07	4.12
$-CO_2H$	0.00	4.44
$-F$	1.67	2.89
$-H$	0.40	1.99
$-CH_2CH_3$	0.28	0.37
$-CH_3$	0.08	1.50
$-OCH_3$	0.00	0.00
$-OH$	0.11	0.93
$-NH_2$	0.00	1.06

Table 5.4. (continued).

	n(O) → n*(B)	
-N$_2$$^+$	466.0	
-NO$_2$	329.3	
-CN	300.3	
-CF$_3$	321.0	
-CO$_2$H	342.8	
-F	236.9	
-H	228.6	
-CH$_2$CH$_3$	178.4	
-CH$_3$	192.5	
-OCH$_3$	20.0	
-OH	122.7	
-NH$_2$	2.1	
	σ(B–O) → σ*(B–X)	σ(B–O) → σ*(B–F)
-N$_2$$^+$	NA[c]	0.37
-NO$_2$	1.29	1.32
-CN	0.58	2.00
-CF$_3$	1.70	1.88
-CO$_2$H	1.17	1.65
-F	1.06	3.04
-H	0.72	2.83
-CH$_2$CH$_3$	0.61	2.90
-CH$_3$	0.52	3.00
-OCH$_3$	0.16	0.79
-OH	0.56	2.40
-NH$_2$	NA[d]	NA[d]
	σ(B–O) → σ*(C–C)	
-N$_2$$^+$	4.66	
-NO$_2$	8.09	
-CN	8.98	
-CF$_3$	9.36	
-CO$_2$H	9.16	
-F	11.34	
-H	11.57	
-CH$_2$CH$_3$	14.60	
-CH$_3$	13.01	
-OCH$_3$	24.84	
-OH	16.55	
-NH$_2$	NA[d]	

Table 5.4. (continued).

σ(C=O) → σ*(B–O)	
$-N_2^+$	0.87
$-NO_2$	0.75
-CN	0.65
$-CF_3$	0.83
$-CO_2H$	1.03
-F	0.47
-H	0.50
$-CH_2CH_3$	0.71
$-CH_3$	0.58
$-OCH_3$	0.32
-OH	0.33
$-NH_2$	NA[d]

	σ(C=O) → σ*(B–X)	σ(C=O) → σ*(B–F)
$-N_2^+$	NA[c]	0.17
$-NO_2$	0.00	0.00
-CN	0.00	0.00
$-CF_3$	0.00	0.00
$-CO_2H$	0.00	0.10
-F	0.00	0.06
-H	0.00	0.00
$-CH_2CH_3$	0.00	0.00
$-CH_3$	0.00	0.00
$-OCH_3$	0.00	0.16
-OH	0.00	0.11
$-NH_2$	0.00	0.00

n(O) → σ*(B–O)	
$-N_2^+$	0.23
$-NO_2$	1.21
-CN	1.22
$-CF_3$	0.72
$-CO_2H$	0.66
-F	1.18
-H	1.03
$-CH_2CH_3$	1.67
$-CH_3$	1.57
$-OCH_3$	4.73
-OH	2.75
$-NH_2$	NA[d]

Table 5.4. (continued).

	σ(B–O) → σ*(C–H)	
-N$_2$$^+$	0.78	
-NO$_2$	2.24	
-CN	2.72	
-CF$_3$	3.13	
-CO$_2$H	2.84	
-F	4.57	
-H	4.76	
-CH$_2$CH$_3$	7.46	
-CH$_3$	5.89	
-OCH$_3$	25.0	
-OH	9.39	
-NH$_2$	NA[d]	
	n(F) → σ*(B–O)[b]	n(X) → σ*(B–O)[b]
-N$_2$$^+$	52.49	NA[e]
-NO$_2$	50.08	NA[e]
-CN	53.78	NA[e]
-CF$_3$	50.91	NA[e]
-CO$_2$H	48.10	NA[e]
-F	78.21	25.11
-H	50.99	NA[e]
-CH$_2$CH$_3$	57.99	6.27
-CH$_3$	56.61	5.37
-OCH$_3$	78.83	60.56
-OH	60.54	41.18
-NH$_2$	NA[d]	NA[d]
	σ(C–C) → σ*(B–O)	
-N$_2$$^+$	2.36	
-NO$_2$	2.48	
-CN	2.58	
-CF$_3$	2.31	
-CO$_2$H	2.40	
-F	1.91	
-H	2.34	
-CH$_2$CH$_3$	2.08	
-CH$_3$	2.23	
-OCH$_3$	0.57	
-OH	1.60	
-NH$_2$	NA[d]	

Table 5.4. (continued).

	σ(C–H) → σ*(B–O)
-N$_2$$^+$	0.00
-NO$_2$	0.09
-CN	0.00
-CF$_3$	0.00
-CO$_2$H	0.00
-F	0.21
-H	0.00
-CH$_2$CH$_3$	0.00
-CH$_3$	0.00
-OCH$_3$	0.19
-OH	0.24
-NH$_2$	NA^d

	σ(B–X) → π*(C=O)	σ(B–F) → π*(C=O)
-N$_2$$^+$	NA^c	0.25
-NO$_2$	0.00	0.24
-CN	0.00	0.00
-CF$_3$	0.75	0.05
-CO$_2$H	0.72	0.00
-F	0.11	0.22
-H	0.84	0.15
-CH$_2$CH$_3$	0.00	0.00
-CH$_3$	0.93	0.34
-OCH$_3$	0.00	0.00
-OH	0.07	0.05
-NH$_2$	0.00	0.00

	σ(B–O) → σ*(C=O)
-N$_2$$^+$	0.70
-NO$_2$	0.40
-CN	0.00
-CF$_3$	0.43
-CO$_2$H	0.66
-F	0.09
-H	0.12
-CH$_2$CH$_3$	0.09
-CH$_3$	0.06
-OCH$_3$	2.53
-OH	0.06
-NH$_2$	NA^d

Table 5.4. (continued).

	σ(B–O) → π*(C=O)	
-N$_2$$^+$	0.00	
-NO$_2$	0.00	
-CN	0.00	
-CF$_3$	0.18	
-CO$_2$H	0.57	
-F	0.00	
-H	0.00	
-CH$_2$CH$_3$	0.00	
-CH$_3$	0.00	
-OCH$_3$	0.00	
-OH	0.00	
-NH$_2$	NA^d	
	σ(B–X) → σ*(C=O)	σ(B–F) → σ*(C=O)
-N$_2$$^+$	NA^c	0.46
-NO$_2$	0.14	1.36
-CN	0.00	1.10
-CF$_3$	0.66	0.97
-CO$_2$H	0.50	1.14
-F	0.54	1.25
-H	1.34	0.45
-CH$_2$CH$_3$	0.95	0.16
-CH$_3$	0.93	0.34
-OCH$_3$	0.06	0.06
-OH	0.33	0.43
-NH$_2$	0.00	0.00
	π(C=O) → σ*(B-O)	
-N$_2$$^+$	0.00	
-NO$_2$	0.00	
-CN	0.00	
-CF$_3$	0.00	
-CO$_2$H	0.25	
-F	0.00	
-H	0.00	
-CH$_2$CH$_3$	0.00	
-CH$_3$	0.00	
-OCH$_3$	0.00	
-OH	0.00	
-NH$_2$	NA^d	

Table 5.4. (continued).

	$\pi(C=C) \rightarrow \pi^*(C=O)$
$-N_2^+$	93.69
$-NO_2$	47.15
$-CN$	43.92
$-CF_3$	44.64
$-CO_2H$	43.58
$-F$	39.42
$-H$	37.82
$-CH_2CH_3$	36.38
$-CH_3$	36.02
$-OCH_3$	29.54
$-OH$	34.06
$-NH_2$	27.66

[a] Y=X or F. All values are in kcal/mol. When an interaction involves the B-F bond, the reported magnitude represents the sum of both interactions involving the B-F bonds.
[b] Only *antiperiplanar* lone pairs are observed to be significant and thus considered.
[c] As displayed in Figure 5.3, the B—N_2^+ distance is 2.59 Å, thus a σ(B-X) bond does not exist.
[d] As displayed in Figure 5.3, the B—O distance is 2.58 Å, thus a σ(B-O) bond does not exist
[e] No *antiperiplanar* orbitals with respect to the σ^*(B-O).

Figure 5.5 displays all linear correlations between stereoelectronic interactions considered and ΔH_{298}. In particular, the total strength of the three $\pi(C=O) \rightarrow \sigma^*(B-Y)$ (Y = F, F, and X) interactions (Table 5.4) yields the highest correlation with ΔH_{298} (Figure 5.5A; $R^2 = 0.98$), where a stronger orbital interaction results in an increased affinity. Moreover, the P-value (7.2×10^{-10}) associated with the F-statistic is much lower than $\alpha = 0.05$ (95% confidence interval), indicating the correlation is hardly a coincidence. As an illustration, a single $\pi(C=O) \rightarrow \sigma^*(B-F)$ interaction between 2-propenal and BF_3 is shown by Figure 5.6, where the π density on the carbonyl group is transferred to the B–F anti-bonding sigma orbital. Thus, the first point of this work is realized, where the binding affinity of the Lewis acid adduct is controlled not by the traditional donor-acceptor model presented by Lewis, but by a transfer of electron

186

density from the dienophile π-system to the antibonding orbitals between boron and its substituents on the Lewis acid after the coordinate covalent bond formed.
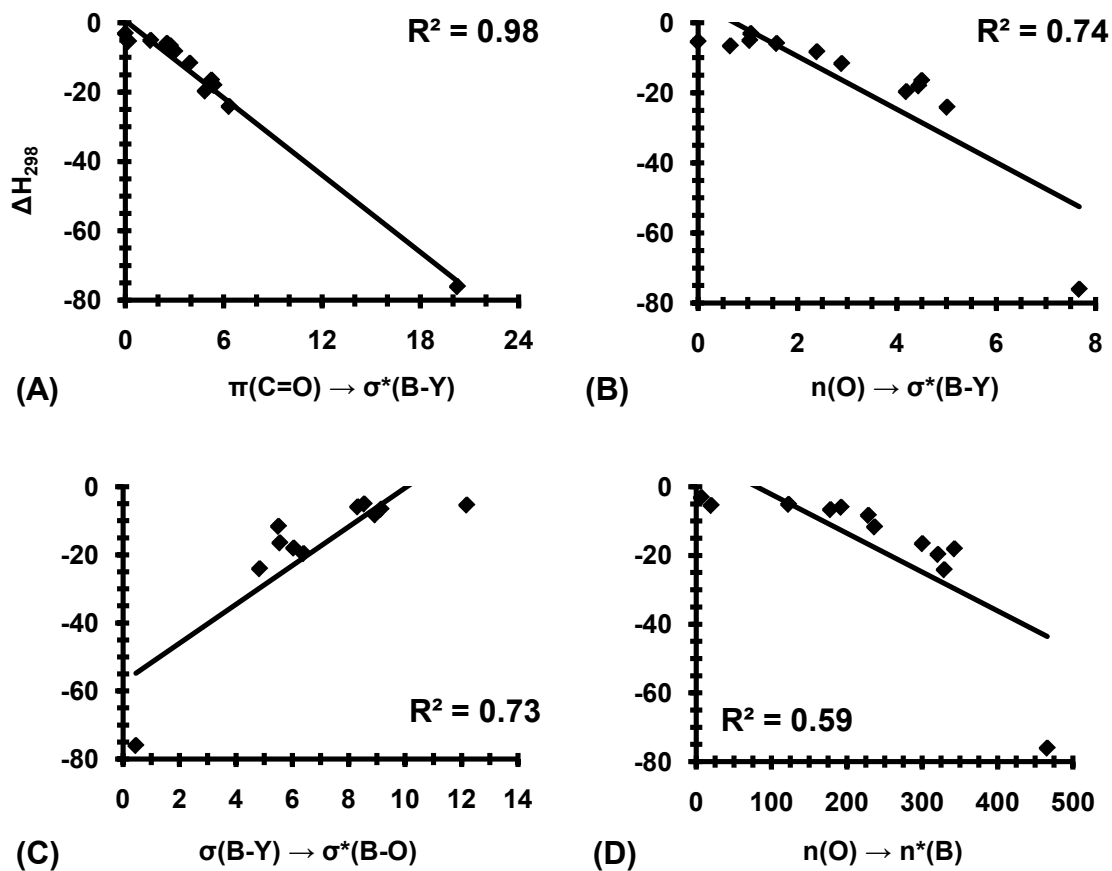
Figure 5.5. Binding enthalpy between $BF_2\mathbf{X}$ and 2-propenal vs. the total strength of each interaction (Table 5.4). The $\sigma(C\text{-}H) \rightarrow \sigma^*(B\text{-}O)$, $\sigma(B\text{-}O) \rightarrow \pi^*(C\text{=}O)$ and $\pi(C\text{=}O) \rightarrow \sigma^*(B\text{-}O)$ interactions are omitted since their strengths are 0.0 kcal/mol for the majority of $\mathbf{X}$ (Table 5.4).

(E) σ(B-O) → σ*(B-Y)

(F) σ(B-O) → σ*(C-C)

(G) σ(C=O) → σ*(B-O)

(H) n(O) → σ*(B-O)

(I) σ(C=O) → σ*(B-Y)

(J) σ(B-O) → σ*(C-H)

Figure 5.5. (continued).

(K) $n(Y) \rightarrow \sigma^*(B-O)$

(L) $\sigma(C-C) \rightarrow \sigma^*(B-O)$

(M) $\sigma(B-Y) \rightarrow \sigma^*(C=O)$

(N) $\sigma(B-O) \rightarrow \sigma^*(C=O)$

(O) $\sigma(B-Y) \rightarrow \pi^*(C=O)$
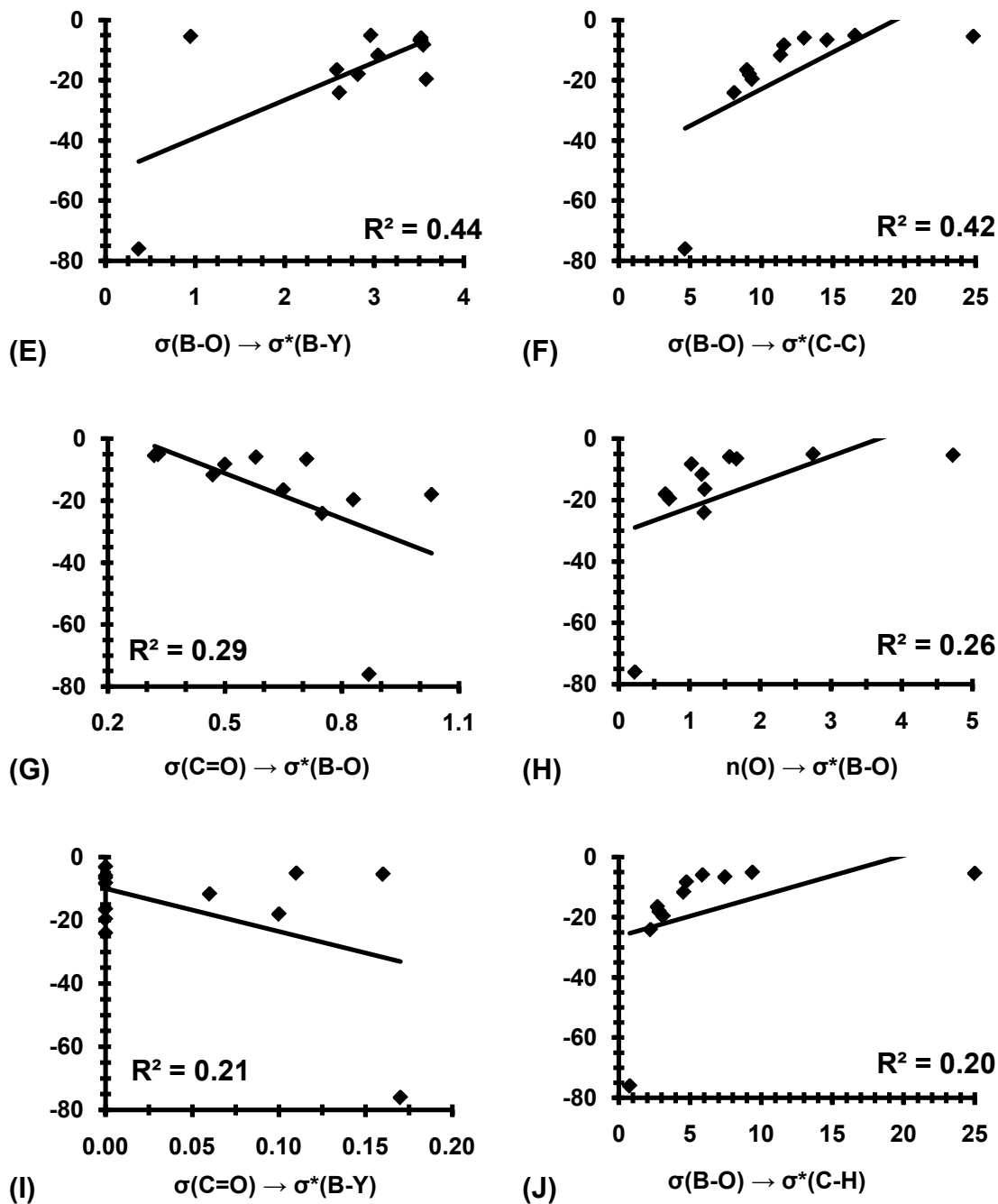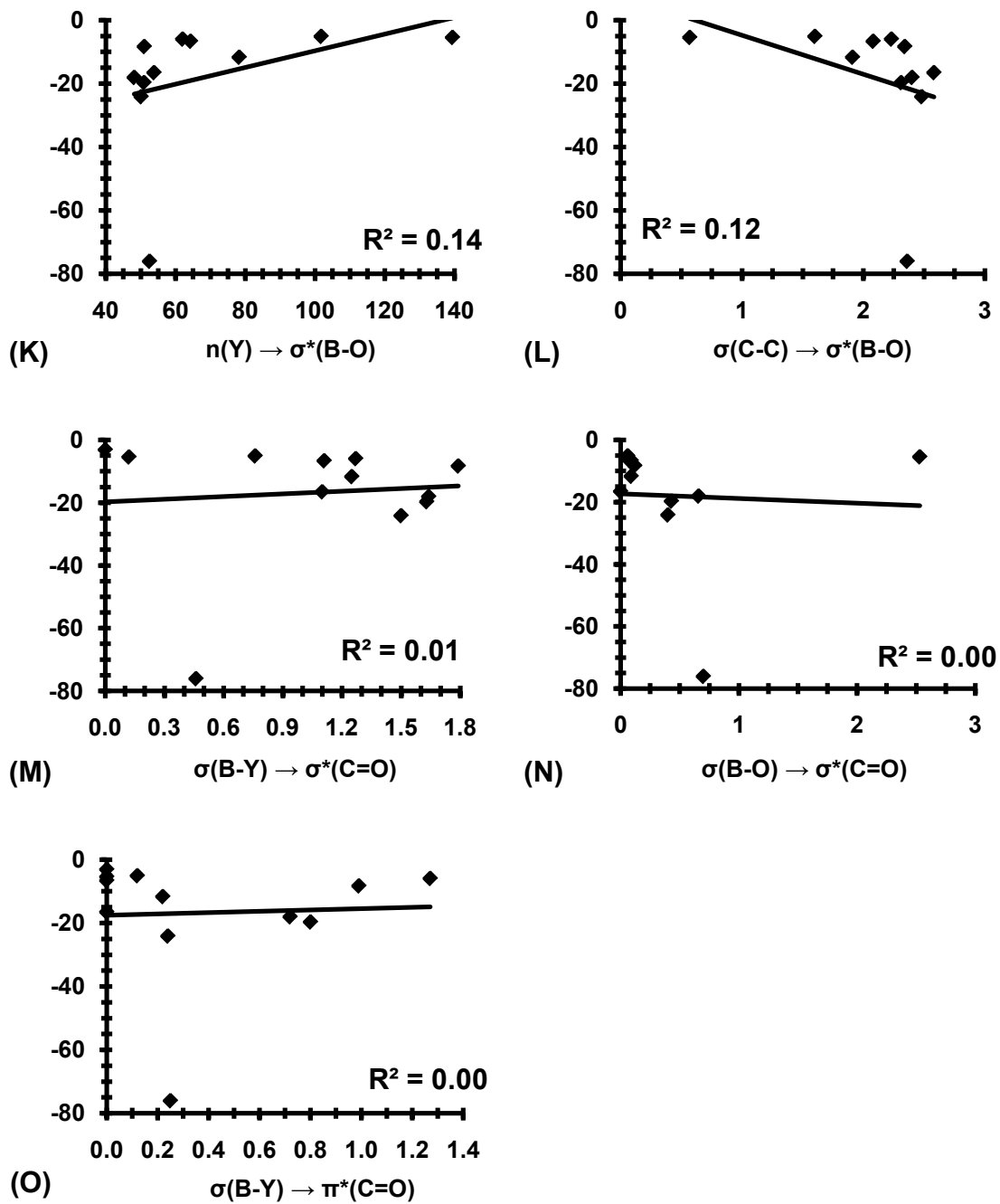
Figure 5.5. (continued).
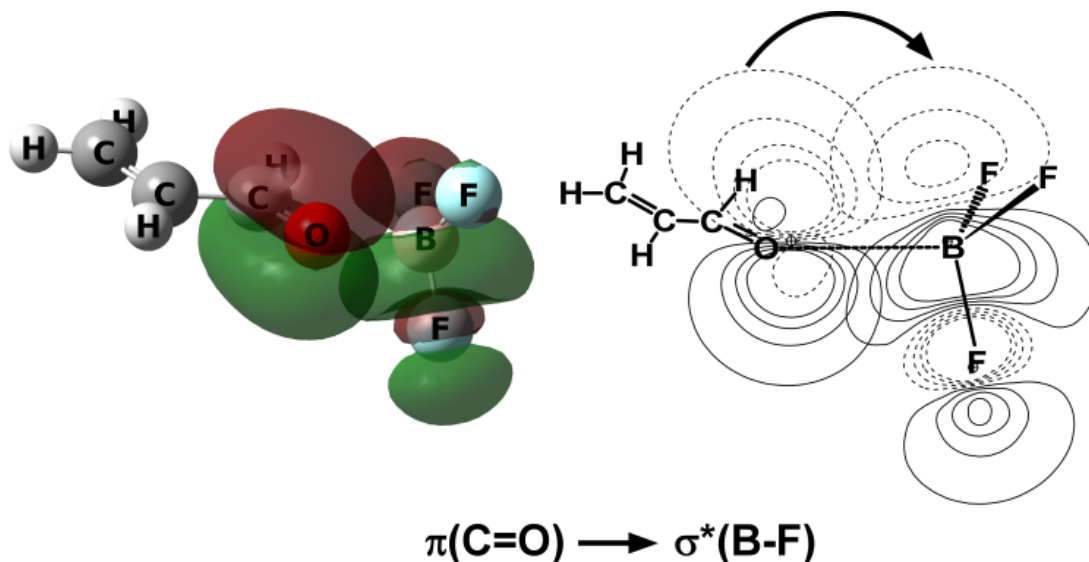
$$\pi(\text{C=O}) \longrightarrow \sigma^*(\text{B-F})$$

Figure 5.6. Orbital overlap corresponding to one of the three possible π(C=O) → σ*(B–F) stereoelectronic interactions within the BF₃ Lewis acid activated dienophile adduct. The strength of this individual interaction is 1.97 kcal/mol.

In the next phase of the investigation, the origin and control of the π(C=O) → σ*(B–Y) (Y = F, F, and **X**) orbital interactions were investigated. Geminal interactions between each of the three substituents coordinated to boron were found to be crucial to the modulation of the π(C=O) → σ*(B–Y) strength. The net effect is that geminal interactions lower the σ* orbitals of the Lewis acid substituents, ultimately leading to efficient orbital overlap with the π(C=O) of the dienophile.

Each antibonding orbital is modulated by the electronic tendencies (EWG or EDG) of the other two geminal substituents. A systematic evaluation of exchanging **X** with EDGs and EWGs reveals that the energy levels of the two σ*(B–F) orbitals decrease and increase, respectively, as compared to when **X** = H (neither EDG nor EWG). For example, when **X** = NO₂ (e.g. an EWG) the average energy level of both

σ*(B–F) orbitals is 1.189 hartrees above the energy level of π(C=O). In contrast, when

$\mathbf{X}$ = NH$_2$ (e.g. an EDG) the average energy level of both σ*(B–F) orbitals is 1.248

hartrees above the energy level of π(C=O). Consequently, there is a lower energy gap

between σ*(B–F) and π(C=O) when $\mathbf{X}$ = NO$_2$ than when $\mathbf{X}$ = NH$_2$, thus a stronger

π(C=O) → σ*(B–F) interaction is observed for when $\mathbf{X}$ = NO$_2$. Figure 5.7 displays the

relative energies of σ*(B–F), as compared to π(C=O), when $\mathbf{X}$ = NO$_2$, H, and NH$_2$.
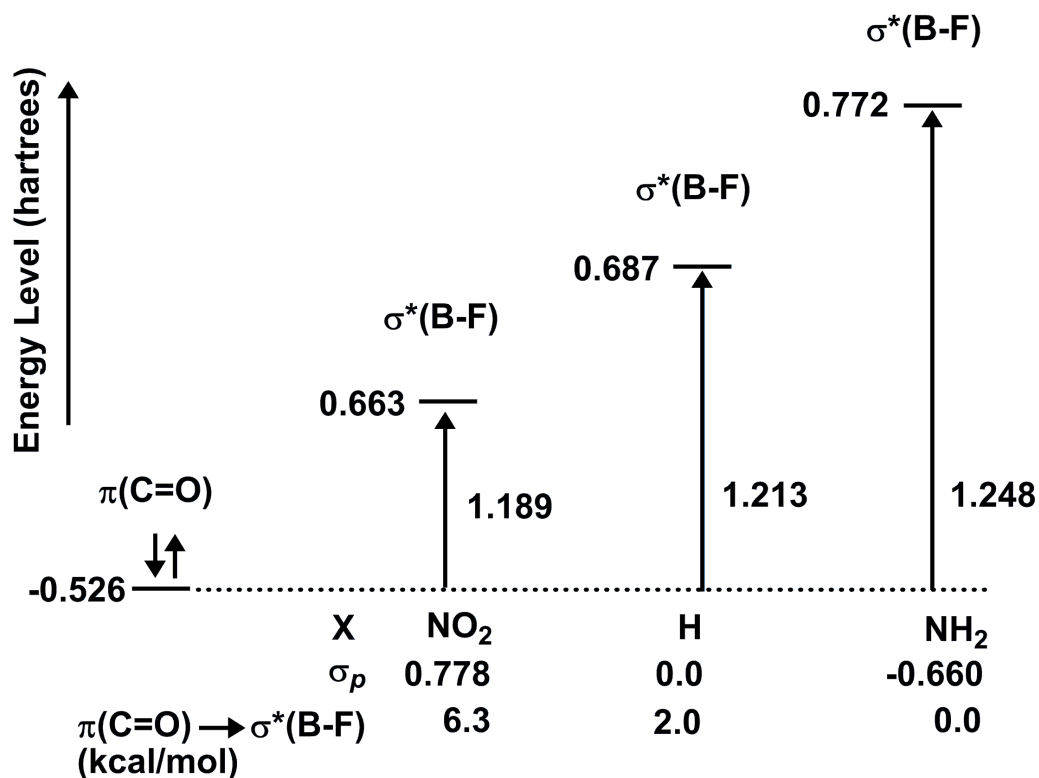
Figure 5.7. Energy diagram comparing the relative average energies of both σ*(B-F) orbitals to π(C=O) when $\mathbf{X}$ = NO$_2$, H, and NH$_2$. All energies are in hartrees and kcal/mol as indicated.

As **X** is systematically exchanged with EDGs and EWGs, its effect upon the geminal σ*(B–F) orbitals has been computed. Figure 5.8 provides a more comprehensive connection between σ_p of **X** and the average energy level of the two geminal σ*(B–F) orbitals, where a stronger EWG substituted on the isolated Lewis acid decreases the average energy level of σ*(B–F) ($R^2 = 0.86$). Subsequently, the lower σ*(B–F) orbitals relative to π(C=O) allow for stronger π(C=O) → σ*(B–F) interactions to occur (Figure 5.9; $R^2 = 0.90$). An EWG decreases the energy levels of the geminal σ*(B–F) orbitals, decreasing the energy gap between σ*(B–F) and the dienophile π(C=O), thus facilitating the π(C=O) → σ*(B–F) hyperconjugation, and increasing the affinity between the Lewis acid and 2-propenal (Figure 5.10; $R^2 = 0.90$). Although **X** is systematically substituted and discussed to illustrate the connection between geminal Lewis acid interactions, σ*(B–F) energy lowering, and π(C=O) → σ*(B–F) strengths, it must be remembered that the two fluorine substituents also influence the other σ*(B–F) and σ*(B–**X**) orbitals of the geminal pairs. However, the systematic impact of **X**'s electronic tendencies upon the energy levels of σ*(B–F) has been discussed for simplicity and clarity. Consequently, it is the total of the three π(C=O) → σ*(B–Y) interactions that is important, where Y = **X**, F and F, as discussed previously and in the following sections.
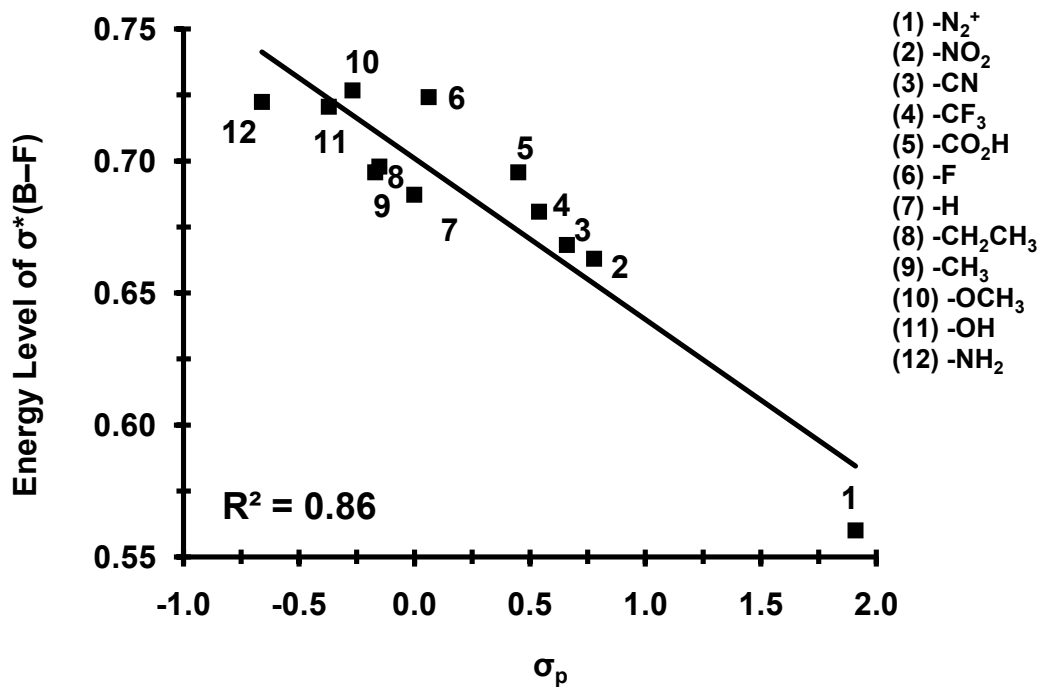
Figure 5.8. Average σ*(B–F) energy level (hartrees) within the isolated BF$_2$**X** Lewis acids vs. Hammett substituent constants, σ$_p$.
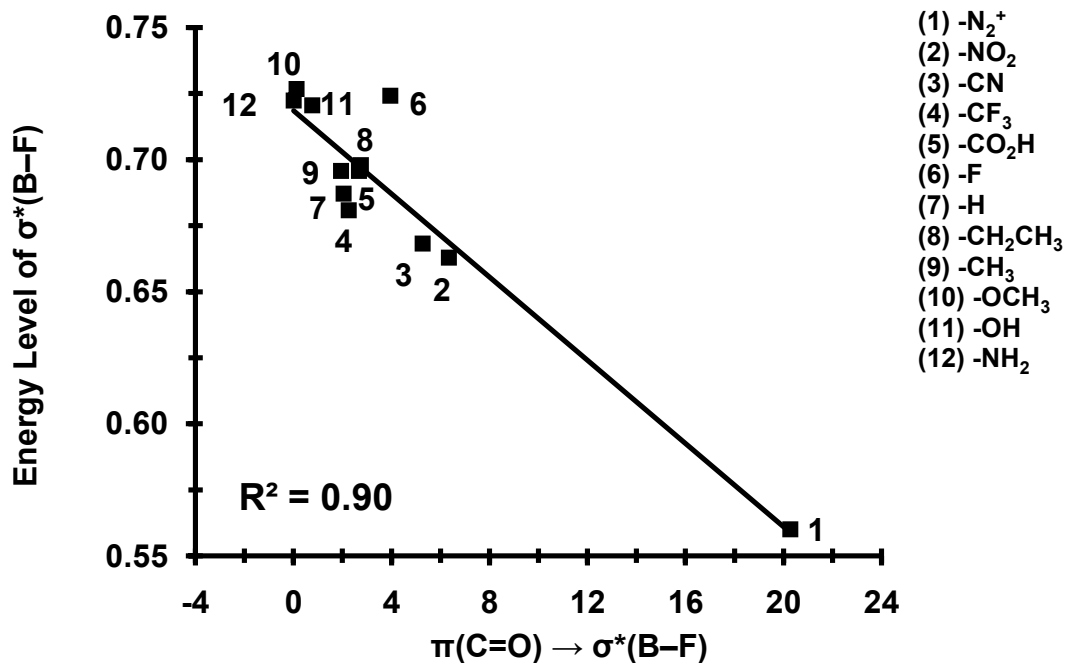
Figure 5.9. Average σ*(B–F) energy level (hartrees) within the isolated BF$_2$**X** Lewis acids vs. the total strength of the two π(C=O) → σ*(B–F) interactions.
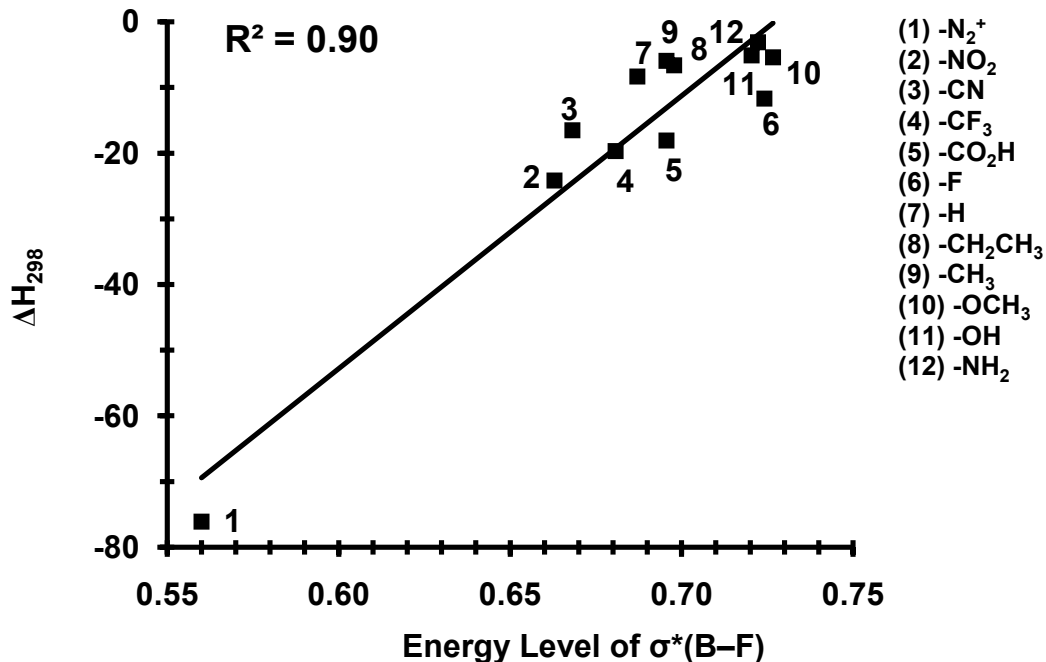
Figure 5.10. Binding enthalpy between 2-propenal and BF$_2$**X**, ΔH_{298} vs. the average σ^*(B–F) energy level. Binding energies and energy levels are in kcal/mol and hartrees, respectively.

Lupton dissected σ_p into 53% resonance ($\mathcal{R}$) and 47% field contributions ($\mathcal{F}$).[337] In attempt to determine which factor influences the average energy level of σ^*(B–F), correlations between the average energy level of σ^*(B–F) and both $\mathcal{F}$ and $\mathcal{R}$ were determined and shown in Figure 5.11. Both correlations are lower than that achieved by considering σ_p. The data suggest that both $\mathcal{R}$ and $\mathcal{F}$ effects collectively influence the energy levels of σ^*(B–Y). In summary, the differences in adduct binding affinity are a direct result of the π(C=O) $\rightarrow \sigma^*$(B–Y) orbital interactions, which are facilitated by geminal interactions between each substituent coordinated to boron and the remaining σ^* orbitals.
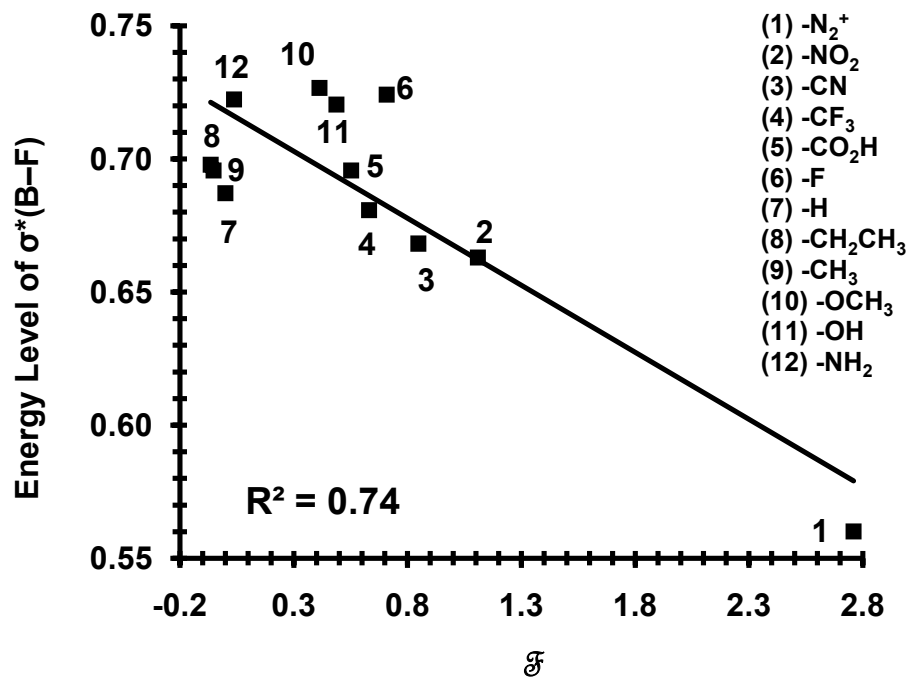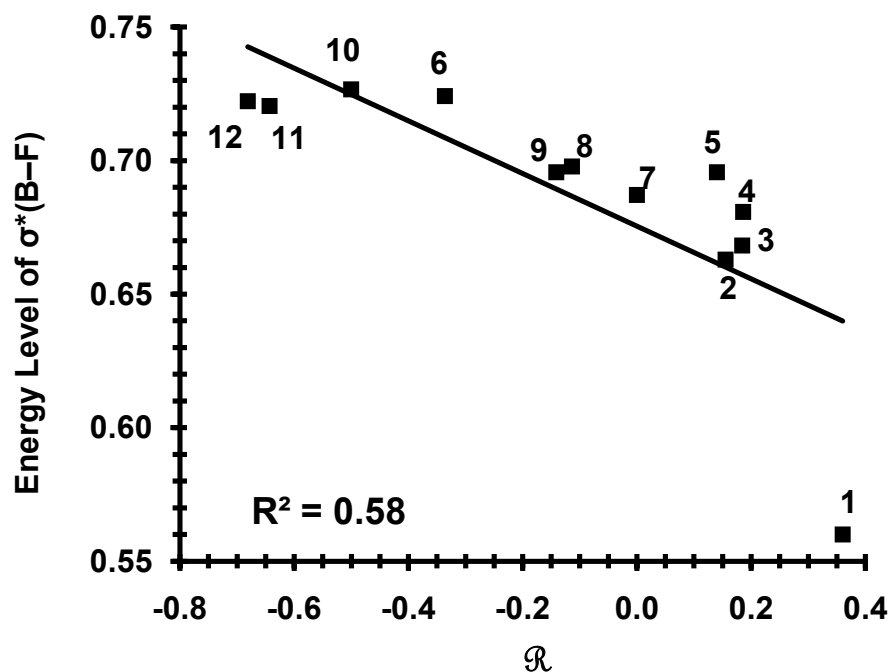
Figure 5.11. Average σ*(B–F) energy level (hartrees) within the isolated BF$_2$**X** Lewis acids vs. Hammett substituent constant, σ$_p$. $\mathscr{R}$ represents the resonance constants and $\mathscr{F}$ represents the field constants.

5.5 Convergence Behavior of Computed Activation Energies

Similar to the study conducted for the ammonia borane coordinate covalent bond (Chapter 3), the convergence behavior of the activation energy for the Diels-Alder reaction between 1,3-butadiene and 2-propenal as a function of basis functions is explored and compared to the experimental activation energy of $\Delta^{\ddagger}E_{298} = 19.7 \pm 0.3$ kcal/mol.[354] The ability of density functionals to predict activation energies of the Diels-Alder reaction has been reported.[178, 334, 355] In particular, B3LYP/6-31G(d) has been reported to be the most accurate, when compared to experiment and higher level computations.[355] However, it has been reported that that B3LYP, employed with larger basis sets, yields activation energies with larger errors, i.e, showed divergent behavior from the experimental value.[355]

A systematic evaluation of the activation energy with M06-2X, M05-2X, and B3LYP as a function of the correlation consistent basis sets (cc-pVXZ; X = D, T, Q, 5) has been performed in order to extrapolate the appropriate electronic energies to the complete basis set limit. The extrapolation scheme proposed by Martin has been employed, where the electronic energy ($E(n)$) is a function of inverse powers of the angular momentum, n (n = D, T, Q, and 5), plus the electronic energy in the limit of the complete basis (E_{∞}) set (Equation 5.1).[197, 356] E_{∞}, A, and B are determined by a self consistent fit.

$$E(n) = E_{\infty} + \frac{A}{n^3} + \frac{B}{n^5} \qquad 5.1$$

It is discovered that M06-2X must be employed with at least the cc-pV5Z basis set (1,278 basis functions) to yield a near converged $\Delta^{\ddagger}E_{298}$ (Figure 5.12). The cc-pV5Z basis set differs from the extrapolated value by 0.2 kcal/mol. The inherent error within the M06-2X functional is exposed in the limit of the complete basis set, where a 1.8 kcal/mol difference with the experimental value of $\Delta^{\ddagger}E_{298} = 19.7 \pm 0.3$ kcal/mol[354] is observed. An additional error of 1.3 kcal/mol is introduced when the smaller and more practical 6-311++G(3df,2p) basis set (412 basis functions) is employed with M06-2X, which is the level found to agree with experimental binding energies of the coordinate covalent bond. Consequently, the M06-2X/6-311++G(3df,2p) predicted activation energy is 16.6 kcal/mol, or 3.1 kcal/mol lower than the experimental value. M05-2X predicted activation energies converge similarly to that observed for the M06-2X functional; however, the inherent error introduced by the M05-2X functional is 3.1 kcal/mol rather than 1.8 kcal/mol.
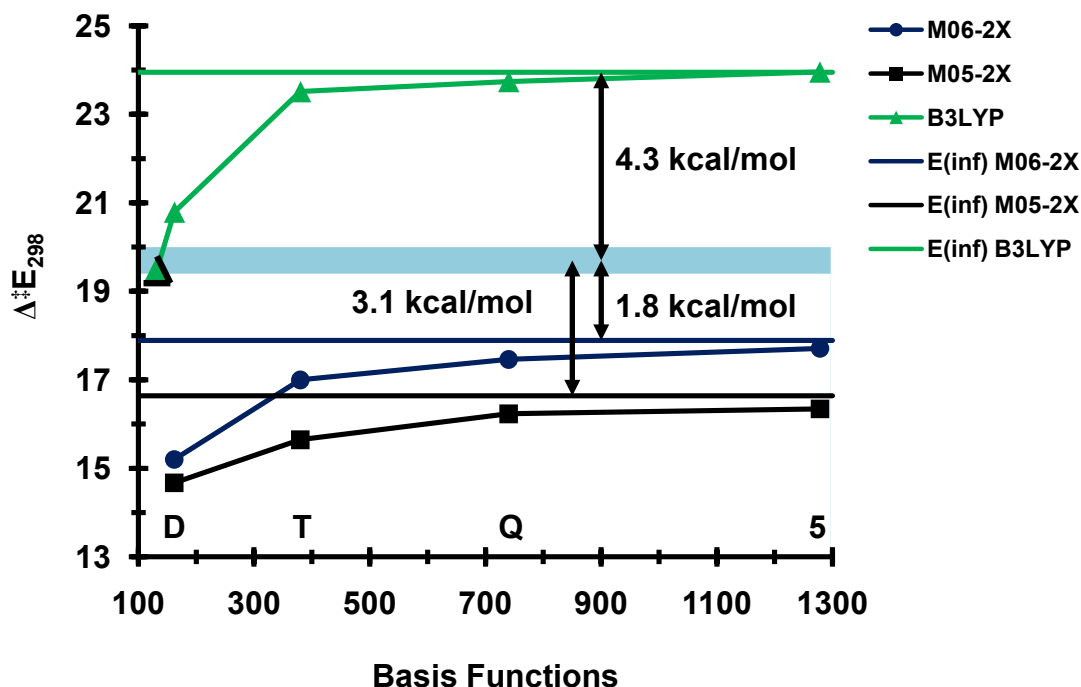
Figure 5.12. Convergence behavior of $\Delta^{\ddagger}E_{298}$ as a function of basis functions. The M06-2X, M05-2X, and B3LYP methods are employed with the cc-pVXZ (X = D, T, Q, and 5) basis sets to extrapolate to the complete basis set limit, E(inf). M06-2X converges toward the experimental value but underestimates the activation energy by 1.8 kcal/mol. B3YLP predicts an accurate activation energy with a small basis set (6-31G(d)); however, it diverges from experiment in the limit of the complete basis set. The light blue box indicates the experimental activation energy of $\Delta^{\ddagger}E_{298}$ = 19.7 ± 0.3 kcal/mol. The data point symbolized by the black outlined triangle is the activation energy predicted by B3LYP/6-31G(d).

Although, B3LYP does not model coordinate covalent bound adducts accurately, [24, 173] its convergence behavior is investigated, since it is a commonly employed functional, as discussed in Chapter 2.7.3. It is interesting to note that the activation energy predicted by B3LYP/6-31G(d) ($\Delta^{\ddagger}E_{298}$ = 19.5 kcal/mol) for the Diels-Alder reaction between 2-propenal and 1,3-butadiene, is in excellent agreement with the experimental value of $\Delta^{\ddagger}E_{298}$ = 19.7 ± 0.3 kcal/mol.[354] However, increasing the basis set and extrapolating to the complete basis set limit reveals that B3LYP diverges from the experimental activation energy by 4.3 kcal/mol. The data suggest that B3LYP/6-31G(d)

allows a unique cancellation of errors to occur, where the final result is in fortuitous agreement with experiment. Such a unique combination of method and basis set is referred to as a "Pauling point," where excellent agreement with experiment is observed by employing a fairly low level of theory, but is eliminated whenever the level of theory is improved by increasing the basis set.[357] Thus, the inherent error found in M06-2X (1.8 kcal/mol) is improved over that found for B3LYP (4.3 kcal/mol).

It is important to note that it is the relative differences in activation barriers ($\Delta\Delta^{\ddagger}E_{298}$) that is of most importance to understand the effect of catalysis. It is assumed that the errors cancel by taking the difference between activation energies of catalyzed and uncatalyzed reactions. Consequently, the $AlCl_3$ catalyzed and uncatalyzed Diels-Alder reaction between 1,3-butadiene and methyl acrylate has been investigated with M06-2X/6-311++G(3df,2p) and compared to experiment.[100] The activation energies for the $AlCl_3$ catalyzed and uncatalyzed Diels-Alder reactions are $\Delta^{\ddagger}E_{298} = 10.4 \pm 1.9$ and 18.0 ± 1.0 kcal/mol, respectively, and thus a relative difference of $\Delta\Delta^{\ddagger}E_{298} = 7.6 \pm 2.1$ kcal/mol is observed. The relative difference of 9.5 kcal/mol as predicted by M06-2X/6-311++G(3df,2p) is within the experimental uncertainty, thus confidence is conveyed in the fact that M06-2X/6-311++G(3df,2p) is able to model the relative differences in activation energies of Lewis acid catalyzed Diels-Alder reactions. Consequently, the practical and efficient M06-2X/6-311++G(3df,2p) basis set is employed to predict Gibbs free activation barriers for all Diels-Alder reactions discussed.

In summary, it is discovered that the energetics associated with the transition structure converge slower in terms of basis functions than compared to those associated

with the coordinate covalent bound ground state. Consequently, a larger basis set must be used, specifically the cc-pV5Z basis set, in order to achieve a near converged activation energy. However, this is neither practical nor efficient. The inherent inaccuracies of the M06-2X formalism in the limit of the complete basis set introduce a 1.8 kcal/mol error, while employing the smaller 6-311++G(3df,2p) basis set introduces an additional 1.3 kcal/mol error, totaling a final error of 3.1 kcal/mol. Although M06-2X/6-311++G(3df,2p) underestimates the activation barriers by *ca* 3.0 kcal/mol, it predicts the relative differences between the catalyzed and uncatalyzed activation energies within experimental uncertainty. Consequently, all Gibbs free activation barriers (Chapter 5.6) are predicted by M06-2X/6-311++G(3df,2p), realizing that the magnitude of each barrier is underestimated by *ca*. 3 kcal/mol, in better agreement than that observed for MP2/6-311++G(3df,2p) and M05-2X/6-311++G(3df,2p), where the differences with experiment are 12.4 and 4.4 kcal/mol, respectively. The combination of B3LYP with 6-31G(d) is recognized to be a Pauling point, where excellent agreement between experiment and theory is observed.

5.6 BF$_2$X Catalyzed and Uncatalyzed Diels-Alder Reaction between 2-Propenal and 1,3-Butadiene

Four reaction pathways are possible for the Diels-Alder reaction between 2-propenal and 1,3- butadiene. Consistent with previous conventions,[108, 358] the transition structures (TSs) are denoted as NC (*endo*, *s-cis* acrolein), XC (*exo*, *s-cis* acrolein), NT (*endo*, *s-trans* acrolein) and XT (*exo*, *s-trans* acrolein) (Figure 5.13).[108, 358]

NC, $\Delta^{\ddagger}G_{298}$ = 29.7 kcal/mol
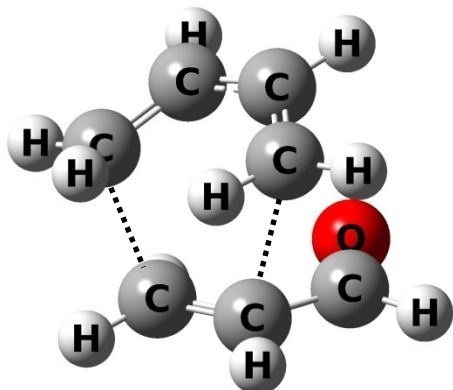
NT, $\Delta^{\ddagger}G_{298}$ = 30.6 kcal/mol
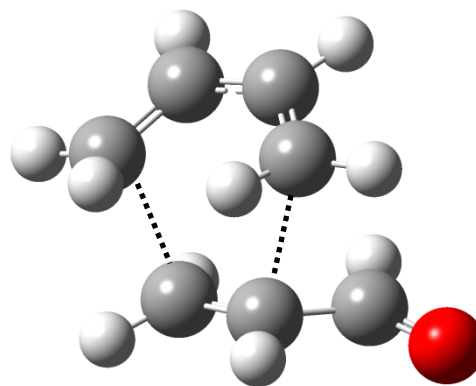
XC, $\Delta^{\ddagger}G_{298}$ = 30.7 kcal/mol
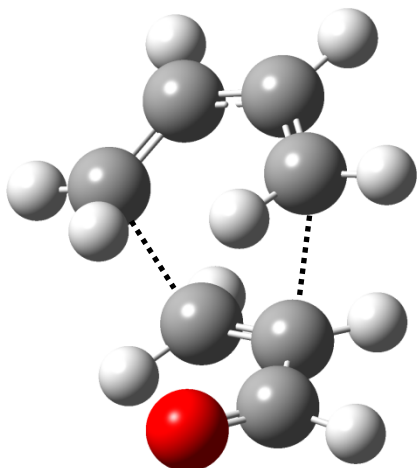
XT, $\Delta^{\ddagger}G_{298}$ = 32.3 kcal/mol
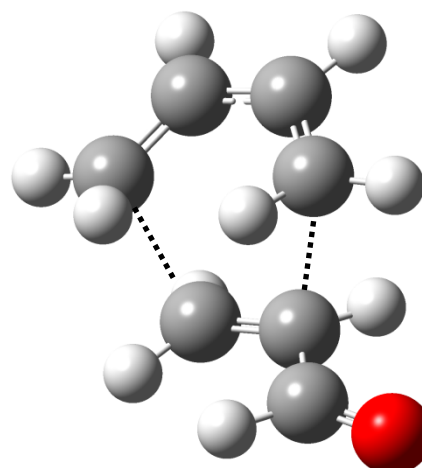
Figure 5.13. Four possible transition structures for the Diels-Alder reaction between 2-propenal and 1,3-butadiene. NC (*endo*, *s-cis* acrolein), XC (*exo*, *s-cis* acrolein), NT (*endo*, *s-trans* acrolein) and XT (*exo*, *s-trans* acrolein). The dashed lines correspond to the C-C forming bonds.

The NC TS has been reported to be the most stable for the same uncatalyzed[345, 358] and BF$_3$ catalyzed[358] Diels-Alder reaction. The stability of the *endo* TS[73] is commonly attributed to stabilizing secondary orbital interactions (SOIs) that are unobtainable during the *exo* reaction pathway, as discussed in Chapter 1.3.1.[104-107]

However, the influence of SOIs upon stereoselectivity remains debated.[109, 110]

Regardless of the stabilizing interactions that promote the *endo* TS, our results regarding

the uncatalyzed Diels-Alder reaction between 1,3 butadiene and 2-propenal indicate that

the NC TS is indeed more stable than the NT, XC, and XT TSs by 0.9, 1.0 and 2.6

kcal/mol, respectively (Figure 5.13). Moreover, the BF_3 catalyzed Diels-Alder reaction

follows the NC reaction pathway as compared to the NT, XC, and XT pathways by 4.2,

2.7, 7.1 kcal/mol, respectively (Figure 5.14). It is suspected that the remaining $BF_2\mathbf{X}$

catalyzed Diels-Alder reactions will follow the lower energy reaction pathway via the

NC transition structure. Consequently, only the NC TSs have been computed, analyzed,

and reported.
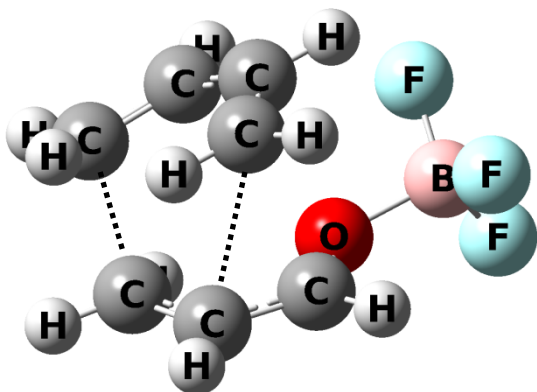
NC, Δ‡G_{298} = 19.1 kcal/mol   **NT, Δ‡G_{298} = 23.3 kcal/mol**
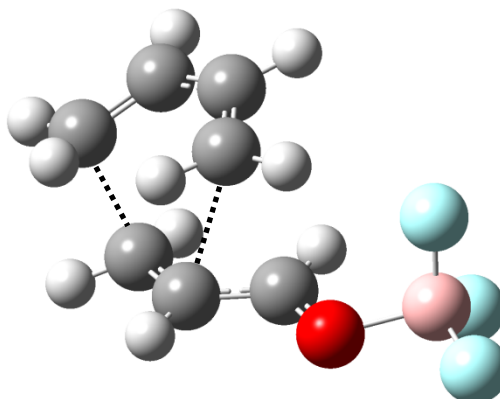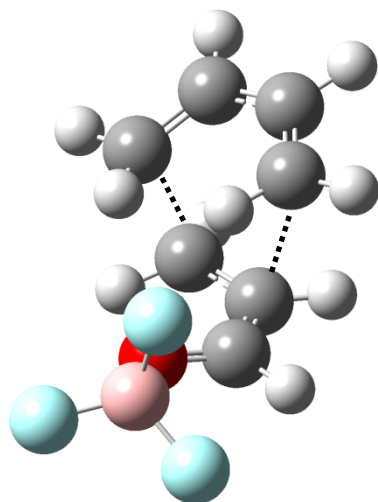
XC, Δ‡G_{298} = 21.8 kcal/mol   **XT, Δ‡G_{298} = 26.2 kcal/mol**
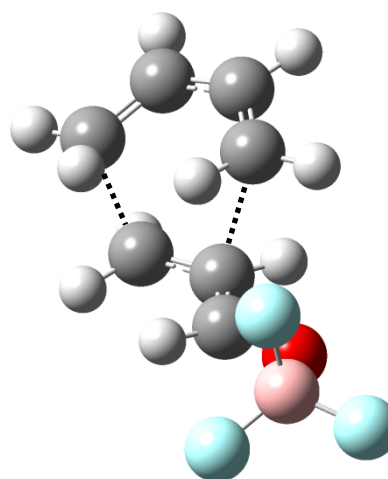
Figure 5.14. Four possible transition structures for the BF_3 catalyzed Diels-Alder reaction between 2-propenal and 1,3-butadiene. NC (*endo*, *s-cis* acrolein), XC (*exo*, *s-cis* acrolein), NT (*endo*, *s-trans* acrolein) and XT (*exo*, *s-trans* acrolein). The dashed lines correspond to the C-C forming bonds.

Activation barriers, Δ‡G_{298}, for BF_2**X** catalyzed Diels-Alder reactions between 1,3-butadiene and 2-propenal decrease as the electron withdrawing nature of **X** increases (Table 5.5), as expected from FMO analysis. Figure 5.15 displays a correlation between

the total strength of the three π(C=O) $\rightarrow$ σ*(B–Y) interactions and the decrease in

$\Delta^{\ddagger}G_{298}$ ($R^2 = 0.81$, P-value $= 1.6 \times 10^{-4}$). Furthermore, as the computed interaction

becomes stronger, the π(C=C) $\rightarrow$ π*(C=O) interaction strengthens (Figure 5.16; $R^2 =$

0.98), indicating that the π(C=O) $\rightarrow$ σ*(B–Y) interaction facilitates dienophile π-

conjugation from π(C=C) to π*(C=O), lowering the energy of the dienophile LUMO,

and ultimately decreasing the activation barrier. The magnitude of the π(C=C) $\rightarrow$

π*(C=O) interaction demonstrated by each BF$_2$**X** activated dienophile is reported in

Table 5.4. As an illustration, the π-conjugation from π(C=C) to π*(C=O) when **X** = F is

shown by Figure 5.17.

When π(C=C) $\rightarrow$ π*(C=O) strengthens, $\Delta^{\ddagger}G_{298}$ decreases (Figure 5.18; $R^2 =$

0.83), further illustrating the intimate connection between dienophile π-conjugation,

initiated by π(C=O) $\rightarrow$ σ*(B–Y), and a lower activation barrier. The synergistic

movement of electron density initiated by the Lewis acid geminal interaction explains

the differences in $\Delta^{\ddagger}G_{298}$ and thus the rate enhancement of the Diels-Alder reaction. It is

natural to assume that as the σ*(B–Y) energy levels are lowered the empty 2p orbital of

boron will be lowered as well. The consequence of lowering the n*(B) orbital should

promote coordinate covalent bonding, where the traditional donor-acceptor

hyperconjugation should strengthen. This is indeed found, where π(C=O) $\rightarrow$ σ*(B–Y)

correlates strongly with n(O) $\rightarrow$ n*(B) (Figure 5.19; $R^2 = 0.95$; P-value $= 2.4 \times 10^{-7}$).

Table 5.5. Substituents, Hammett Constants, and Gibbs Free Activation Energies for the $BF_2\textbf{X}$ Catalyzed Diels-Alder Reaction between 2-propenal and 1,3-butadiene.[a]

X	σ_p [336, 337]	$\Delta^{\ddagger}G_{298}$
$-N_2^+$	1.910	NA[a]
$-NO_2$	0.778	13.1
$-CN$	0.660	15.8
$-CF_3$	0.540	18.6
$-CO_2H$	0.450	19.2
$-F$	0.062	19.1
$-H$	0.000	20.1
$-CH_2CH_3$	-0.151	19.9
$-CH_3$	-0.170	20.7
$-OCH_3$	-0.268	23.4
$-OH$	-0.370	21.9
$-NH_2$	-0.660	28.5

[a] All energies are in kcal/mol.
[b] After many attempts, a TS with $\textbf{X}=N_2^+$ was unable to be located.

(1) $-NO_2$
(2) $-CN$
(3) $-CF_3$
(4) $-CO_2H$
(5) $-F$
(6) $-H$
(7) $-CH_2CH_3$
(8) $-CH_3$
(9) $-OCH_3$
(10) $-OH$
(11) $-NH_2$

$R^2 = 0.81$
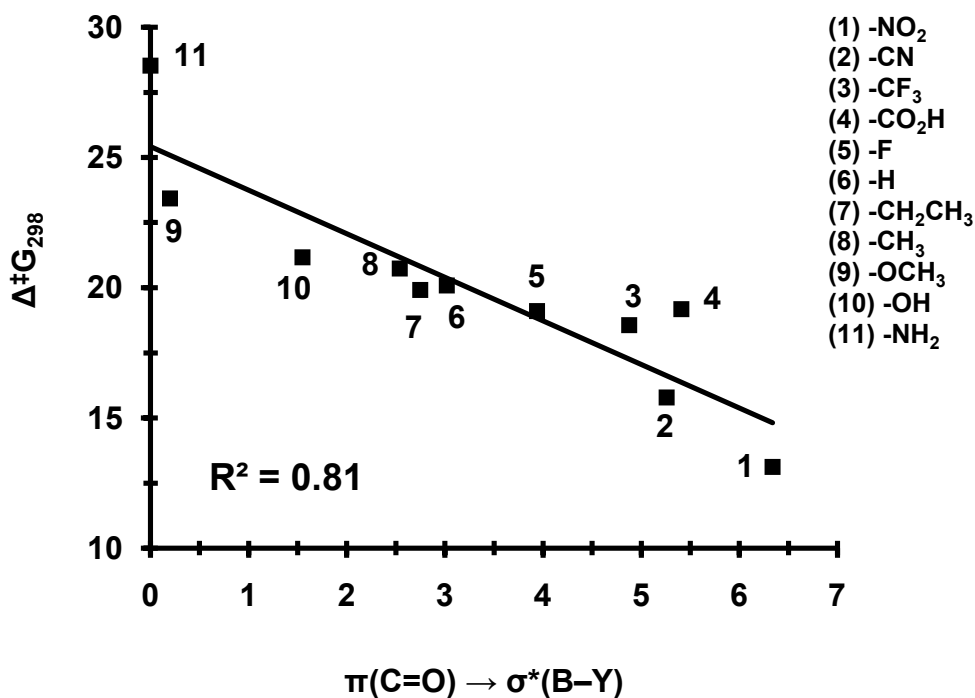
$\pi(C=O) \rightarrow \sigma^*(B-Y)$

Figure 5.15. Gibbs free activation energy, $\Delta^{\ddagger}G_{298}$, for the $BF_2\textbf{X}$ catalyzed Diels-Alder reaction between 1,3-butadiene and 2-propenal vs. the total strength of the three $\pi(C=O) \rightarrow \sigma^*(B-Y)$ interactions (Y = $\textbf{X}$, F and F). All values are in kcal/mol.
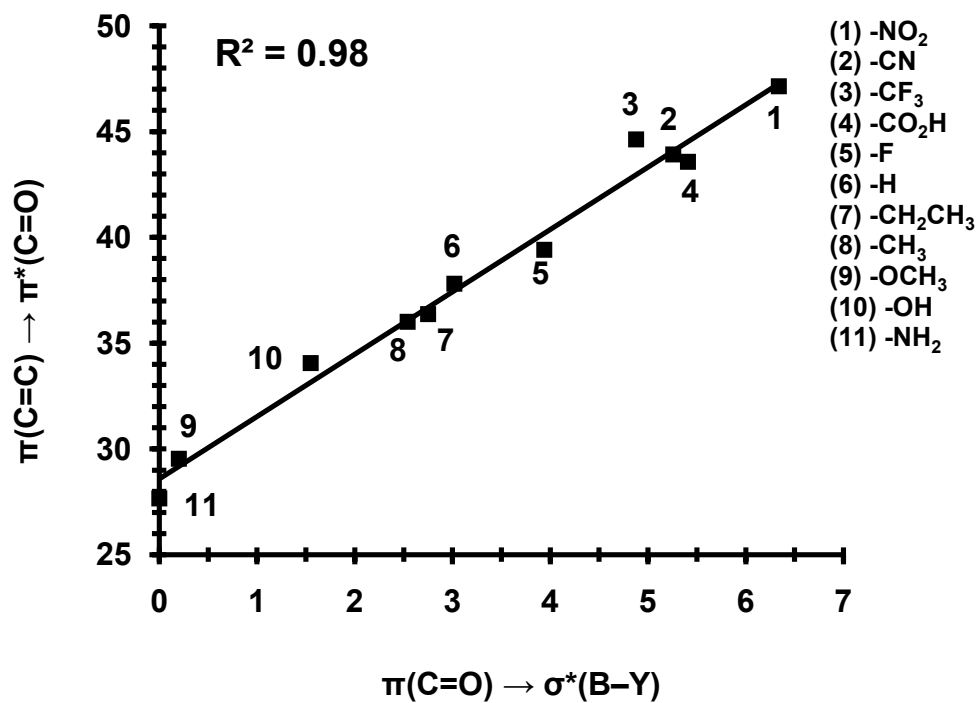
Figure 5.16. The strength of $\pi(C=C) \to \pi^*(C=O)$ vs. the total strength of the three $\pi(C=O) \to \sigma^*(B-Y)$ interactions ($Y = \mathbf{X}$, F and F). All values are in kcal/mol.
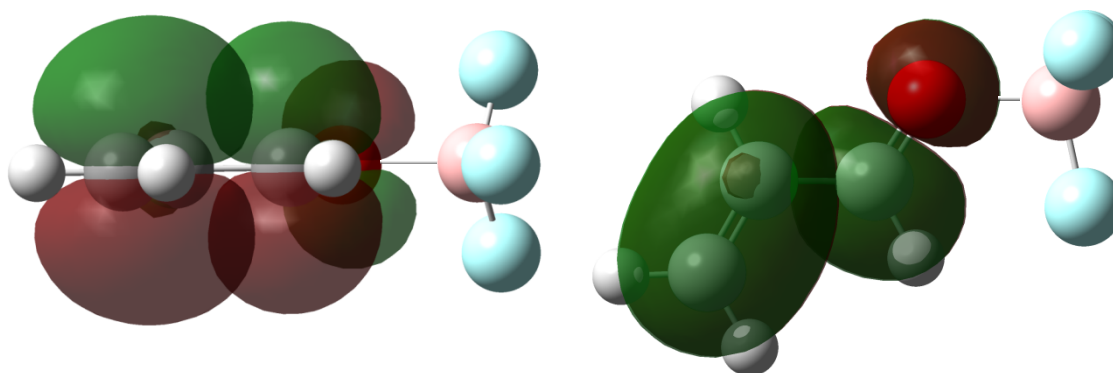
Figure 5.17. Orbital overlap corresponding to the $\pi(C=O) \to \pi^*(C=O)$ stereoelectronic interaction within the BF$_3$ Lewis acid activated dienophile adduct. The strength of this individual interaction is 39.42 kcal/mol.
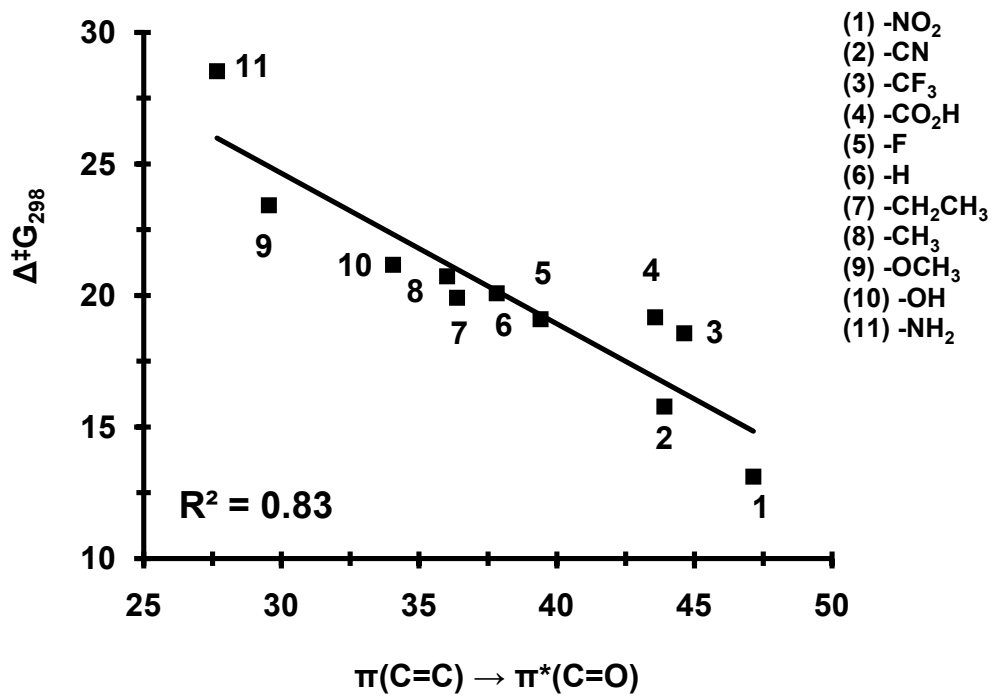
Figure 5.18. Gibbs free activation energy, $\Delta^{\ddagger}G_{298}$, for the $BF_2\mathbf{X}$ catalyzed Diels-Alder reaction between 1,3-butadiene and 2-propenal vs. the strength of $\pi(C=C) \rightarrow \pi^*(C=O)$. All values are in kcal/mol.
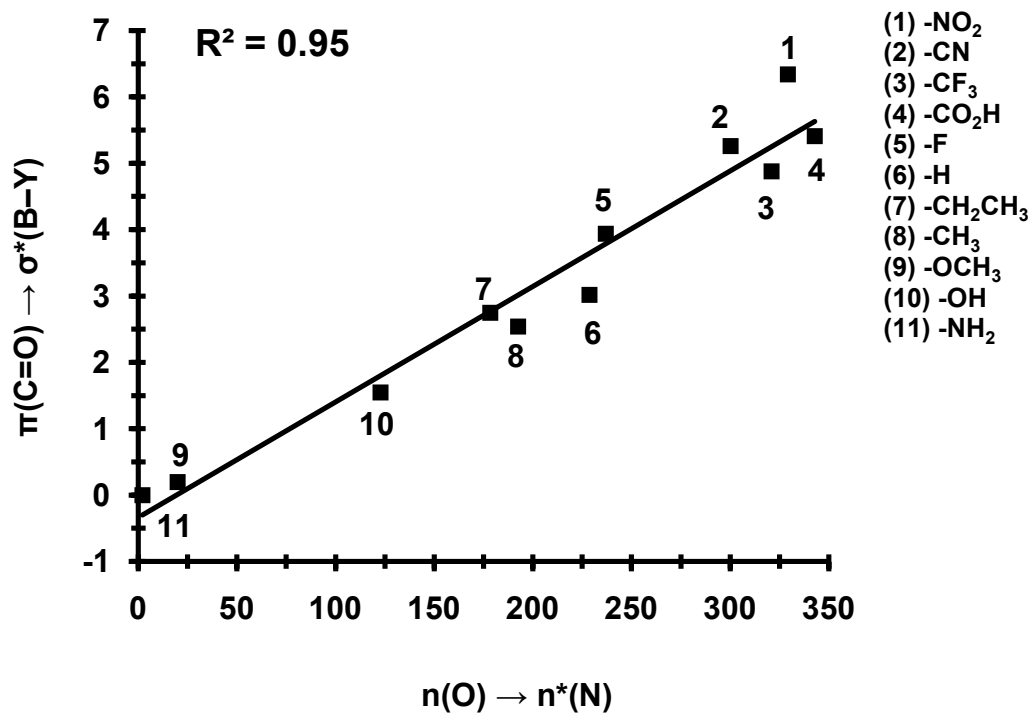
Figure 5.19. The total strength of the three $\pi(C=O) \rightarrow \sigma^*(B–Y)$ interactions ($Y = X$, F and F) within the BF_2X activated 2-propenal vs. the strength of the main donor-acceptor interaction necessary for the formation of the coordinate covalent bond, $n(O) \rightarrow n^*(B)$. All values are in kcal/mol.

5.7 Analysis of Four Additional Lewis Acids (BH_3, BCl_3, $B(OH)_3$ and $B(CF_3)_3$)

In order to extend the investigation beyond the specific case of each boron Lewis acid possessing two $\sigma^*(B–F)$ orbitals, four additional Lewis acids have been investigated (BH_3, BCl_3, $B(OH)_3$, and $B(CF_3)_3$), which do not possess $\sigma^*(B–F)$ orbitals. The total strength of the three $\pi(C=O) \rightarrow \sigma^*(B–X)$ ($X = H$, Cl, O, C) interactions increases across the Lewis acid activated dienophiles, as OH < H < F < Cl < CF$_3$, where the magnitude is 0.0, 3.90, 3.94, 7.36 and 7.74 kcal/mol, respectively, in line with

increasing σ_p (-0.37 < 0.0 < 0.062 < 0.23 < 0.54). Consequently, $\Delta^{\ddagger}G_{298}$ is expected to

decrease as OH > H > F > Cl > CF$_3$, which is in fact the case, as predicted activation

barriers are $\Delta^{\ddagger}G_{298}$ = 28.6, 22.5, 19.1, 13.5 and 11.9 kcal/mol, respectively (Figure 5.20;

R^2 = 0.90). The data suggest that the π(C=O) → σ*(B–**X**) interactions govern the rate

enhancement of the Diels-Alder reaction with and without imposing the constraint of the

boron Lewis acid possessing two σ*(B–F) orbitals.

Figure 5.20. Gibbs free activation energy, $\Delta^{\ddagger}G_{298}$, for the B**X**$_3$ catalyzed Diels-Alder reaction between 1,3-butadiene and 2-propenal vs. the total strength of the three π(C=O) → σ*(B–**X**) interactions (**X**= OH, H, F, Cl, CF$_3$). All values are in kcal/mol.

5.8 Conclusions

In summary, the identified Lewis acid geminal interactions govern both the binding affinity of adduct formation and the activation barrier of the Diels-Alder reaction. The geminal interactions lower the σ*(B–Y) orbitals, promoting the transfer of electron density from the carbonyl group of the dienophile. The donation from the carbonyl group initiates π-conjugation across the dienophile, lowering the π*(C=C) involved in the pericyclic process, and ultimately decreases the activation barrier. The results are consistent with Fukui's traditional FMO model, but provide a level of detail that has not been reported previously. The presented quantitative connection between geminal Lewis acid interactions and the modulation of the dienophile LUMO provides a fundamental understanding of how the rates of common organic reactions are controlled through coordinate covalent bond involvement.

It is discovered that B3LYP/6-31G(d) is a Pauling point, thus when the basis set is improved, the predicted activation energies diverge from experiment. B3LYP/6-31G(d) establishes a unique cancelation of errors, introduced by the approximate exchange-correlation functional and the basis set truncation. As a result, B3LYP/6-31G(d) yields a fortuitous result in excellent agreement with experiment. M06-2X predicted activation energies converge toward the experimental value, in contrast to B3YLP; however, the converged value underestimates the barrier by *ca.* 2 kcal/mol. M06-2X in conjunction with the 6-311++G(3df,2p) basis set underestimates the barrier by *ca.* 3 kcal/mol; however, the errors cancel when the differences in

activation barriers are compared, and thus the relative differences are modeled accurately.

REFERENCES

1.   Lewis, G. N., Valence and the electron. *Trans. Faraday Soc.* **1923,** 19, 452.

2.   Lewis, G. N., The Definition of Acids and Bases. In *Valence and the Structure of Atoms and Molecules*, 1st ed.; Chemical Catalog Co.: New York, 1923; 142.

3.   Langmuir, I., The arrangement of electrons in atoms and molecules. *J. Am. Chem. Soc.* **1919,** 41, 868.

4.   Lewis, G. N., The atom and the molecule. *J. Am. Chem. Soc.* **1916,** 38, 762.

5.   Lewis, G. N., The chemical bond. *J. Chem. Phys.* **1933,** 1, 17.

6.   Langmuir, I., The structure of atoms and the octet theory of valence. *Proc. Am. Acad. Sci.* **1919,** 5, 252.

7.   Pauling, L. C., *The Nature of the Chemical Bond and the Structure of Molecules and Crystals. An Introduction to Modern Structural Chemistry*. 3rd ed.; Cornell University Press: Ithaca, NY, 1960; p 644.

8.   Langmuir, I., Isomorphism, isosterism and covalence. *J. Am. Chem. Soc.* **1919,** 41, 1543.

9.   Gillespie, R. J.; Popelier, P. L. A., *Chemical Bonding and Molecular Geomoetry*. 1st ed.; Oxford University Press: New York, 2001; p 90.

10.   Gillespie, R. J.; Robinson, E. A., Gilbert N. Lewis and the chemical bond: the electron pair and the octet rule from 1916 to the present day. *J. Comput. Chem.* **2007,** 28, (1), 87.

11.   Sidgwick, N. V.; Powell, H. M., Stereochemical types and valency groups. *Proc. R. Soc. London, Ser. A* **1940,** 176, 153.

12.   Lennard-Jones, J., The spatial correlation of electrons in molecules. *J. Chem. Phys.* **1952,** 20, 1024.

13. Linnett, J. W., Modification of the Lewis-Langmuir octet rule. *J. Am. Chem. Soc.* **1961,** 83, 2643.

14. Heitler, W.; London, F., Interaction of neutral atoms and homopolar binding according to the quantum mechanics. *Z. Phys.* **1927,** 44, 455.

15. Frenking, G.; Shaik, S., 90 Years of Chemical Bonding [Special Issue]. *J. Comput. Chem.* **2006,** 28, (1).

16. Kovacs, A.; Esterhuysen, C.; Frenking, G., The nature of the chemical bond revisited: an energy-partitioning analysis of nonpolar bonds. *Chem.Eur. J.* **2005,** 11, (6), 1813.

17. Nguyen, T.; Sutton, A. D.; Brynda, M.; Fettinger, J. C.; Long, G. J.; Power, P. P., Synthesis of a stable compound with fivefold bonding between two chromium(I) centers. *Science* **2005,** 310, (5749), 844.

18. Boudreaux, E. A.; Baxter, E., More QR-SCMEH-MO calculations on group VIB transition metal molecules, M_2 (M = Cr, Mo, W, Sg) valence and valence-core effects. *Int. J. Quantum Chem.* **2004,** 100, (6), 1170.

19. Haaland, A., Covalent and dative bonds to main group metals, a useful difference. *Angew. Chem., Int. Ed.* **1989,** 101, (8), 1017.

20. Wittig, G., Ylides and ylide reactions. *Angew. Chem.* **1951,** 63, (1), 15.

21. Linton, E. P., The dipole moments of amine oxides. *J. Am. Chem. Soc.* **1940,** 62, 1945.

22. Chatt, J., Coordinate link in chemistry. *Nature* **1950,** 165, 637.

23. Mulliken, R. S., Molecular compounds and their spectra. II. *J. Am. Chem. Soc.* **1952,** 74, 811.

24. Plumley, J. A.; Evanseck, J. D., Covalent and ionic nature of the dative bond and account of accurate ammonia borane binding enthalpies. *J. Phys. Chem. A* **2007,** 111, (51), 13472.

25.   Zhong, D.; Zewail, A. H., Femtosecond dynamics of dative bonding: concepts of reversible and dissociative electron transfer reactions. *Proc. Natl. Acad. Sci. U. S. A.* **1999,** 96, (6), 2602.

26.   Thorne, L. R.; Suenram, R. D.; Lovas, F. J., Microwave spectrum, torsional barrier, and structure of borane monoammoniate. *J. Chem. Phys.* **1983,** 78, (1), 167.

27.   Mayer, E., Symmetrical cleavage of diborane by ammonia in solution. *Inorg. Chem.* **1972,** 11, (4), 866.

28.   Lide, D. R., *CRC Handbook of Chemistry and Physics*. 88th ed.; CRC Press: Bosca Raton, 2007; p 2640.

29.   Luo, Y.-R., *Comprehensive Handbook of Chemical Bond Energies*. 1st ed.; CRC Press: Boca Rota, 2007; p 1655.

30.   Kuchitsu, K., Comparison of molecular structures determined by electron diffraction and spectroscopy. Ethane and diborane. *J. Chem. Phys.* **1968,** 49, (10), 4456.

31.   Beagley, B.; Monaghan, J. J.; Hewitt, T. G., Electron-diffraction studies of tetramethylsilane and hexamethyldisilane, and discussion of the lengths of silicon-carbon bonds. *J. Mol. Struct.* **1971,** 8, (4), 401.

32.   Almenningen, A.; Fernholt, L.; Haaland, A.; Weidlein, J., The molecular structure of the complex trimethylaluminum trimethylphosphine, $(CH_3)_3AlP(CH_3)_3$, determined by gas phase electron diffraction. *J. Organomet. Chem.* **1978,** 145, (1), 109.

33.   Gordon, F.; Stone, A.; West, R., *Advances in Organometallic Chemistry*. 1st ed.; Elsevier Inc.: Oxford, 2008; p 470.

34.   Henrickson, C. H.; Duffy, D.; Eyman, D. P., Lewis acidity of alanes. Interactions of trimethylalane with amines, ethers, and phosphines. *Inorg. Chem.* **1968,** 7, (6), 1047.

35.   Dixon, D. A.; Gutowski, M., Thermodynamic properties of molecular borane amines and the $[BH_4^-][NH_4^+]$ salt for chemical hydrogen storage systems from ab initio electronic structure theory. *J. Phys. Chem. A* **2005,** 109, (23), 5129.

36.   Grant, D. J.; Dixon, D. A., Thermodynamic properties of molecular borane phosphines, alane amines, and phosphine alanes and the $[BH_4^-][PH_4^+]$, $[AlH_4^-][NH_4^+]$, and $[AlH_4^-][PH_4^+]$ salts for chemical hydrogen storage systems from ab Initio electronic structure theory. *J. Phys. Chem. A* **2005,** 109, (44), 10138.

37.   Nguyen, M. T.; Nguyen, V. S.; Matus, M. H.; Gopakumar, G.; Dixon, D. A., Molecular mechanism for H_2 release from BH_3NH_3,including the catalytic role of the lewis acid BH_3. *J. Phys. Chem. A* **2007,** 111, (4), 679.

38.   Huang, J. L.; Pan, C. H.; Lii, D. F., Investigation of the BN films prepared by low pressure chemical vapor deposition. *Surf. Coat. Technol.* **1999,** 122, (2-3), 166.

39.   Lii, D.-F.; Huang, J.-L.; Tsui, L.-J.; Lee, S.-M., Formation of BN films on carbon fibers by dip-coating. *Surf. Coat. Technol.* **2002,** 150, (2-3), 269.

40.   Einset, E. O.; Patibandla, N.-B.; Luthra, K. L., Processing conditions for boron nitride coatings in fiber bundles via chemical vapor deposition. *J. Am. Ceram. Soc.* **1994,** 77, (12), 3081.

41.   Karim, M. Z.; Cameron, D. C.; Murphy, M. J.; Hashmi, M. S. J., Vapor deposited boron nitride thin films: a review. *Proc. Inst. Mech. Eng., IMechE Conf.* **1991**, (7), 181.

42.   Fisher, L.; Holme, T., MM3 parameterization for the B-N dative bond. *J. Comput. Chem.* **2001,** 22, (9), 913.

43.   Hall, I. H.; Spielvogel, B. F.; Sood, A., The antineoplastic activity of trimethylamine carboxyboranes and related esters and amides in murine and human tumor cell lines. *Anti-Cancer Drugs* **1990,** 1, (2), 133.

44.   Burnham, B. S., Synthesis and pharmacological activities of amine-boranes. *Curr. Med. Chem.* **2005,** 12, (17), 1995.

45.   Gibson, A.; Fernandes, F.; Wallace, P.; McFadzean, I., Selective inhibition of thapsigargin-induced contraction and capacitative calcium entry in mouse anococcygeus by trifluoromethylphenylimidazole (TRIM). *Br. J. Pharmacol.* **2001,** 134, (2), 233.

46.   Clementi, E.; Meldolesi, J., Pharmacological and functional properties of voltage-independent Ca_2^+ channels. *Cell Calcium* **1996,** 19, (4), 269.

47.   Putney, J. W., Jr., The pharmacology of capacitative calcium entry. *Mol. Interventions* **2001,** 1, (2), 84.

48.   Sood, A.; Sood, C. K.; Spielvogel, B. F.; Hall, I. H.; Wong, O. T., Synthesis, cytotoxicity, hypolipidemic and anti-inflammatory activities of amine-boranes and esters of boron analogues of choline and thiocholine. *J. Pharm. Sci.* **1992,** 81, (5), 458.

49.   Arrhenius, S. A., On the dissociation of substances dissolved in water. *Z. Phys. Chem* **1887,** 1, 631.

50.   Brønsted, J. N., Some remarks on the concept of acids and bases. *Recl. Trav. Chim. Pays-Bas* **1923,** 42, 718.

51.   Lowry, M., The electronic theory of valency. Part IV. The origin of acidity. *Trans. Faraday Soc.* **1924,** 20, 13.

52.   Lowry, T. M., Uniqueness of hydrogen. *Chem. Ind. (London)* **1923,** 42, 43.

53.   Wade, L. G., *Organic Chemistry*. 5th ed.; Pearson Education , Inc.: Upper Saddle River, NJ, 2003; p 1296.

54.   Anslyn, E. V.; Dougherty, D. A., *Modern Physical Organic Chemistry*. 1st ed.; University Science: Sausalito, CA, 2006; p 1104.

55.   Lewis, G. N., Acids and bases. *J. Franklin Inst.* **1938,** 226, 293.

56.   Lewis, G. N., *Valence and the Structure of Atoms and Molecules*. 1st ed.; Chemical Catalog Company: New York, 1923; p 172.

57. Pearson, R. G., *Benchmark Papers in Inorganic Chemistry: Hard and Soft Acids and bases*. 1st ed.; Dowden: Stroudsburgh, 1973; p 480.

58. Pearson, R. G., Hard and soft acids and bases (HSAB). I. Fundamental principles. *J. Chem. Educ.* **1968,** 45, (9), 581.

59. Pearson, R. G., Hard and soft acids and bases (HSAB). II. Underlying theories. *J. Chem. Educ.* **1968,** 45, (10), 643.

60. Pearson, R. G., Hard and soft acids and bases. *J. Am. Chem. Soc.* **1963,** 85, (22), 3533.

61. Gutmann, V.; Steininger, A.; Wychera, E., Donor strengths in 1,2-dichloroethane. *Monatsh. Chem.* **1966,** 97, (2), 460.

62. Mayer, U.; Gutmann, V.; Gerger, W., Acceptor number. Quantitative empirical parameter for the electrophilic properties of solvents. *Monatsh. Chem.* **1975,** 106, (6), 1235.

63. Gutmann, V., Empirical approach to molecular interactions. *Coord. Chem. Rev.* **1975,** 15, (2-3), 207.

64. Drago, R. S.; Wayland, B. B., A double-scale equation for correlating enthalpies of Lewis acid-base interactions. *J. Am. Chem. Soc.* **1965,** 87, (16), 3571.

65. Drago, R. S., Quantitative evaluation and prediction of donor-acceptor interactions. *Struc. Bonding (Berlin)* **1973,** 15, 73.

66. Marks, A. P.; Drago, R. S., Prediction and correlation of the enthalpies of gas-phase ionic reactions. *Inorg. Chem.* **1976,** 15, (8), 1800.

67. Christe, K. O.; Dixon, D. A.; McLemore, D.; Wilson, W. W.; Sheehy, J. A.; Boatz, J. A., On a quantitative scale for Lewis acidity and recent progress in polynitrogen chemistry. *J. Fluorine Chem.* **2000,** 101, (2), 151.

68. Luder, W. F.; Zuffanti, S., *The Electronic Theory of Acids and Bases*. 1st ed.; John Wiley & Sons, Inc.: New York, 1946; p 165.

69. Jensen, W. B., The Lewis acid-base definitions: A status report. *Chem. Rev.* **1978,** 78, (1), 1.

70. Mortimer, C. T., Molecular Addition Compunds. In *Reaction Heats and Bond Strengths*, 1st ed.; Pergamon Press: New York, 1962; 107.

71. Diels, O.; Alder, K., Syntheses in the hydroaromatic series. I. Addition of "diene" hydrocarbons. *Liebigs Ann.* **1928,** 460, 98.

72. Fringuelli, F.; Taticchi, A., *The Diels-Alder Reaction: Selected Practical Methods*. 1st ed.; John Wiley & Sons, Ltd.: Baffins Lane, England, 2002; p 340.

73. Nicolaou, K. C.; Snyder, S. A.; Montagnon, T.; Vassilikogiannakis, G., The Diels-Alder reaction in total synthesis. *Angew. Chem., Int. Ed.* **2002,** 41, (10), 1668.

74. Jorgensen, K. A., Catalytic asymmetric hetero-Diels-Alder reactions of carbonyl compounds and imines. *Angew. Chem., Int. Ed.* **2000,** 39, (20), 3558.

75. Boger, D. L.; Weinreb, S. M., *Hetero Diels-Alder Methodolgy in Organic Synthesis*. 1st ed.; Academic Press: San Diego, CA, 1987; p 366.

76. Pindur, U.; Lutz, G.; Otto, C., Acceleration and selectivity enhancement of Diels-Alder reactions by special and catalytic methods. *Chem. Rev.* **1993,** 93, (2), 741.

77. Konovalov, A. I.; Kiselev, V. D., Diels-Alder reaction. Effect of internal and external factors on the reactivity of diene-dienophile systems. *Russ. Chem. Bull.* **2003,** 52, (2), 293.

78. Vidis, A.; Laurenczy, G.; Kusters, E.; Sedelmeier, G.; Dyson, P. J., High-pressure effects on the Diels-Alder reaction in room temperature ionic liquids. *J. Phys. Org. Chem.* **2007,** 20, (2), 109.

79. Giguere, R. J., Nonconventional reaction conditions: ultrasound, high pressure, and microwave heating in organic synthesis. *Org. Synth.: Theory Appl.* **1989,** 1, 103.

80. Fringuelli, F.; Piermatti, O.; Pizzo, F.; Vaccaro, L., Recent advances in Lewis acid catalyzed Diels-Alder reactions in aqueous media. *Eur. J. Org. Chem.* **2001**, (3), 439.

81. Pan, C.; Wang, Z., Catalytic asymmetric formation of carbon-carbon bond in the presence of water. *Coord. Chem. Rev.* **2008,** 252, (5-7), 736.

82. Sinou, D., Asymmetric organometallic-catalyzed reactions in aqueous media. *Adv. Synth. Catal.* **2002,** 344, (3+4), 221.

83. Bolm, C.; Rantanen, T.; Schiffers, I.; Zani, L., Protonated chiral catalysts: Versatile tools for asymmetric synthesis. *Angew. Chem., Int. Ed.* **2005,** 44, (12), 1758.

84. Akiyama, T., Stronger Brønsted acids. *Chem. Rev.* **2007,** 107, (12), 5744.

85. Shen, J.; Tan, C.-H., Brønsted-acid and Brønsted-base catalyzed Diels-Alder reactions. *Org. Biomol. Chem.* **2008,** 6, (18), 3229.

86. Fischer, T.; Sethi, A.; Welton, T.; Woolf, J., Diels-Alder reactions in room-temperature ionic liquids. *Tetrahedron Lett.* **1999,** 40, (4), 793.

87. Welton, T., Room-temperature ionic liquids. solvents for synthesis and catalysis. *Chem. Rev.* **1999,** 99, (8), 2071.

88. Avalos, M.; Babiano, R.; Cintas, P.; Jimenez, J. L.; Palacios, J. C., Greener media in chemical synthesis and processing. *Angew. Chem., Int. Ed.* **2006,** 45, (24), 3904.

89. Chiappe, C.; Pieraccini, D., Ionic liquids: solvent properties and organic reactivity. *J. Phys. Org. Chem.* **2005,** 18, (4), 275.

90. Vidis, A.; Kusters, E.; Sedelmeier, G.; Dyson, P. J., Effect of Lewis acids on the Diels-Alder reaction in ionic liquids with different activation modes. *J. Phys. Org. Chem.* **2008,** 21, (4), 264.

91.   Fringuelli, F.; Minuti, L.; Pizzo, F.; Taticchi, A., Reactivity and selectivity in Lewis acid-catalyzed Diels-Alder reactions of 2-cyclohexenones. *Acta Chem. Scand.* **1993,** 47, (3), 255.

92.   Oh, T.; Reilly, M., Reagent-controlled asymmetric Diels-Alder reactions. A review. *Org. Prep. Proced. Int.* **1994,** 26, (2), 129.

93.   Fujimoto, H.; Inagaki, S.; Fukui, K., On the donor-acceptor relationship in cyclic additions. *J. Am. Chem. Soc.* **1976,** 98, (9), 2670.

94.   Fukui, K., Recognition of stereochemical paths by orbital interaction. *Acc. Chem. Res.* **1971,** 4, (2), 57.

95.   Fukui, K., Role of frontier orbitals in chemical reactions. *Science* **1982,** 218, (4574), 747.

96.   Fleming, I., *Pericyclic Reactions*. 1st ed.; Oxford University Press: Oxford, UK, 1998; p 96.

97.   Sauer, J.; Sustmann, R., Mechanistic aspects of the Diels-Alder reaction: a critical review. *Angew. Chem., Int. Ed.* **1980,** 92, (10), 773.

98.   Anh, N. T., *Fronteir Orbitals: A Practical Guide*. 1st ed.; John Wiley & Sons Ltd.: West Sussex, England, 2007; p 287.

99.   Yates, P.; Eaton, P., Acceleration of the Diels-Alder reaction by aluminum chloride. *J. Am. Chem. Soc.* **1960,** 82, (16), 4436.

100.   Inukai, T.; Kojima, T., Aluminum chloride catalyzed diene condensation. IV. Kinetic study of butadiene-methyl acrylate reaction. *J. Org. Chem.* **1967,** 32, (4), 872.

101.   Inukai, T.; Kojima, T., Aluminum chloride catalyzed diene condensation. VI. Partial rate factors of 2-phenyl-, 2-chloro-, 2-trifluoromethyl-, and 2-cyanobutadienes in reactions with methyl acrylate. Differential Hammettt correlation. *J. Org. Chem.* **1971,** 36, (7), 924.

102.   Kojima, T.; Inukai, T., Aluminum chloride catalyzed diene condensation. V. Selectivity--reactivity relation of dienophiles toward butadiene, isoprene, and 2-trifluoromethyl butadiene. *J. Org. Chem.* **1970,** 35, (5), 1342.

103.   Hoffmann, R.; Woodward, R. B., Conservation of orbital symmetry. *Acc. Chem. Res.* **1968,** 1, (1), 17.

104.   Salem, L., Intermolecular orbital theory of the interaction between conjugated systems. II. Thermal and photochemical cycloadditions. *J. Am. Chem. Soc.* **1968,** 90, (3), 553.

105.   Alston, P. V.; Ottenbrite, R. M.; Cohen, T., Secondary orbital interactions determining regioselectivity in the Diels-Alder reaction. 3. Disubstituted dienes. *J. Org. Chem.* **1978,** 43, (10), 1864.

106.   Houk, K. N., Role of secondary orbital interactions in cycloaddition reactions. *Tetrahedron Lett.* **1970**, (30), 2621.

107.   Singleton, D. A., A [4 + 3] transition state for a [4 + 2] cycloaddition. A new secondary orbital interaction in Diels-Alder reactions. *J. Am. Chem. Soc.* **1992,** 114, (16), 6563.

108.   Birney, D. M.; Houk, K. N., Transition structures of the Lewis acid-catalyzed Diels-Alder reaction of butadiene with acrolein. The origins of selectivity. *J. Am. Chem. Soc.* **1990,** 112, (11), 4127.

109.   Garcia, J. I.; Mayoral, J. A.; Salvatella, L., Do secondary orbital interactions really exist? *Acc. Chem. Res.* **2000,** 33, (10), 658.

110.   Wannere, C. S.; Paul, A.; Herges, R.; Houk, K. N.; Schaefer, H. F., III; Schleyer, P. v. R., The existence of secondary orbital interactions. *J. Comput. Chem.* **2007,** 28, (1), 344.

111.   Frisch, M. J.; Trucks, G. W.; Schlegel, H. B.; Scuseria, G. E.; Robb, M. A.; Cheeseman, J. R.; Montgomery Jr., J. A.; Vreven, T.; Kudin, K. N.; Burant, J. C.; Millam, J. M.; Iyengar, S. S.; Tomasi, J.; Barone, V.; Mennucci, B.; Cossi, M.; Scalmani, G.; Rega, N.; Petersson, G. A.; Nakatsuji, H.; Hada, M.; Ehara, M.; Toyota, K.; Fukuda, R.; Hasegawa, J.; Ishida, M.; Nakajima, T.; Honda, Y.; Kitao, O.; Nakai, H.; Klene, M.; Li, X.; Knox, J. E.; Hratchian, H. P.; Cross, J. B.; Adamo, C.; Jaramillo, J.; Gomperts, R.; Stratmann, R. E.; Yazyev, O.;

Austin, A. J.; Cammi, R.; Pomelli, C.; Ochterski, J.; Ayala, P. Y.; Morokuma, K.; Voth, G. A.; Salvador, P.; Dannenberg, J. J.; Zakrzewski, V. G.; Dapprich, S.; Daniels, A. D.; Strain, M. C.; Farkas, O.; Malick, D. K.; Rabuck, A. D.; Raghavachari, K.; Foresman, J. B.; Ortiz, J. V.; Cui, Q.; Baboul, A. G.; Clifford, S.; Cioslowski, J.; Stefanov, B. B.; Liu, G.; Liashenko, A.; Piskorz, P.; Komaromi, I.; Martin, R. L.; Fox, D. J.; Keith, T.; Al-Laham, M. A.; Peng, C. Y.; Nanayakkara, A.; Challacombe, M.; Gill, P. M. W.; Johnson, B.; Chen, W.; Wong, M. W.; Gonzalez, C.; Pople, J. A. *Gaussian 03*, Revision E.01; Gaussian, Inc.: Pittsburgh PA, 2004

112. Bylaska, E. J.; Jong, W. A. d.; Govind, N.; Kowalski, K.; Straatsma, T. P.; Valiev, M.; Wang, D.; Apra, E.; Windus, T. L.; Hammond, J.; Nichols, P.; Hirata, S.; Hackler, M. T.; Zhao, Y.; Fan, P. D.; Harrison, R. J.; Dupuis, M.; Smith, D. M. A.; Nieplocha, J.; Tipparaju, V.; Krishnan, M.; Wu, Q.; Voorhis, T. V.; Auer, A. A.; Nooijen, M.; Brown, E.; Cisneros, G.; Fann, G. I.; Fruchtl, H.; Garza, J.; Hirao, K.; Kendall, R.; Nichols, J. A.; Tsemekhman, K.; Wolinski, K.; Anchell, J.; Bernholdt, D.; Borowski, P.; Clark, T.; Clerc, D.; Dachsel, H.; Deegan, M.; Dyall, K.; Elwood, D.; Glendening, E.; Gutowski, M.; Hess, A.; Jaffe, J.; Johnson, B.; Ju, J.; Kobayashi, R.; Kutteh, R.; Lin, Z.; Littlefield, R.; Long, X.; Meng, B.; Nakajima, T.; Niu, S.; Pollack, L.; Rosing, M.; Sandrone, G.; Stave, M.; Taylor, H.; Thomas, G.; Lenthe, J. v.; Wong, A.; Zhang, Z. *NWChem, A Computational Chemistry Package for Parallel Computers*, version 5.1; Pacific Northwest National Laboratory: Richland, WA, 2007

113. E. D. Glendening; J. K. Badenhoop; A. E. Reed; J. E. Carpenter; J. A. Bohmann; C. M. Morales; Weinhold, F. *NBO 5.G*, Theoretical Chemistry Institute, University of Wisconsin: Madison, WI, 2001.; http://www.chem.wisc.edu/~nbo5.

114. McQuarrie, D. A.; Simon, J. D., *Physical Chemistry: A Molecular Approach*. 1st ed.; University Science Books: Sausalito, 1997; p 1360.

115. Trindle, C.; Shillady, D., *Electronic Structure and Modeling, Connections Between Theory and Software*. 1st ed.; CRC Press: Boca Raton, 2008; p 484.

116. Nakashima, H.; Nakatsuji, H., Solving the Schrödinger equation for helium atom and its isoelectronic ions with the free iterative complement interaction (ICI) method. *J. Chem. Phys.* **2007,** 127, (22), 224104/1.

117. Nakashima, H.; Nakatsuji, H., Solving the electron-nuclear Schrödinger equation of helium atom and its isoelectronic ions with the free iterative-complement-interaction method. *J. Chem. Phys.* **2008,** 128, (15), 154107/1.

118. Born, M.; Oppenheimer, R., Quantum theory of the molecules. *Ann. Phys* **1927,** 84, 457.

119. Eckart, C., The theory and calculation of screening constants. *Phys. Rev.* **1930,** 36, 878.

120. Leach, R. A., *Molecular Modeling Principles and Applications*. 2nd ed.; Pearson Education: Harlow, 2001; p 744.

121. Jensen, F., *Introduction to Computational Chemistry*. 2nd ed.; John Wiley & Sons Ltd: The Atrium, 2007; p 599.

122. Foresman, J. B.; Frisch, A., *Exploring Chemistry with Electronic Structure Methods*. 2nd ed.; Gaussian, Inc: Pittsburgh, 1996; p 302.

123. Head-Gordon, M.; Head-Gordon, T., Analytic MP2 frequencies without fifth-order storage. Theory and application to bifurcated hydrogen bonds in the water hexamer. *Chem. Phys. Lett.* **1994,** 220, (1-2), 122.

124. Møller, C.; Plesset, M. S., *Phys. Rev.* **1934,** 46, 618.

125. Sousa, S. F.; Fernandes, P. A.; Ramos, M. J., General performance of density functionals. *J. Phys. Chem. A* **2007,** 111, (42), 10439.

126. Krishnan, R.; Schlegel, H. B.; Pople, J. A., Derivative studies in configuration-interaction theory. *J. Chem. Phys.* **1980,** 72, (8), 4654.

127. Pople, J. A.; Binkley, J. S.; Seeger, R., Theoretical models incorporating electron correlation. *Int. J. Quant. Chem. Symp.* **1976,** 10, 1.

128. Boys, S. F., Electronic wave functions. II. A calculation for the ground state of the beryllium atom. *Proc. R. Soc. London, Ser. A* **1950,** 201, 125.

129. Boys, S. F., Electronic wave functions. I. A general method of calculation for the stationary states of any molecular system. *Proc. R. Soc. London, Ser. A* **1950,** 200, 542.

130. Ramachandran, C. N.; De Fazio, D.; Cavalli, S.; Tarantelli, F.; Aquilanti, V., Revisiting the potential energy surface for the He + H_2^+ -> HeH^+ + H reaction at the full configuration interaction level. *Chem. Phys. Lett.* **2009,** 469, (1-3), 26.

131. Gauss, J.; Cremer, D., Analytical evaluation of energy gradients in quadratic configuration interaction theory. *Chem. Phys. Lett.* **1988,** 150, (3,4), 280.

132. Pople, J. A.; Head-Gordon, M.; Raghavachari, K., Quadratic configuration interaction. A general technique for determining electron correlation energies. *J. Chem. Phys.* **1987,** 87, (10), 5968.

133. Scuseria, G. E.; Schaefer, H. F., III, Is coupled cluster singles and doubles (CCSD) more computationally intensive than quadratic configuration interaction (QCISD)? *J. Chem. Phys.* **1989,** 90, (7), 3700.

134. Lee, T. J.; Rendell, A. P.; Taylor, P. R., Comparison of the quadratic configuration interaction and coupled-cluster approaches to electron correlation including the effect of triple excitations. *J. Phys. Chem.* **1990,** 94, (14), 5463.

135. Boehme, M.; Frenking, G., The Cu-C bond dissociation energy of $CuCH_3$. A dramatic failure of the QCISD(T) method. *Chem. Phys. Lett.* **1994,** 224, (1-2), 195.

136. Zhao, Y.; Truhlar, D. G., Density functionals with broad applicability in chemistry. *Acc. Chem. Res.* **2008,** 41, (2), 157.

137. Koch, W.; Houlhausen, M. C., *A Chemist's Guide to Density Functional Theory*. 2nd ed.; Wiley-VCH: Weinheim, 2001; p 293.

138. Xu, X.; Goddard, W. A., III, The X3LYP extended density functional for accurate descriptions of nonbond interactions, spin states, and thermochemical properties. *Proc. Natl. Acad. Sci. U. S. A.* **2004,** 101, (9), 2673.

139. Kohn, W.; Meir, Y.; Makarov, D. E., van der Waals energies in density-functional theory. *Phys. Rev. Lett.* **1998,** 80, (19), 4153.

140. van Mourik, T.; Gdanitz, R. J., A critical note on density functional theory studies on rare-gas dimers. *J. Chem. Phys.* **2002,** 116, (22), 9620.

141. Zhao, Y.; Schultz, N. E.; Truhlar, D. G., Design of density functionals by combining the method of constraint satisfaction with parametrization for thermochemistry, thermochemical kinetics, and noncovalent interactions. *J. Chem. Theory Comput.* **2006,** 2, (2), 364.

142. Mackie, I. D.; DiLabio, G. A., Interactions in large, polyaromatic hydrocarbon dimers: application of density functional theory with dispersion corrections. *J. Phys. Chem. A* **2008,** 112, (43), 10968.

143. Grimme, S., Accurate description of van der Waals complexes by density functional theory including empirical corrections. *J. Comput. Chem.* **2004,** 25, (12), 1463.

144. Schwabe, T.; Grimme, S., Double-hybrid density functionals with long-range dispersion corrections: higher accuracy and extended applicability. *Phys. Chem. Chem. Phys.* **2007,** 9, (26), 3397.

145. Tarnopolsky, A.; Karton, A.; Sertchook, R.; Vuzman, D.; Martin, J. M. L., Double-hybrid functionals for thermochemical kinetics. *J. Phys. Chem. A* **2008,** 112, (1), 3.

146. Morgado, C.; Vincent, M. A.; Hillier, I. H.; Shan, X., Can the DFT-D method describe the full range of noncovalent interactions found in large biomolecules? *Phys. Chem. Chem. Phys.* **2007,** 9, (4), 448.

147. Kohn, W.; Hohenberg, P., Inhomogenous electron gas. *Phys. Rev.* **1964,** 136, (3B), B864.

148. Kohn, W.; Sham, L. J., Quantum density oscillations in an inhomogeneous electron gas. *Phys. Rev.* **1965,** 137, (6A), 1697.

149. Sham, J.; Kohn, W., Self-consistent equations including exchange and correlation effects. *Phys. Rev.* **1965,** 140, (4A), 1133.

150. Slater, J. C., A simplification of the Hartree-Fock method. *Phys. Rev.* **1951,** 81, (3), 385.

151. Painter, G. S., Density functional description of molecular bonding within the local spin density approximation. *J. Phys. Chem.* **1986,** 90, (22), 5530.

152. Becke, A. D., Density-functional exchange-energy approximation with correct asymptotic behavior. *Phys. Rev. A* **1988,** 38, (6), 3098.

153. Perdew, J. P.; Yue, W., Accurate and simple density functional for the electronic exchange energy: generalized gradient approximation. *Phys. Rev. B* **1986,** 33, (12), 8800.

154. Becke, A. D., Density functional calculations of molecular bond energies. *J. Chem. Phys.* **1986,** 84, (8), 4524.

155. Perdew, J. P.; Burke, K.; Ernzerhof, M., Generalized gradient approximation made simple. *Phys. Rev. Lett.* **1996,** 77, (18), 3865.

156. Lee, C.; Yang, W.; Parr, R. G., Development of the Colle-Salvetti correlation-energy formula into a functional of the electron density. *Phys. Rev. B.* **1988,** 37, 785.

157. Becke, A. D., Correlation energy of an inhomogeneous electron gas: a coordinate-space model. *J. Chem. Phys.* **1988,** 88, (2), 1053.

158. Becke, A. D., Density-functional thermochemistry. IV. A new dynamic correlation functional and implications for exact-exchange mixing. *J. Chem. Phys.* **1996,** 104, (3), 1040.

159. Van Voorhis, T.; Scuseria, G. E., A novel form for the exchange-correlation energy functional. *J. Chem. Phys.* **1998,** 109, (2), 400.

160. Zhao, Y.; Lynch, B. J.; Truhlar, D. G., Development and assessment of a new hybrid density functional model for thermochemical kinetics. *J. Phys. Chem. A* **2004,** 108, (14), 2715.

161. Lynch, B. J.; Fast, P. L.; Harris, M.; Truhlar, D. G., Adiabatic connection for kinetics. *J. Phys. Chem. A* **2000,** 104, (21), 4811.

162. Zhao, Y.; Truhlar, D. G., Hybrid meta density functional theory methods for thermochemistry, thermochemical kinetics, and noncovalent interactions: The MPW1B95 and MPWB1K models and comparative assessments for hydrogen bonding and van der Waals interactions. *J. Phys. Chem. A* **2004,** 108, (33), 6908.

163.   Zhao, Y.; Truhlar, D. G., The M06 suite of density functionals for main group thermochemistry, thermochemical kinetics, noncovalent interactions, excited states, and transition elements: two new functionals and systematic testing of four M06-class functionals and 12 other functionals. *Theor. Chem. Acc.* **2008,** 120, (1-3), 215.

164.   Becke, A. D., Density-functional thermochemistry. III. The role of exact exchange. *J. Chem. Phys.* **1993,** 98, (7), 5648.

165.   Zhao, Y.; Schultz, N. E.; Truhlar, D. G., Exchange-correlation functional with broad accuracy for metallic and nonmetallic compounds, kinetics, and noncovalent interactions. *J. Chem. Phys.* **2005,** 123, (16), 161103/1.

166.   Curtiss, L. A.; Raghavachari, K.; Trucks, G. W.; Pople, J. A., Gaussian-2 theory for molecular energies of first- and second-row compounds. *J. Chem. Phys.* **1991,** 94, (11), 7221.

167.   Vosko, S. H.; Wilk, L.; Nusair, M., Accurate spin-dependent electron liquid correlation energies for local spin density calculations: a critical analysis. *Can. J. Phys.* **1980,** 58, (8), 1200.

168.   Zhao, Y.; Gonzalez-Garcia, N.; Truhlar, D. G., Benchmark database of barrier heights for heavy atom transfer, nucleophilic substitution, association, and unimolecular reactions and its use to test theoretical methods. *J. Phys. Chem. A* **2005,** 109, (9), 2012.

169.   Zhao, Y.; Truhlar, D. G., A density functional that accounts for medium-range correlation energies in organic chemistry. *Org. Lett.* **2006,** 8, (25), 5753.

170.   Wodrich, M. D.; Corminboeuf, C.; Schreiner, P. R.; Fokin, A. A.; Von Schleyer, P., How accurate are DFT treatments of organic energies? *Org. Lett.* **2007,** 9, (10), 1851.

171.   Schultz, N. E.; Zhao, Y.; Truhlar, D. G., Density functionals for Inorganometallic and organometallic chemistry. *J. Phys. Chem. A* **2005,** 109, (49), 11127.

172.   Harvey, J. N., On the accuracy of density functional theory in transition metal chemistry. *Annu. Rep. Prog. Chem., Sect. C: Phys. Chem.* **2006,** 102, 203.

173. Plumley, J. A.; Evanseck, J. D., Hybrid meta-generalized gradient functional modeling of boron-nitrogen coordinate covalent bonds. *J. Chem. Theory Comput.* **2008,** 4, (8), 1249.

174. Perdew, J. P. In *Proceedings of the 21st annual international symposium on the electronic etructure of eolids*, Berlin, 1991; Ziesche, P.; Eschrig, H., Akademie Verlag: Berlin, 1991;

175. Perdew, J. P.; Burke, K.; Wang, Y., Generalized gradient approximation for the exchange-correlation hole of a many-electron system. *Phys. Rev. B* **1996,** 54, (23), 16533.

176. Adamo, C.; Barone, V., Exchange functionals with improved long-range behavior and adiabatic connection methods without adjustable parameters: the mPW and mPW1PW models. *J. Chem. Phys.* **1998,** 108, (2), 664.

177. Perdew, J. P.; Wang, Y., Accurate and simple analytic representation of the electron-gas correlation energy. *Phys. Rev. B* **1992,** 45, (23), 13244

178. Jones, G. O.; Guner, V. A.; Houk, K. N., Diels-Alder reactions of cyclopentadiene and 9,10-dimethylanthracene with cyanoalkenes: The performance of density functional theory and hartree-fock calculations for the prediction of substituent effects. *J. Phys. Chem. A* **2006,** 110, (4), 1216.

179. Lynch, B. J.; Truhlar, D. G., Small representative benchmarks for thermochemical calculations. *J. Phys. Chem. A* **2003,** 107, (42), 8996.

180. Zhao, Y.; Truhlar, D. G., Benchmark databases for nonbonded interactions and their use to test density functional theory. *J. Chem. Theory Comput.* **2005,** 1, (3), 415.

181. Koehl, R. M.; Odom, G. K.; Scuseria, G. E., The use of density matrix expansions for calculating molecular exchange energies. *Mol. Phys.* **1996,** 87, (4), 835.

182. Van Voorhis, T.; Scuseria, G. E., Exchange energy functionals based on the density matrix expansion of the Hartree-Fock exchange term. *Mol. Phys.* **1997,** 92, (3), 601.

183. Zhao, Y.; Truhlar, D. G., Exploring the limit of accuracy of the global hybrid meta density functional for main-group thermochemistry, kinetics, and noncovalent interactions. *J. Chem. Theory Comput.* **2008,** 4, (11), 1849.

184. Davidson, E. R.; Feller, D., Basis set selection for molecular calculations. *Chem. Rev.* **1986,** 86, (4), 681.

185. Cramer, C. J., *Essentials of Computational Chemistry: Theories and Models*. 2nd ed.; John Wiley & Sonds Ltd.: West Sussex, 2004; p 596.

186. Slater, J. C., Atomic shielding constants. *Phys. Rev.* **1930,** 36, 57.

187. Hehre, W. J.; Stewart, R. F.; Pople, J. A., Self-consistent molecular-orbital methods. I. Use of Gaussian expansions of Slater-type atomic orbitals. *J. Chem. Phys.* **1969,** 51, (6), 2657.

188. Hehre, W. J.; Ditchfield, R.; Pople, J. A., Self-consistent molecular orbital methods. XII. Further extensions of Gaussian-type basis sets for use in molecular orbital studies of organic molecules. *J. Chem. Phys.* **1972,** 56, (5), 2257.

189. Frisch, M. J.; Pople, J. A.; Binkley, J. S., Self-consistent molecular orbital methods. 25. Supplementary functions for Gaussian basis sets. *J. Chem. Phys.* **1984,** 80, (7), 3265.

190. Krishnan, R.; Binkley, J. S.; Seeger, R.; Pople, J. A., Self-consistent molecular orbital methods. XX. A basis set for correlated wave functions. *J. Chem. Phys.* **1980,** 72, (1), 650.

191. Binkley, J. S.; Pople, J. A.; Hehre, W. J., Self-consistent molecular orbital methods. 21. Small split-valence basis sets for first-row elements. *J. Am. Chem. Soc.* **1980,** 102, (3), 939.

192. Ditchfield, R.; Hehre, W. J.; Pople, J. A., Self-consistent molecular-orbital methods. IX. Extended Gaussian-type basis for molecular-orbital studies of organic molecules. *J. Chem. Phys.* **1971,** 54, (2), 724.

193. Hariharan, P. C.; Pople, J. A., Influence of polarization functions on MO hydrogenation energies. *Theor. Chim. Acta* **1973,** 28, (3), 213.

194.   Kendall, R. A.; Dunning, T. H., Jr.; Harrison, R. J., Electron affinities of the first-row atoms revisited. Systematic basis sets and wave functions. *J. Chem. Phys.* **1992,** 96, (9), 6796.

195.   Dunning, T. H., Jr., Gaussian basis sets for use in correlated molecular calculations. I. The atoms boron through neon and hydrogen. *J. Chem. Phys.* **1989,** 90, (2), 1007.

196.   Feller, D.; Peterson, K. A., Probing the limits of accuracy in electronic structure calculations: Is theory capable of results uniformly better than "chemical accuracy"? *J. Chem. Phys.* **2007,** 126, (11), 114105/1.

197.   Dunning, T. H., Jr., A road map for the calculation of molecular binding energies. *J. Phys. Chem. A* **2000,** 104, (40), 9062.

198.   Peterson, K. A., Gaussian basis sets exhibiting systematic convergence to the complete basis set limit. *Ann. Rep. in Comp. Chem.* **2007,** 3, 195.

199.   Woon, D. E., Accurate modeling of intermolecular forces: a systematic Moeller-Plesset study of the argon dimer using correlation-consistent basis sets. *Chem. Phys. Lett.* **1993,** 204, (1-2), 29.

200.   Peterson, K. A.; Kendall, R. A.; Dunning, T. H., Jr., Benchmark calculations with correlated molecular wave functions. III. Configuration interaction calculations on first row homonuclear diatomics. *J. Chem. Phys.* **1993,** 99, (12), 9790.

201.   Kestner, N. R.; Combariza, J. E., Basis set superposition errors: theory and practice. *Rev. Comput. Chem.* **1999,** 13, 99.

202.   Boys, S. F.; Bernardi, F., The calculation of small molecular interactions by the differences of separate total energies: some total energies: Some procedures with reduced errors. *Mol. Phys.* **1970,** 19, (4), 553.

203.   Simon, S.; Duran, M.; Dannenberg, J. J., How does basis set superposition error change the potential surfaces for hydrogen-bonded dimers? *J. Chem. Phys.* **1996,** 105, (24), 11024.

204. Jagielska, A.; Moszynski, R.; Piela, L., Ab initio theoretical study of interactions in borazane molecule. *J. Chem. Phys.* **1999,** 110, (2), 947.

205. Giesen, D. J.; Phillips, J. A., Structure, bonding, and vibrational frequencies of CH_3CN-BF_3: New insight into medium effects and the discrepancy between the experimental and theoretical Geometries. *J. Phys. Chem. A* **2003,** 107, (20), 4009.

206. Gutowski, M.; Van Duijneveldt, F. B.; Chalasinski, G.; Piela, L., Proper correction for the basis set superposition error in SCF calculations of intermolecular interactions. *Mol. Phys.* **1987,** 61, (1), 233.

207. Gutowski, M.; Van Duijneveldt, F. B.; Chalasinski, G.; Piela, L., Comment. Does the Boys and Bernardi function counterpoise method actually overcorrect the basis set superposition error? *Chem. Phys. Lett.* **1986,** 129, (3), 325.

208. Gutowski, M.; Chalasinski, G., Critical evaluation of some computational approaches to the problem of basis-set-superposition error. *J. Chem. Phys.* **1993,** 98, (7), 5540.

209. Bultinck, P.; Langenaeker, W.; Lahorte, P.; De Proft, F.; Geerlings, P.; Van Alsenoy, C.; Tollenaere, J. P., The electronegativity equalization method II: Applicability of different atomic charge schemes. *J. Phys. Chem. A* **2002,** 106, (34), 7895.

210. Mulliken, R. S., Electronic population analysis on LCAO-MO [linear combination of atomic orbital-molecular orbital] molecular wave functions. I. *J. Chem. Phys.* **1955,** 23, 1833.

211. Lowdin, P. O., Nonorthogonality problem. *Adv. Quantum Chem.* **1970,** 5, 185.

212. Bader, R. F. W., Atoms in molecules. *Acc. Chem. Res.* **1985,** 18, (1), 9.

213. Reed, A. E.; Weinstock, R. B.; Weinhold, F., Natural population analysis. *J. Chem. Phys.* **1985,** 83, (2), 735.

214. Young, D. C., *Computational Chemistry: A Practical Guide for Applying Techniques to Real-World Problems.* 1st ed.; John Wiley & Sons, Inc.: New York, 2001; p 370.

215. Gross, K. C.; Seybold, P. G.; Hadad, C. M., Comparison of different atomic charge schemes for predicting pKa variations in substituted anilines and phenols. *Int. J. Quantum Chem.* **2002,** 90, (1), 445.

216. Clark, A. E.; Sonnenberg, J. L.; Hay, P. J.; Martin, R. L., Density and wave function analysis of actinide complexes: What can fuzzy atom, atoms-in-molecules, Mulliken, Lowdin, and natural population analysis tell us? *J. Chem. Phys.* **2004,** 121, (6), 2563.

217. Glendening, E. D.; Weinhold, F., Natural resonance theory. I. General formalism. *J. Comput. Chem.* **1998,** 19, (6), 593.

218. Glendening, E. D.; Weinhold, F., Natural resonance theory. II. Natural bond order and valency. *J. Comput. Chem.* **1998,** 19, (6), 610.

219. Glendening, E. D.; Badenhoop, J. K.; Weinhold, F., Natural resonance theory. III. Chemical applications. *J. Comput. Chem.* **1998,** 19, (6), 628.

220. Reed, A. E.; Curtiss, L. A.; Weinhold, F., Intermolecular interactions from a natural bond orbital, donor-acceptor viewpoint. *Chem. Rev.* **1988,** 88, (6), 899.

221. Weinhold, F.; Landis, C., *Valency and Bonding: A Natural Bond Orbital Donor - Acceptor Perspective.* 1st ed.; Cambridge University Press: Cambridge, 2005; p 749.

222. Foster, J. P.; Weinhold, F., Natural hybrid orbitals. *J. Am. Chem. Soc.* **1980,** 102, (24), 7211.

223. Pophristic, V.; Goodman, L., Hyperconjugation not steric repulsion leads to the staggered structure of ethane. *Nature* **2001,** 411, (6837), 565.

224. Weinhold, F., Chemistry: A new twist on molecular shape. *Nature* **2001,** 411, (6837), 539.

225. Schreiner, P. R., Teaching the right reasons: Lessons from the mistaken origin of the rotational barrier in ethane. *Angew. Chem., Int. Ed.* **2002,** 41, (19), 3579.

226.   Bickelhaupt, F. M.; Baerends, E. J., The case for steric repulsion causing the staggered conformation of ethane. *Angew. Chem., Int. Ed.* **2003,** 42, (35), 4183.

227.   Mo, Y.; Wu, W.; Song, L.; Lin, M.; Zhang, Q.; Gao, J., The magnitude of hyperconjugation in ethane: a perspective from ab initio valence bond theory. *Angew. Chem., Int. Ed.* **2004,** 43, (15), 1986.

228.   Weinhold, F., Rebuttal to the Bickelhaupt-Baerends case for steric repulsion causing the staggered conformation of ethane. *Angew. Chem., Int. Ed.* **2003,** 42, (35), 4188.

229.   Mo, Y.; Gao, J., Theoretical analysis of the rotational barrier of ethane. *Acc. Chem. Res.* **2007,** 40, (2), 113.

230.   Acevedo, O.; Evanseck, J. D., Transition states and transition structures. In *Computational Medicinal Chemistry for Drug Discovery*, 1st ed.; 2004; 323.

231.   Chandler, D., *Introduction to Modern Statistical Mechancis*. 1st ed.; Oxford University Press: New York, 1987; p 274.

232.   McQuarrie, D. A.; Simon, J. D., *Molecular Thermodynamics*. 1st ed.; University Science Books: Sausalito, 1999; p 656.

233.   Carroll, F. A., *Perspectives on Structure and Mechanism*. 1st ed.; Brooks/Cole Publishing Company: Pacific Grove, 1998; p 944.

234.   Merrick, J. P.; Moran, D.; Radom, L., An evaluation of harmonic vibrational frequency scale factors. *J. Phys. Chem. A* **2007,** 111, (45), 11683.

235.   Scott, A. P.; Radom, L., Harmonic vibrational frequencies: An evaluation of Hartree-Fock, Møller-Plesset, quadratic configuration interaction, density functional theory, and semiempirical scale factors. *J. Phys. Chem.* **1996,** 100, (41), 16502.

236.   Rauhut, G.; Pulay, P., Transferable scaling factors for density functional derived vibrational force fields. *J. Phys. Chem.* **1995,** 99, (10), 3093.

237. Shaik, S., The Lewis legacy: the chemical bond-a territory and heartland of chemistry. *J. Comput. Chem.* **2007,** 28, (1), 51.

238. Kauffman, G. B., *Classics in Coordination Chemistry, Part 1: The Selected Papers of Alfred Werner*. 1st ed.; Dover Inc.: New York, 1968; p 190.

239. Guryanova, E. N.; Goldshtein, I. P.; Romm, I. P., *Donor-Acceptor Bond*. 1st ed.; Halsted/Wiley: Chichester, 1975; p 366.

240. Gutmann, V., *The Donor-Acceptor Approach to Molecular Interactions*. 1st ed.; Plenum Press: New York, 1978; p 279.

241. Jonas, V.; Frenking, G.; Reetz, M. T., Comparative theoretical study of lewis acid-base complexes of BH_3, BF_3, BCl_3, $AlCl_3$, and SO_2. *J. Am. Chem. Soc.* **1994,** 116, (19), 8741.

242. Umeyama, H.; Morokuma, K., Molecular orbital studies of electron donor-acceptor complexes. 3. Energy and charge decomposition analyses for several strong complexes: carbon monoxide-borane, ammonia-borane, methylamine-borane, trimethylamine-borane, and ammonia-boron trifluoride. *J. Am. Chem. Soc.* **1976,** 98, (23), 7208.

243. Rayon, V. M.; Sordo, J. A., On the nature of the interaction in donor-acceptor van der Waals complexes: $BH_3\cdots CO$, $BF_3\cdots CO$, $BH_3\cdots NH_3$ and $BF_3\cdots NH_3$. *THEOCHEM* **1998,** 426, 171.

244. LeTourneau, H. A.; Birsch, R. E.; Korbeck, G.; Radkiewicz-Poutsma, J. L., Study of the dative bond in 2-aminoethoxydiphenyl borate at various levels of theory: Another poor performance of the B3LYP method for B-N dative bonds. *J. Phys. Chem. A* **2005,** 109, (51), 12014.

245. Gilbert, T. M., Tests of the MP2 model and various DFT models in predicting the structures and B-N bond dissociation energies of amine-boranes $(X_3C)_mH_{3-m}B-N(CH_3)_nH_{3-n}$ (X = H, F; m = 0-3; n = 0-3): Poor performance of the B3LYP approach for dative B-N bonds. *J. Phys. Chem. A* **2004,** 108, (13), 2550.

246. Bauschlicher, C. W., Jr.; Ricca, A., On the interaction of CO and NH_3 with BH_3 and BF_3. *Chem. Phys. Lett.* **1995,** 237, (1,2), 14.

247.   Anane, H.; Boutalib, A.; Nebot-Gil, I.; Tomas, F., Comparative G2(MP2) study of H_3NBX_3 and H_3PBX_3 (X = H, F, and Cl) donor-acceptor complexes. *J. Phys. Chem. A* **1998,** 102, (35), 7070.

248.   Anane, H.; Boutalib, A.; Nebot-Gil, I.; Francisco, T., G2(MP2)2mrr01 study of the substituent effects in the $H_3BXH_nMe_{3-n}$ (X = N, P; n = 0-3) donor-acceptor complexes. *Chem. Phys. Lett.* **1998,** 287, (5,6), 575.

249.   Gurvich, L. V.; Veyts, I. V.; Alcock, C. B., *Thermodynamic Properties of Individual Substances*. 4th ed.; CRC Press: Boca Raton, 1994; p 106

250.   Allendorf, M. D.; Melius, C. F., Thermochemistry of molecules in the B-N-Cl-H system: ab initio predictions using the BAC-MP4 method. *J. Phys. Chem. A* **1997,** 101, (14), 2670.

251.   Anane, H.; El Houssame, S.; El Guerraze, A.; Jarid, A.; Boutalib, A.; Nebot-Gil, I.; Tomas, F., Ab initio molecular orbital study of the substituent effect on ammonia and phosphine-borane complexes. *THEOCHEM* **2004,** 709, (1-3), 103.

252.   Brown, H. C.; Bartholomay, H., Jr.; Taylor, M. D., Acid-base studies in gaseous systems. II. The anomalous base strength of the methylamines; a new manifestation of steric strain. *J. Am. Chem. Soc.* **1944,** 66, 435.

253.   Cox, J. D.; Wagman, D. D.; Medvedev, V. A., *CODATA Key Values for Thermodynamics*. 1st ed.; Hemisphere Publishing Corp.: New York, 1989; p 285.

254.   Bhat, K. L.; Howard, N. J.; Rostami, H.; Lai, J. H.; Bock, C. W., Intramolecular dative bonds involving boron with oxygen and nitrogen in boronic acids and esters: a computational study. *THEOCHEM* **2005,** 723, (1-3), 147.

255.   Nxumalo, L. M.; Andrzejak, M.; Ford, T. A., The vibrational spectra of the boron halides and their molecular complexes. 3. Ab initio predictions of the structures, snergetics, and mulliken atomic charges of the complexes of boron trifluoride with some linear nitrogen donors. *J. Chem. Inf. Comput. Sci.* **1996,** 36, (3), 377.

256.   This work was funded in part by the National Science Foundation and the Department of Energy (CHE-0723109, CHE-0321147, and CHE-030008P) and the Department of Education (P116Z040100, P116Z050331, and P116Z080180).

257. Suenram, R. D.; Thorne, L. R., Microwave spectrum and dipole moment of borane monoammoniate. *Chem. Phys. Lett.* **1981,** 78, (1), 157.

258. Curtiss, L. A.; Redfern, P. C.; Raghavachari, K., Gaussian-4 theory. *J. Chem. Phys.* **2007,** 126, (8), 084108/1.

259. Coyle, T. D.; Kaesz, H. D.; Stone, F. G. A., Molecular addition compounds of boron. II. Thiophane-borane and related adducts. *J. Am. Chem. Soc.* **1959,** 81, 2989.

260. Kulevsky, N.; Sveum, L., BX_3; complexes of some pyridine N-oxides. *J. Inorg. Nucl. Chem.* **1965,** 27, (9), 2111.

261. Christov, V. C.; Ivanov, I. K., Alkatrienyl sulfoxides and sulfones, VIII: Diels-Alder reaction of 3-methylpenta-1,2,4-trienyl phenyl sulfoxide with maleic anhydride. *Synth. Commun.* **2007,** 37, (18), 3201.

262. Maruoka, K.; Akakura, M.; Saito, S.; Ooi, T.; Yamamoto, H., Asymmetric Diels-Alder Reaction of Unsymmetrical Maleates. A Chemical Access to Chiral, Unsymmetrical cis-Cyclohexene-1,2-dicarboxylates. *J. Am. Chem. Soc.* **1994,** 116, (14), 6153.

263. Corey, E. J., Catalytic enantioselective Diels-Alder reactions: methods, mechanistic fundamentals, pathways, and applications. *Angew. Chem., Int. Ed.* **2002,** 41, (10), 1650.

264. Kabalka, G.; Borella, S.; Yao, M.-L., Boron trihalide mediated substitution of hydroxyl groups with alkenyl, alkynyl, and allyl moieties. *Synthesis* **2008**, (2), 325.

265. Li, C.; Wang, J., Lewis acid catalyzed propargylation of arenes with o-propargyl trichloroacetimidates: Synthesis of 1,3-diarylpropynes. *J. Org. Chem.* **2007,** 72, (19), 7431.

266. Huang, J.-W.; Shi, M., Lewis acid $BF_3.OEt_2$-catalyzed Friedel-Crafts reaction of methylenecyclopropanes with arenes. *Tetrahedron Lett.* **2003,** 44, (52), 9343.

267. Olah, G. A.; Kuhn, S. J., Selective Friedel-Crafts reactions. I. Boron halide catalyzed haloalkylation of benzene and alkylbenzenes with fluorohaloalkanes. *J. Org. Chem.* **1964,** 29, (8), 2317.

268. D'Aniello, F.; Mann, A.; Mattii, D.; Taddei, M., Stereoselective "ene" reaction of allylsilanes with amino aldehydes. An application to the synthesis of potential HIV-1 protease inhibitors. *J. Org. Chem.* **1994,** 59, (14), 3762.

269. Mayr, H.; Gorath, G., Kinetics of the reactions of carboxonium ions and aldehyde boron trihalide complexes with alkenes and allylsilanes. *J. Am. Chem. Soc.* **1995,** 117, (30), 7862.

270. Malladi, R. R.; Li, N.-S.; Tejedor, D.; Kabalka, G. W., Boron trifluoride mediated synthesis of 1,3-disubstituted 1,2-dihydronaphthalenes. *Synth. Commun.* **2000,** 30, (19), 3613.

271. Bellur, E.; Langer, P., Convenient synthesis of e-halo-b-keto esters and g,g'-dibromoalkanones by regio- and chemoselective reaction of 2-alkylidenetetrahydrofurans with boron trihalides: A "ring-closure ring-cleavage" strategy. *J. Org. Chem.* **2005,** 70, (10), 3819.

272. Bhatt, M. V.; Kulkarni, S. U., Cleavage of ethers. *Synthesis* **1983**, (4), 249.

273. Pons, J.-M.; Santelli, M., *Lewis Acids and Selectivity in Organic Synthesis*. 1st ed.; CRC-Press: New York, 1996; p 352.

274. Miller, J. M.; Onyszchuk, M., Heat of formation of boron tribromide-acetonitrile. *Can. J. Chem.* **1965,** 43, (6), 1877.

275. Bax, C. M.; Katritzky, A. R.; Sutton, L. E., N-Oxides and related compounds. IX. The electric dipole moments of pyridine- and trimethylamine-boron trihydride and trihalide complexes. *J. Chem. Soc.* **1958**, 1258.

276. Shriver, D. F.; Swanson, B., Nature of the donor-acceptor interaction in boron trihalide complexes. Vibrational spectra and vibrational analysis of acetonitrile-boron trichloride and acetonitrile-boron tribromide. *Inorg. Chem.* **1971,** 10, (7), 1354.

277. Brown, H. C.; Holmes, R. R., The catalytic halides. XIV. The heats of reaction of pyridine and nitrobenzene with boron trifluoride, trichloride and tribromide; the relative acceptor properties of the boron halides. *J. Am. Chem. Soc.* **1956,** 78, 2173.

278. Miller, J. M.; Onyszchuk, M., The relative acceptor power of boron trihalides toward acetonitrile by proton nuclear magnetic resonance measurements. *Can. J. Chem.* **1966,** 44, (8), 899.

279. Rothe, E. W.; Mathur, B. P.; Reck, G. P., Measurement of boron trihalide electron affinities: correlation with boron-nitrogen adduct strengths. *Inorg. Chem.* **1980,** 19, (4), 829.

280. Kuhn, S. J.; McIntyre, J. S., Reactions of amides and related compounds. I. Nuclear magnetic resonance (proton) investigation of N,N-dimethylformamide-Lewis acid adducts and remarks on the relative strength of Lewis acids. *Can. J. Chem.* **1965,** 43, (2), 375.

281. Mente, D. C.; Mills, J. L.; Mitchell, R. E., Gas-phase calorimetry of trimethyl Group Va bases with boron Lewis acids. *Inorg. Chem.* **1975,** 14, (1), 123.

282. Miller, J. M.; Onyszchuk, M., The relative acceptor power of boron trihalides and borane toward trimethylamine determined by proton N.M.R. (nuclear magnetic resonance) measurements. *Can. J. Chem.* **1964,** 42, (7), 1518

283. Bent, H. A., An appraisal of valence-bond structures and hybridization in compounds of the first-row elements. *Chem. Rev.* **1961,** 61, 275.

284. Bondi, A., van der Waals volumes and radii. *J. Phys. Chem.* **1964,** 68, (3), 441.

285. Pearson, R. G., Absolute electronegativity and hardness: application to inorganic chemistry. *Inorg. Chem.* **1988,** 27, (4), 734.

286. Hirao, H.; Omoto, K.; Fujimoto, H., Lewis acidity of boron trihalides. *J. Phys. Chem. A* **1999,** 103, (29), 5807.

287. Branchadell, V.; Oliva, A., The Lewis acidity scale of boron trihalides. An ab initio study. *THEOCHEM* **1991,** 82, (1-2), 75.

288. Branchadell, V.; Oliva, A., Complexes between formaldehyde and boron trihalides. An ab initio study. *J. Am. Chem. Soc.* **1991,** 113, (11), 4132.

289. Branchadell, V.; Sbai, A.; Oliva, A., Density functional study of complexes between Lewis acids and bases. *J. Phys. Chem.* **1995,** 99, (17), 6472.

290. Brown, D. G.; Drago, R. S.; Bolles, T. F., The linear ΔH-$\Delta \nu_{C=O}$ relation for ethyl acetate adducts and its significance for donor-acceptor interactions. *J. Am. Chem. Soc.* **1968,** 90, (21), 5706.

291. Cotton, F. A.; Leto, J. R., Acceptor properties, reorganization energies, and π bonding in the boron and aluminum halides. *J. Chem. Phys.* **1959,** 30, 993.

292. Rowsell, B. D.; Gillespie, R. J.; Heard, G. L., Ligand close-packing and the Lewis acidity of BF_3 and BCl_3. *Inorg. Chem.* **1999,** 38, (21), 4659.

293. Bessac, F.; Frenking, G., Why is BCl_3 a stronger Lewis acid with respect to strong bases than BF_3? *Inorg. Chem.* **2003,** 42, (24), 7990.

294. Bessac, F.; Frenking, G., Chemical bonding in phosphane and amine complexes of main group elements and transition metals. *Inorg. Chem.* **2006,** 45, (17), 6956.

295. Liebman, J. F., The Lewis acidity of the boron trihalides. *Struct. Chem.* **1990,** 1, (4), 395.

296. Miller, J. M.; Lanthier, G. F., Mass spectra of trimethylamine adducts of the boron trihalides and some mixed trihalides. *J. Chem. Soc. A* **1971**, (2), 346.

297. Fenwick, J. T. F.; Wilson, J. W., Thermochemical investigation into the Lewis acidity of the boron atom in some triaryloxyboranes. *Inorg. Chem.* **1975,** 14, (7), 1602.

298. Swanson, B.; Shriver, D. F.; Ibers, J. A., Nature of the donor-acceptor bond in acetonitrile-boron trihalides. The structures of the boron trifluoride and boron trichloride complexes of acetonitrile. *Inorg. Chem.* **1969,** 8, (10), 2182.

299. Frenking, G.; Fau, S.; Marchand, C. M.; Gruetzmacher, H., The π-donor ability of the halogens in cations and neutral molecules. A theoretical study of AX_3^+,

AH$_2$X$^+$, YX$_3$, and YH$_2$X (A = C, Si, Ge, Sn, Pb; Y = B, Al, Ga, In, Tl; X = F, Cl, Br, I). *J. Am. Chem. Soc.* **1997,** 119, (28), 6648.

300. Brinck, T.; Murray, J. S.; Politzer, P., A computational analysis of the bonding in boron trifluoride and boron trichloride and their complexes with ammonia. *Inorg. Chem.* **1993,** 32, (12), 2622.

301. Kutzelnigg, W., Chemical bonding in the higher major group elements. *Angew. Chem., Int. Ed.* **1984,** 23, (4), 272.

302. Lappert, M. F.; Litzow, M. R.; Pedley, J. B.; Riley, P. N. K.; Tweedale, A., Bonding studies of compounds of boron and the Group IV elements. II. Ionization potentials of boron halides and mixed halides by electron impact and by molecular orbital calculations. *J. Chem. Soc. A* **1968**, (12), 3105.

303. Cho, H. G.; Cheong, B. S., A theoretical investigation of the structure and vibrational frequencies of CH$_3$CN-BF$_3$ and CH$_3$CN-BCl$_3$. *THEOCHEM* **2000,** 496, (1-3), 185.

304. Hirota, F.; Miyata, K.; Shibata, S., Ab initio study on the charge-transfer complexes of boron trihalide with ammonia, trimethylamine, phosphine and trimethylphosphine. *THEOCHEM* **1989,** 60, 99.

305. Cai, Z.-T.; Li, C.-R.; Zhang, R.-Q.; Deng, C.-H., Theoretical studies on Lewis acidity scale and bonding character of boron trihalides BX$_3$(X=F, Cl, Br, I) by DV-Xa quantum chemical approach. *Chin. J. Chem.* **1997,** 15, (1), 17.

306. Mo, Y.; Lin, M.; Wu, W.; Zhang, Q.; Schleyer, P. v. R., Orbital deletion procedure and its applications. *Sci. China, Ser. B: Chem.* **1999,** 42, (3), 253.

307. Ghosh, D. C.; Jana, J., Frontier orbital and density functional study of the variation of the hard-soft behavior of monoborane (BH$_3$) and boron trifluoride (BF$_3$) as a function of angles of reorganization from planar (D$_{3h}$) to pyramidal (C$_{3v}$) shape. *Int. J. Quantum Chem.* **2003,** 92, (6), 484.

308. Allred, A. L., Electronegativity values from thermochemical data. *J. Inorg. Nucl. Chem.* **1961,** 17, 215.

309. Clementi, E.; Raimondi, D. L.; Reinhardt, W. P., Atomic screening constants from S.C.F. II. Atoms with 37 to 86 electrons. *J. Chem. Phys.* **1967,** 47, (4), 1300.

310. Goodman, L.; Sauers, R. R., Diffuse functions in natural bond orbital analysis. *J. Comput. Chem.* **2007,** 28, (1), 269.

311. Allendorf, M. D.; Melius, C. F.; Osterheld, T. H., A model of the gas-phase chemistry of boron nitride CVD from BCl_3 and NH_3. *Mater. Res. Soc. Symp. Proc.* **1996,** 410, (Covalent Ceramics III--Science and Technology of Non-Oxides), 459.

312. Allen, L. C., Electronegativity is the average one-electron energy of the valence-shell electrons in ground-state free atoms. *J. Am. Chem. Soc.* **1989,** 111, (25), 9003.

313. Sanderson, R. T., Principles of electronegativity. Part I. General nature. *J. Chem. Educ.* **1988,** 65, (2), 112.

314. Allred, A. L.; Rochow, E. G., A scale of electronegativity based on electrostatic force. *J. Inorg. Nucl. Chem.* **1958,** 5, 264.

315. Mulliken, R. S., Electronic structure of molecules. XI. Electroaffinity, molecular orbitals and dipole moments. *J. Chem. Phys.* **1935,** 3, 573.

316. Mulliken, R. S., New electroaffinity scale; together with data on valence states and on valence ionization potentials and electron affinities. *J. Chem. Phys.* **1934,** 2, 782.

317. Bratsch, S. G., Revised Mulliken electronegativities. I. Calculation and conversion to Pauling units. *J. Chem. Educ.* **1988,** 65, (1), 34.

318. Neter, J.; Wasserman, W.; Kutner, M. H., *Applied Linear Statistical Models: Regression, Analysis of Variance, and Experimental Designs*. Third ed.; Richard D. Irwin Inc.: 1990; p 1184.

319. Beste, A.; Kramer, O.; Gerhard, A.; Frenking, G., Theoretical studies of inorganic compounds. Part 9. The Lewis basicity of diaminocarbene. A theoretical study of donor-acceptor complexes of $C(NH_2)_2$, NH_3, and CO with

the Lewis acids EF_3, ECl_3 (E = B, Al, Ga, In), TiF_4, and $TiCl_4$. *Eur. J. Inorg. Chem.* **1999**, (11), 2037.

320.   Krahl, T.; Kemnitz, E., The very strong solid Lewis acids aluminum chlorofluoride (ACF) and bromofluoride (ABF)-synthesis, structure, and Lewis acidity. *J. Fluorine Chem.* **2006,** 127, (6), 663.

321.   Krossing, I.; Bihlmeier, A.; Raabe, I.; Trapp, N., Structure and characterization of $CI_3^+[Al(OC(CF_3)_3)_4]^-$; Lewis acidities of CX_3^+ and BX_3. *Angew. Chem., Int. Ed.* **2003,** 42, (13), 1531.

322.   Timoshkin, A. Y.; Suvorov, A. V.; Bettinger, H. F.; Schaefer, H. F., III., Role of the terminal atoms in the donor-acceptor complexes MX_3-D (M = Al, Ga, In; X = F, Cl, Br, I; D = YH_3, YX_3, X^-; Y = N, P, As). *J. Am. Chem. Soc.* **1999,** 121, (24), 5687.

323.   Pervova, Y. V.; Korobov, M. V.; Sidorov, L. N., Heats of bond cleavage in chlorofluoroaluminate ($AlCl_nF_{4-n}^-$) ions. *Zh. Fiz. Khim.* **1992,** 66, (5), 1199.

324.   Ball, D. W., Ab initio studies of AlH_3-H_2O, AlF_3-H_2O, and $AlCl_3$-H_2O Complexes. *J. Phys. Chem.* **1995,** 99, (34), 12786.

325.   Trusov, V. I.; Suvorov, A. V., Thermodynamic study of vaporous aluminum bromide-ammonia ($AlBr_3.NH_3$) and aluminum iodide-ammonia ($AlI_3.NH_3$). *Zh. Neorg. Khim.* **1974,** 19, (12), 3253.

326.   Timoshkin, A. Y.; Bettinger, H. F.; Schaefer, H. F., III., The chemical vapor deposition of aluminum nitride: Unusual cluster formation in the gas phase. *J. Am. Chem. Soc.* **1997,** 119, (24), 5668.

327.   Mercier, H. P. A.; Moran, M. D.; Schrobilgen, G. J.; Suontamo, R. J., Energetics of hydride and electron pair attachment to $EX_3^{0/+}$ (E=B, C, Al, Si and X=F, Cl, Br, I) and the study of bonding trends among $EX_3^{0/+}$, $EX_3^{2-/-}$, and $EX_3H^{-/0}$ by use of ELF and NBO analyses. *J. Fluorine Chem.* **2004,** 125, (11), 1563.

328.   Ryu, D. H.; Lee, T. W.; Corey, E. J., Broad-spectrum enantioselective Diels-Alder catalysis by chiral, cationic oxazaborolidines. *J. Am. Chem. Soc.* **2002,** 124, (34), 9992.

329. Corma, A.; Garcia, H., Lewis Acids: from conventional homogeneous to green homogeneous and heterogeneous catalysis. *Chem. Rev.* **2003,** 103, (11), 4307.

330. Li, C.-J., Organic reactions in aqueous media with a focus on carbon-carbon bond formations. A decade update. *Chem. Rev.* **2005,** 105, (8), 3095.

331. Yamamoto, H.; Futatsugi, K., "Designer acids": Combined acid catalysis for asymmetric synthesis. *Angew. Chem., Int. Ed.* **2005,** 44, (13), 1924.

332. Denmark, S. E.; Fu, J., Catalytic enantioselective addition of allylic organometallic reagents to aldehydes and ketones. *Chem. Rev.* **2003,** 103, (8), 2763.

333. Yamamoto, Y., From s- to p-electrophilic lewis Acids. Application to selective organic transformations. *J. Org. Chem.* **2007,** 72, (21), 7817.

334. Ess, D. H.; Jones, G. O.; Houk, K. N., Conceptual, qualitative, and quantitative theories of 1,3-dipolar and Diels-Alder cycloadditions used in synthesis. *Adv. Synth. Catal.* **2006,** 348, (16 + 17), 2337.

335. Ruben, E. A.; Plumley, J. A.; Chapman, M. S.; Evanseck, J. D., Anomeric effect in high energy phosphate bonds. Selective destabilization of the scissile bond and modulation of the exothermicity of hydrolysis. *J. Am. Chem. Soc.* **2008,** 130, (11), 3349.

336. Hammettt, L. P., Effect of structure upon the reactions of organic compounds. Benzene derivatives. *J. Am. Chem. Soc.* **1937,** 59, 96.

337. Swain, C. G.; Lupton, E. C., Jr., Field and resonance components of substituent effects. *J. Am. Chem. Soc.* **1968,** 90, (16), 4328.

338. Frisch, M. J.; Trucks, G. W.; Schlegel, H. B.; Scuseria, G. E.; Robb, M. A.; Cheeseman, J. R.; Scalmani, G.; Barone, V.; Mennucci, B.; Petersson, G. A.; Nakatsuji, H.; Caricato, M.; X. Li; Hratchian, H. P.; A. F. Izmaylov; Bloino, J.; Zheng, G.; Sonnenberg, J. L.; Hada, M.; Ehara, M.; Toyota, K.; Fukuda, R.; Hasegawa, J.; Ishida, M.; Nakajima, T.; Honda, Y.; Kitao, O.; Nakai, H.; Vreven, T.; J. A. Montgomery, J.; Peralta, J. E.; Ogliaro, F.; Bearpark, M.; Heyd, J. J.; Brothers, E.; Kudin, K. N.; Staroverov, V. N.; Kobayashi, R.; Normand, J.; Raghavachari, K.; Rendell, A.; Burant, J. C.; Iyengar, S. S.; Tomasi, J.; Cossi, M.; Rega, N.; Millam, J. M.; Klene, M.; Knox, J. E.; Cross, J. B.; Bakken, V.;

Adamo, C.; Jaramillo, J.; Gomperts, R.; Stratmann, R. E.; Yazyev, O.; Austin, A. J.; Cammi, R.; Pomell, C.; Ochterski, J. W.; Martin, R. L.; Morokuma, K.; Zakrzewski, V. G.; Voth, G. A.; Salvador, P.; Dannenberg, J. J.; Dapprich, S.; Daniels, A. D.; Farkas, O.; Foresman, J. B.; J. V. Ortiz, J. C.; Fox., D. J. *Gaussian 09, Revision A.01*, Gaussian, Inc.: Wallingford, CT, 2009

339.   Reed, A. E.; Weinhold, F., Natural localized molecular orbitals. *J. Chem. Phys.* **1985,** 83, (4), 1736.

340.   Miertus, S. S., E.; Tomasi, J., Electrostatic interaction of a solute with a continuum. A direct utilization of ab initio molecular potentials for the prevision of solvent effects. *Chem. Phys.* **1981,** 55, (1), 117.

341.   Cossi, M. B., V.; Cammi, R.; Tomasi, J., Ab initio study of solvated molecules: a new implementation of the polarizable continuum model. *Chem. Phys. Lett.* **1996,** 225, (4-6), 327.

342.   Aguilar, M. A.; Olivares del Valle, F. J., Nonequilibrium solvation: An ab initio quantum-mechanical method in the continuum cavity model approximation. *J. Chem. Phys.* **1993,** 98, (9), 7375.

343.   Tomasi, J.; Persico, M., Molecular interactions in solution: An overview of methods based on continuous distributions of the solvent. *Chem. Rev.* **1994,** 94, (7), 2027.

344.   Klamt, A.; Jonas, J., Treatment of the outlying charge in continuum solvation models. *J. Chem. Phys.* **1996,** 105, (22), 9972.

345.   Kong, S.; Evanseck, J. D., Density functional theory study of aqueous-phase rate acceleration and endo/exo selectivity of the butadiene and acrolein Diels-Alder reaction. *J. Am. Chem. Soc.* **2000,** 122, 10418.

346.   Corey, E. J.; Lee, T. W., The formyl C-H$\cdot$O hydrogen bond as a critical factor in enantioselective Lewis-acid catalyzed reactions of aldehydes. *Chem. Commun.* **2001,** 15, 1321.

347.   Alkorta, I.; Elguero, J., Non-conventional hydrogen bonds. *Chem. Soc. Rev.* **1998,** 27, 163.

348.   Gung, B. W.; Xue, X.; Roush, W. R., The origin of diastereofacial control in allylboration reactions using tartrate ester derived allylboronates: Attractive interactions between the Lewis acid coordinated aldehyde carbonyl group and an ester carbonyl oxygen. *J. Am. Chem. Soc.* **2002,** 124, 10692.

349.   Gung, B. W.; Wolf, M. A., A study of the electronic structures of boron trifluoride complexes with carbonyl compounds by ab initio MO methods. *J. Org. Chem.* **1992,** 57, (5), 1370.

350.   Mackey, M. D.; Goodman, J. M., Conformational preferences of R^1R^2C:O$^.$H$_2$BF complexes. *Chem. Commun.* **1997,** 24, 2388.

351.   Goodman, J. M., Molecular orbital calculations on R^1R^2C=O$^.$H$_2$BF complexes: Anomeric stabilisation and conformational preferences. *Tetrahedron Lett.* **1992,** 33, (47), 7219.

352.   Feng, Y.; Liu, L.; Zhao, S.-W.; Wang, J.-T.; Guo, Q.-X., Origin of conformational restriction in complexes of formyl compounds with boron Lewis acids and their related systems. *J. Phys. Chem. A* **2004,** 108, (42), 9196.

353.   Carroll, F. A., Substituent Effects and Linear Free Energy Relationships. In *Perspectives on Structure and Mechanism in Organic Chemistry*, 1st ed.; Brooks/Cole Publishing Company: Pacific Grove, 1998; 366.

354.   Kistiakowaki, G. B.; Lacher, J. R., The knetices of some gaseous Diels-Alder reactions. *J. Am. Chem. Soc.* **1936,** 58, 123.

355.   Guner, V.; Khuong, K. S.; Leach, A. G.; Lee, P. S.; Bartberger; D., M.; Houk, K. N., A standard set of pericyclic reactions of hydrocarbons for the benchmarking of computational methods: The performance of ab initio, density functional, CASSCF, CASPT2, and CBS-QB3 methods for the prediction of activation barriers, reaction energetics, and transition state geometries. *J. Phys. Chem. A* **2003,** 107, (51), 11445.

356.   Martin, J. M. L., Ab initio total atomization energies of small molecules — towards the basis set limit. *Chem. Phys. Lett.* **1996,** 259, (5-6), 669.

357.   Loewdin, P. O., Some comments on the present situation of quantum chemistry in view of the discussions at the Dubrovnik workshop on the electronic structure of molecules. *Pure Appl. Chem.* **1989,** 61, (12), 2185.

358.   García, J. I.; Martinez-Merino, V.; Mayoral, J. A.; Salvatella, L., Density functional theory study of a Lewis acid catalyzed Diels-Alder reaction. The butadiene + acrolein paradigm. *J. Am. Chem. Soc.* **1998,** 120, 2415.